Design of an Airborne Launch Vehicle for an Air Launched Space Booster

University of Michigan
Aerospace 490/590 Advanced Airplane Design
Winter 1993

ABSTRACT

DESIGN OF AN AIRBORNE LAUNCH VEHICLE FOR AN
AIR LAUNCHED SPACE BOOSTER

University of Michigan
Aerospace 490/590 Advanced Airplane Design
Winter 1993

A conceptual design is presented for a carrier vehicle for an air launched space booster. This airplane is capable of carrying a 500,000 pound satellite launch system to an altitude over 40,000 feet for launch. The airplane features a twin fuselage configuration for improved payload and landing gear integration, a high aspect ratio wing for maneuverability at altitude, and is powered by six General Electric GE-90 engines. The analysis methods used and the systems employed in the airplane are discussed. Launch costs are expected to be competitive with existing launch systems.

Team Members:
Chin Chao
Rich Choi
Scott Cohen
Brian Dumont
Mauricius Gibin
Rob Jorden
Stefan Poth, Team Leader

Advisor:
Dr. David Levy

Graduate Assistant:
John Blow

TABLE OF CONTENTS

(This page left intentionally blank.)

LIST OF SYMBOLS

Variables

Symbol	Meaning	Unit
A	Area	in^2, ft^2
A	Aspect ratio	-
b	Span	ft
C	Chord	ft
C	Cost	$
CEF	Cost escalation factor	-
C_D	Drag coefficient	-
C_{do}	Zero lift drag	-
C_{di1}	Linear lift induced drag constant	-
C_{di2}	Parabolic lift induced drag constant	-
C_L	Lift coefficient	-
$C_{L\alpha}$	Lift curve slope	rad^{-1}
C_l	Rolling moment coefficient	-
$C_{l\beta}$	Change in rolling moment due to side slip	rad^{-1}
$C_{l\delta A}$	Change in rolling moment due to lateral control	rad^{-1}
$C_{l\delta R}$	Change in rolling moment due to directional control	rad^{-1}
$C_{n\beta}$	Change in yawing moment due to side slip	rad^{-1}
$C_{n\delta A}$	Change in yawing moment due to lateral control	rad^{-1}
$C_{n\delta R}$	Change in yawing moment due to directional control	rad^{-1}
C_Y	Side force coefficient	-
$C_{Y\beta}$	Change in side force due to side slip	rad^{-1}
$C_{Y\delta A}$	Change in side force due to lateral control	rad^{-1}
$C_{Y\delta R}$	Change in side force due to directional control	rad^{-1}
D	Drag	lbf
d	Distance	ft
F	Force	lbf
F_Y	Side force	lbf
g	Gravitational acceleration	ft/sec^2
h	Altitude	ft
k	Constant	-
L	Lift	lbf
LCC	Life cycle cost	$

L_T	Rolling moment	ft•lbf
l	Moment arm	ft
$\dot{m}$	Airflow	slug/sec
M	Mach number	-
M	Moment	ft•lbf
N	Number	-
N_T	Yawing moment	ft•lbf
n	Load factor	g
OWE	Operational weight empty	lbf
P	Power	hp
P	Pressure	psi
r	Radius	ft
S	Field length	ft
S	Reference area	ft^2
SM	Static margin	%
T	Thrust	lbf
t	Time	hr, min, sec
U_1	Velocity	ft/sec
V	Velocity	mph, kts, ft/sec
$\overline{V}$	Volume coefficient	-
$\dot{v}$	Acceleration	ft/sec^2
W	Weight	lbf
x	Distance	ft
$\overline{x}$	Distance	-

Greek symbols

Symbol	Meaning	Unit
α	Angle of attack	°
β	Side slip angle	°
Δ	Change in	-
δ	Deflection angle	°
ρ	Density	$slug//ft^3$
η	Efficiency	-
Λ	Sweep angle	°
λ	Taper ratio	-
ϕ	Bank angle	°

τ	Shear stress	lbf/in^2
μ_f	Static coefficient of friction	-

Subscripts

Symbol	Meaning
A	Aileron
A	Airplane
ACQ	Acquisition
a	Absolute
a	Air
ac	Aerodynamic center
aedr	Airframe engineering and design
ampr	Empty structure
app	Approach conditions
arm	Hydraulic arm
av	Available
bleed	Bleed air
c	Capture
c/4	Quarter-chord
cg	Center of gravity
CONSMAT	Consumable materials
cool	Cooling
cr	Critical
cr	Cruise
D	Dive
DEPOT	Depot
DISP	Disposal
dst	development support and testing
e	Elevator
eff	Effective
electrical	Electrical
emergency	Emergency landing conditions
extracted	Total extracted
F	Fuselage
f	Flaps
f	Fuel

fin	Financing
flaps	Flaps
fta	Flight test airplane
fto	Flight test operations
gas	Gaseous flow
h	Horizontal tail
hydraulic	Hydraulic
inl/inc	Inlet
L	Landing
LE	Leading edge
launch	Launch conditions
launch turn	During launch turn
lever	Lever arm
lim	Limit
MISC	Miscellaneous
max	Maximum
mc	Minimum control
mechanical	Mechanical
mission	Complete mission
OPS	Operations
o	Effective
ol	Zero lift
PERSIND	Indirect personnel
PERSDIR	Direct personnel
POL	Fuel, oil, and lubricant
PROT	Prototype
p	Payload
pin	Eclipse/Gryphon connection pin
pneumatic	Bleed air
pro	Profit
R	Root
R	Rudder
RDTE	Research, development, test, and evaluation
r	Root
ramp	Ramp conditions
ref	Reference location

req	Required
reqd	Required
stall	Stall conditions
SPARES	Spare parts
TO	Take off conditions
t	Tip
to	Take off conditions
touch down	Touch down conditions
tsf	Test and simulation facilities
tst/av	Uninstalled available
ult	Ultimate
v	Vertical tail
WB	Wing and body
w	Wing

Abbreviations

Symbol	Meaning
APU	Auxiliary power unit
CAD	Computer aided design
CFD	Computational fluid dynamics
CNC	Computer numerical control
GD	General Dynamics
IMU	Inertial measurement unit
NC	Numerical control
OSC	Orbital Sciences Corporation
RAT	Ram air turbine

(This page left intentionally blank.)

LIST OF FIGURES & TABLES

Figures

Tables

(This page left intentionally blank.)

ACKNOWLEDGMENTS

The Aerospace 490/590 Advance Airplane Design team would like to thank the following people without whose aid this project would not have been possible:

Dr. David Levy - for committing the time so we could undertake this project
John Blow - for his help as teaching assistant
Mr. Bob Lovell of OSC - for giving us the idea for this project
Prof. William Anderson - for his help with the wing weight calculations
W'Lance Kallenberg - for his help generating the NC mill cutter paths
Prof. Peter Washabaugh - for his help with model fabrication
Mr. Terry Larrow - for his help with model fabrication
Mr. Warren Eaton - for his help with wind tunnel testing and model fabrication
Mr. Darren De Zeeuw - for use of his Quadtree CFD code and for his help in boundary layer modeling
Mr. Dennis Berry of Boeing - for providing us with useful methods in propulsion calculations
Mr. Ron Bengelink of Boeing - for helping us integrate the drag of the booster into the airplane drag
and especially all those people who took Aerospace 481 in the Fall of 1992 and started us on this journey:

Maize Team
Steve Battle
Mike Fisher
Enrique Garcia
Frank Gulczinski
Scot May
Kevin McGuirk
Rob Mitchell
Thuc Nguyen
Benjamin Place
Tracy Scott
Guan Soh
Matt Taylor
Ryan Waddington
Matthew Wagner
Charla Widmer

Blue Team
Brett Deutscher
Jeff Felkowski
Andrew Flotten
Rolf Kappe
Kevin Kilburn
Jack Kobus
Sara Lewis
Brian Nehez
Michael Ol
Bilal Rathur
Rance Stehower
Cynthia Tarr
Kevin Williamson

(This page left intentionally blank.)

1. INTRODUCTION

One way of reducing the total weight of a booster is to launch the booster from an airborne platform. This allows for a lower booster vehicle weight for the same payload capacity. Among the advantages to this approach are that the kinetic and potential energy of the airborne platform are added to that of the space booster and that the launch takes place above a substantial portion of the atmosphere so that aerodynamic drag forces are reduced. One such design is the Pegasus, manufactured by the Orbital Sciences Corporation. The Pegasus has a total weight of 42,000 pounds and a payload weight of 900 pounds. It has been carried aloft and launched by a Boeing B-52 and future launches are planned from a modified Lockheed L-1011.

In the future there may be a market for an air launched booster an order of magnitude larger. A space booster of this size would be capable of placing one or more satellites into geosynchronous earth orbit or a heavy payload into low earth orbit. Such a large booster would require a new airplane to be purpose built for its launch since no current airplane could carry such a heavy space booster to a high altitude. The design for such an airplane has been undertaken. This report details almost ten months of work on this project.

The University of Michigan Aerospace 490/590 Advanced Airplane Design class has designed the Eclipse, an aircraft whose primary mission is to act as a launch platform for a space booster weighing 500,000 pounds. Other mission requirements include a mission radius of 750 statute miles, a launch altitude of at least 40,000 feet, the ability to use existing airport facilities with minimal or no modification, and use of materials and processes which are already in existence or are planned for introduction in the very near future. Low cost for the airplane is also a priority since an increased airplane cost could make the launch system uncompetitive.

This report presents the design of the Eclipse. First, the mission for which the airplane was designed is presented, followed by an overview of the design. Then, the work in each of the technical areas is presented in depth. Next, the wind tunnel testing is discussed. Finally, the conclusions of the design team and some recommendations are presented.

(This page left intentionally blank.)

2. MISSION DESCRIPTION

2.1 Design Criteria

There are six main criteria for which the Eclipse is designed. These criteria are:

- The ability to carry a 500,000 pound payload which can be dropped in flight
- The ability to drop the payload above 40,000 feet
- A 750 statute mile mission radius
- The ability to perform a 2.2g post launch maneuver
- The ability to use existing airport facilities with minimal modification to the airport
- The use of existing production methods and equipment

Each of these criteria imposes a point for which an engineering design compromise must be made.

The design analysis is performed for an aborted mission which imposes the harshest conditions on the airplane. In the case of a last second aborted launch, the Eclipse would have to return to the airfield with the Gryphon attached since dropping such an expensive piece of hardware would be ill-advised. This means higher drag and therefore higher fuel burn, as well as a higher weight, for the return portion of the flight.

Planned airplane use is six missions per year over a ten year lifetime. The plan for six missions per year is based on a market study of current demand for launches of similar class boosters. The ten year lifetime is based on an estimate of when the next generation of space boosters will be in use. Only two airplanes will be built. The first will be fully functional while the second will be a structural spare, lacking avionics and engines.

2.2 Mission Profile

Figure 2.2.1 shows the mission profile which the Eclipse will perform. This mission is made up of nine segments:

1. Engine start, warm-up, taxi, and take off
2. Climb to best cruise altitude and accelerate to best cruise Mach number
3. Outbound cruise of 750 miles at best cruise altitude and best cruise Mach number
4. One hour loiter to prepare for launch
5. Launch maneuver designed for maximum booster/airplane separation
6. Inbound cruise of 750 miles at best cruise altitude and Mach number

7. Descent to sea level
8. One hour loiter to account for fuel reserve and any time spent in the landing pattern
9. Landing, taxi, and engine stop

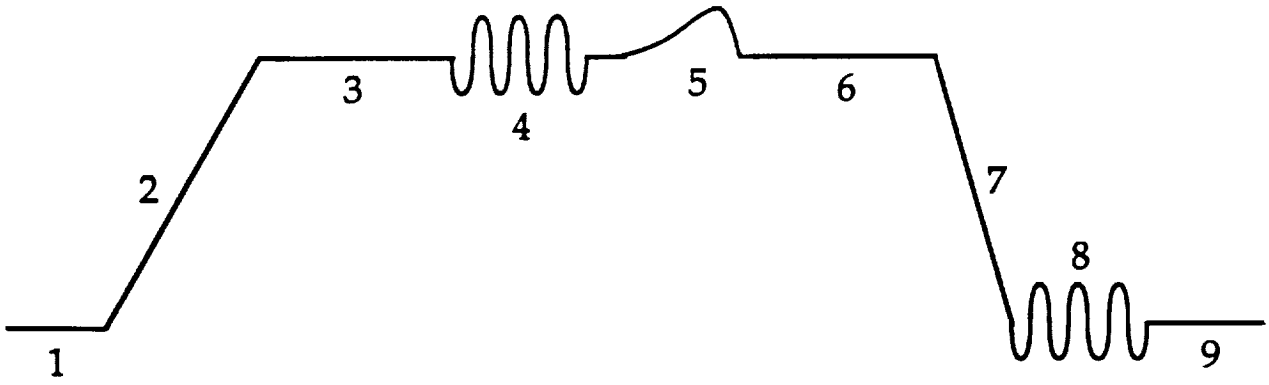

Fig. 2.2.1 Mission Profile

Performance calculations are based on this mission profile. Again, assuming an aborted launch. Two other missions are considered, the minimum fuel mission and the ferry mission. The minimum fuel mission does not have any cruise which allows for a higher launch altitude. The ferry mission is a point to point cartage of the space booster.

3. CONFIGURATION DESCRIPTION

In order to meet the unusual mission specifications set out for the Eclipse, an unusual airplane design has been developed. The Eclipse is a twin fuselage aircraft with the booster mounted beneath the wing between the two fuselages. A conventional tail-aft configuration is used with a cruciform layout. A high aspect ratio wing is employed to increase maneuverability at high altitude. Six engines power the Eclipse. These engines are a planned growth version of the General Electric GE-90 rated at 100,000 pounds of thrust at take off. This chapter gives a brief overview of the Eclipse.

3.1 Design History

This design project began in the fall of 1992 at the suggestion of Mr. Bob Lovell from the Orbital Sciences Corporation (OSC). OSC currently manufactures the Pegasus, a 42,000 pound air launched space booster with a payload capacity of 900 pounds. Mr. Lovell suggested that in the future OSC might look into a booster which is an order of magnitude larger. Such a large booster would require a purpose built aircraft since no current production airplane is capable of fulfilling the mission requirements.

The Aerospace 481 Airplane Design class began this project with each person in the 35 member class doing a basic layout and sizing for an aircraft capable of carrying a 250,000 pound booster. This lower weight was chosen as it was not known if a realistic design was feasible which could carry a 500,000 pound booster. The designs which were developed can be grouped into three broad categories: the conventional designs, the twin fuselage designs, and the other designs, which include flying wings and airplanes with elaborate schemes for conformally mounting the payload. Based on each person's design, the class was split into two groups for a continued design with a payload weight of 500,000 pounds. The increase to a higher weight was warranted as the feasibility of the design goal was proven by the individual projects. One group, consisting of people who looked at conventional designs, was tasked to design a conventional airplane. The other group was asked to come up with a more unusual design and decided upon a twin fuselage airplane. In the end, both designs had about the same characteristics: a weight of about 1.4 million pounds and a wing span of about 300 feet. Along with that, each airplane had its share of problems. For instance, the conventional design had a problem with landing gear integration while the fuselages of the twin fuselage design could not carry the loads which would be imposed on them. In addition, both airplanes had fuselage volume that was not put to any good use.

In January of 1993, seven of the members of the Aerospace 481 class decided to continue the design to see if a truly feasible design could be formulated. The class was formed under the title Aerospace 490/590 Advanced Airplane Design. Since each existing design had its share of problems, an analysis was made as to which design should be continued. Also, a third airplane design was reevaluated at this point, the flying wing. The flying wing showed promise since it does not have one of the big flaws in each of the other designs, wasted fuselage volume. The class decided to pursue the flying wing design and found that stability and control was a problem with this design for this mission. Sent back to step one, but much wiser about stability and control issues, the team decided to pursue a twin fuselage design since it showed promise from a landing gear and payload integration standpoint and was also more aesthetically pleasing.

The twin fuselage design, named the Eclipse, was taken through a Class II analysis, plus some special analysis when it was deemed necessary. After nearly ten months of work on the design, a realistic design has been formulated. This is the design which is presented in this report.

The University of Michigan Aerospace System Design class designed the Gryphon, an air launched space booster which can be carried and launched by the Eclipse. There was a significant amount of interchange between the classes in an attempt to optimize the system. Details of the Gryphon can be found in a summary paper (Appendix A) or in the Project Gryphon final report.[15]

3.2 Configuration Overview

Table 3.2.1 lists the major dimensions, weights, and performance numbers for the Eclipse. Figures 3.2.1 and 3.2.2 present the top and front views of the airplane. Figure 3.2.3 shows two longitudinal cross sections of the left fuselage. Figure 3.2.4 is an isometric view of the Eclipse.

3.3 Comparison with Existing Aircraft

It is important to compare the Eclipse with existing aircraft. This serves both to prove that the results are reasonable and to reavow that the design criteria cannot be met by existing airplanes. In Table 3.3.1, the Eclipse is compared with three other aircraft: the Boeing 747-400, the Lockheed C-5A, and the Antonov An-225. Figure 3.3.1 presents this comparison as a chart, with each value normalized to the Eclipse, which is assigned the value 1. Figure 3.3.2 is a top view which compares the size of the Eclipse with a Boeing 747-400.

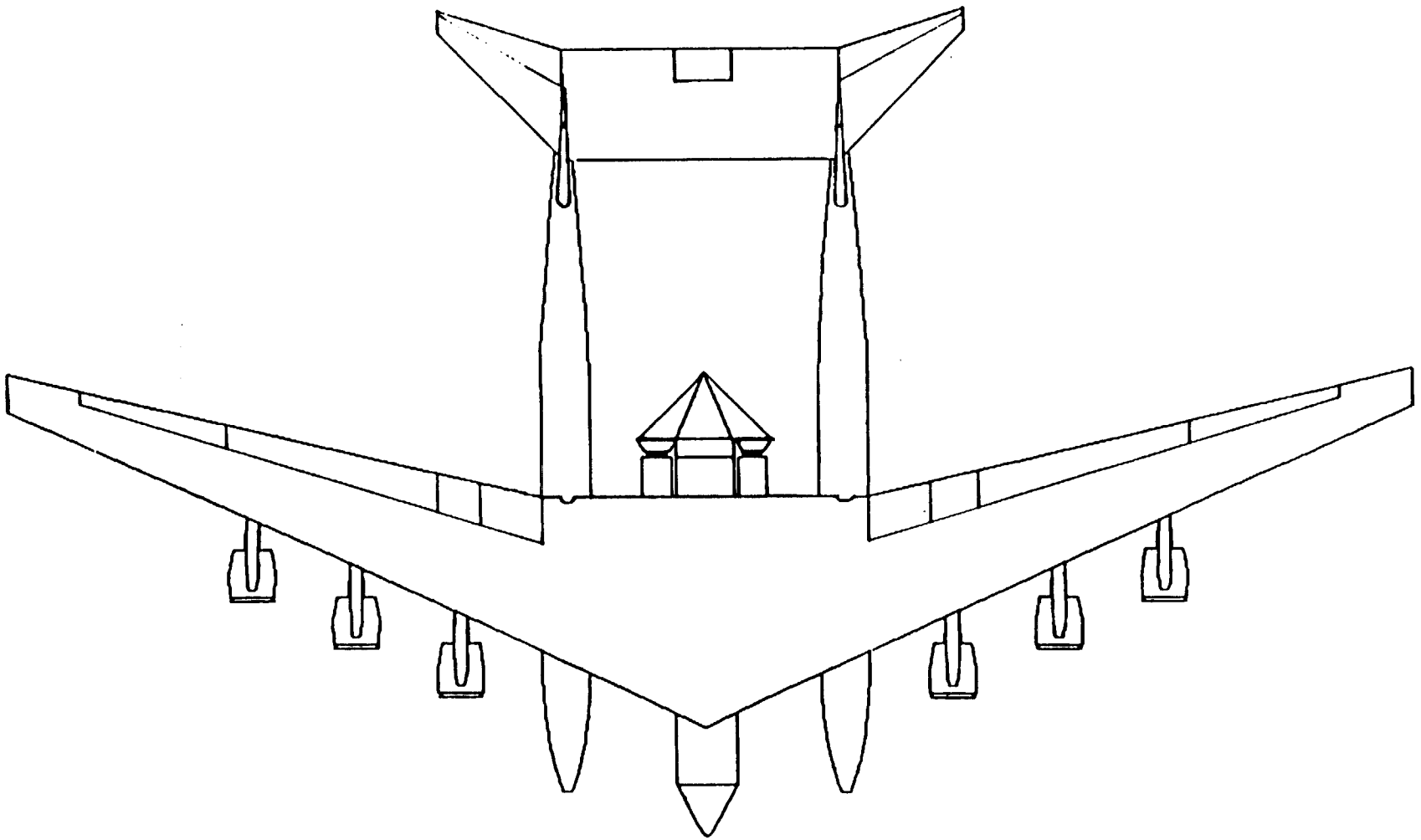

Fig. 3.2.1 Eclipse top view

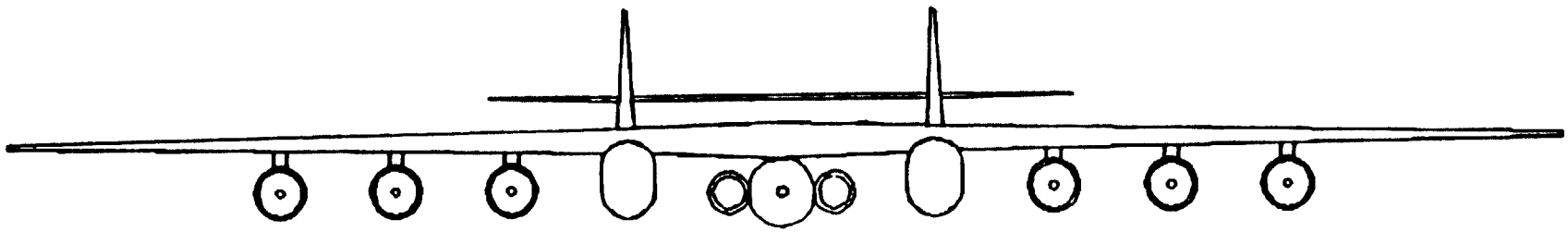

Fig. 3.2.2 Eclipse front view

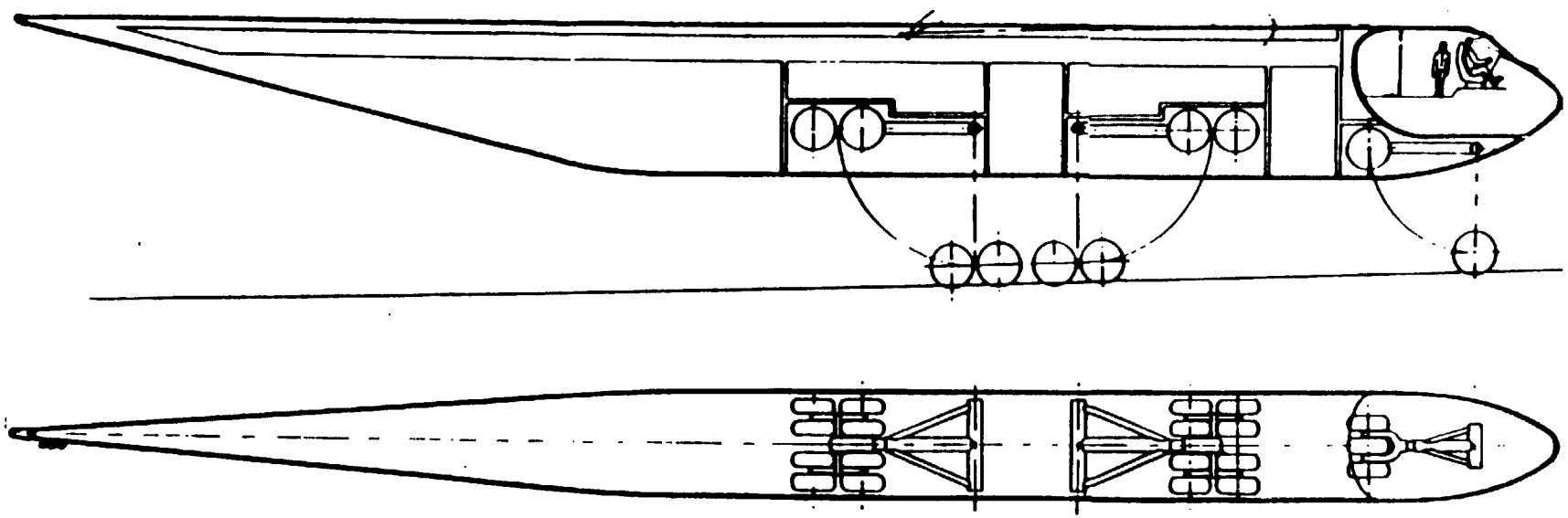

Fig. 3.2.3 Fuselage longitudinal cross sections

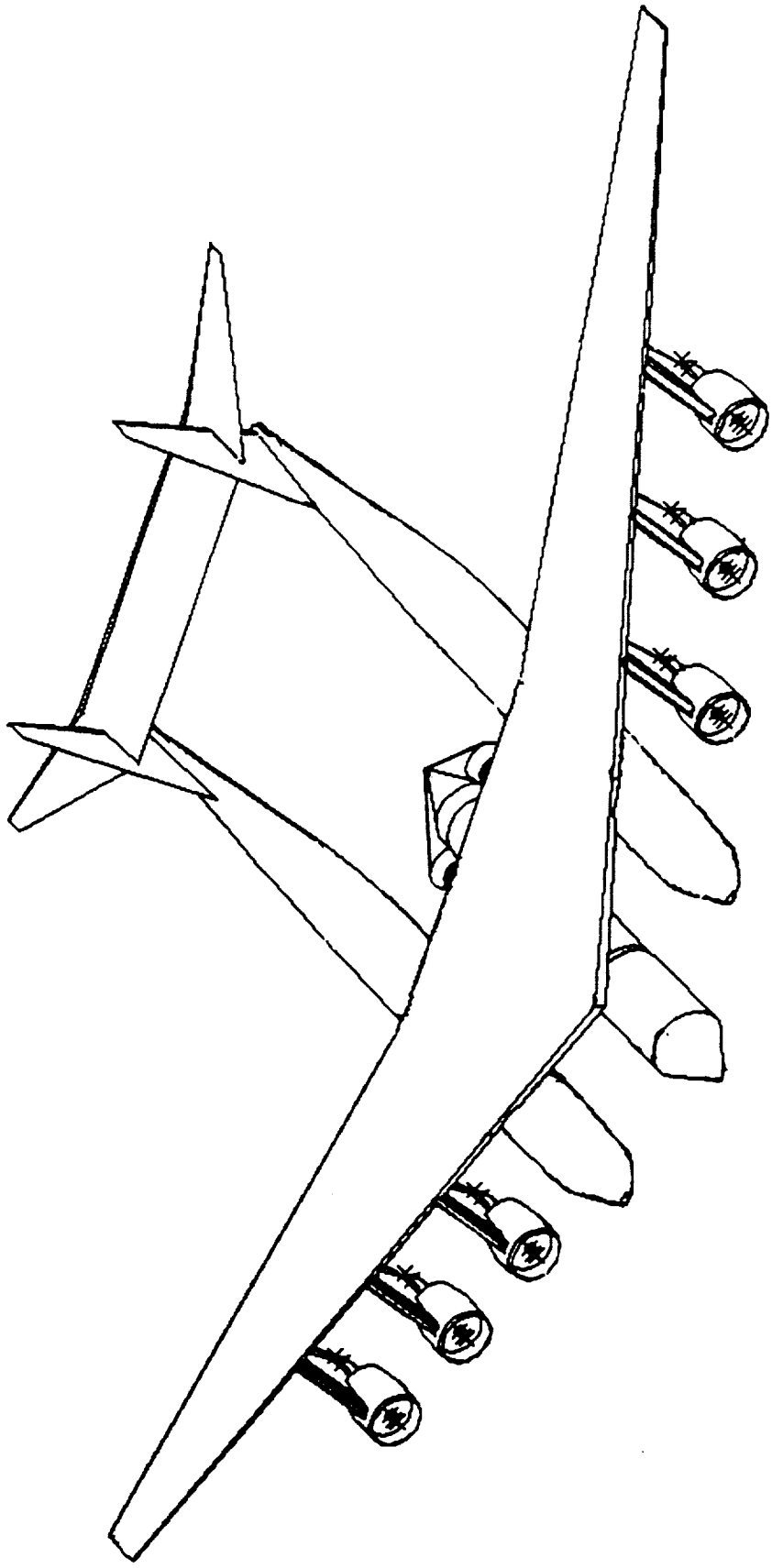

Fig. 3.2.4 Eclipse isometric view

Table 3.2.1 Major airplane parameters

W_{TO} (lbf)	1,227,000	Length (ft)	188.6
W_p (lbf)	479,000*	Height (ft)	62.4
W_f (lbf)	241,000**	S_v (ft^2) each	950
OWE (lbf)	541,000	S_h (ft^2)	3700
S (ft^2)	11,750	T_{TO} (lbf)	574,700
b (ft)	368	T/W (-)	0.489
A (-)	11.53	S_{TO} (ft)	4,300
$\Lambda_{c/4}$ (°)	22.1	S_L (ft)	3,400
W/S (lbf/ft^2)	104.4	h_{launch} (ft)	43,300
V_{cr} (mph)	515		

* University of Michigan Gryphon space booster

** includes 37,000 pounds of ramp fuel

Table 3.3.1 Airplane comparison

	Eclipse	747-400	C-5A	An-225
W_{TO} (lbf)	1,227,000	870,000	837,000	1,323,000
W_p (lbf)	479,000	144,000	261,000	344,000*
W_f (lbf)	241,000**	387,000	332,500	N/A
OWE (lbf)	541,000	339,000	243,500	N/A
S (ft^2)	11,750	5,500	6,500	N/A
b (ft)	368	211	222.7	290
Length (ft)	188.6	231.8	247	275.6
Height (ft)	62.4	63.4	65	59.3
W/S (lbf/ft^2)	104.4	158.2	131	N/A
T/W (-)	0.489	0.28	0.20	0.23

* this is the maximum payload that has been carried, published W_p = 551,000 lbf

** this includes fuel burned prior to take off which is not included in W_{TO}, maximum W_f = 350,000 lbf

It is interesting to note that while the Eclipse would not be the heaviest airplane ever built, it would have the largest wing span. The span surpasses even the Hughes H-4 Hercules, better known as the "Spruce Goose", which has a wing span of 320 feet. It is also important to notice that the An-225 could carry a payload of 500,000 pounds but, based on the performance with the maximum payload carried to date, it would not be able to meet the altitude or range requirements when doing so. The high thrust-to-weight ratio, necessitated by the altitude requirement, translates directly into very good take off and climb performance. The low wing loading, also necessitated by the altitude requirement, allows the post launch maneuver to be performed.

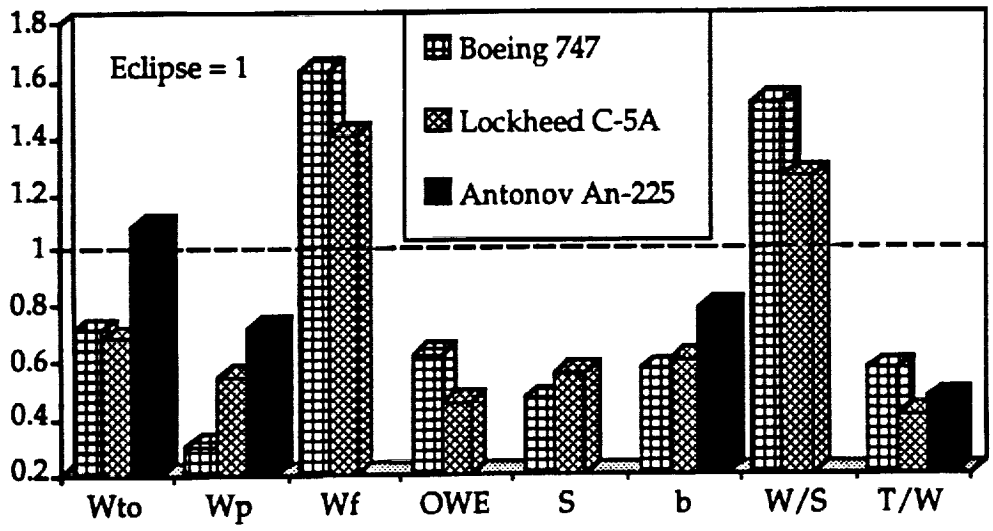

Fig. 3.3.1 Airplane comparison

3.4 Analysis Overview

As stated previously, the design was taken through a Class II analysis, plus some special analysis where it was deemed necessary. The basic idea and major results of each area of analysis is presented here.

3.4.1 Propulsion

The propulsion work centers on three items:

- engine selection
- sizing the nacelles and their placement on the wing
- determination of installed thrust available

Engine selection for this airplane is simple since only one engine meets the criteria with only six engines. The engine is a growth version of the General Electric GE-90 rated at 100,000 pounds of thrust at take off.

Engine nacelle sizing is based on the physical dimensions of the engine and the air flow needed into the engine for proper engine operation. The sizing is done using existing methods which minimize losses and interference effects.

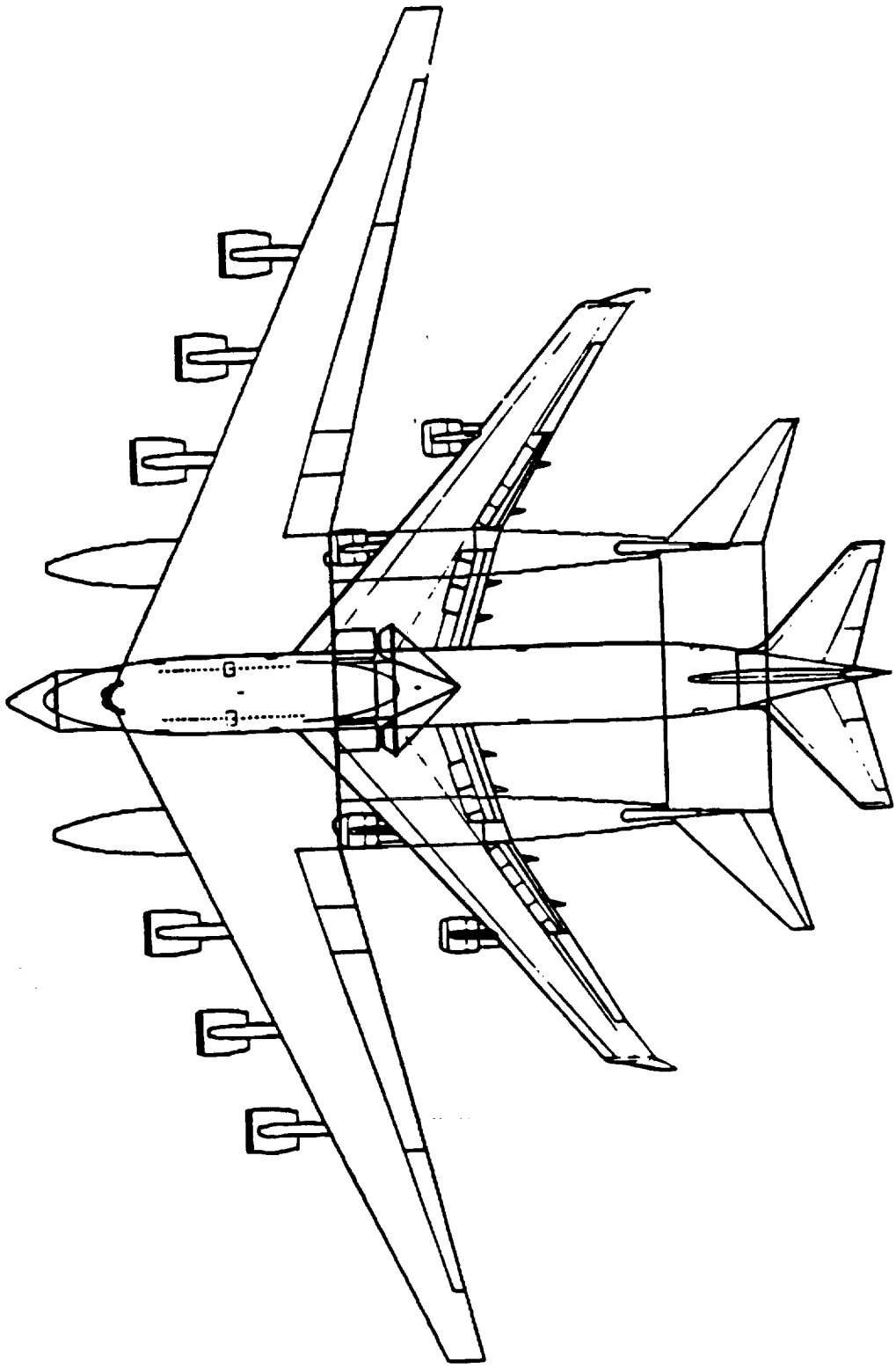

Fig. 3.3.1 Airplane comparison

Thrust losses due to installation effects are calculated using empirical formulas for mechanical, electrical, and pneumatic extraction. The installed thrust curves are then available for performance calculations. Table 3.4.1 lists some of the example thrust numbers.

Table 3.4.1 Thrust values per engine

Uninstalled T_{TO} (lbf) (M = 0, h = 0 ft)	100,000
Installed T_{TO} (lbf)	95,800
Uninstalled T_{CT} (lbf) (M = 0.78, h = 39,000 ft)	14,400
Installed T_{CT} (lbf)	14,100

3.4.2 Aerodynamics

The aerodynamics calculations focus on four issues:

- airfoil selection
- drag calculations
- flap sizing
- performance analysis

The airfoil selection is made to minimize drag while maximizing the lift for the critical parts of the mission. The airfoil is a NASA 14-percent thick supercritical airfoil. The aerodynamic characteristics of the airfoil with variation of angle of attack must also be known. To this end, a computational fluid dynamics (CFD) code is employed to supplement the semi-empirical methods. The CFD method employed is not successful for finding stall, but does supply a transition point which is used on the wind tunnel model.

Drag polar determination is based on semi-empirical methods which focus on wetted area. There is also a need to account for the interference losses associated with the payload mounted so close to the wing. Table 3.4.2 highlights the drag polars.

Flaps are sized to meet take off and landing speed criteria. Along with size, the most appropriate type of flap must be chosen. A single slotted Fowler flap with an area of 670 ft^2 is employed for this application.

Performance analysis is done, in conjunction with the propulsion work, to find the location, speed, and attitude of the airplane at any given moment during the flight. This allows for an accurate calculation of the fuel needed to complete the mission. Table 3.4.3 lists some of the important performance parameters.

Table 3.4.2 Drag polars

$C_{L_{\alpha\ cr}}$ (M = 0.78)	8.827
Cruise (M = 0.78, h = 40,000 ft w/ Gryphon)	$C_D = 0.0170 - 0.0012C_L + 0.0390C_L^2$
Cruise (M = 0.78, h = 40,000 ft clean)	$C_D = 0.0150 - 0.0011C_L + 0.0364C_L^2$
Loiter (M = 0.78, h = 44,000 ft w/ Gryphon)	$C_D = 0.0146 - 0.0016C_L + 0.0397C_L^2$
Loiter (M = 0.45, h = 10,000 ft clean)	$C_D = 0.0144 - 0.0052C_L + 0.0414C_L^2$

Table 3.4.3 Performance parameters

S_{TO} (ft)	4,300
S_L (ft)	3,400
h_{launch} (ft)	43,300
$n_{launch\ turn}$	2.2g
$r_{launch\ turn}$ (ft)	9200
$t_{mission}$	6 hr 55 min

3.4.3 Structures and weights

The structures and weights calculations look into four items:

- V-n diagram
- component weights
- longitudinal center of gravity
- structural considerations

The V-n diagram is needed to determine the loads acting on the airplane during flight. Two are made, one is for forces acting during an airplane maneuver while the other is for gust induced loads.

Component weight estimations are made using semi-empirical methods, analytical methods, or manufacturer supplied data. These values are calibrated with actual production aircraft to improve the accuracy of the prediction.

Longitudinal center of gravity calculation is made by assigning each airplane component a center of gravity. These can then be used, in conjunction with the component weights, to find the airplane center of gravity. The center of gravity is 53.43 feet behind the forward most point of the wing. The fuel and payload centers of gravity are coincident with the airplane center of gravity to eliminate shifts during the course of the mission which may worsen performance.

Other structural considerations, such as sizing of wing spars and fuselage pieces, are also considered. These include closing the fuselage section for greater structural strength and the number of spars in the wing.

3.4.4 Stability and control

Stability and control is concerned with two issues:

- longitudinal stability
- lateral and directional stability

Longitudinal stability involves sizing the horizontal tail to allow for take-off rotation, trim at cruise, and static margin at cruise. Pertinent horizontal tail parameters are listed in table 3.4.4.

Table 3.4.4 Horizontal tail parameters

S_h (ft^2)	3700
$\bar{x}_{cg_h}$ (-)	5.81*
$\bar{x}_{ac_h}$ (-)	5.68*
l_h (ft)	117.0
SM_{cr} (%)	5.2
SM_{TO} (%)	14.4

* measured from 50 feet in front of the forward most point of the wing

Lateral and directional stability sizes the vertical tail to limit airplane rolling moment, side force, and yawing moment. There is also a critical sizing of the vertical tails to maintain control in a one engine-out flight condition during take off rotation. Table 3.4.5 documents several of the important vertical tail and one engine-out parameters.

3.4.5 Systems

Six main airplane systems are designed:

- payload integration
- landing gear
- hydraulic system
- ectrical system
- ..ight c ntrol system
- fuel system

In addition, several issues relevant to the crew, such as visibility and crew training, are discussed.

Table 3.4.5 Vertical tail parameters

S_V (ft^2) each	950
$\bar{x}_{cg_V}$ (-)	5.48*
$\bar{x}_{ac_V}$ (-)	5.38*
l_V (ft)	94.86
$C_{n\beta}$ (rad^{-1})	0.1556
$C_{l\beta}$ (rad^{-1})	-0.1297
One engine-out ϕ (°)	4.0
One engine-out β (°)	5.0
One engine-out δ_R (°)	25.4
One engine-out δ_A (°)	7.4
V_{mc} (ft/sec)	231

* measured from 50 feet in front of the forward most point of the wing

3.4.6 Cost Analysis

Finally, what can make or break a design, its cost, is analyzed. A cost to build only two airplanes is formulated. This amounts to $1.715 billion for the one flying airplane and one structural spare, or an airplane cost of $28.6 million per mission for a 60 mission lifetime. Including the $22.1 million cost to buy a Gryphon, the launch cost comes to $50.7 million which is very competitive with today's launch systems.

(This page left intentionally blank.)

4. PROPULSION

4.1 Introduction

The goal of propulsion integration is to ensure that the propulsion system is well designed based on the mission goals and the requirements imposed by other aircraft components. In order to accomplish this goal, three primary tasks need to be completed. The assumptions made in propulsion integration to complete these tasks and the methods that are employed are detailed in the following discussion. The three tasks are:

- Engine selection
- Engine nacelle sizing
- Determination of installed thrust available

4.2 Discussion

The first step in the work is to decide what power plant should be used for the Eclipse. Due to the extreme thrust requirements for this aircraft, six General Electric GE-90 engines are used which, in a growth version, are expected to produce more than 100,000 pounds of thrust each. Since the time of engine selection, General Electric has tested the 87,400 pound thrust variant of the GE-90 at 105,400 pounds thrust which bodes well for an engine capable of meeting our specifications being produced. The methods used are from references which supply the detailed methods used in sizing the engine nacelles and determining the installed thrust available.[6,9]

4.2.1 Engine nacelle sizing

The first step in sizing the engine nacelle is to determine the engine inlet area, A_C, using:

$$A_C = \frac{\dot{m}_a}{\rho \cdot U_1} \tag{4.2.1}$$

where:

$\dot{m}_a$ = engine air mass flow [slug/sec]

ρ = air density [slug/ft^3]

U_1 = air velocity [ft/sec]

With engine data received from General Electric, $\dot{m}_a$ is determined from the fan flow rate to be 104.03 slug/sec. With an assumed take off speed of 288 ft/sec at sea level standard conditions, the inlet area is calculated to be 161.17 ft^2. This translates into an inlet diameter of 14.33 feet.

The other dimensions of the nacelle are determined based on the size of the GE-90 engine and dimensional comparisons with the General Electric CF6-32C. The relationships of the nacelle to the pylon and wing are based on nacelle location graphs with parameters chosen to minimize interference drag.[6,9] These parameters are determined as fractions of the wing chord length. The nacelle and pylon dimensions are shown in Figures 4.2.1 and 4.2.2, the side and front views.

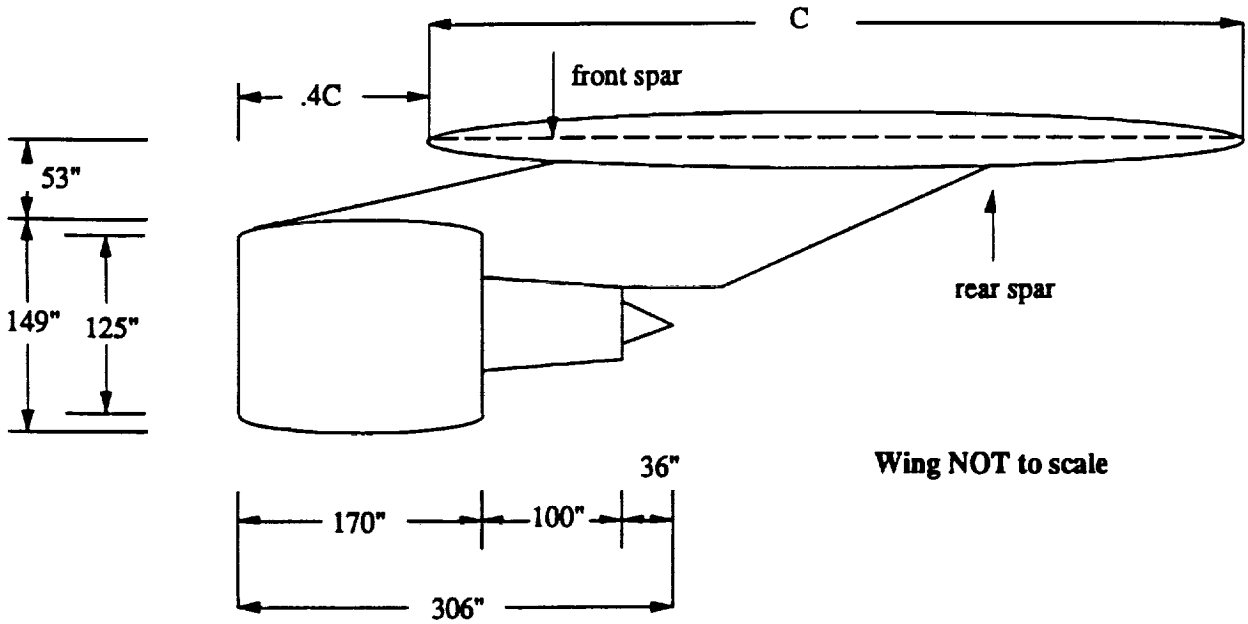

Fig. 4.2.1 Nacelle and pylon side view

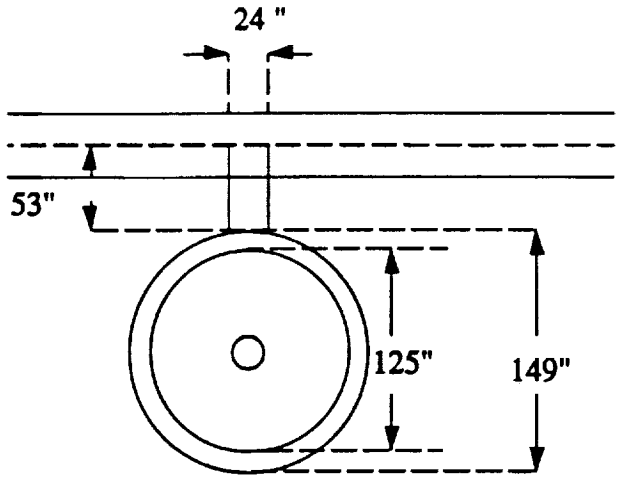

Fig. 4.2.2 Nacelle and pylon front view

In order to minimize interference effects which would lower engine efficiency, the nacelles are placed with approximately one and a quarter nacelle diameters between them. One and a quarter nacelle diameters are also left between the fuselages and the inboard nacelle for the same reason.

4.2.2 Determination of Installed Thrust Available

The first step in determining the installed thrust available is to calculate the power extracted due to mechanical extraction, electrical extraction, and pneumatic extraction. This is done using the following semi-empirical equations:[6]

$$P_{extracted} = P_{electrical} + P_{mechanical} + P_{pneumatic} \tag{4.2.2}$$

$$P_{electrical} = 0.00070 W_{TO} \tag{4.2.3}$$

$$P_{mechanical} = 0.00060 W_{TO} \tag{4.2.4}$$

$$P_{pneumatic} = \left(\frac{\dot{m}_{bleed}}{\dot{m}_a}\right)\left(\frac{T_{reqd} U_1}{550}\right) \tag{4.2.5}$$

$$\dot{m}_{bleed} = k \cdot \dot{m}_a \tag{4.2.6}$$

where:

$P_{extracted}$ = extracted power [hp]

$P_{electrical}$ = electrical power required by the airplane [hp]

$P_{mechanical}$ = mechanical power required by the airplane [hp]

$P_{pneumatic}$ = pneumatic power required by the airplane [hp]

W_{TO} = take off weight [lbf]

$\dot{m}_{bleed}$ = bleed air mass flow [slug/sec]

T_{reqd} = thrust required [lbf]

k = bleed air constant

In this case, the bleed air constant equals 0.015. This value is due to the fact that there are no deicing requirements for this airplane and only a small cabin must be pressurized. The values for power extracted are determined at the take off weight for various velocities. These values are shown in Figures 4.2.3 and 4.2.4.

The second step in determining the installed thrust available is to find the uninstalled thrust available. This data is acquired from a GE-90 cycle deck run which can be found in Appendix D.[16]

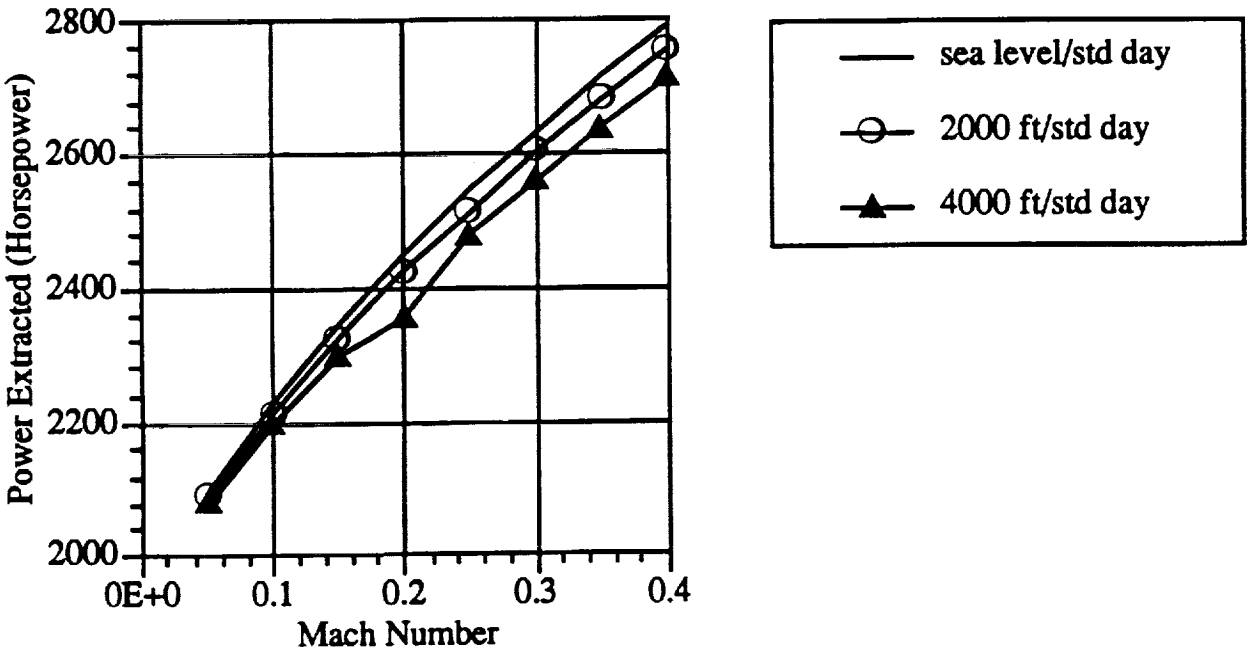

Fig. 4.2.3 Power extracted at take off for various field altitudes at standard conditions

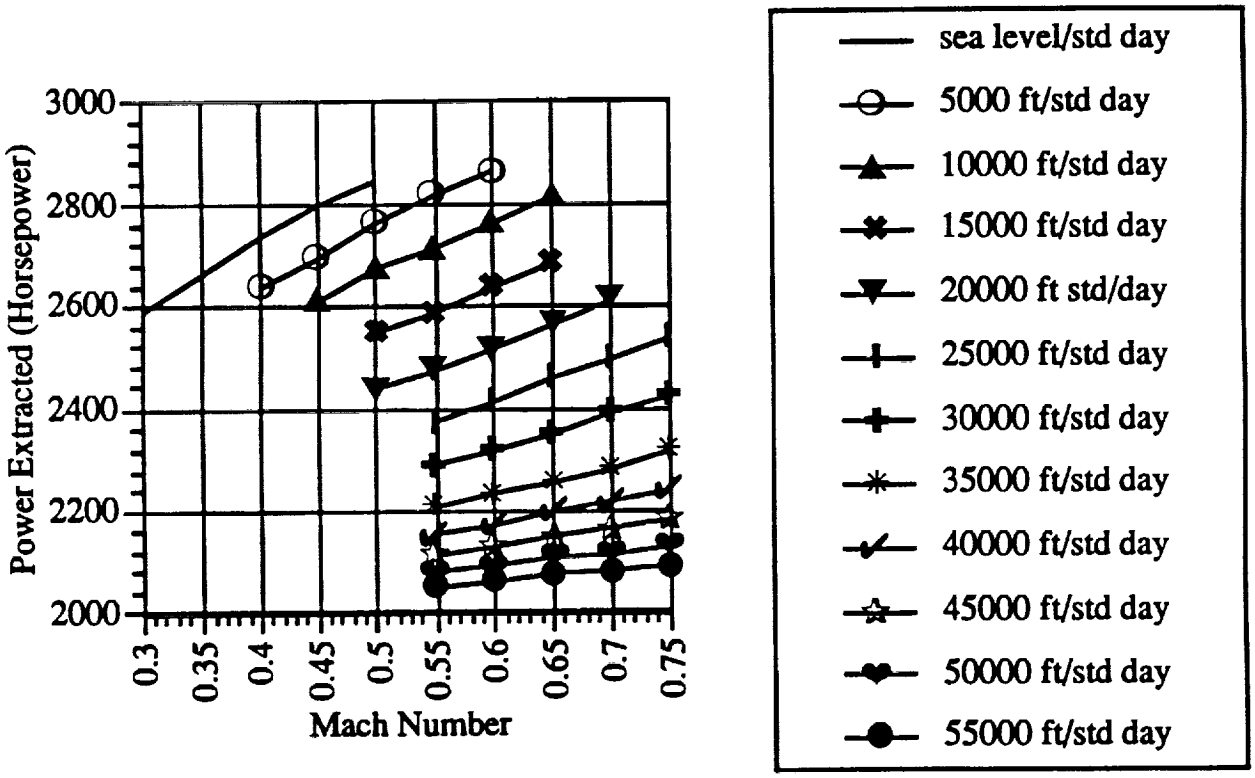

Fig. 4.2.4 Power extracted at maximum climb rate for various altitudes at standard conditions

The final step is to determine the installed thrust available using the following equation:[6]

$$T_{av} = \left[\left(T_{tst/av} \right) \left\{ 1 - 0.35 k_T M_1 \left(1 - \eta_{inl/inc} \right) \right\} - 550 \left(\frac{P_{extracted}}{U_1} \right) \right] \tag{4.2.7}$$

where:

T_{av} = installed thrust available [lbf]

$T_{tst/av}$ = uninstalled thrust available [lbf]

k_T = constant

M_1 = flight Mach number

$\eta_{inl/inc}$ = inlet efficiency

However, the thrust data received from General Electric accounted for the pressure drop across the engine ($\eta_{inl/inc} = 1$), so the equation is reduced to:

$$T_{av} = T_{tst/av} - 550 \left(\frac{P_{extracted}}{U_1} \right) \tag{4.2.8}$$

This calculation is performed at various velocities and altitudes, and the results are shown in Figure 4.2.5. The curves are extrapolated to cover the entire Mach number range at each altitude for use in performance calculations.

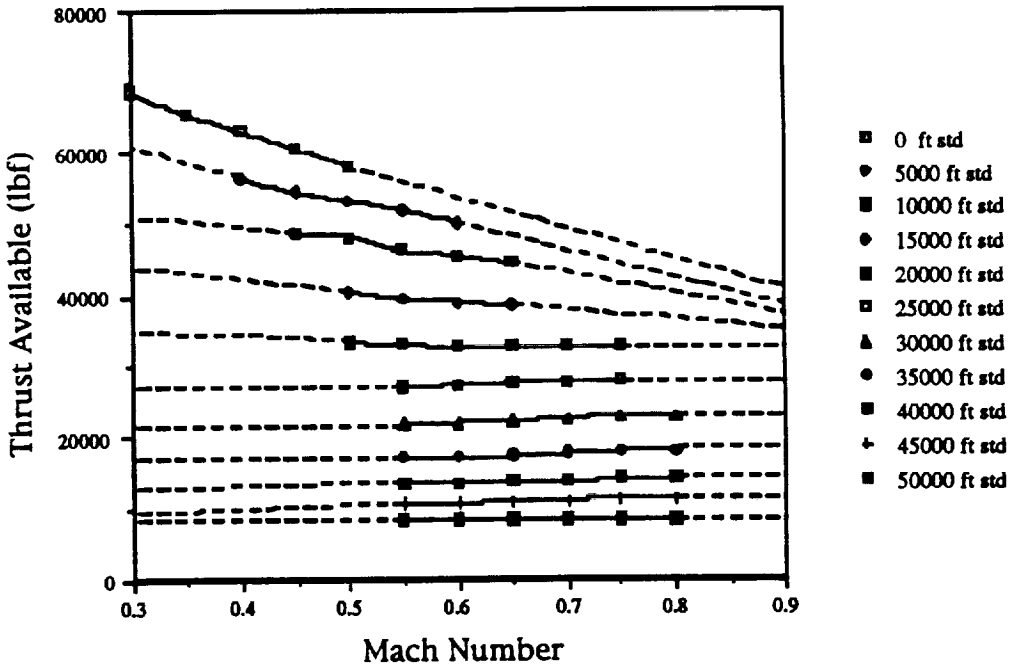

Fig. 4.2.5 Installed thrust available at maximum climb for various altitudes at standard conditions

(This page left intentionally blank.)

5. AERODYNAMICS

Aerodynamics is concerned with the flow of air around the airplane. In addition, the performance calculations and sizing of the lifting surfaces fall under the auspices of aerodynamics. The aerodynamics calculations focus on four issues:

- airfoil selection
- drag calculations
- flap sizing
- performance analysis

5.1 Assumptions & Pertinent Data

5.1.1 Equivalent wing drawing

For calculations involving the lift curves and drag polars, an aerodynamically equivalent wing is used. Table 5.1.1 lists the parameters of this equivalent wing.

Table 5.1.1 Equivalent wing parameters

S (ft^2)	11750
A (-)	11.53
b (ft)	368
λ (-)	0.19
C_r (ft)	53.64
C_t (ft)	10.2
Λ_{LE} (°)	25

Figure 5.1.1 shows a drawing of the equivalent wing along with the actual wing. Note that although the trailing edges are very close, they are not at the same sweep angle. The equivalent wing has a slightly smaller trailing edge sweep angle to account for the area lost by not having a yehudi.

5.1.2 Important numbers

Some important parameters used in the aerodynamics calculations are found in Table 5.1.2. A 1.5° angle of incidence for the main wing was used, as this is the cruise angle of attack of the main wing.

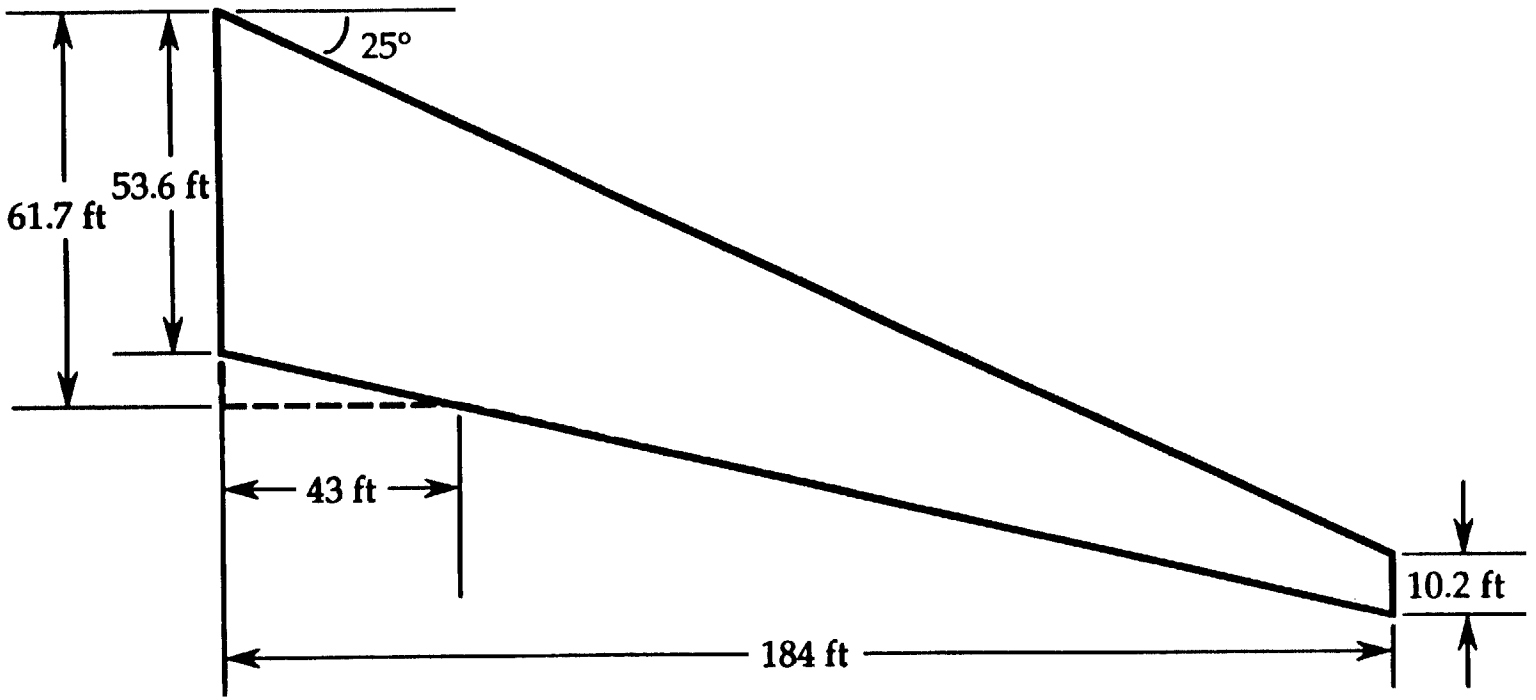

Figure 5.1.1 - Overlay of Equivalent Wing and Actual Wing

Table 5.1.2 Aerodynamic parameters

M_{CR} (-)	0.78
V_{TO} (ft/sec)	231
V_L (ft/sec)	240.5
V_{stall} (ft/sec)	210
V_{mc} (ft/sec)	231

5.1.3 Planform drawings of aerodynamic surfaces

Figures 5.1.2, 5.1.3, and 5.1.4 show the planform drawings of the main wing, horizontal tail, and vertical tail, respectively.

5.2 Airfoil Selection & Data

The airfoil is a NASA supercritical 14-percent thick airfoil.[10] The reason for this choice is largely due to critical Mach number (M_{CR}) considerations. Due to the immense wingspan of this airplane, the sweep must be mild to lighten the structure. Since the Eclipse will cruise at M = 0.78, a supercritical airfoil is necessary to minimize wave drag. A leading edge sweep angle of 25° is chosen. For a normal force coefficient of 0.75, significant wave drag is not encountered until about M = 0.73. At cruise, $M_{eff} = 0.78 \cdot \cos(25°) = 0.707$, which is below M_{CR}.

As can be seen from the numbers just presented, a sweep of 25° is not needed. In fact, a sweep of only 20.6° is necessary. The extra 4.4° of sweep is used for two reasons. First, since the cruise altitude and speed were not fixed at the outset, a buffer was desired. Second, since the shape of the Eclipse's airfoil almost certainly will not be to the same tolerances as the test airfoil due to inaccuracies in manufacturing such a large wing, it was desirable to add a factor of safety.

The shape of this airfoil is shown in Figure 5.2.1. The lift curve and drag polar for this airfoil at M = 0.71 are given in Figures 5.2.2 and 5.2.3. From the lift curve shown in Figure 5.2.5, Cl_α = 10.007 and α_{ol} = -2.955°. This scales by a Prandtl-Glauert transformation to Cl_α = 7.047 and α_{ol} = -2.955° at M = 0.

As can be seen from Figure 5.2.2, there is no available data for this airfoil in the nonlinear range of angle of attack. For this reason, a computational fluid dynamics (CFD) code is used to attempt to simulate separation.[19] More specifically, an Euler method is first used to solve the inviscid flow solution. From these results, Thwaite's method is used to evaluate the boundary layer behavior. Since this version of Thwaite's method estimates a laminar boundary layer, it will predict separation before the actual separation point. However, turbulent flow models that are

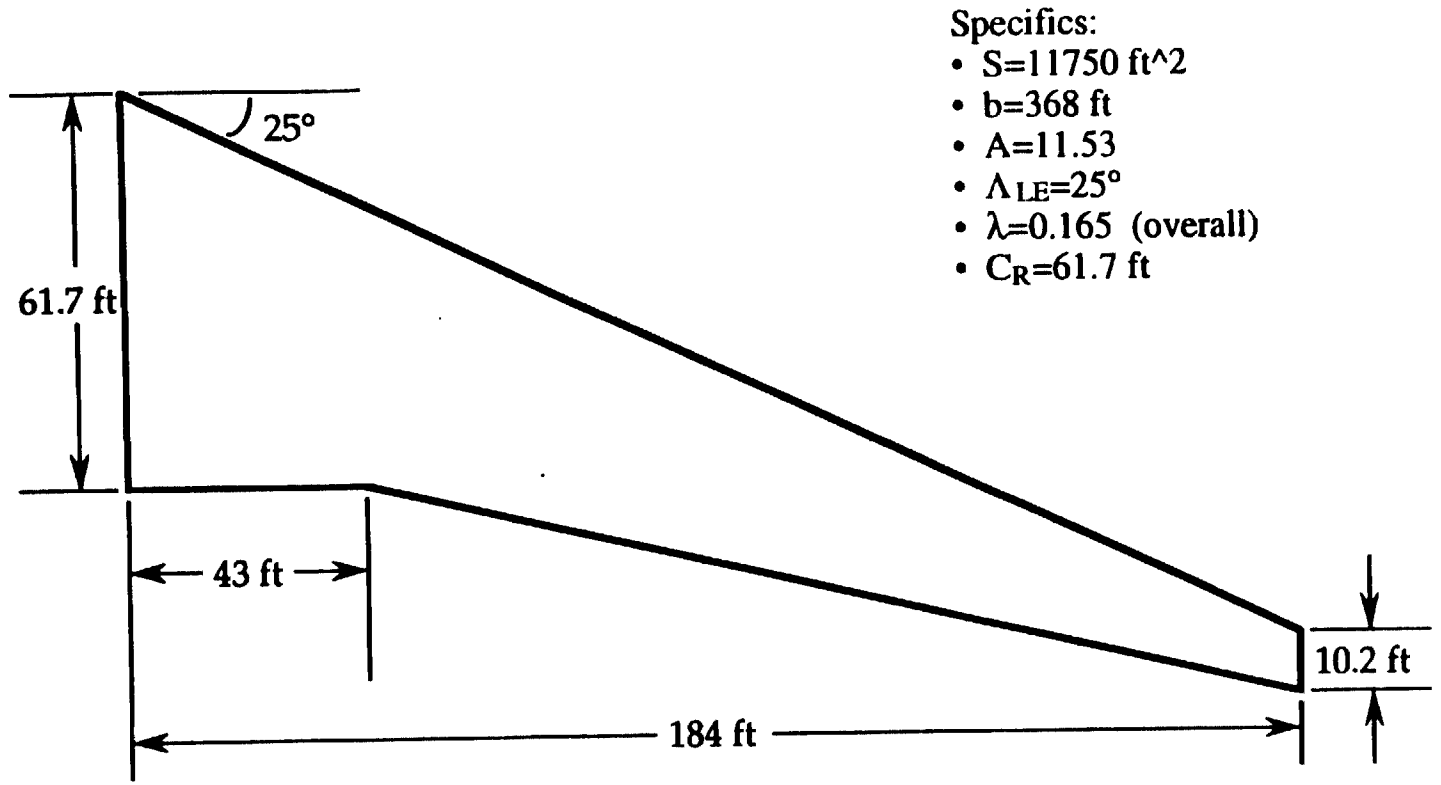

Figure 5.1.2 - Main Wing Planform

S_h	3700 ft^2	δ_e @ t.o.	-6.4°
A_h	6	δ_e @ cruise	1.7°
λ_h (overall)	0.2	S_e	670 ft^2
$\overline{V}_h$	0.905		
$\bar{x}_h$	2.87		

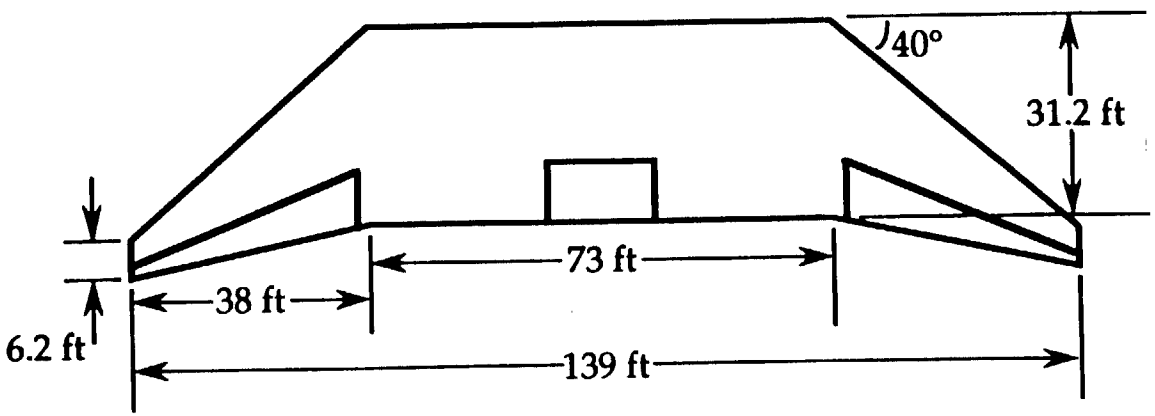

Figure 5.1.3 - Horizontal Tail Planform

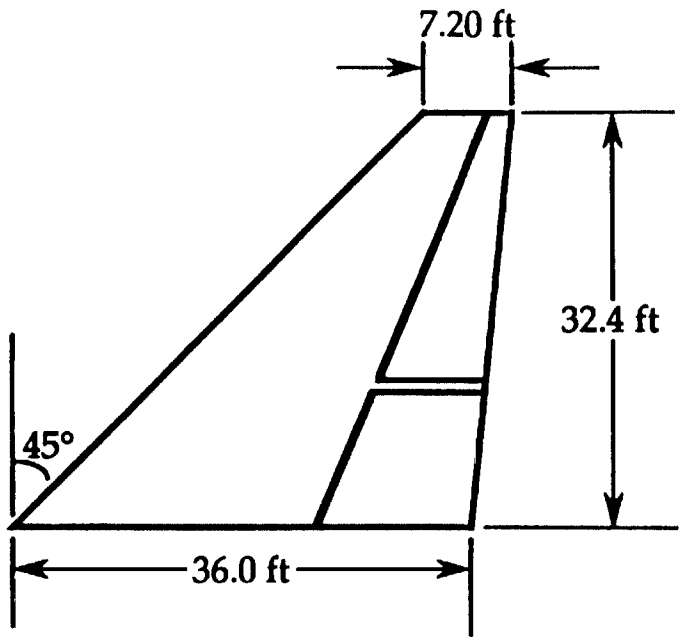

S_v	700 ft^2
A_v	1.5
λ_v	0.2
$\overline{V}_v$	0.032
$\bar{x}_v$	2.713
V_{mc}	238 mph

Figure 5.1.4 Vertical Tail Planform

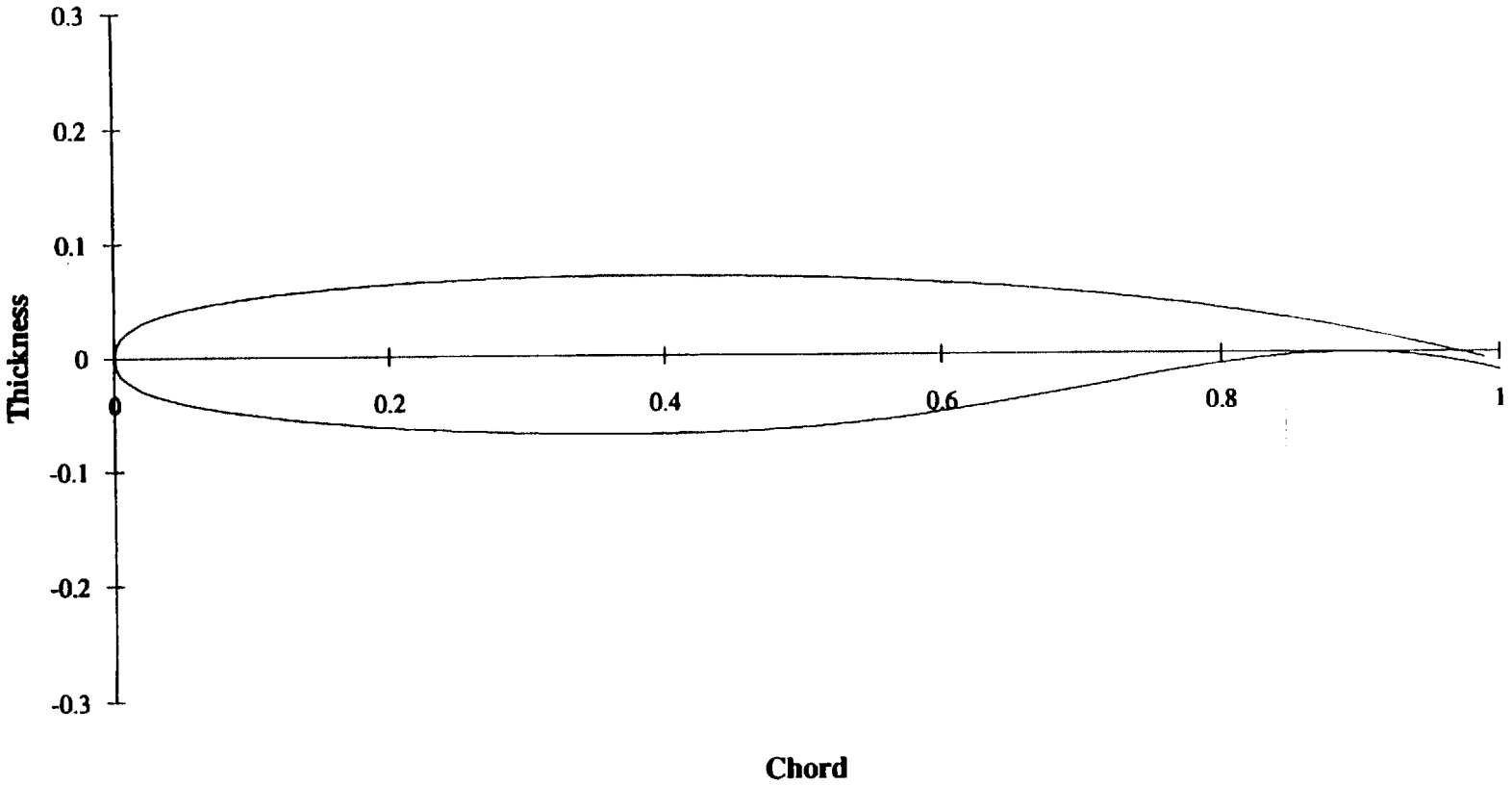

Figure 5.2.1 - Airfoil Cross-Section

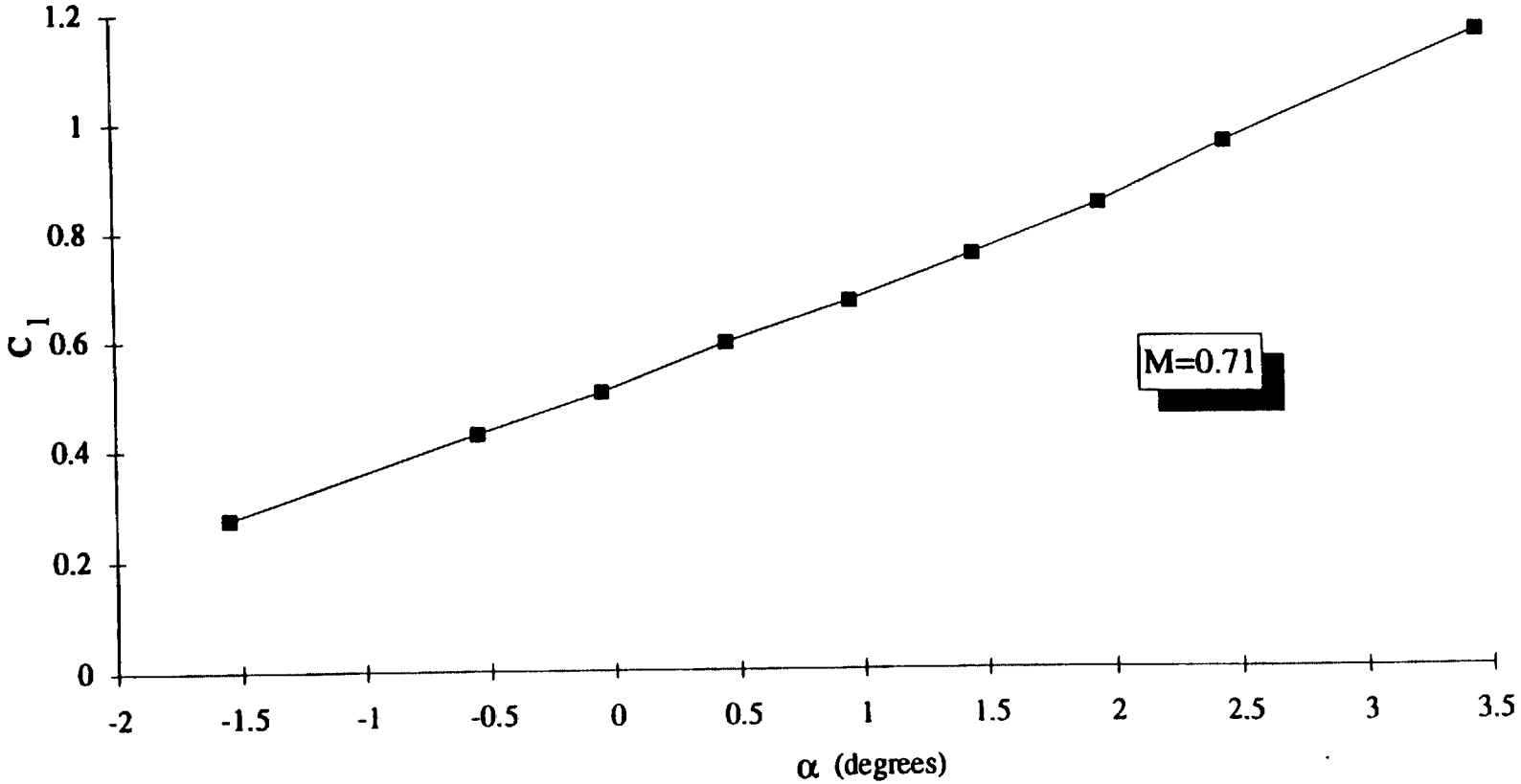

Figure 5.2.2 - Lift Coefficient versus Angle of Attack for NASA 14-percent thick Supercritical Airfoil

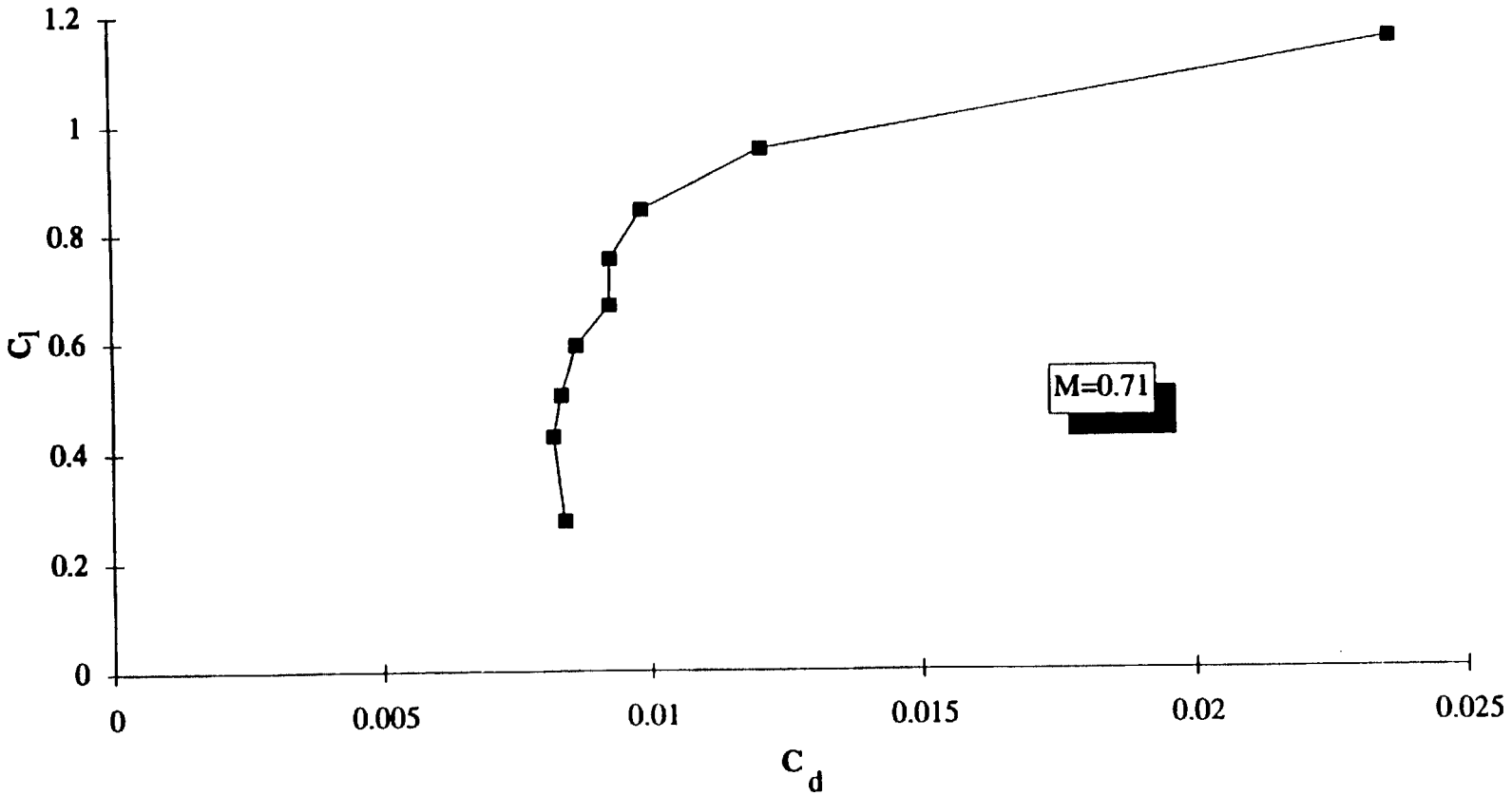

Figure 5.2.3 - Drag Polar for NASA 14-percent thick Supercritical Airfoil

good near stall are very difficult to come by and could not be employed. Unfortunately, this method is more conservative than expected. Separation is found at 72% of the chord at M = 0.71 and $\alpha = 0°$. Since this is the design condition of the airfoil, separation is unlikely to occur here. Therefore, this estimate is too conservative to be of use. However, there is something to be gained from this work. A point of transition to turbulence can be found which was used on the wind tunnel model to trip the flow at the correct point. Further details can be found in Appendix B.1.

5.3 Lift Curves & Wing Moment Coefficients

The lift curves for the wing, wing and fuselage, and airplane were calculated (in the linear range) for Mach numbers between 0.2 and 0.8 in increments of 0.05. For the same Mach Numbers, moment coefficients were calculated for the main wing in order to analyze trim. These calculations were done with semi-empirical methods.[6] Some assumptions that were made include:

1) A half-chord sweep angle of 17° for the horizontal tail. This was found by simply scaling the half-chord sweep angles of the two portions of the tail by area.
2) A value of Cdo was needed for each lift curve. These values depend on altitude. The altitude that will correspond to a given Mach Number in the mission profile was used. For Mach numbers for which no drag polar have been calculated, interpolation was employed.
3) The lift curve slope for the tail was found for a NACA 0009 airfoil. The actual airfoil is a NACA 0010 outboard and NACA 0008 inboard, but the change due to thickness appears to be minor.

The lift curve slope varied from 6.4353 at M = 0.20 to 9.0929 at M = 0.80. A full break down of the numbers and further details of the calculations can be found in Appendix B.2.

5.4 Drag Polars

5.4.1 Methodology

Most of the drag components for the Eclipse are calculated using semi-empirical methods from Roskam.[6] However, there are some exceptions. The nacelle drag is calculated using the semi-empirical method found in Raymer.[11] Roskam's method approximates the nacelle by a fuselage. Due to the extremely wide fan diameter of the GE-90, the fineness ratio is very low. This causes Roskam's drag prediction to be much larger than could be reasonably expected. Raymer's book suggests a method for nacelles which gave a drag prediction which was much more in line with the nacelle's percentage of airplane wetted area. When finding the zero-lift drag on the wing, the wing-fuselage interference factor is squared to account for the second fuselage.

Once the clean drag polars were calculated for the Eclipse, the next step was to account for the Gryphon. Using the final external geometry of the Gryphon, a drag polar for the Gryphon alone was obtained. To account for the interference of the Gryphon on the Eclipse, an empirical method was employed.[17] The method for combining the drag polars has three steps:

1) Assume the effective angle of attack on the Gryphon to be zero because the chord of the wing is so large that it will force the flow around the Gryphon. This is not be the case for the tip of the Gryphon, but that effect is of an order less than the error in the interference calculations.
2) For the portion of the wing that is directly affected by the Gryphon, add a 10% increment to the drag to account for the changed flow field that the Gryphon will directly impose on the wing.
3) After all other drag polar calculations are done, add 5% to the final drag for other interference caused by the Gryphon.

Further details of the calculations can be found in Appendix B.3.

5.4.2 Results

A few of the final drag polars are shown in Table 5.4.1. The complete results can be found in Appendix B.3.

Table 5.4.1 Drag polars

Flight condition	Drag polar
Cruise (M = 0.78, h = 40,000 ft w/ Gryphon)	$C_D = 0.0170 - 0.0012C_L + 0.0390C_L^2$
Cruise (M = 0.78, h = 40,000 ft clean)	$C_D = 0.0150 - 0.0011C_L + 0.0364C_L^2$
Loiter (M = 0.78, h = 44,000 ft w/ Gryphon)	$C_D = 0.0146 - 0.0016C_L + 0.0397C_L^2$
Loiter (M = 0.45, h = 10,000 ft clean)	$C_D = 0.0144 - 0.0052C_L + 0.0414C_L^2$

5.5 Flap Sizing

Flaps are sized using Class I methods.[2] The placement of the flaps followed two criteria:

1) The flaps must be outboard of the fuselages. The placement of the Gryphon makes it impossible to place flaps in the inboard section.
2) The flaps must be as far inboard as possible while conforming to condition 1.

This leads to the flap configuration shown in Figure 5.5.1.

The flaps chosen are 30% chord single slotted Fowler flaps. Important parameters are show in Table 5.5.1.

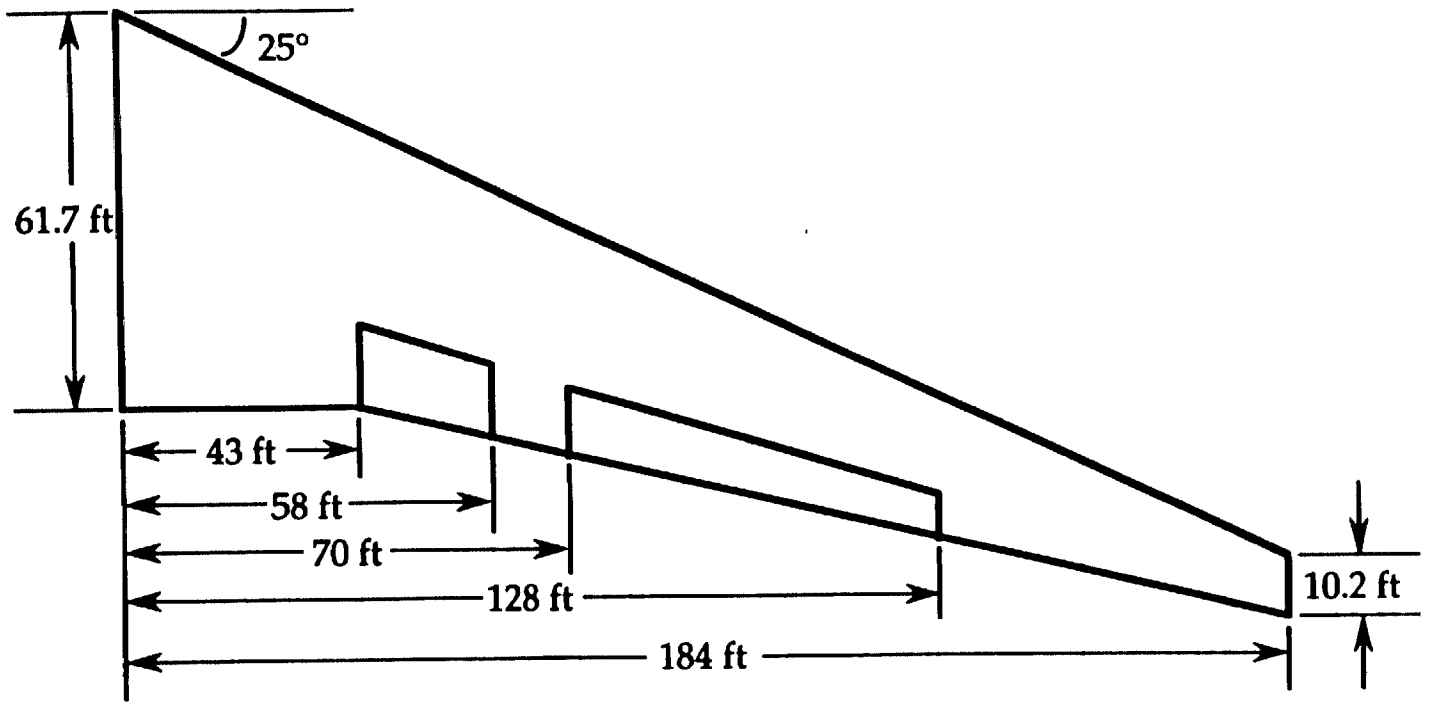

Figure 5.5.1 - Main Flap Configuration

Table 5.5.1 Important flap parameters

Sflaps	1346.4 ft^2
cf/c	0.3
δTO	20°
VTO	286 ft/s
WTO	1265000 lbf
δL	45°
Vstall	185 ft/s
Vapp	240.5 ft/s
WL	1265000 lbf
ΔCL_{max}	1.18

5.6 Thrust Required

To find the thrust required, the following formulas are employed:

$$C_L = \frac{W}{\frac{1}{2}\rho \cdot S \cdot V^2}$$

$$C_D = C_{do} + C_{di1} \cdot C_L + C_{di2} \cdot C_L{}^2$$

$$T_{req} = D = \frac{1}{2}\rho \cdot S \cdot V^2 \cdot C_D \qquad (5.6.1)$$

$$\therefore T_{req} = \frac{1}{2}\rho \cdot S \cdot V^2 \left[C_{do} + C_{di1} \frac{W}{\frac{1}{2}\rho \cdot S \cdot V^2} + C_{di2} \left[\frac{W}{\frac{1}{2}\rho \cdot S \cdot V^2} \right]^2 \right]$$

From the drag polar, weight, wing area, altitude, and velocity, thrust required is obtained.

5.7 Spanwise Lift Distribution

To analyze the high angle of attack characteristics of the Eclipse, it is necessary to know the angle of attack at which the wing will begin to stall. It is therefore assumed that the wing would begin to stall when the effective angle of attack of any section of the wing reached the maximum angle of attack for our airfoil. To find this effective angle of attack, Prandtl's lifting line theory was refined to account for wing sweep. The result is shown in Figure 5.7.1 which shows:

$$\frac{\alpha_o}{\alpha_a} = f(y) \qquad (5.7.1)$$

where α_o is the effective angle of attack and α_a is the absolute angle of attack:

$$\alpha_a=\alpha-\alpha_{ol} \qquad (5.7.2)$$

where α is the geometric angle of attack and α_{ol} is the zero-lift angle of attack.

This data and the wing planform leads directly to Figure 5.7.2, the spanwise lift distribution across the wing.

5.8 Performance Analysis

The purpose of this analysis is to predict the airplane position, weight and flight attitude, i.e. lift-to-drag ratio and angle of attack at any given moment of the mission from the beginning to the end of the flight. Calculations are based on structural weight, propulsion, and aerodynamic analysis results.[18] The complete method for performance calculations is found in Appendix C.

The most unfavorable scenario, an aborted launch mission with both loiters, is assumed.

With engine data from the manufacturer, it is possible to obtain the fuel flow, and hence the specific fuel consumption, for any power setting, at any altitude. The weight of fuel burned can then be determined, for a given interval of time or distance traveled.

To ensure reliable results, instead of using Class II methods, a more precise approach is applied: analyzing individual distance or time breakdown, depending on the mission portion being analyzed. By upgrading the airplane weight, drag polar values and flight altitude after each breakdown, it is possible to calculate the new thrust and lift necessary, and hence the new flight condition. The advantage of this method is that many of the values that had to be otherwise assumed in a Class II analysis (such as average specific fuel consumption, thrust required, time to accomplish each mission portion, required angle of attack, lift-to-drag ratio, altitude) can now be determined.

With a three-coordinate system (0x as the horizontal distance and 0z as the altitude), it is not only possible to compute the flight path velocity, but also the rate of climb and/or descent, during any mission portion.

Two other mission scenarios are studied as well. In the ferry mission, the space booster is unfueled and the extra payload capacity is used to carry fuel for the Eclipse. The maximum fuel load of 350,000 pounds is carried. Instead of a gradually climbing cruise, the cruise is assumed to be at a constant altitude of 35,000 feet. In the minimum fuel mission, there is no cruise segment.

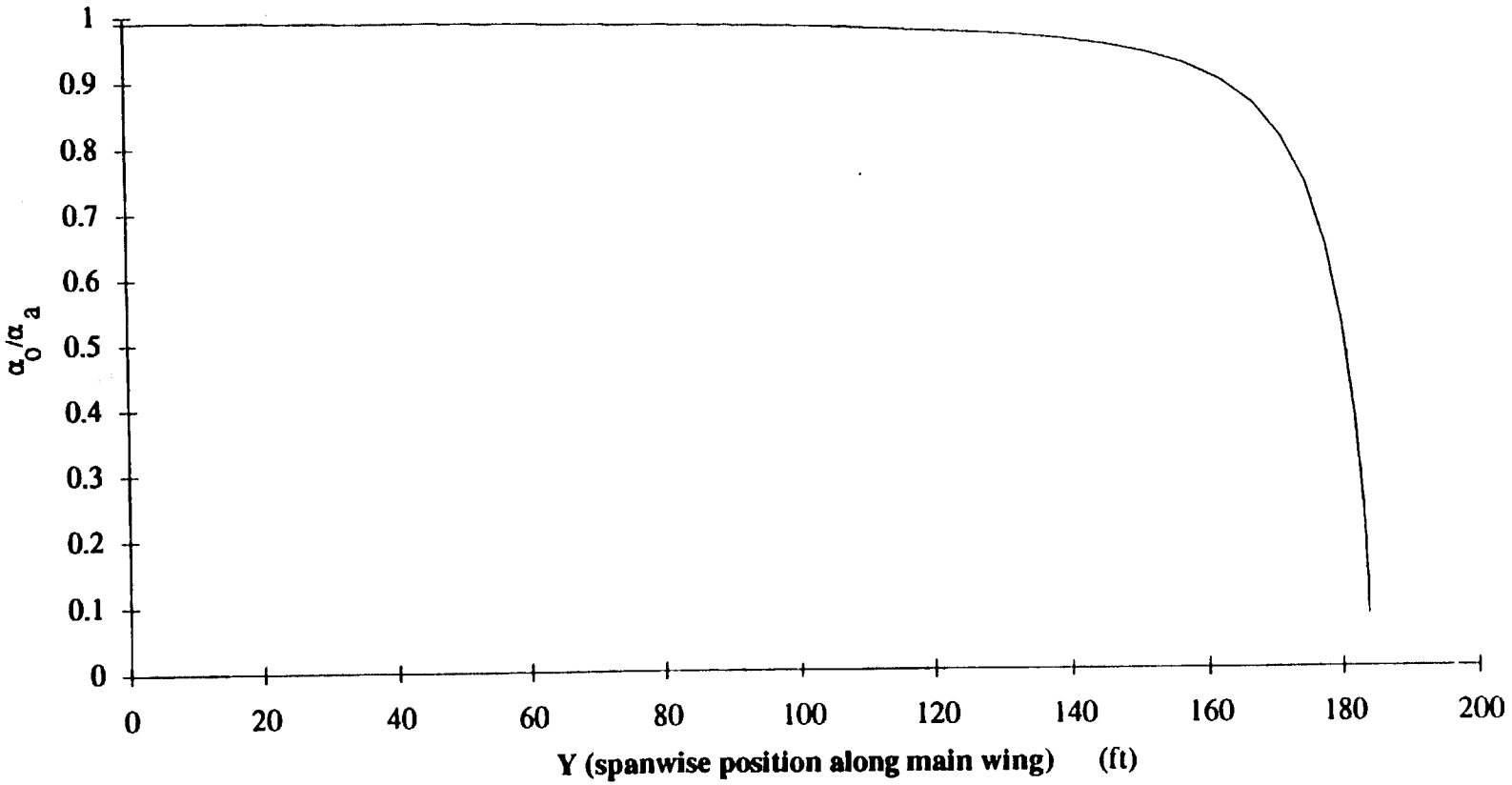

Figure 5.7.1 Spanwise effective angles of attack / absolute angles of attack at cruise

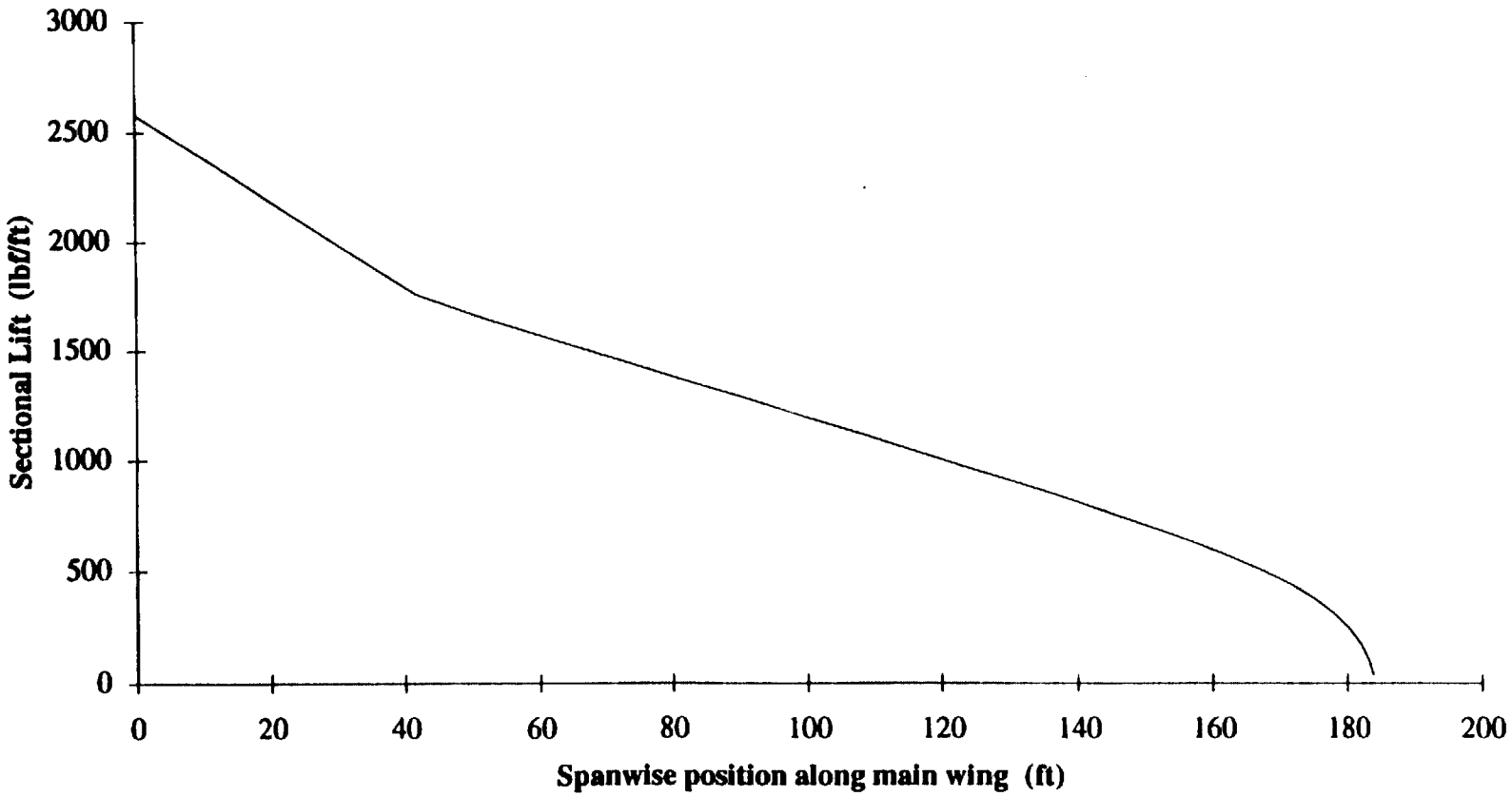

Figure 5.7.2 Lift distribution at cruise

Any range from the airfield comes from the distance covered during the climb. Since the Eclipse has a lower weight, a higher launch altitude is possible.

5.8.1 Analysis results

Important results of the performance analysis are contained in Table 5.8.1. The results of the minimum fuel and ferry mission performance analysis are found in Tables 5.8.2 and 5.8.3, respectively.

Table 5.8.1 Performance results

W_{ramp} (lbf)	1,264,000
W_{TO} (lbf)	1,227,000
W_{fuel} (lbf)	241,000
S_{TO} (ft)	4,300
S_L (ft)	3,400
$S_{Lemergency}$ (ft)	3,900
$V_{touch\ down}$ (ft/sec)	221
$V_{emergency\ touch\ down}$ (ft/sec)	241
h_{launch} (ft)	43,300
$n_{launch\ turn}$ (g)	2.2
$r_{launch\ turn}$ (ft)	9,200
$t_{mission}$	6 hr 55 min

Table 5.8.2 Minimum fuel mission performance

W_{to} (lbf)	1,143,000
W_{fuel} (lbf)	157,000
h_{launch} (ft)	45,800
$r_{launch\ turn}$ (ft)	11,500
$t_{mission}$	4 hr 11 min

Table 5.8.3 Ferry mission performance:

W_{to} (lbf)	1,135,000
W_p (lbf)	278,000
h_{cr} (ft)	35,000
Range (mi)	4,300
$t_{mission}$	11 hr 14 min

5.8.2 Comments

The take off field length is very short, in comparison to the average length (approximately 9,000 to 11,000 feet) for commercial and military carrier airplanes. This is because the Eclipse is overpowered at take off, due to the fact that the design requirement is to lift a 500,000 pound payload to above 40,000 feet. The total field length is based to clear a 35 foot high obstacle at the end of the flare arc, for both a soft or hard maneuver. Accelerating force takes into account thrust

and drag variations due to acceleration. The runway is also sized for an emergency landing at take off weight, with the brakes applied three seconds after touchdown.

The velocity during climb is constrained to 250 knots below 10,000 feet, and to constant indicated speed of 600 ft/sec until critical Mach number is reached (at 20,000 feet). From there on, climb is performed at constant Mach number. The distance covered during climb is subtracted from the cruise range. The service ceiling (rate of climb limit of 500 ft/min) at the end of climb almost coincides with the best cruise altitude at the beginning of the cruise portion.

The best cruise altitude is below the service ceiling. The airplane is still left with 541 to 587 ft/min of rate of climb for the outbound cruise and with 563 to 648 ft/min for the inbound cruise.

The initial loiter altitude is set to coincide with the final cruise altitude. The angle of attack that yields minimum thrust required is chosen.

In order to choose the best receding maneuver for the airplane after booster separation, various turn maneuvers were analyzed. The low wing loading of the airplane assists in being able to perform this maneuver. The best maneuver is a flat turn at critical Mach number at the maximum possible load factor, n = 2.17. This is neither the maximum turn rate nor the minimum turn diameter condition, both of which exceed other constraints. Since the airplane is so close to the service ceiling, a climbing maneuver is not a better choice. A descending maneuver was discounted since the drop time is short and a descent would slow the separation. Speed cannot be increased without a sizeable increase in drag due to wave drag effects associated with exceeding critical Mach number.

The ground run is short, even when assuming no thrust reverse and brakes applied 3 seconds after touchdown. This result is very sensitive to drag coefficient, which cannot be determined from the drag polar because of the presence of spoilers (used as speed brakes). Since there is no spoiler data to date for this project, a value was assumed for C_D. This is also the only value assumed in this analysis.

A 2,500 foot gain in launch altitude is associated with the minimum fuel mission. The manufacturer of the space booster may find this valuable in increasing the performance of the booster. The 4,300 mile range for the ferry mission is sufficient for a coast-to-coast cartage, carrying the booster from the assembly site to an alternate launch site.

6. STRUCTURES & WEIGHTS

Structures and weights work focuses on designing adequate structure to take the loads imposed on the aircraft and subsequently estimating the weight of the structure. In addition, center of gravity calculations are done. The structures and weights work is focused on four main issues:

- V-n diagram
- Component weights
- Longitudinal center of gravity
- Structural considerations

6.1 V-n Diagram

The first step in structural calculations is to determine the maximum forces which will be acting on the airplane in flight. This is done by creating a gust and a maneuver V-n diagram.[5] The two V-n diagrams are presented in Figures 6.1.1 and 6.1.2. Table 6.1.1 lists the important values needed for V-n diagram construction and the important results, V_D and n_{ult}.

Table 6.1.1 V-n diagram parameters

$C_{L\ max}$	1.46
V_D (keas)	300
n_{lim} (g)	2.5
n_{ult} (g)	3.75

6.2 Estimation of Eclipse Component Weights

This section summarizes the calculation of estimated component weights of the Eclipse. These estimates are based upon: semi-empirical, statistical methods, manufacturer's data, and analytical methods. The components which will be discussed in this section are broken down as follows:

- Fuselages
- Horizontal tail
- Vertical tails
- Crew and mission specific equipment
- Gryphon
- Engines, nacelles, and pylons
- Forward landing gear
- Main landing gear

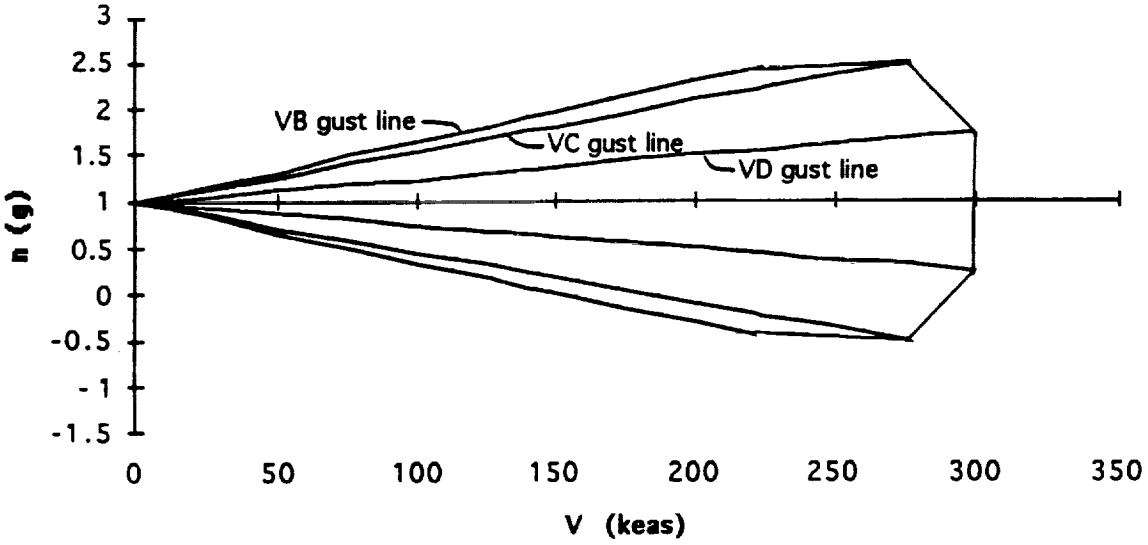

Fig. 6.1.1 V-n gust diagram

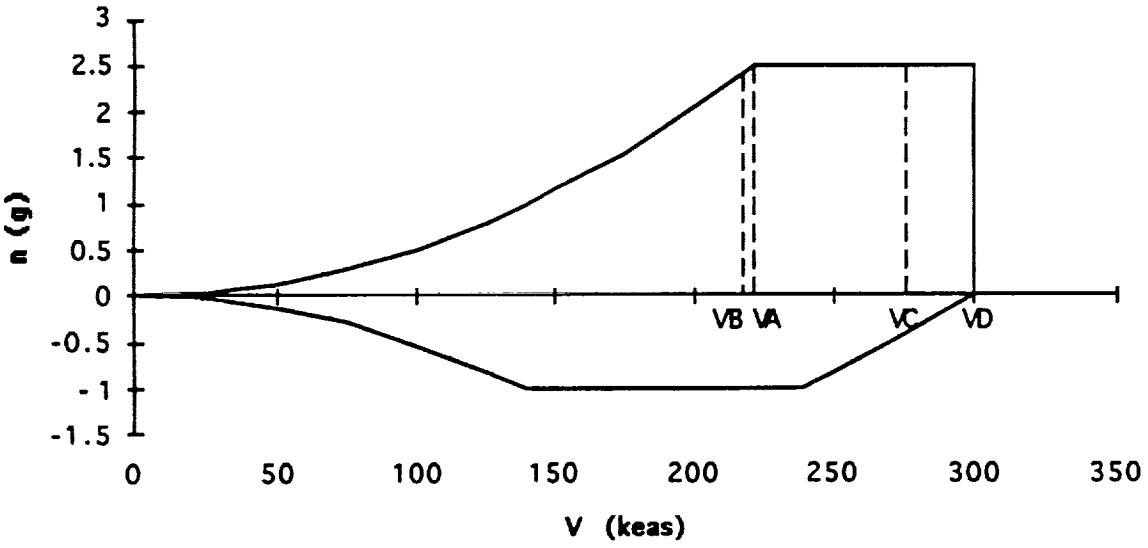

Fig. 6.1.2 V-n maneuver diagram

- Fixed equipment
- Mission fuel
- Main wing

The fuselage weight is calculated using semi-empirical methods consisting of Raymer's method for cargo/transport weights,[11] and Torenbeek's method for transport airplanes.[5] The results for each of these methods is calibrated for an MD-80 fuselage, which is slightly smaller in diameter, but the same overall length. This analysis yields an average weight for two fuselages of 85,200 pounds.

The horizontal and vertical tail weights are each evaluated using three different semi-empirical methods. The results of these three methods are averaged and then calibrated using the empennage weight of a C-5 Galaxy. The six equations used are:

- General Dynamics (GD) method for commercial transport airplanes (horizontal tail)[5]
- Torenbeek method for transport airplanes (horizontal tail)[5]
- Raymer method for cargo/transport weights (horizontal tail)[11]
- GD method for commercial transport airplanes (vertical tail)[5]
- Torenbeek method for transport airplanes (vertical tail)[5]
- Raymer method for cargo/transport weights (vertical tail)[11]

The weights for the horizontal tail are averaged, as are those for the two vertical tails. The combined average empennage weight is then calibrated using a correction factor of 0.85, derived from the empennage weight of the Lockheed C-5A. This analysis yields a horizontal tail weight of 28,100 pounds and a weight for two vertical tails of 14,800 pounds.

A 2,000 pound allowance is made for the three crew members and any Gryphon specific equipment which must be placed in the cockpit of the Eclipse.

The weight of the Gryphon is set at the final design weight of 479,000 pounds.[15]

The combined weight of engines and nacelles is provided by General Electric Aircraft Engines and set at 22,000 pounds each.[16] An additional 1,000 pounds is allowed for the weight of each engine pylon. This yields a total weight for six engines, nacelles, and pylons of 138,000 pounds.

A conservative estimate for landing gear weight is made using Torenbeek's method for Commercial Transport Airplanes.[5] This estimate is based on a gross take off weight of

1,460,000 pounds and was not iterated as take off weight decreased. The result is calibrated using the landing gear weight of the Lockheed C-5A. This method yields a weight for the nose gear of 7,100 pounds and a weight for the main gear of 64,200 pounds.

As with landing gear, fixed equipment weights are based upon a gross take off weight of 1,460,000 pounds and were not updated. The results are slightly conservative and are estimated in the following manner. A set of fixed equipment weights for other large aircraft is averaged with the results predicted by GD and Torenbeek methods.[5] Results are listed in Table 6.2.1.

Table 6.2.1 Fixed equipment weights (all weights in pounds)

Component	Similar aircraft	GD	Torenbeek	Average
Flight controls	13,629	15,982	8,028	12,500
Hydraulics and pneumatics	8,150	11,240	11,240	10,000
Electrical systems	6,534	5,403	N/A	6,000
Avionics, electronics, and instrumentation	10,679	17,563	6,956	11,000
Auxiliary power	2,038	5,620	5,620	4,000
Oxygen	562	19	50	100
Air conditioning, pressurization	7,236	216	1,391	1,500
Gryphon specific miscellaneous systems	N/A	N/A	N/A	5,000
Total fixed equipment				50,100

The mission fuel requirement was developed using analytical methods based upon the following parameters:

- Mission profile
- Aerodynamic characteristics of the Eclipse and Gryphon
- Weight of the Eclipse and Gryphon
- Engine performance data provided by General Electric Aircraft Engines

This analysis yields a total mission fuel weight (excluding ramp fuel) of 207,000 pounds and a total fuel weight of 241,000 pounds.

Semi-empirical methods for wing weight estimation yield a weight of 252,000 pounds.[5,11] This is twenty percent of the take off weight of the airplane. No other airplane has a wing group weight percentage which is so large. Since the semi-empirical method seems to be high in comparison with existing aircraft, an analytical method is employed. The configuration of the airplane with its high aspect ratio wing, twin fuselages, and many distributed and point loads providing bending relief for the wing is well suited to an analytical solution. The method used is an analytic method for wing group weight determination for twin fuselage aircraft.[12] The method predicts the structural weight necessary to resist shear and bending moments along the wing based upon all distributed and point loads placed on the wing. Semi-empirical methods

were then used to estimate the weight of non-structural components of the wing, i.e. leading edge, flaps, ailerons, and spoilers. A separate analysis was made using this model for a single fuselage and center mounted payload. This value is then used to calibrate the wing group weight percentage with that of existing aircraft. The analysis yielded a wing group weight of 151,900 pounds which is twelve percent of the airplane take off weight. This is a much more reasonable solution. A by-product of this is an extra savings of 5000 pounds, or 0.4 percent of airplane take off weight, due to the extra bending relief provided by the two fuselages. The calculations are detailed in Appendix E.

6.3 Determination of the Longitudinal Center of Gravity of the Eclipse

The longitudinal center of gravity is computed as follows.

$$x_{cg} = \frac{\sum w_i x_{cg_i}}{\sum w_i} \qquad (6.3.1)$$

where the w_i are the individual component weights determined in the preceding sections and the x_{cg_i} are the individual component centers of gravity relative to a common reference datum. All x_{cg_i} are measured relative to a reference datum 50 feet forward of the forward most part of the wing.

The fuselage center of gravity is estimated at 40% of the length of the fuselage. This places its center of gravity at 107.33 feet aft of the reference datum.

The center of gravity of the horizontal tail is assumed at 42% of chord at 38% of semi-span. This places the horizontal tail center of gravity at 214.03 feet aft of the datum.

The center of gravity of the vertical tails is assumed at 42% of chord at 38% of span. This places the vertical tail center of gravity at 202.05 feet aft of the datum.

Crew and equipment are housed within the aircraft cockpit. Their center of gravity is therefore 45 feet aft of the reference datum.

The Gryphon is located at the center of gravity of the aircraft so as to minimize adverse changes in aircraft handling qualities due to sudden center of gravity changes at launch. This is fixed after the airplane is balanced at 103.43 feet aft of the reference datum.

The engines are located placed on the wing so as to minimize interference with the wing and each other. This involved placing engines at 64, 92, and 120 feet of semi-span. Based upon pylon design, this yields a center of gravity for each engine pair at 72.84, 83.90, and 94.96 feet aft of the reference datum.

The nose gear center of gravity is placed 45 feet aft of the reference datum. This is the correct position for the gear in the down position. However, after studying the change in center of gravity due to landing gear retraction, it was found that the landing gear retracting causes a center of gravity shift of slightly over 1/2 inch. This is considered negligible.

The center of gravity of the main gear is placed seven feet aft of the aircraft center of gravity. This location is at 110.43 feet aft of the reference datum. Due to the retraction kinematics of the main gear, there is no center of gravity shift due to main gear retraction.

Based on preliminary systems plans, and the goal of placing most of the systems within the aircraft wing, the fixed equipment center of gravity is placed 80 feet aft of the reference datum.

The center of gravity of the mission fuel is placed at the aircraft center of gravity so as to eliminate changes in aircraft handling qualities over the course of the mission. As with the payload, this is located at 103.43 feet aft of the reference datum.

The center of gravity of the main wing is estimated to be at 40% of chord at 40% of semi-span from centerline. This yields a center of gravity at 97.17 feet aft of the reference datum.

6.4 Summary of Weight and Balance Calculations

Table 6.4.1 is a summary of the component weights and their centers of gravity. It also includes the total airplane weight and center of gravity. Figure 6.4.1 shows the center of gravity locations used in the longitudinal center of gravity analysis.

6.5 Structural Considerations

Several structural issues were considered on a qualitative level in the design. The fuselage has an oblong shape so that the landing gear can be fully retracted within the fuselage and still allow for a large closed section. This large closed section significantly stiffens the structure. There is a pressurized compartment in the left fuselage for the crew. This pressurized section is a cylinder

Reference datum

Numbers correspond to Table 6.4.1

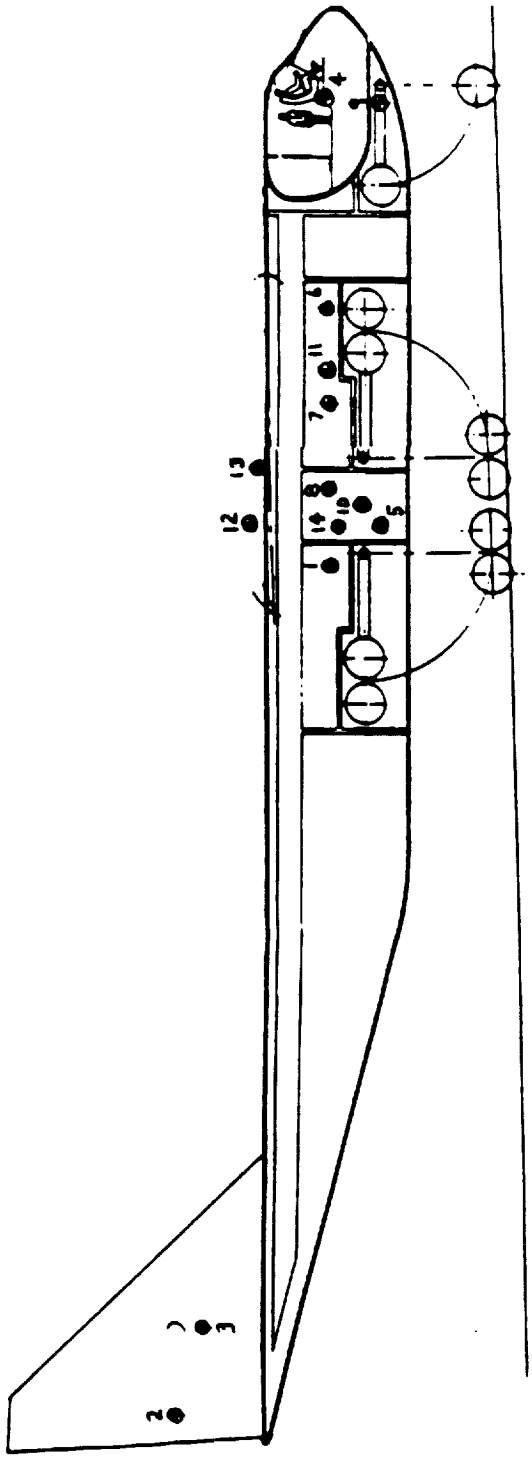

Fig. 6.4.1 Longitudinal center of gravity

which fits inside the exterior contour of the airplane. A cylinder was chosen to minimize the possibility of fatigue due to pressure cycling. The wing has four main spars located at 17, 38 (maximum airfoil thickness), 54, and 70 percent of the chord. In addition, between the fuselages a fifth spar runs parallel to and 12.5 feet in front of the trailing edge of the wing. This spar aids in the distribution of the loads from the space booster. Two reinforced ribs are used for the mounting system for the booster. These ribs start at the first spar and extend out the back of the wing to provide attachment points for the payload. The twin fuselage design with a horizontal tail spanning the two fuselages has an added advantage of creating a large shear cell. This should significantly lower the structure needed to carry the loads. This would be seen in a weight savings over a comparable single fuselage design. The two forward horizontal tail spars intersect the two rear vertical tail spars. This minimizes the extra structure needed to carry the tail loads.

Table 6.4.1 Weight and balance summary

No.	Component	Weight (lbf)	Center of gravity (ft)
1	Fuselages	85,200	107.33
2	Horizontal tail	28,100	214.03
3	Vertical tails	14,800	202.05
4	Crew and mission specific equipment	2,000	45.00
5	Gryphon	479,000	103.43
	Engines, nacelles, and pylons		
6	#3 & #4	46,000	72.84
7	#2 & #5	46,000	83.90
8	#1 & #6	46,000	94.96
9	Forward landing gear	7,100	45.00
10	Main landing gear	64,200	110.43
11	Fixed equipment	50,100	80.00
12	Mission fuel (excluding ramp fuel)	207,000	103.43
13	Main wing	151,900	97.17
14	Take off weight	1,227,400	103.43

7. STABILITY & CONTROL

The central question of aircraft stability is whether an equilibrium of moment and forces can be maintained at a given flight configuration. This requirement of flight equilibrium implies that there must exist a configuration orientation corresponding to each allowable flight condition, such that a disturbance would result in a tendency to return to steady state, followed by the eventual recovery of the steady state. Examples of internally generated disturbances include changes in control surface deflection, changes in center of gravity location, and changes in airplane configuration. Some examples of externally generated disturbances are turbulence and changes in altitude and temperature. Both the lateral and longitudinal stability and control are evaluated.

For internally and externally generated disturbances, the airplane must be able to operate such that a pilot can fly a mission and maneuver the airplane without undue effort on his part, with or without assistance from an automatic control system. Again the airplane must be designed so that it has a build-in tendency to diminish the motions resulting from internal of external deviations. Civilian and military operators translate this into detailed specifications for ride quality and upset recovery quality.

7.1 Horizontal Tail Sizing and Longitudinal Stability

The final result is a tail of 3700 ft^2, with planform as shown in Figure 5.3.3. Discussion of the elevators shown in Figure 5.3.3 can be found in section 7.2.

The horizontal tail sizing is done on the basis of three criteria:

- Take off rotation
- Trim at cruise
- Static margin at cruise

7.1.1 Horizontal tail sizing due to take off rotation

Based on the seven forces and two moments acting on the airplane at take off and shown in Figure 7.1.1, the take off rotation is analyzed.

To find the needed elevator deflection/size and tail size, the moments about the median point between where the main gear struts meet the runway are analyzed. At the present time, the change in moment due to elevators is not accounted for. This moment should be small, and since the

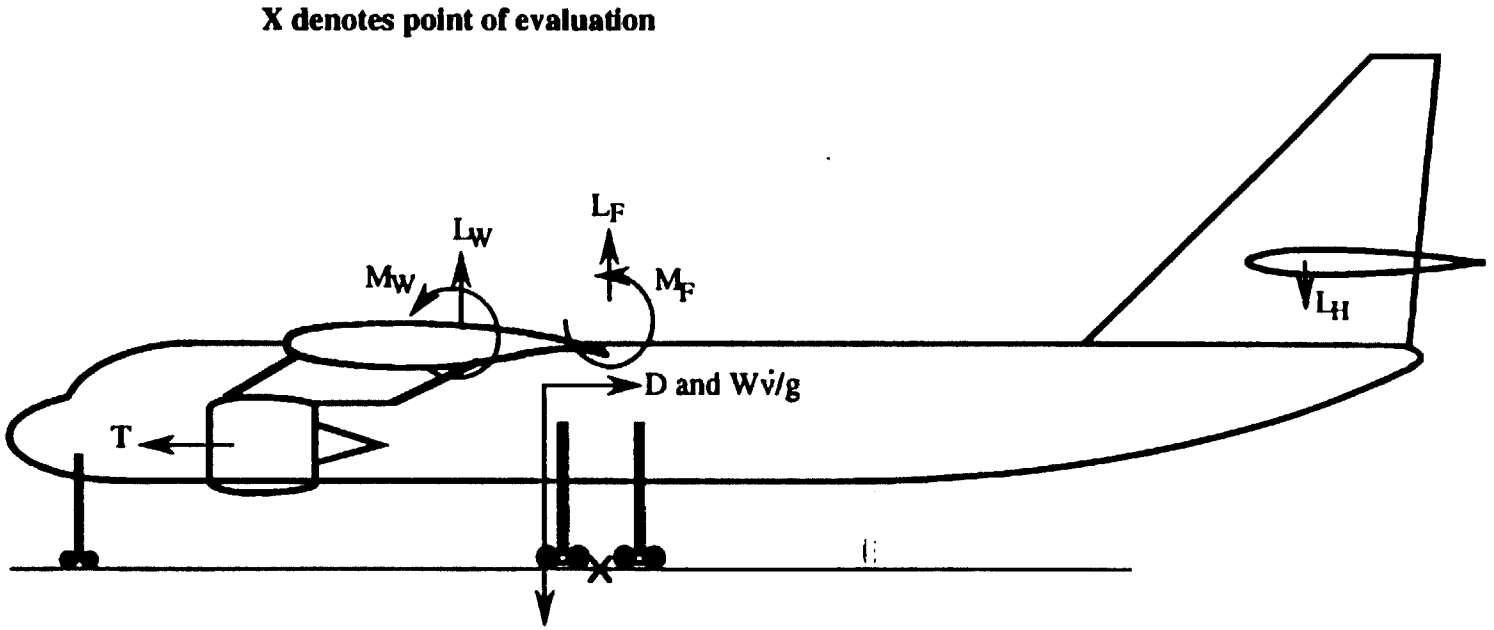

Figure 7.1.1 - Take off Rotation Analysis

elevators are deflected upward, this estimate is overly conservative. While this requirement does size the elevators, it does not size the tails.

$$M = 0 = L\left(x_{ref} - x_{ac_w}\right) + M_w + L_F\left(x_{ref} - x_F\right) + M_F$$
$$+W\left(x_{ref} - x_{cg}\right) + T\left(z_{ref} - z_T\right) + L_h\left(x_{ref} - x_{ac_h}\right) \qquad (7.1.1)$$
$$+M_h + D\left(z_{ref} - z_{cg}\right) + \frac{W}{g}\dot{V}\left(z_{ref} - z_{cg}\right) + M_e$$

where:

M = total airplane moment [ft•lbf]
M_e = moment due to elevator deflection [ft•lbf]
M_F = fuselage moment [ft•lbf]
M_h = moment due to horizontal tail [ft•lbf]
M_w = wing moment [ft•lbf]
D = airplane drag (acting at center of gravity) [lbf]
L = lift due to the wing [lbf]
L_F = fuselage lift [lbf]
L_h = horizontal tail lift [lbf]
T = airplane thrust [lbf]
W = airplane weight [lbf]
x_{ac_h} = longitudinal horizontal tail center of gravity [ft]
x_{ac_w} = longitudinal wing aerodynamic center [ft]
x_{cg} = longitudinal airplane center of gravity [ft]
x_F = longitudinal location of equivalent fuselage lift [ft]
x_{ref} = longitudinal landing gear rotation point [ft]
z_{cg} = center of gravity height [ft]
z_{ref} = landing gear rotation height [ft]
z_T = thrust height [ft]
g = gravitational acceleration [ft/sec^2]
$\dot{V}$ = instantaneous acceleration [ft/sec^2]

7.1.2 Horizontal tail sizing due to trim at cruise

This is done in the same manner as take off rotation except that the moments are summed about the center of gravity. It is not the driving factor.

$$M = 0 = L\left(x_{cg} - x_{ac_w}\right) + M_w + T\left(z_{cg} - z_T\right) + L_h\left(x_{cg} - x_{ac_h}\right) + M_h + M_e \qquad (7.1.2)$$

7.1.3 Tail sizing due to static margin at cruise

This is the criteria that has sized the horizontal tail. Use of a cruciform tail has significantly decreased the downwash. The tail's moment arm is very low, so this savings in downwash is crucial. The lift curves and downwash values are obtained as explained in section 5.2. The aerodynamic center is then found by semi-empirical methods:[6]

$$\bar{x}_{ac_A} = \frac{C_{L_{\alpha_{WB}}} \bar{x}_{ac_{WB}} + C_{L_{\alpha_H}} \eta_H \frac{S_H}{S}\left(1 - \left[\frac{d\varepsilon}{d\alpha}\right]_H\right)\bar{x}_{ac_h}}{C_{L_{\alpha_A}}} \qquad (7.1.3)$$

where:

$\bar{x}_{ac_A}$ = location of airplane aerodynamic center

$\bar{x}_{ac_h}$ = location of horizontal tail aerodynamic center

$\bar{x}_{ac_{WB}}$ = location of wing/body aerodynamic center

$C_{L\alpha\,A}$ = airplane lift curve slope [rad^{-1}]

$C_{L\alpha\,h}$ = horizontal tail lift curve slope [rad^{-1}]

$C_{L\alpha\,WB}$ = wing/body lift curve slope [rad^{-1}]

η_h = horizontal tail efficiency

S = wing reference area [ft^2]

S_h = horizontal tail reference area[ft^2]

$\left[\frac{d\varepsilon}{d\alpha}\right]_h$ = horizontal tail downwash

To properly size the horizontal tail, an X-plot was employed. The X-plot shows the variation of center of gravity and aerodynamic center location as a result of varying tail area. From this plot, the tail area needed for a certain static margin can easily be deduced. The aerodynamic center varies as in equation 7.1.3. The center of gravity shifts to wherever 42% of chord is on a given geometry. The X-Plot is shown in Figure 7.1.2. A static margin of 5% was chosen for the final horizontal tail sizing. A value lower than the traditional 10% was chosen because the tail was unreasonably large to meet the 10% requirement. A 5% static margin will require a stability augmentation system to ensure safe operations.

7.2 Flight Control Surface Sizing

The elevators are 30% chord, 60% span, plain flaps with an area of 670 ft^2 that deflect -2.35° on take off and 1.7° during cruise. These elevators can be seen in Figure 5.3.3. The central elevator

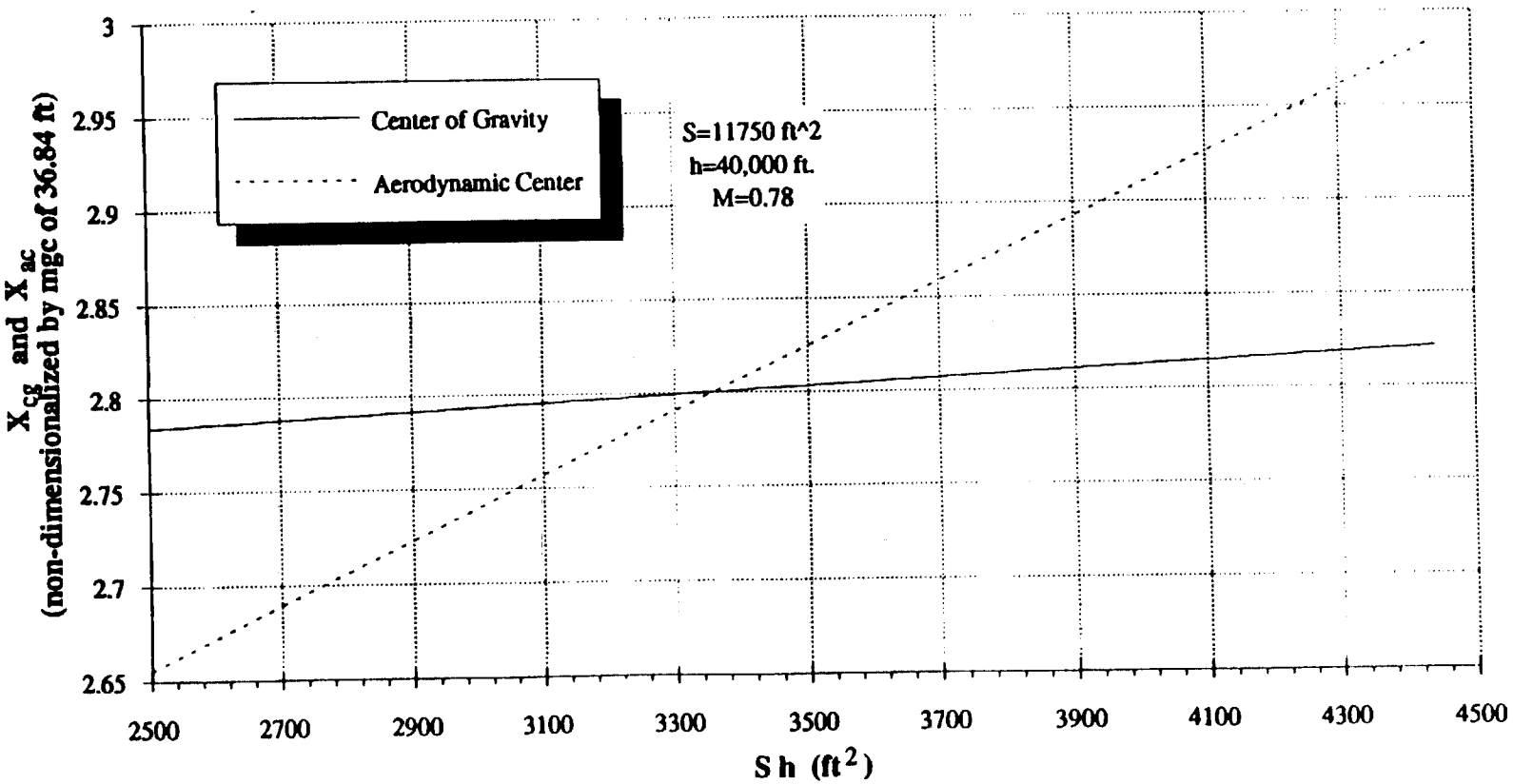

Figure 7.1.2 - X-Plot at Cruise Conditions

piece is also used for the stability augmentation system. The sizing factor for the elevators is take off rotation, as explained in section 7.1.1.

The sizing of the ailerons is closely related to the overall directional and lateral control of the airplane. With various airplane dimension and performance parameter, the ailerons are sized from the steady flight equations of motion and the directional and lateral equations of motion for the outboard engine-out flight condition. These equations are listed in the stability and control section of this report.[6,7]

The two coefficients due to aileron deflection which contribute to the overall stability are the rolling moment coefficient, Cl_{δ_a}, and the yawing moment coefficient, Cn_{δ_a}. The size force coefficient, Cy_{δ_a}, and several other partial contributions of control derivatives are neglected because their values become insignificant when normalized with respect to the reference wing area. Furthermore, the perturbed forces and moments induced during flight are also ignored as they have a relatively small effect on the overall flight characteristics due to the size of the Eclipse. Table 7.2.1 lists the final attributes of the ailerons.

Table 7.2.1 Aileron characteristics

Total area	500 ft^2
Inboard ailerons	
Semi–span ratio (in/out)	.34/.39
Outboard ailerons	
Semi-span ratio (in/out)	.75/.95

7.3 Lateral and Directional Stability Analysis

7.3.1 Methodology

The lateral and directional stability analysis is carried out for the worst case scenario. In this case, the one engine-out condition with an outboard engine inoperable at take off rotation is the worst. This is the worst because it imposes the largest moment on the aircraft. It should be noted here that a two engine-out during take off condition was also analyzed. The vertical tail size, which is dependent on wing area, is very sensitive to the bank angle allowed. Since the bank angle during take off is restricted to 5° as specified by FAR 25, for a two engine-out take off condition the Eclipse would require at least 3700 ft^2 of vertical tail area or a much higher rotation speed. An engineering decision is made to forego meeting the two engine-out criteria to save the weight associated with larger tails. This should not be a problem since the airplane will be used infrequently and well maintained, lowering the odds of a two engine-out situation.

During the outboard engine-out take off flight condition, the unbalanced forces induce a sideslip angle, β, which gives rise to a rolling moment, L_T, a side force, F_Y, and a yawing moment, N_T.

The steady state rolling moment, side force, and yawing moment depend on:

- Mach number and Reynold's number
- Angle of attack
- Angle of sideslip
- Dynamic pressure
- Control deflections of aileron, spoiler, rudder or other lateral-directional control surfaces

The effect of Mach number and angle of attack are accounted for in an indirect way, by evaluating the derivative at the required velocity during take off rotation (V_{mc} = 231 ft/sec) and the angle of attack at take off (9°). The Reynold's number effects are usually small and are therefore neglected in this analysis. The dynamic pressure is also accounted for in an indirect way, by multiplying a non-dimensional coefficient by the dynamic pressure and the appropriate geometric parameters.

Typically, the minimum control speed (V_{mc}) is calculated as a percentage above the stall speed. For this airplane, this resulted in a high rotation speed and a resultant large vertical tail area. Therefore, V_{mc} is assumed at a value above the stall speed where the tails are a reasonable size. The error in these calculations makes this a reasonable assumption.

The next three sections summarizes the results of the total airplane rolling moment, side-force, and yawing moment analysis.

7.3.2 Total airplane rolling moment

Airplane rolling moment is nondimensionalized as:

$$L_T = C_l \cdot q \cdot S \cdot b \qquad (7.3.1)$$

where C_l is the total airplane rolling moment coefficient, q is the dynamic pressure, S is the wing reference area, and b is the wing span. The relationship between the total rolling moment coefficient and the functional dependence among the side slip angle and the control deflections is usually expressed as:

$$C_l = C_{l_\beta}\beta + C_{l_{\delta A}}\delta A + C_{l_{\delta R}}\delta R \qquad (7.3.2)$$

where:

C_{l_β} = change in rolling moment coefficient due to a unit side slip angle

$C_{l_{\delta A}}$ = change in rolling moment coefficient due to a unit change in lateral control (aileron) deflection

$C_{l_{\delta R}}$ = change in rolling moment coefficient due to a unit change in directional control (rudder) deflection

The derivative are evaluated at constant Mach number and constant angle of attack. Table 7.3.1 summarizes the results of the rolling moment coefficients analysis.

Table 7.3.1 Results of the rolling moment coefficient calculation

C_{l_β}	-0.1297 rad^{-1}
$C_{l_{\delta A}}$	0.1431 rad^{-1}
$C_{l_{\delta R}}$	0.0073 rad^{-1}

7.3.3 Total airplane side-force

Airplane side force is nondimensionalized as:

$$FY = CY \cdot q \cdot S \qquad (7.3.3)$$

where CY is the total airplane side-force coefficient.

The functional dependence of the side-force coefficient CY on the sideslip angle, β, rudder deflection angle, δR, and aileron deflection angle, δA, is usually expressed as:

$$C_Y = C_{Y_\beta}\beta + C_{Y_{\delta R}}\delta R + C_{Y_{\delta A}}\delta A \qquad (7.3.4)$$

where:

C_{Y_β} = change side-force coefficient due to a unit side slip angle

$C_{Y_{\delta A}}$ = change in side-force coefficient due to a unit change in lateral control (aileron) deflection

$C_{Y_{\delta R}}$ = change in side-force coefficient due to a unit change in directional control (rudder) deflection

Again, the derivatives are evaluated at constant Mach number and constant angle of attack. Table 7.3.2 summarizes the results of the side-force coefficients analysis.

Table 7.3.2 Results of the side-force coefficient calculation

C_{Y_β}	-0.7794 rad^{-1}
$C_{Y_{\delta A}}$	0 rad^{-1}
$C_{Y_{\delta R}}$	0.1839 rad^{-1}

7.3.4 Total airplane yawing moment

Airplane Yawing moment is nondimensionalized as:

$$N_T = C_N \cdot q \cdot S \cdot b \tag{7.3.5}$$

where C_N is the total airplane yawing moment coefficient. The relationship between the total yawing moment coefficient and the functional dependence among the side slip angle and the control deflections is usually expressed as:

$$C_n = C_{n_\beta}\beta + C_{n_{\delta A}}\delta A + C_{n_{\delta R}}\delta R \tag{7.3.6}$$

where:

C_{n_β} = change in yawing moment coefficient due to a unit sideslip angle

$C_{n_{\delta A}}$ = change in yawing moment coefficient due to a unit change in lateral control (aileron) deflection

$C_{n_{\delta R}}$ = change in yawing moment coefficient due to a unit change in directional control (rudder) deflection

The derivative are evaluated at constant Mach number and constant angle of attack. Table 7.3.3 summarizes the results of the yawing moment coefficients analysis.

Table 7.3.3 Results of the yawing moment coefficient calculation

C_{n_β}	0.1556 rad^{-1}
$C_{n_{\delta A}}$	-0.0275 rad^{-1}
$C_{n_{\delta R}}$	-0.0474 rad^{-1}

7.3.5 Configuration analysis

With the force and control derivative coefficients determined from the previous three sections, the stable airplane configuration for the outboard engine out during take off can be determined from the following stability matrix:

$$\begin{Bmatrix} F_Y \\ L_T \\ N_T \end{Bmatrix} = \begin{bmatrix} C_{Y_\beta} qS & C_{Y_{\delta A}} qS & C_{Y_{\delta R}} qS \\ C_{l_\beta} qSb & C_{l_{\delta A}} qSb & C_{l_{\delta R}} qSb \\ C_{n_\beta} qSb & C_{n_{\delta A}} qSb & C_{n_{\delta R}} qSb \end{bmatrix} \begin{Bmatrix} \beta \\ \delta A \\ \delta R \end{Bmatrix} + \frac{W \cdot \sin\phi}{q \cdot S} \tag{7.3.7}$$

With the vertical tail parameters listed in table 7.3.4, the stability matrix (equation 7.3.7) is solved with the following results.

β (Sideslip angle) = 5.0°

δA (Aileron deflection) = 7.4°

δR (Rudder deflection) = 25.4°

ϕ (Banking Angle) = 4.0°

Table 7.3.4 Vertical tail parameters

S_V (total) (ft^2)	1900
S_V (individual) (ft^2)	950
A_V	1.5
λ_V	0.2
b_V (ft)	37.75
Λ_V (°)	45
C_{r_V} (ft)	41.94
C_{t_V} (ft)	8.388
V_{mc} (ft/sec)	231

All the parameters are within the regulatory limits as specified in FAR 25. Force and moments used for this calculation are listed in Table 7.3.5.

Table 7.3.5 Force and moments for one engine-out during take off

F_y	5401 lbf
L_t	-1377000 ft•lbf
N_t	-10758000 ft•lbf

8. SYSTEMS

Six of the main systems on the Eclipse were designed. Also, some issues related to crew safety and comfort were considered. The six systems are:

- Payload integration
- Landing gear
- Hydraulic system
- Electrical system
- Flight control system
- Fuel system

8.1 Payload Integration

This section details the airplane/space booster interface for one payload which can be carried by the Eclipse, the Gryphon which was designed by the University of Michigan Aerospace System Design class.[15] In the same manner that booster stages must be interconnected in order for the system to function, the Gryphon must be physically and functionally attached to the Eclipse in order to take advantage of the air-launched system. There are several area which are important to the interface from the airplane standpoint, including:

- Physical attachment from the Eclipse to the Gryphon/drop mechanism
- Power connections to the Eclipse in the pre-drop phase
- Placement of support systems on the Eclipse

Details of the mating process can be found in the Gryphon report. A general mission scenario begins the moment any of the base components leave their manufacturing center and become the property of the launch company. Each component is received and constructed into a complete launch booster, and then mated with the payload. Then, as the launch window approaches the Gryphon is rolled out to the Eclipse and connected and fueled. The Eclipse either uses its prime facility as its base of operations (for Geosynchronous orbits), or flies to the secondary launch facility (for Polar orbits). When the launch criteria have been met, a technician on the Eclipse handles the release/launch phase.

8.1.1 Aircraft/booster interface

Since the Gryphon is an air launched space booster, the interface attachments between the launch aircraft and booster are of vital importance. The Eclipse was designed solely for launch

of the Gryphon space booster. In fact, the Eclipse could be considered the Gryphon's first stage. There were two designs considered for the Eclipse/Gryphon interface:

- Space Shuttle/Boeing 747-100 attachment
- Orbital Sciences Corporation's Pegasus/Lockheed L-1011 interface

These designs were analyzed and compared to see which would best fit the requirements for the Gryphon/Eclipse attachment. Some of the design parameters considered were:

- Pin layout
- Release mechanism geometry
- Materials
- Drop transient
- G-force loads

Both designs were considered based off of these criteria. It was determined that a design similar to OSC's Pegasus/Lockheed L-1011 interface would be used. This design was chosen because it was similar to this project, proven to work, and easier to analyze. However, the Shuttle attachment design was considered throughout the analysis stage. The following sections give overviews of the specifications of the Gryphon/Eclipse interface attachments. A final section will review the specifics of the overall design, show the layout of the components and costs.

8.1.1.1 Pin layout

In order to fully analyze the different possibilities, a finite element model was constructed on the CAD program I-DEAS. It was determined to run different configurations using finite element models in order to find the best pin layout on the Gryphon. The parameters determining the best pin configuration were:

- Distribution of forces on pins
- Stability of configuration
- Structural dynamics

Having approximately the same force on each pin would mean only one type of hook and pin combination had to be designed. This would greatly reduce design work and manufacturing costs. Having the same forces on each hook/pin combination would also make the system easier to manufacture. A symmetric system would also help in design and analysis.

First, it was determined to align the center of gravity of the Eclipse and the Gryphon as best as possible. This would ensure some stability and displace the loading on the interface mechanism evenly. Second, the farther apart the pins on the Gryphon, the more stable it would be when hanging off the Eclipse. This is because the moments created by the hook/pin mechanism would be greater the farther they were from the center of gravity. Therefore, it was determined that there would be two pins located as far back as possible. Finally, the Gryphon, unlike the Pegasus, did not have a wing in which the pins could be placed. The pins would have to be placed externally since there was no space to place any type of external structure within the Gryphon. Also, they would have to be placed where extra internal rings could fit or at the booster interstages.

8.1.1.2 Release mechanism geometry

The geometry of the release mechanism is based on the Pegasus/Lockheed L-1011 release mechanism. The release mechanism is very flexible in its operation. The moment arms and control rods are similar to the one used on the Pegasus/Lockheed L-1011 interface except that they are notably larger. This, of course, is due to the larger weight of the Gryphon requires the mechanical linkages to be proportionally large to prevent buckling and beam bending. This system, as seen from the Figures 8.1.1 and 8.1.2, will release two pins at the same time. That is, the lever arm rotates the connecting rods evenly. The hook on the right is released when the connecting rod is pulled up by the lever arm. The hook on the left is released when the connecting rod is pulled down by the lever arm. This system can release four hooks simultaneously if two more are place on the main axle of the lever arm.

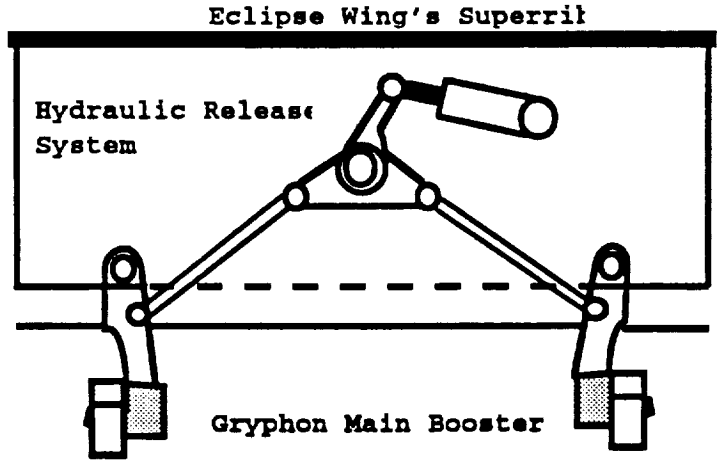

Fig. 8.1.1 Side view layout of release mechanism geometry (before release)

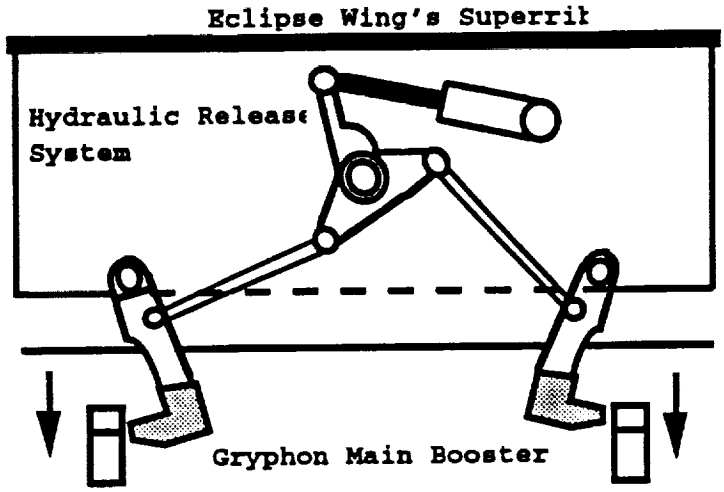

Fig. 8.1.2 Side view layout of release mechanism geometry (after release)

8.1.1.3 Materials

The material used for the structural members throughout the interface system is a heat treated, quenched and tempered, steel alloy ASTM-A242. The specifics of this material are summarized in Table 8.1.1. This alloy was chosen due to the fact that it is the strongest construction material in yield shear strength.

Table 8.1.1 Steel alloy ASTM-A242 properties

Specific weight (psi)	0.284
Ultimate tensile strength (ksi)	120
Yield tensile strength (ksi)	100
Yield shear strength (ksi)	55
Modulus of elasticity (10^6 psi)	29
Modulus of rigidity (10^6 psi)	11.5
Coefficient of thermal exp. (10^{-6}/°F)	6.5
Ductility percent elongation (2 in.)	18

8.1.1.4 Drop transient

Another important consideration involved in air launched vehicles is a smooth drop transient. This involves simultaneous release of all the attachments between the launch and launching vehicle. This was found to be an important consideration from studying OSC's Pegasus launches. The fifth attachment hook was added to keep the Pegasus "straight" on the L-1011 to reduce drooping and deflection. By doing this, OSC cut down on the vibrations that might have damaged the payload resonating at the natural frequency. In the design of the Gryphon/Eclipse interface, the drop transient was to be as "straight" as possible so it could be dropped without causing damage to the payload or any of the internal components.

8.1.1.5 G-force loads

It was necessary to know the maximum g-force the Eclipse will perform in normal flight. This was important so that the Gryphon/Eclipse interface could be designed with a worst case load. The maximum g-force is 2.5. This was then multiplied by the structural factor of safety and the dynamic loading coefficient to obtain the overall system factor of safety of 4.

8.1.1.6 Gryphon/Eclipse system overview

Taking into account all of the parameters just discussed, the Gryphon/Eclipse interface mechanism was designed. The best configuration was found to be two four point, attachment systems on the second stage, symmetric about the center of gravity (Figure 8.1.3). Note, the reference coordinates were taken from the end of the LR-91 nozzle. As can be seen, all of the pins lie within the second stage. With the exception of pins 1 and 2, a circular support structure had to be designed at the pin locations. The first two pins were purposefully placed at the interstage between stage 1 and stage 2 due to the structure required there. Pins 5 and 6 are placed at the attach ring required for the struts connecting the two castor 120 engines. Many assumptions were made (i.e. rigid elements, etc.) in this model. However, the purpose of this model was to find the best distribution of attach points for the statically indeterminate loading. Some of the key aspects of this system are shown in Table 8.1.2.

Table 8.1.2 Important system aspects of the Gryphon/Eclipse interface

Hook Cross Sectional Area	16 in^2
Maximum Pin Length	27 in
Total System Weight	11,100 lbf
Total Pin Weight	1328 lbf

The pin sizing was determined by the shear force equation for square cross sections:

$$\tau = \frac{3}{2}\frac{F}{A} \tag{8.1.1}$$

where τ is the shear stress, F is the shear force and A is the cross sectional area. Using the maximum shear force for the steel alloy ASTM-A242 of 55 ksi, and the force per pin from the finite element model of 402 kips, the cross sectional area was found to be 10.96 square inches with the system factor of safety of 4. However, due to manufacturing constraints and the desire for a simple cross section, this cross section was increased to 16 square inches so that the hook would be 4 inches by 4 inches (Figure 8.1.4).

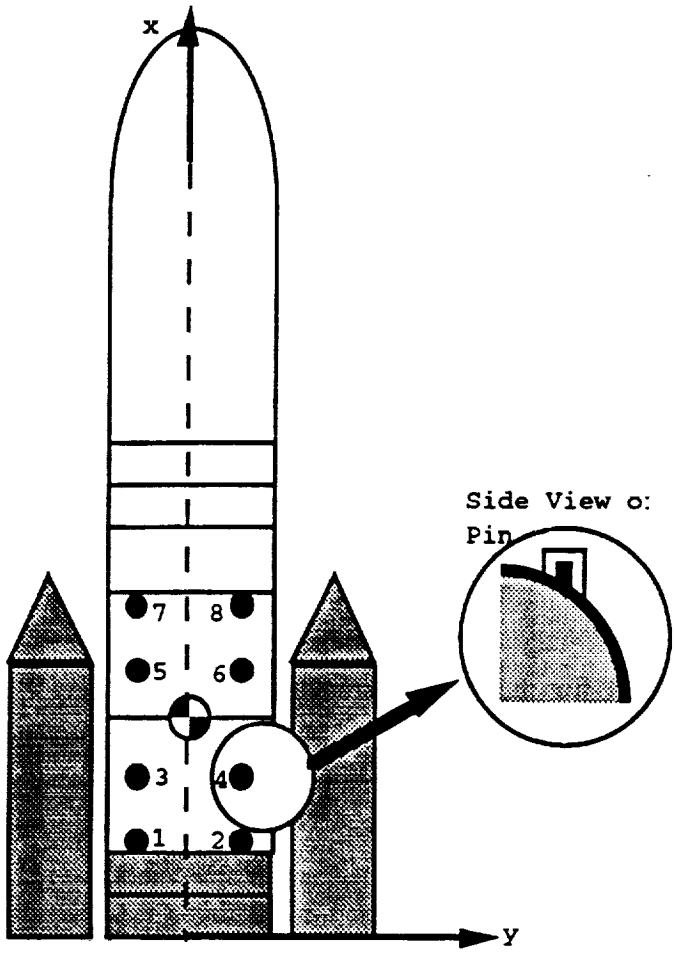

Fig. 8.1.3 Top down location of attach pins on Gryphon

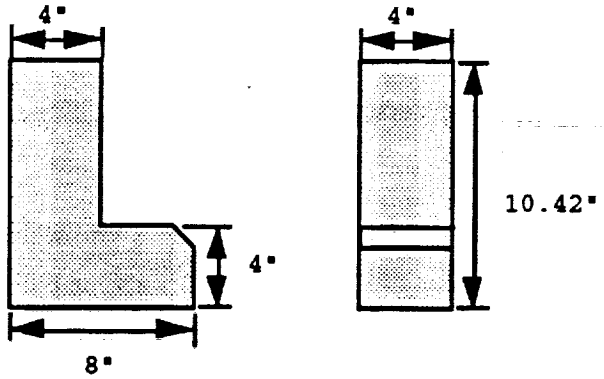

Fig. 8.1.4 Hook dimensions showing side and front views

The hydraulic force to operate the system was calculated using a worst case load. The hydraulic force was calculated by using the forces on the pin/hook combination, the friction coefficient between the pin and hook and the geometry and the lengths of the lever arm and

connecting rods. The hydraulic pressure provided by the plane is 5000 psi. It was noted that pumps could be added for emergency pressure loss and additional hydraulic force if needed. Using the hydraulic pressure, the pistons were sized by calculating the worst case load force required. The sizing of the hydraulic actuators was determined from the sum of the forces on the lever arm in the equations:

$$\Sigma M = \mu_f (F_{pin1} + F_{pin2}) (d_{lever}) - F_{hydraulic} (d_{arm}) = 0 \quad (8.1.2)$$

$$P_{hydraulic} = \frac{F_{hydraulic}}{A} \quad (8.1.3)$$

where:

ΣM = sum of the moments about the lever arm [ft•lbf]

μ_f = static coefficient of friction for steel on steel

F_{pin} = forces of a pin [lbf]

d_{lever} = distance of the connectors on the lever arm [ft]

$F_{hydraulic}$ = hydraulic force [psi]

d_{arm} = length of the hydraulic arm [ft]

$P_{hydraulic}$ = hydraulic pressure from the plane [psi]

A = cross sectional area of the hydraulic piston [in^2]

After inserting the values for these equations, it was found that the hydraulic needed to have a cross sectional area of 10.54 inches for the worst case loading.

8.1.2 Power connection

Since systems on the Gryphon need an external power supply for the pre-drop phase of the mission, an umbilical power cord is needed to connect the Eclipse and the Gryphon. The umbilical cord will be extending from the underside of the Eclipse next to the right forward most attachment point and will be securely attached to the Gryphon. At the point on the umbilical cord closest to the Gryphon there will be placed a cartridge-actuated wire cutter, the most reliable form of wire disconnect available.

8.1.3 Placement of support system on the Eclipse

One crew member is required on the Eclipse for Gryphon related work. The crew member's duties are to:

- relay Gryphon related information to Eclipse crew
- monitor Gryphon status
- switch Gryphon between external and internal power
- update Gryphon inertial measurement unit prior to release

- prepare and enable Gryphon for release
- activate release mechanism
- download and verify mission data
- capture, record, and display data from the Gryphon and its payload

The launch panel operator consists of the following equipment: two computers, an inertial measuring unit, a mass data storage system, the release panel, and three monitors. Two of the monitors will be television screens filming the forward and aft ends of the Gryphon. The third monitor will be a liquid crystal display used to visually monitor the computers, inertial measurement unit, and data storage system. Through a keyboard the crew member will be able to manually switch between these displays.

The launch panel operator's equipment will be assembled into a desk unit as seen in Figure 8.1.5. The top shelving unit will consist of three shelves that are 19 inches high. The overall dimensions of the unit are 6' x 5' x 2'. As seen in the figure, all hardware except for the monitors and the keyboard will be placed in the shelving unit. The front of the shelving unit will be covered to prevent equipment from falling out during the mission. The desk unit is approximately 6' x 3' x 6' and will include a swivel chair bolted to the floor. The monitors will be placed at a 45 degree angle and in a semi-circle on the desk to ensure easy viewing. The keyboard will be located in the middle of the semi-circle. The entire unit (shelving and desk) will be placed on the right wall of the fuselage, behind the raised platform for the pilot and copilot.

The final piece of equipment that needs to be placed on the Eclipse is a power rectifier. The rectifier will convert the 28 volt, 400 Hz AC power supply from the Eclipse engines to a 28 volt DC supply that can be used by the Gryphon systems. The rectifier unit will be approximately eight inches square and weigh ten pounds. It will be placed in a convenient location between the forward most attach points in order to have easy access to the avionics bay on the Gryphon.

8.2 Landing Gear Integration

The Eclipse landing gear will be of a quadracycle configuration. Each fuselage contains two main gear struts just aft of the airplane center of gravity and one nose gear strut just below the cockpit. The main gear struts are 17.8 and 18 feet long and the nose gear struts are 14.5 feet long. These strut lengths allow the aircraft to meet all tip-over, stability, and tail-strike criterion. Additionally, each eight-wheel main gear strut and each three-wheel steerable, nose gear strut is

able to retract within the fuselages of the aircraft. Details of the sizing calculations can be found in Appendix F.

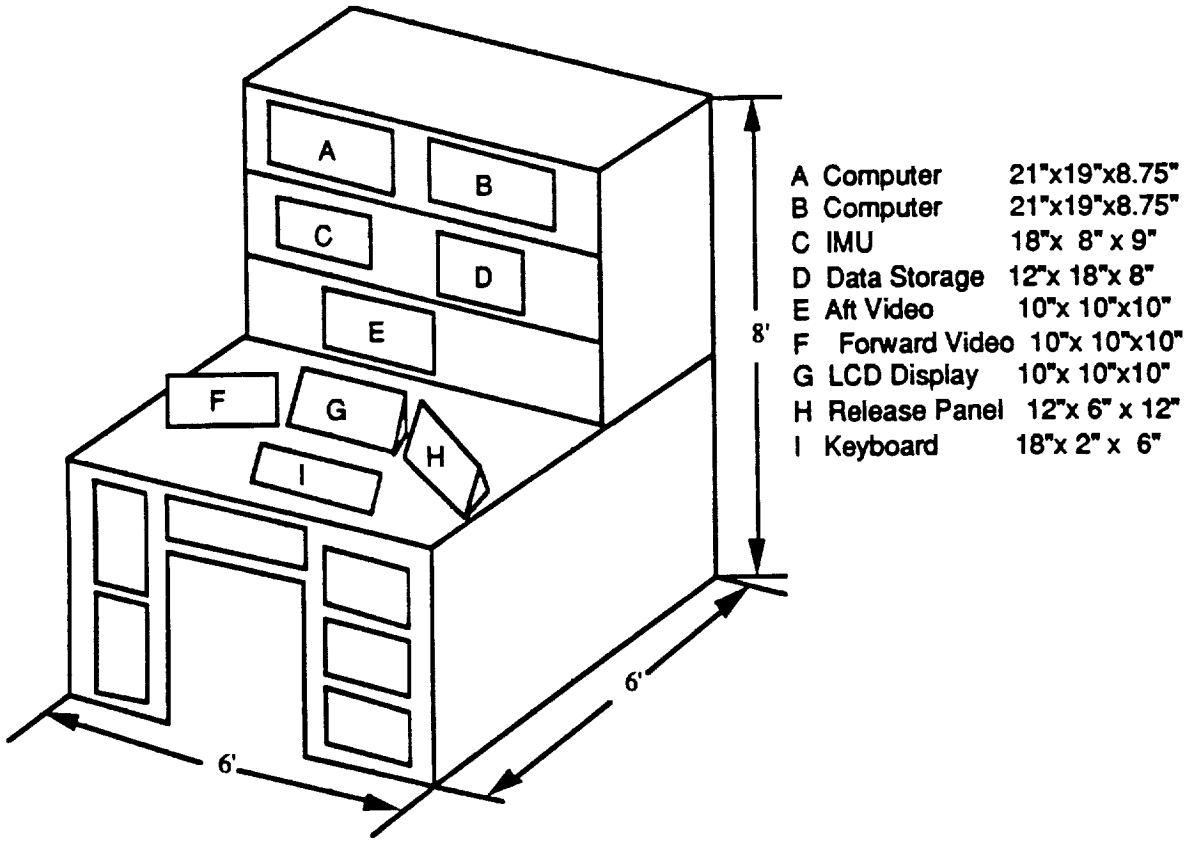

Fig. 8.1.5 Launch panel operator station

8.2.1 Landing gear requirements

The landing gear serves a number of functions. These include, but are not limited to:

- Absorbing landing shocks, and transferring loads to the airframe
- Allowing for ground maneuvering
- Providing braking capability
- Supporting the aircraft on the ground without damaging the runway

Additionally, the landing gear is configured so as to meet requirements of stability, tip-over, and tail-strike angle.

8.2.2 Strut length and position requirements

The aircraft must meet two requirements which set the minimum length of the landing gear. These are the lateral tip-over angle and the tail-strike requirement. The aircraft must be able to

land with 5° of roll without striking wingtips or engine nacelles on the ground. Also, on take off rotation the aircraft must be capable of rotating without striking the tail of the aircraft on the runway. The wing has a 1.5° angle of incidence. Since the wing stalls at approximately 11° angle of attack, it is only necessary to be able to rotate 10°. A 10.5° rotation angle is designed, leaving a small margin for safety. This yields main landing gear struts 17.8 and 18 feet long, and nose gear struts 14.5 feet long. This leaves a ground-clearance below the fuselages, at the main gear, of 12 feet and 6 feet below the Gryphon. The 1.5° nose-down angle of the fuselage, combined with the 1.5° angle of incidence of the main wing allows for perfectly horizontal mounting of the Gryphon payload, as well as minimal induced drag during the take off run.

8.2.3 Main gear position criteria

The position of the main landing gear are dictated by several considerations. The main gear must be far enough behind the center of gravity so that when the aircraft is at its maximum rotation angle, the center of gravity is still forward of the main gear. This prevents the aircraft from ever settling on its tail. However, if the center of gravity is too far forward of the main gear, rotation of the aircraft becomes difficult and the horizontal tail grows in size.

8.2.4 Nose gear position criteria

The position of the nose gear is dictated by the need for a minimum of 8% of the aircraft weight resting on the nose for effective steering. This also reduces any unintended bouncing of the nose gear off the runway. However, within this requirement, the nose gear moment arm should be as long as possible.

8.2.5 Final length and location of landing gear

The above requirements dictate that the aft main struts be 18 feet long, the forward main struts be 17.8 feet long, and the nose gear struts be 14.5 feet long. The lowered nose gear is positioned immediately below the cockpit, approximately 58 feet in front of the aircraft center of gravity. The lowered position for the forward main gear is approximately 2 feet aft of the center of gravity, and the aft main gear is positioned approximately 12 feet aft of the center of gravity.

8.2.6 Wheel configuration

Each of the four main gear struts possess and eight-wheel landing gear truck in a dual-twin-tandem configuration. This configuration was first used on the Convair B-58, which also had to place a large number of wheels within a relatively small fuselage. This configuration allows us to place the necessary number of wheels within the available fuselage volume. The fuselage, 13 feet wide at its widest point has enough internal volume to easily fit the landing gear in this

configuration. The maximum design static load for each main tire is approximately 37,200 pounds. An isometric view of the main gear bogey is shown in Figure 8.2.1. Figure 8.2.2 shows the main gear fit within the fuselage.

Each of the two steerable nose-gear struts has a three-wheel truck in a triple configuration. The static load on each nose gear wheel is only 25,000 pounds, and the dynamic loads which the nose wheel encounters also correspond to a maximum design static load of approximately 25,000 pounds. By using tires which are rated for a significantly higher load, a lower tire pressure can be used increasing the tire lifespan, reducing the chance of a tire blow-out on landing, and most importantly, reducing the risk of causing significant runway damage when landing near maximum gross weight. Figure 8.2.2 shows the nose gear fit within the fuselage.

8.2.7 Tire parameters

To deal with the large static loads associated with such a large aircraft, and to prevent runway damage the aircraft is supported on 38 identical tires. Each is a commercially available B.F. Goodrich tire 50 inches in diameter, and 21 inches wide. These tires operate at a pressure of under 160 psi.

8.2.8 Potential runways

This configuration gives a runway load classification number of approximately 65 for normal landings and approximately 100 for an aborted mission. This means that for a normal mission, the aircraft can operate from any concrete runway of the proper length. In the event of an aborted mission, the Eclipse can land on any well maintained concrete runway currently used by Boeing 747s and Lockheed L-1011s.

8.2.9 Retraction kinematics

The nose gear of the aircraft retracts upwards and aft into the fuselage. In order to reduce center of gravity travel due to retraction of the fairly heavy and relatively long main gear, the forward main gear retracts upward and forward, while the aft main gear retracts upward and aft. Figure 8.2.3 shows the a top and side view of the left fuselage, highlighting the retraction kinematics.

The gear doors are broken into several sections lengthwise. The sections near the hinge points of the gear remain open as long as the gear is down and locked. The remaining sections open to allow the gear to be raised or lowered, and then close again to reduce drag during take off and landing.

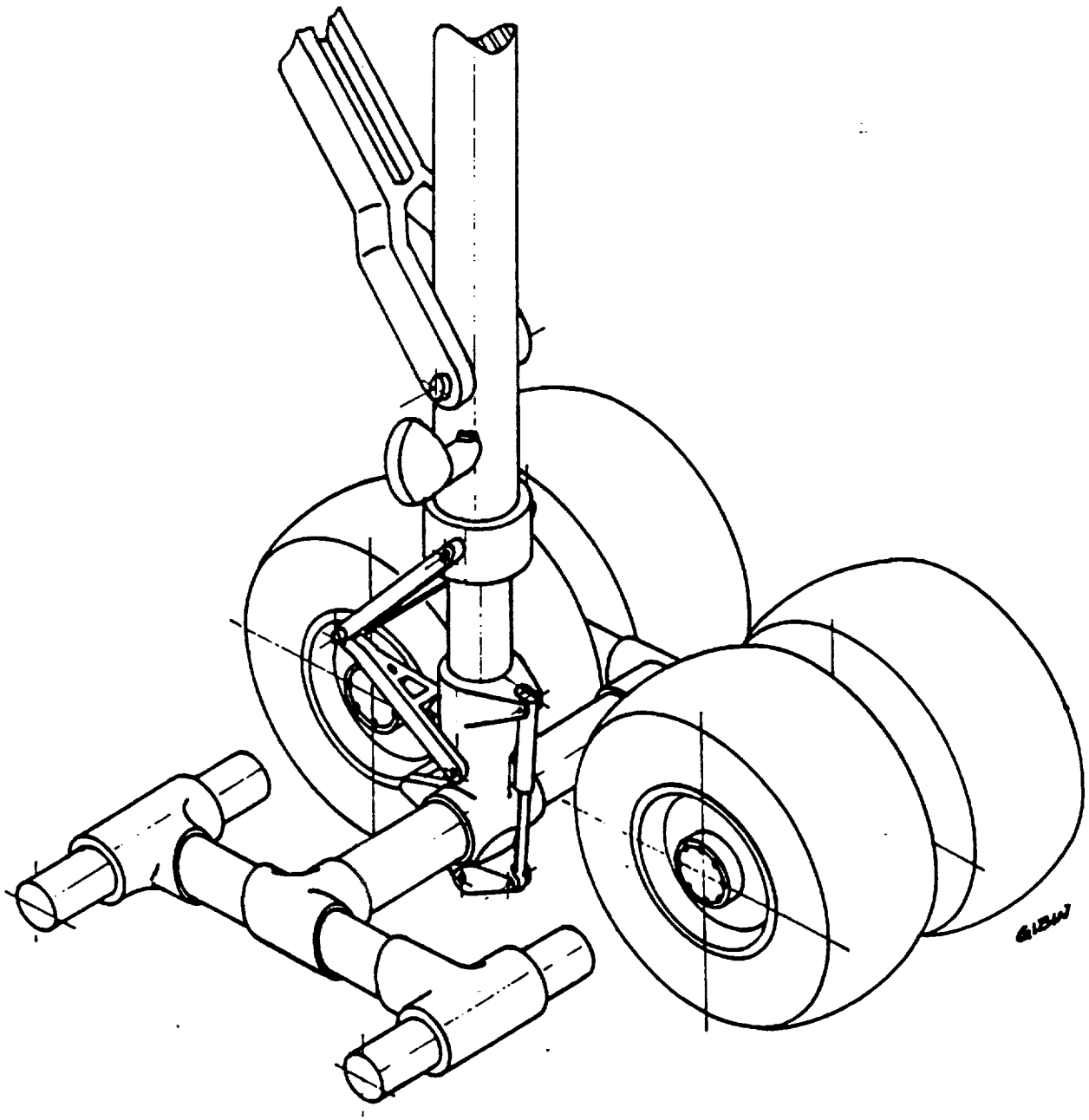

Fig. 8.2.1 Main gear bogey isometric

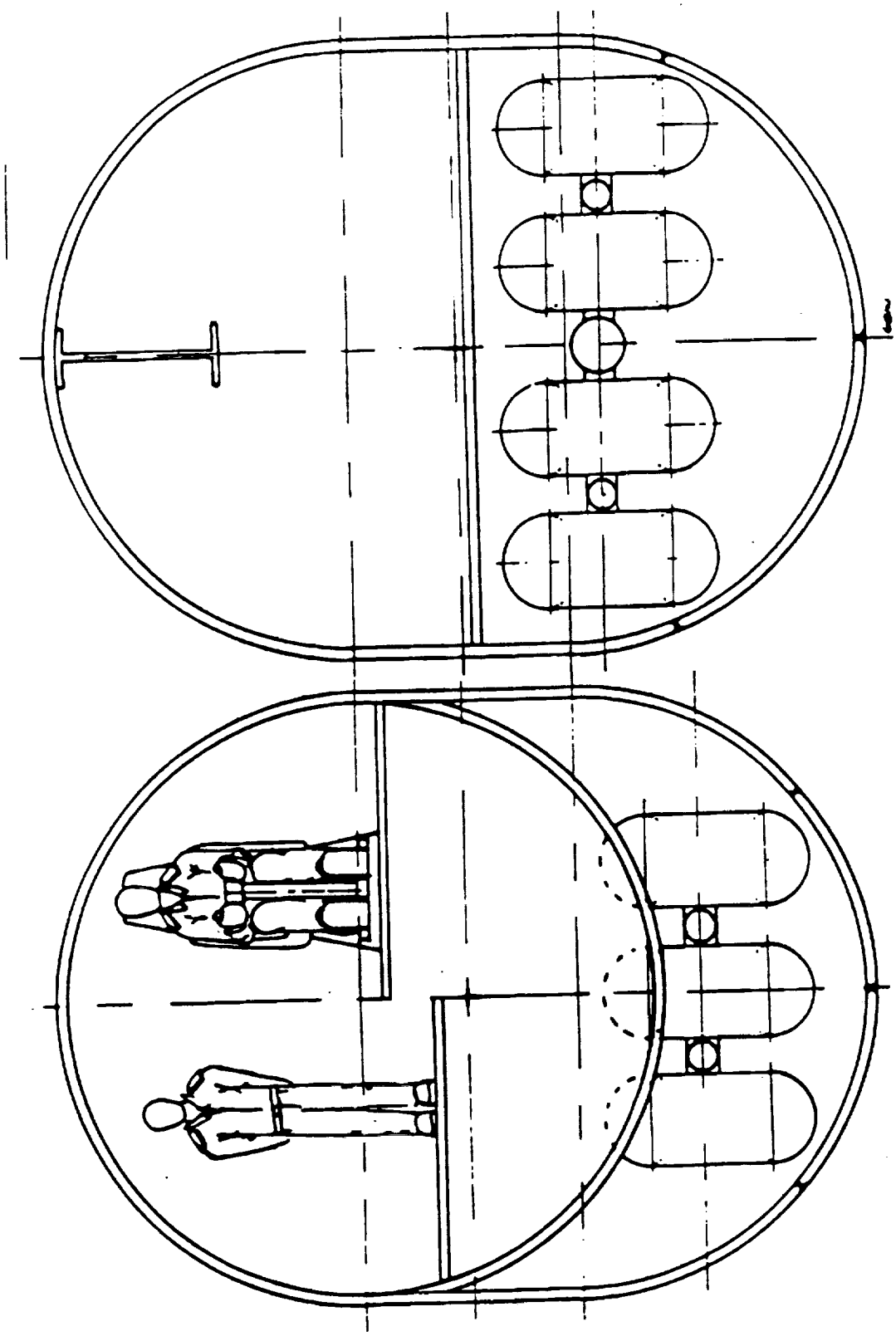

Fig. 8.2.2 Left fuselage lateral cross sections

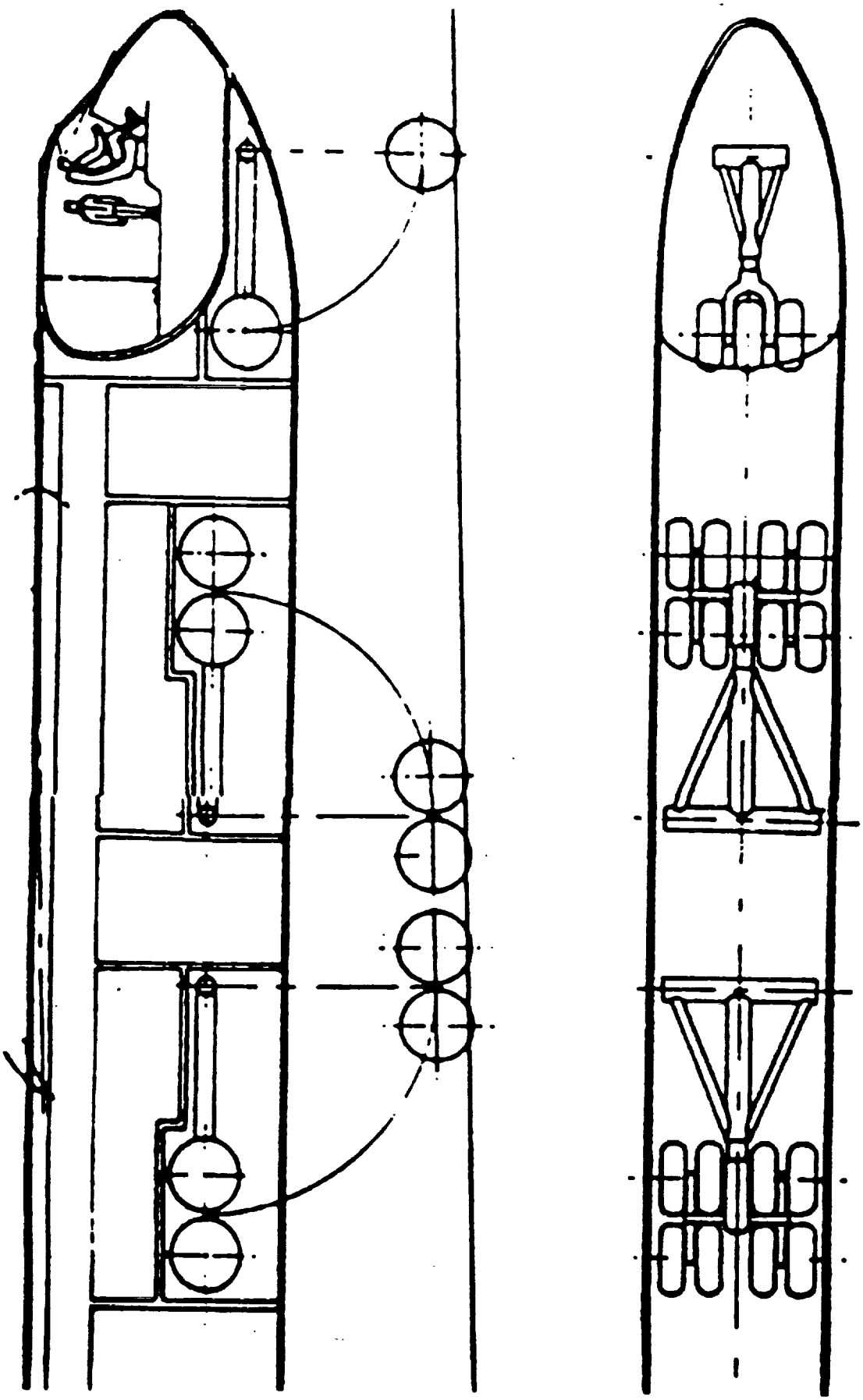

Fig. 8.2.3 Left fuselage longitudinal cross sections

The drag strut on each gear is hinged. The upper portion of the drag strut is tied to a hydraulic actuator which is used to raise or lower the gear. The down-lock on the hinged drag strut is hydraulically actuated, but is spring loaded so that is may be locked without hydraulic pressure, but cannot be unlocked without hydraulic pressure. All hydraulic actuators in the landing gear are dual redundant, and at least one system is needed to raise the gear. However, in the event of the total loss of hydraulics to the landing gear, they may be lowered and locked in the down position by a free-fall method. In this unlikely event, the non-functioning actuators are disconnected from the gear and gear doors. The landing gear is then allowed to drop under its own weight. If necessary, this could by supplemented by a 2g turn, doubling the apparent weight of the gear.

8.2.10 Braking systems

Braking is accomplished by carbon, anti-lock brakes. Differential braking to the left and right main gears is used to supplement rudder control at high speeds and nose wheel steering at lower speeds. These brakes are also dual redundant.

8.3 Hydraulic System Layout

In this section some fundamental design layout for Eclipse's hydraulic system will be discussed. The material includes:

- Design options and philosophy
- Overall system characteristics
- System components analysis
- Hydraulic power distribution
- Individual system layout
- Overall system layout

8.3.1 Design options and philosophy

In designing the power system to drive the actuators, the three most common options were considered. These options are:

1) electromechanical system
2) electrohydrostatic system
3) conventional hydraulic system

During the system selection process, numerous possibilities and considerations were reviewed and argued. However, the driving criteria in designing the system is not much different from the team's overall philosophy. That is, ease of assembly and simplicity in design.

A electromechanical system consists of individual actuators with self-contained electric motors which drive the output shafts via gear boxes. Characteristics of the system depend on the magnetic field strength capability of its electric motors. In general, the electromechanical system suffers in the size, volume, and performance when compared to a conventional hydraulic system. Its actuators are bulkier, heavier, and system response is slower. In addition, it consists of small parts and therefore, is not suitable for the Eclipse.

The electrohydrostatic actuator is a recent development in hydraulic technology. This actuator does not need an airplane hydraulic system because it has its own miniature hydraulic system, including a pump driven by an electric motor. It is primarily designed for fly-by-wire or fly-by-light flight control systems. The Eclipse is controlled via a mechanical signaling system. Therefore, the electrohydrostatic system is not suitable in our design.

A conventional hydraulic system moves the actuator via fluid power in the form of flow and pressure. The advantages of this system are its flexibility, ease of control, and proven feasibility. The primary disadvantage in a conventional hydraulic system is its need for system redundancy. Despite its drawbacks, the conventional hydraulic system represents the most feasible choice among the options considered and it is implemented in the Eclipse.

8.3.2 Overall system characteristics

While the functions of hydraulic system vary from one airplane to another, they are typically separated into primary and secondary systems. A primary system requires higher levels of redundancy because of the criticality to flight. It consists of the primary flight control surfaces such as the aileron, elevator, and rudder. The secondary systems are considered to be in the same class as any other structural member of the aircraft and require a lower number of system redundancy. Examples of these are the landing gear system, landing flaps, and the ground steering unit. Table 8.3.1 lists the primary and secondary systems for the Eclipse.

Most hydraulic systems today operate at a pressure between 3,000-5,000 psi. The major advantages of higher operating pressure are a reduction in weight and installed volume. With advancement in hydraulic technologies, the 5,000 psi hydraulic system is becoming the industry standard and it is the system implemented in Eclipse. Further reduction in weight and installed

volume is possible via implementation of an 8,000 psi system. In such system the problem of sealing between relative moving surfaces such as a piston and cylinder becomes quite severe and costly seals capable withstanding high pressure differential are used. After the preliminary benefit analysis, the advantages of an 8,000 psi system does not justify extra cost incurred for implementation in the Eclipse.

Table 8.3.1 Primary and secondary systems for the Eclipse

Primary	Secondary
Rudders	Braking system
Elevators	Trim units
Ailerons	Ground steering system
	Landing gear system
	Trailing edge flaps
	Thrust reverses
	Payload drop system
	Spoilers
	Flap system

The system can use any standard aviation hydraulic fluid as its operating fluid. This mineral hydrocarbon fluid provides chemical stability needed in high pressure operating environment.

Four independent hydraulic systems are used in Eclipse to ensure safe flight operations. These systems are designated as the left, central, auxiliary, and right system for future references. In addition, each system uses three independent pumps to further ensure flight criticality. Preliminary design approximates the system flow rate at 300 liters per minute (75 gal/min), but the final number depends on specific system characteristics such as the rate of control system operation. Table 8.3.2 summarizes the overall characteristics of Eclipse's hydraulic system.

Table 8.3.2 Main characteristics of hydraulic design

Operating pressure	5,000 psi
Number of systems	four
Pumps per system	three
Flow rate	300 liter / min
Reservoir	four independent
Operating Fluid	standard aviation hydraulic fluid

8.3.3 System component analysis

The hydraulic system consists of the following components:

8.3.3.1 Hydraulic fluid reservoir

The size of reservoir depends on the system flow rate, system volume, and other characteristics. Reservoirs of the left and central systems are located in the left landing gear housing while the other two reservoirs are in the right landing gear housing. This arrangement represents the best layout in terms of balancing system redundancy and accessibility.

8.3.3.2 Hydraulic pump

The hydraulic pump is the heart of the system which transforms the mechanical input into fluid power. The machine used is a positive displacement pump which provides a flow proportional to the input speed. Table 8.3.3 lists characteristics of some hydraulic pumps.

Table 8.3.3 Characteristics of hydraulic pumps

Type	Pressure Range (psi)	Maximum Flow Rate (liter/min)	Overall Efficiency (%)
Gear	290 - 3000	1 - 700	60 - 70
Vane	290 - 3500	2 - 1200	70 - 80
Piston (axial)	290 - 5500	2 - 2000	90 - 95
Piston (in-line axial)	5000 - 10000	1500 - 5000	90 +

As with the other components in the system, increasing pressures, flow rates, and reducing the weight of the pump results in a higher price for the units. It is important to note, however, the critical factor in aircraft systems is mainly weight and criticality to flight whereas in industrial systems is usually cost. From Table 8.3.3, axial–piston pump provides the best efficiency and flexibility for Eclipse's operating pressure range. Indeed this is now the standard type of pump used in aircraft applications.

Table 8.3.4 lists pump distribution among different systems and their power sources. Note that there are two different types of primary hydraulic pumps: engine driven and electric driven. An auxiliary power unit (APU) driven pump is included to further insure redundancy. On top of these there is a ram air turbine (RAT) driven pump, if all else fails. Each system operates with two pumps with an alternate pump for emergency operation as listed below.

Table 8.3.4 Hydraulic pump distribution

System	Left (LT)	Center(CT)	Auxiliary(AU)	Right(RT)
Main Pumps	Engines 1, 2	Engines 3, 4	2 Electric	Engines 5, 6
Alternate Pump	Electric	APU	RAT	Electric

8.3.3.3 Servo actuator

Control units used in Eclipse comprise a servo-valve and actuator coupled together in the manner indicated in Figure 8.3.1 which shows a valve with mechanical input and a feedback lever between valve and jack output to achieve proportionality.

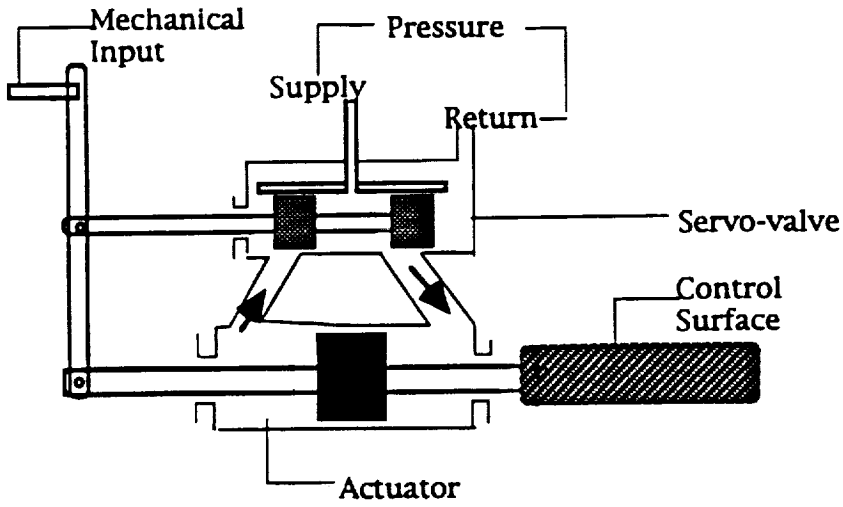

Fig. 8.3.1 Servo-actuator

8.3.3.4 Accumulators

These units are the 'capacitor' in hydraulic system and can be used to store energy or even absorb energy to eliminate sudden surge in pressure. The action of the accumulator is dependent on the compression and subsequent expansion of a specific mass of gas, held in a cylinder behind a piston. There is one accumulator for each hydraulic system located in the main landing gear bays near the system reservoir.

8.3.3.5 Filter

Filters are extremely important in a high pressure system. Because valves contain elements with such small clearances between relative moving parts, it is necessary to filter out particles down to four microns for typical servo-actuator. The filter is design according to the maximum operating pressure.

8.3.3.6 Lines and valves

Lines and valves are used for fluid distribution to all operating points and pilot controls.

8.3.4 Hydraulic Power Distribution

Figure 8.3.2 shows the distribution of hydraulic power to flight controls. Note that there are four levels of redundancy for primary flight control surfaces, with each individual control surface powered by three separate systems. If three hydraulic systems failed during flight operation, the remaining system could still provide hydraulic power to all primary flight controls.

Secondary flight controls are considered as any other structural member on the aircraft and only two levels of redundancy are used.

Figure 8.3.3 indicates the hydraulic power distribution to secondary service systems. Again, only two levels of redundancy are used. Table 8.3.5 lists these system under normal and under emergency operation.

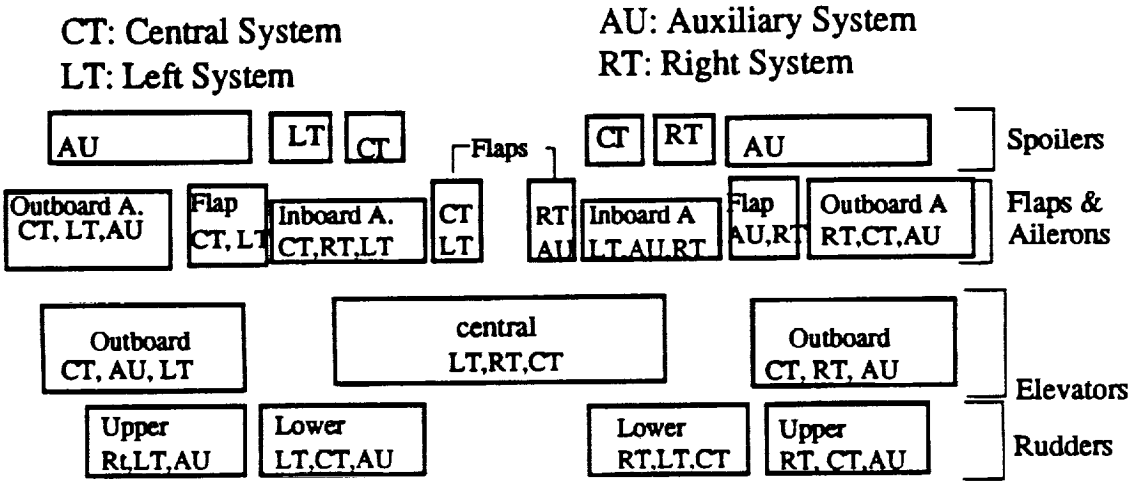

Fig. 8.3.2 Distribution of hydraulic power to flight controls

Table 8.3.5 Emergency operation of secondary systems

Power system	Normal hydraulic system	Emergency operation
Landing gear	Left and right	Manual and "free fall"
Steering	Center and right	Differential braking
Brakes - inboard	Left	Outboard braking available, accumulator pressure
Brakes - outboard	Auxiliary	Inboard brakes available, accumulator pressure
Launching system	Center and auxiliary	Electrohydrostatic actuator

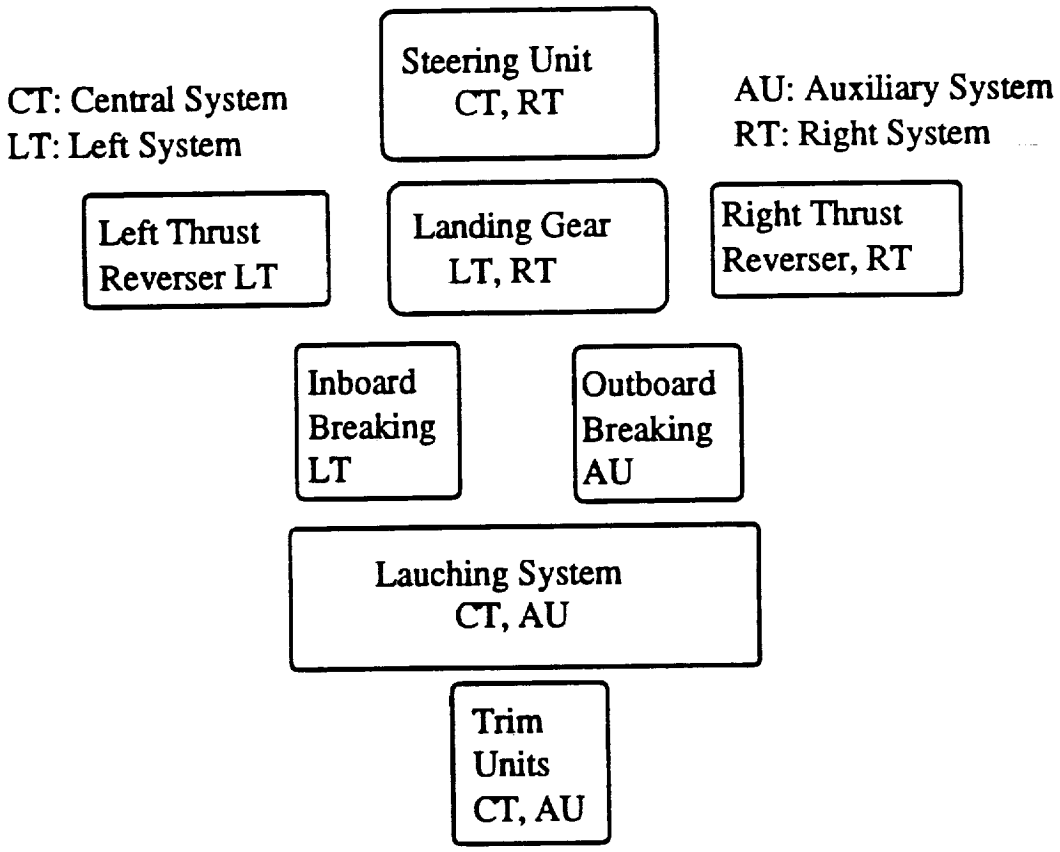

Fig. 8.3.3 Distribution of hydraulic power to secondary systems

8.3.5 Individual System Layout

Table 8.3.6 lists functions of individual systems.

Figures 8.3.4 and 8.3.5 exhibit schematic views of each system with system components, pressure lines and return lines. Note that each system is truly independent with its own pumps, regulator, accumulator, and reservoir. Servo-actuators of primary flight control surfaces represent the only system links and are connected as shown.

8.3.6 Overall systems layout

Figure 8.3.6 shows the hydraulic routing on the Eclipse. Note the followings:

1) Four systems are positioned at four corners of the fuselage for maximum spacing between systems to prevent complete hydraulic failure.

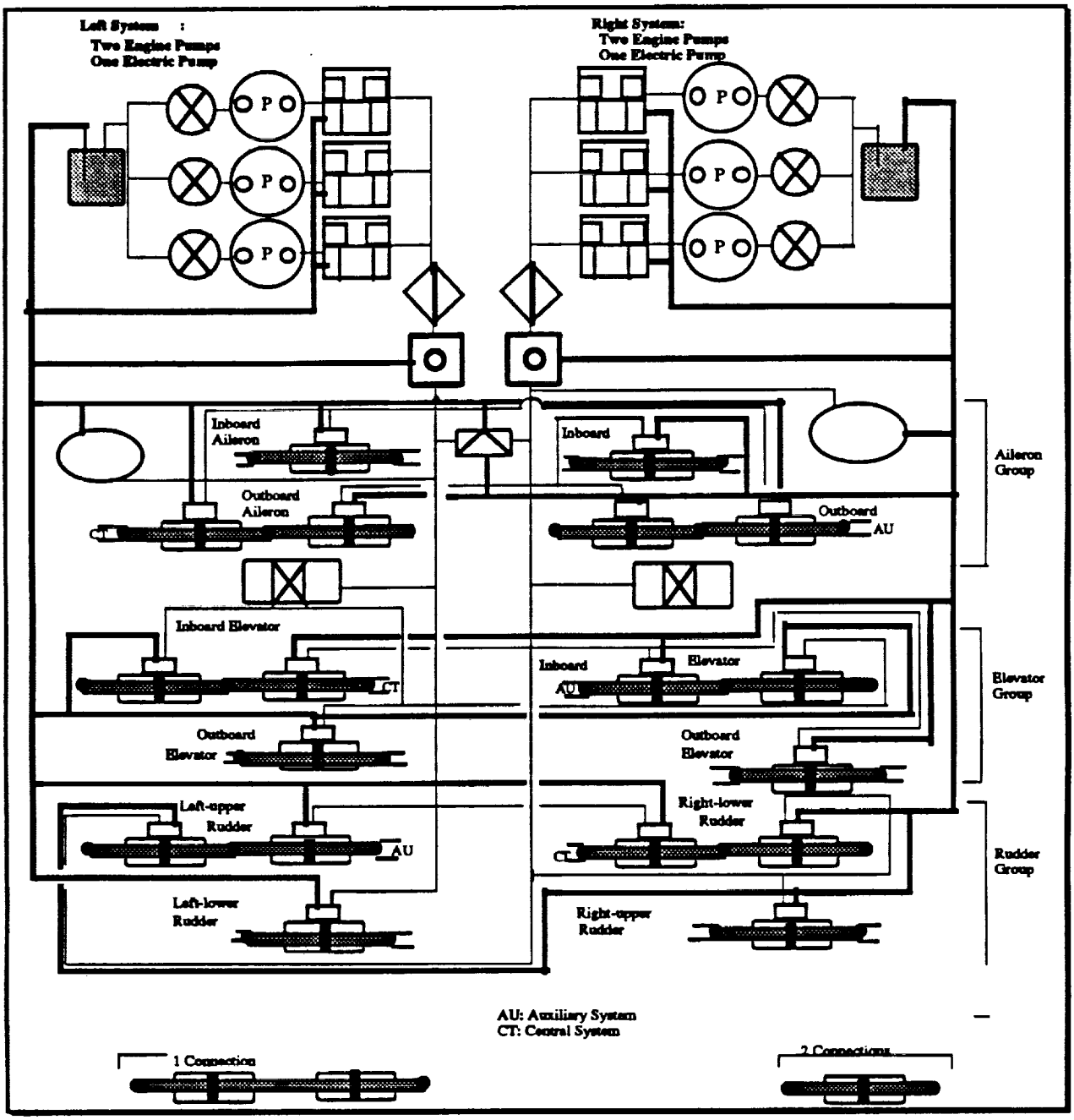

	Pump		Reservoir		Shut off valve		Check valve
	Secondary flight control		Filter		Pressure regulator		Accumu-lator
	Actuator		Secondary systems		Pressure line		Return line

Fig. 8.3.4 Schematic hydraulic diagram: left and right systems

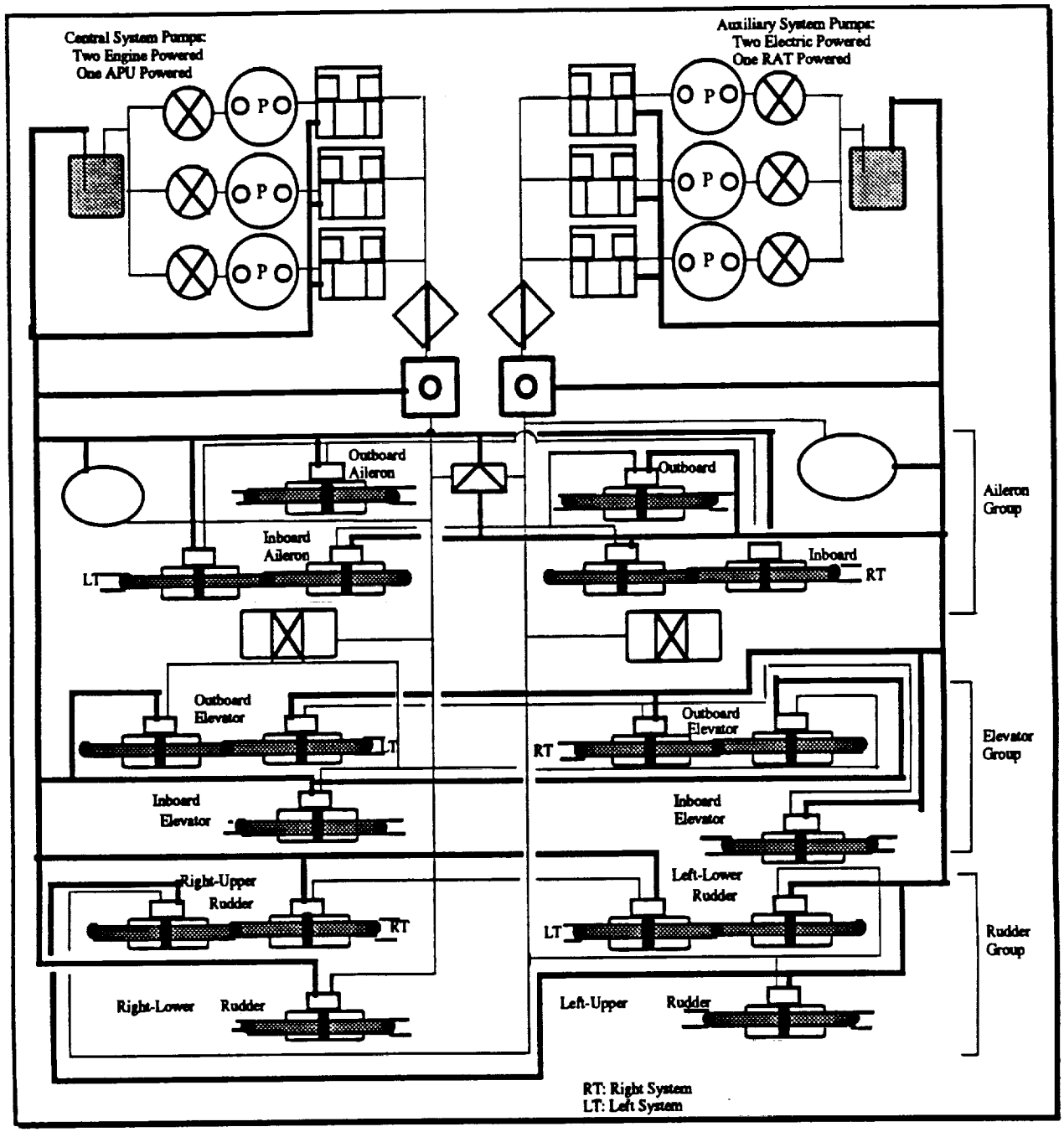

P	Pump		Reservoir		Shut off valve		Check valve
	Secondary flight control		Filter		Pressure regulator		Accumu-lator
	Actuator		Secondary systems		Pressure line		Return line

Fig. 8.3.5 Schematic hydraulic diagram: center and auxiliary systems

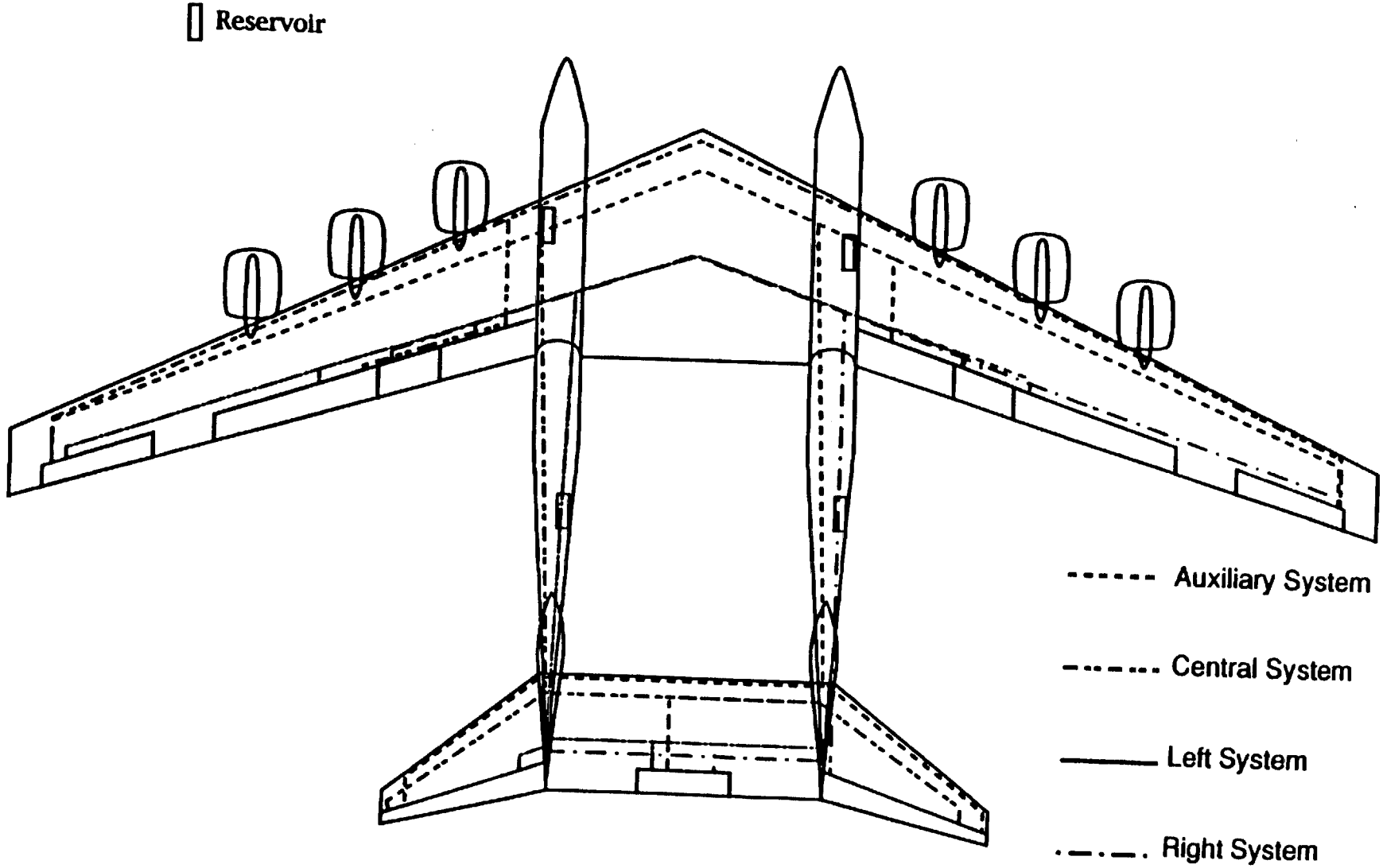

Fig. 8.3.6 Hydraulic routing

2) On the wings, the vertical tails, and the horizontal tails, left and central systems are routed in front of the first wing spar at 17 percent of the chord. Right and auxiliary systems are positioned behind the third spar at 70 percent of the cord. This combination provides the ideal balance between service accessibility and system redundancy.
3) Locations of reservoir for individual systems are spread out to ensure redundancy. They are also located near the surface for better accessibility.
4) Each primary control surface is powered by three independent systems via three independent servo-actuator units as shown.

Table 8.3.6 Individual system functions break–down

System	Left (LT)	Center (CT)	Auxiliary (AU)	Right (RT)
Main pumps	Engines 1, 2	Engines 3, 4	2 Electric	Engines 5, 6
Alternate pump	Electric	APU	RAT	Electric
Ailerons	Left: Out, In	Left: Out	Left: In	Left: In
	Right: In	Right: In,Out	Right: In, Out	Right:In, Out
Elevators	Left	Left	Left, Central	Central
	Central	Right	Right	Right
Rudders	Left: Up,Low	Left: Low	Left: Up, Low	Left: Up
	Right: Low	Right: Up, Low	Right: Up	Right: Up,Low
Spoiler Groups	Left: Center	Left: In	Left: Out	Right: Center
		Right: In	Right: Out	
Flap Groups	Left: In, Out	Right: In,Out	Left: In,Out	Right: In,Out
Thrust Reverses	Left			Right
Trim Units		Primary	Primary	
Steering		Primary		Primary
Braking	Inboard		Outboard	
Landing Gears	Normal			Normal
Launching System		Normal	Normal	

Left: Out = Left side, outboard unit Right: In, Out = Right side, inboard and outboard units

8.4 Electrical system layout

The purpose of this section is to discuss the preliminary electrical system design of the Eclipse. The material in this section includes:

- Sizing of electrical system
- Primary and secondary power generation systems
- Schematic layout of electrical system
- Primary electric-powered systems
- Components locations

8.4.1 Sizing of electrical system

Preliminary design is based on two types of electrical load requirements, essential load and normal operating load. Essential load requirements are determined by the minimum electrical power necessary for safe flight operation. Normal operating load requirements are determined by the maximum sum of all electrical power during certain phase of the mission. At this stage of the design, electrical power requirements of individual components are unknown, overall electrical power required, therefore, is approximated form a similar sized aircraft, the Boeing 747. Although the Boeing 747 is significantly smaller in size than the Eclipse, the Boeing 747 also requires more electrical loads throughout its fuselage to accommodate commercial passengers. The Eclipse on the other hand, lacks such requirement, and thus the electrical power requirements should be similar on both aircraft. Table 8.4.1 approximates the electrical power requirements of the Boeing 747.

Table 8.4.1 Electrical load summary

Operating Phase	Normal Load (KVA)	Essential Load (KVA)
Loading	60	20
Start & Taxi	135	38
Takeoff & Climb	145	42
Cruise	140	35
Descent & Land	160	65
Ground Operation	45	35

It should be noted, however, the mission specification of the Boeing 747 differs significantly from design criteria of the Eclipse, hence the electrical requirements could greatly vary from one operating phase to another. The purpose of this chapter is to provide a preliminary electrical system design for the Eclipse, further requirement analysis is needed for feasible implementation.

8.4.2 Primary and secondary power generation

From Table 8.4.1, approximately 160 KVA is needed for maximum normal operating load and 65 KVA for essential load requirements. When industry standard 90 KVA AC generators are used, the system requires three generators for overall system operation. The design also uses a back-up generator to ensure system safety.

Batteries are also used as a secondary option in the system design. The principal functions of the battery system are:

1) To maintain DC system voltage under transient conditions (The starting of large DC motor-driven accessories, such as pumps, requires high input current which would lower the bus voltage momentarily unless the batteries are available to assume a share of the load)

2) to supply power for short term heavy loads, when generator or ground power is not available
3) to supply limited amounts of power under emergency conditions

Batteries are mounted on an acid-proof, non-absorbent tray secured on the aircraft structure. They are installed in individual compartments designed to provide adequate heat dissipation and gas ventilation.

Although batteries are capable of providing temporary power, their capacity is restricted to the supply of power under emergency conditions and does not permit wide range of use on the ground. It is necessary, therefore, to incorporate a separate circuit through which power from an external ground power unit may be connected to the Eclipse's electrical system. The ground power units supplies the electrical power necessary for starting of engines, mounting of Gryphon, service lighting, and routine system checks.

An additional measure of safety is obtained by using a free-fall RAT to provide prolonged electrical and hydraulic power when all engines failed. The RAT is placed in the nose of the right fuselage based on the following considerations:
1) avoid interference flows induced by the Gryphon
2) provide clearance from the fuel tank
3) provide clearance in case of engine disperse
4) avoid position conflicts with landing gears and other operating structures
5) ensure free stream air availability

Figure 8.4.1 shows the positioning of RAT and engine powered generators on the Eclipse.

8.4.3 Schematic layout of the electrical system

Figure 8.4.2 shows a schematic view of Eclipse's electrical system. Note the following:

1) Three AC engine-driven generators and APU powered generator are used for normal and essential loading. In addition, one RAT driven generator supplies electrical power for emergency operation. External AC ground power supply and DC battery systems provide additional secondary power support.
2) Various AC and DC operating systems connecting to output buses.
3) DC power derived from AC generators via transformer/rectifier systems. AC power derived from the battery system via inverts. Figure 8.4.1 shows the position of these electrical components.

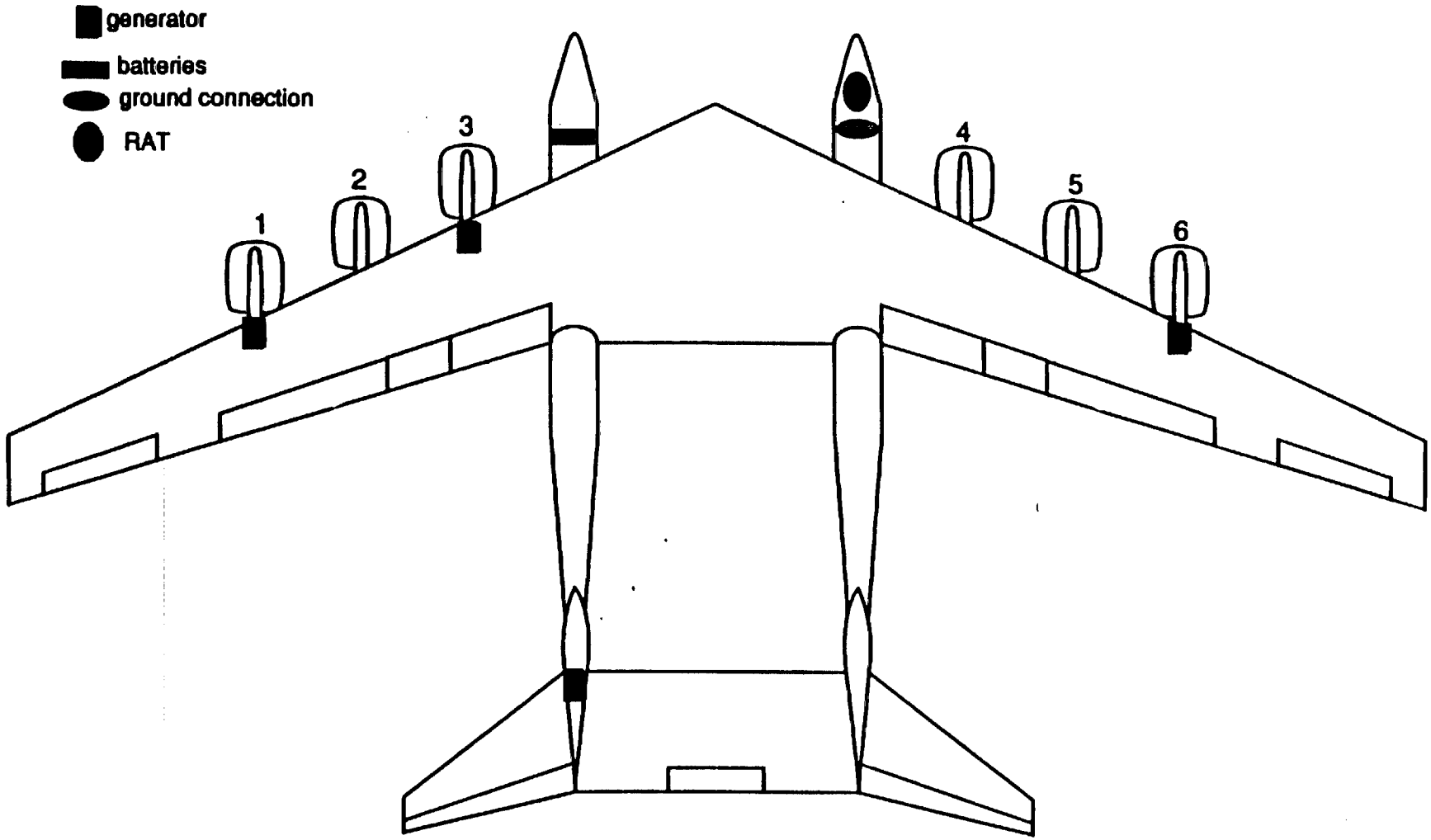

Fig. 8.4.1 Electrical system layout

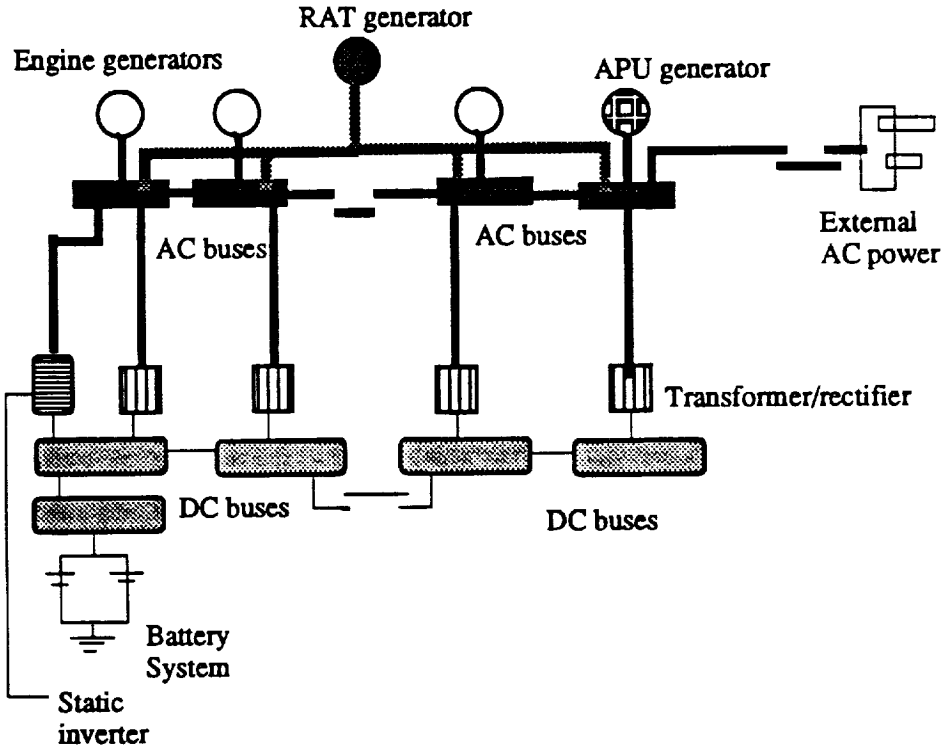

Fig. 8.4.2 Schematic electrical diagram

8.4.4 Electrical power utilization

Electric power is provided to the following systems:

1) Six engine starter motor systems
2) External Lighting
   (i) The marking of an aircraft's position by means of navigation lights
   (ii) Position marking via flashing lights
   (iii) Forward illumination for landing and taxiing
   (iv) Illumination for wings and engines to check for icing
   (v) Illumination for evacuation after an emergency landing
3) Internal lighting
   (i) Illumination of cockpit instruments and control panels
   (ii) Illumination for cabin and cockpit operations
   (iii) Indication and warning system of operating conditions
4) Fire detection and extinguishing systems
5) De-icing and anti-icing systems
6) Landing gear position indication system
7) Anti-skid control system

8) Other general services

8.5 Flight Control System

The purpose of this section is to describe the components of the flight control system as well as their location and description. Also described are some of the major factors behind the design. As with other systems, much of the Eclipse's flight controls were designed following the examples of existing aircraft. For the Eclipse's flight controls, the main aircraft under scrutiny are the Boeing 767 and the Lockheed C-5A Galaxy.

8.5.1 Design considerations

Due to the size of the Eclipse, it is an immediate requirement that all primary flight control systems be irreversible. Otherwise, the pilot will not be able to create a sufficient force to counteract the tremendous amount of aerodynamic forces generated by the large control surfaces.

The next option that must be considered is how the control surfaces will be signaled. This is a difficult design problem to consider. On one hand, mechanical systems offer ease in certification, greater redundancy, and they are much cheaper to develop and maintain than fly–by–wire or fly–by–light systems. However, there is a tremendous operational cost advantage to be gained by having the lighter weight provided by fly-by–wire or fly–by–light systems. The high initial cost involved in developing the hardware and especially the software for the fly–by–wire systems is not justified in our design. Therefore, the Eclipse's flight controls would be mechanically signaled and hydraulically powered.

The operation of the Eclipse's flight controls can be simplified as follows: input is supplied by the pilot through the control yoke. The control yoke applies/releases tension in a stranded cable which, through a designated series of pulleys, pulls/releases a piston inside a control valve. This control valve regulates the amount of hydraulic pressure required to move the hydraulic actuator (and thus the control surface) in the desired direction.

Since the actuator operations are covered in the hydraulic section, the reminder of this section will only cover the mechanical aspects of the flight controls.

8.5.2 Layout of primary flight controls

The primary controls are separated as follows:

Lateral Control: Ailerons

Longitudinal Control: Elevators
Directional Control: Rudders

The layouts of the lateral, longitudinal, and directional controls are shown in Figures 8.5.1, 8.5.2, and 8.5.3, respectively. The cable runs are shown in Figure 8.5.4. In designing these layouts, the following items must be considered: physical clearances, redundancy, forces required, stability, auto flight controls, and a number of other issues. The two redundant mechanical systems are both placed behind the last spar of the wing and tail surfaces and following the side of the fuselage. Similar to hydraulics, the flight control systems have built in redundancy from the presence of the control yokes and pedals. In other word, if the cable in one of the system breaks, the other system would still have control authority of the primary flight surfaces.

Also included in the design are auto pilot controls which must be taken into account. These control inputs act in much the same way as a hydraulic powered control yoke or pedal. The auto pilot, feel, and trim controls enter the system as shown in Figures 8.5.1, 8.5.2, and 8.5.3.

8.5.3 Layout of secondary flight controls.

The secondary flight controls are as follows:
Flaps, Spoilers
Lateral, longitudinal, and directional trim
Engine fuel controls

The layout of the auto pilot and trim controls is included in Figures 8.5.1, 8.5.2, and 8.5.3. Throttle controls are shown in Figure 8.5.5. Other than the large number of engines, there is really no difference between engine controls of the Eclipse and that of any other modern aircraft. The engine controls of the Eclipse are modeled after those of the Boeing 767.

8.6 Fuel System

Once the fuel weight is calculated the fuel volume needed is calculated by dividing the fuel weight by 50.4 ft^3/lbf, the inverse density of jet fuel. For the purpose of other possible mission for the aircraft, and for increased fairing range, an additional 90,000 pounds of fuel was allocated for as auxiliary fuel supply. In addition to the 260,000 pounds already required, this brought the total fuel tank capacity of the Eclipse to 6950 ft^3. Tanks were then placed in the wing, outside of the turbine burst area, to allow for this fuel volume.

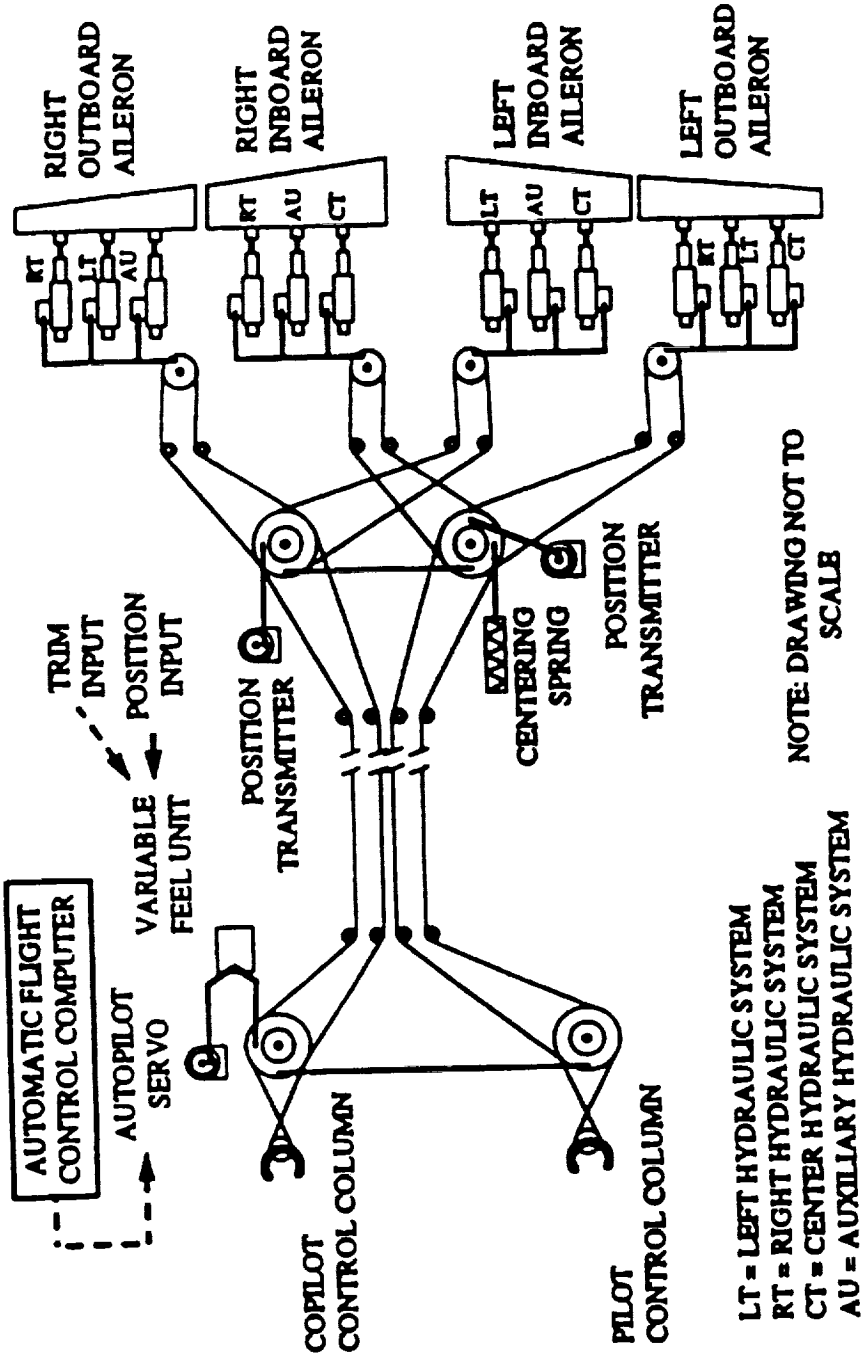

Fig. 8.5.1 Lateral control layout

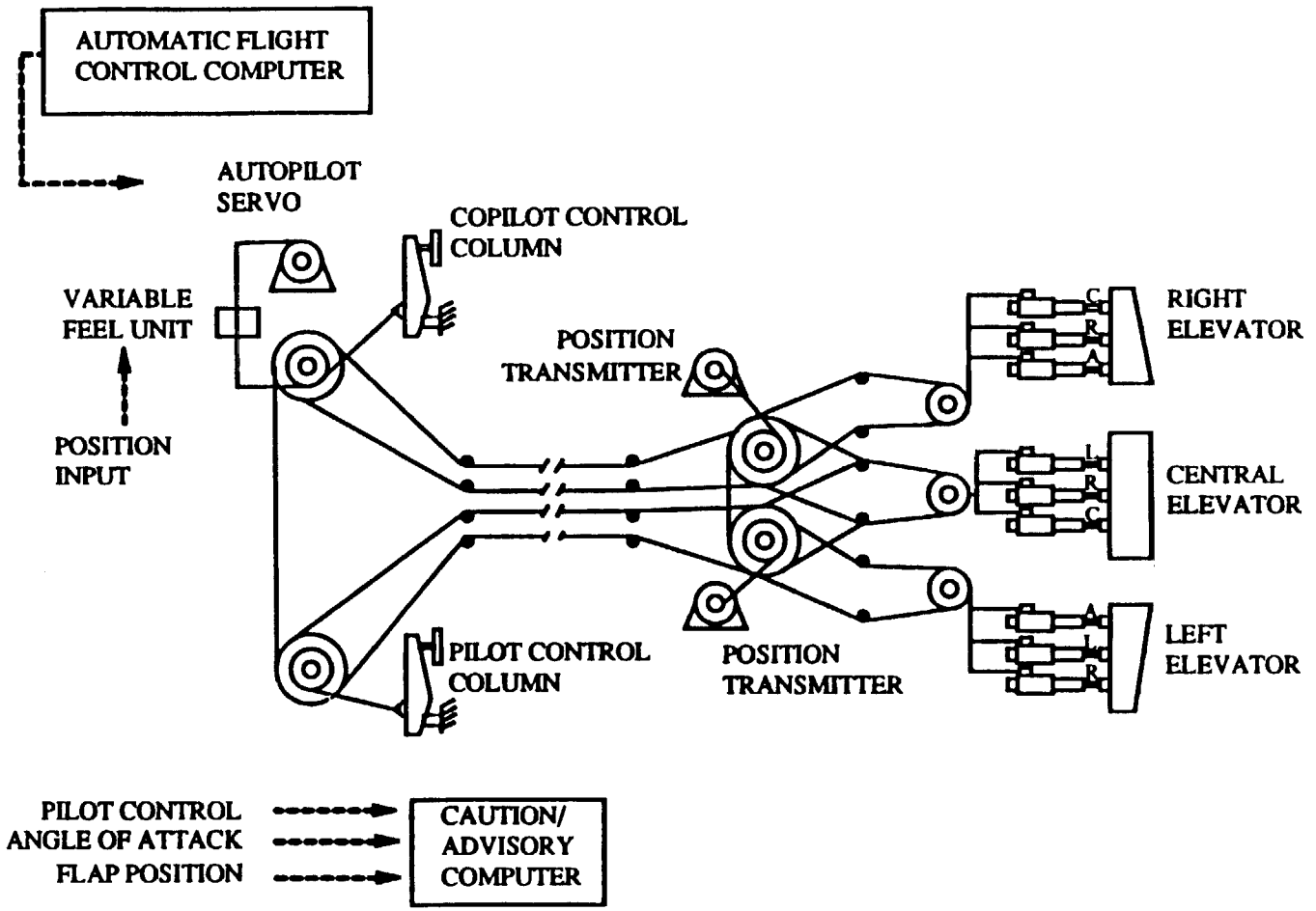

Fig. 8.5.2 Longitudinal control layout

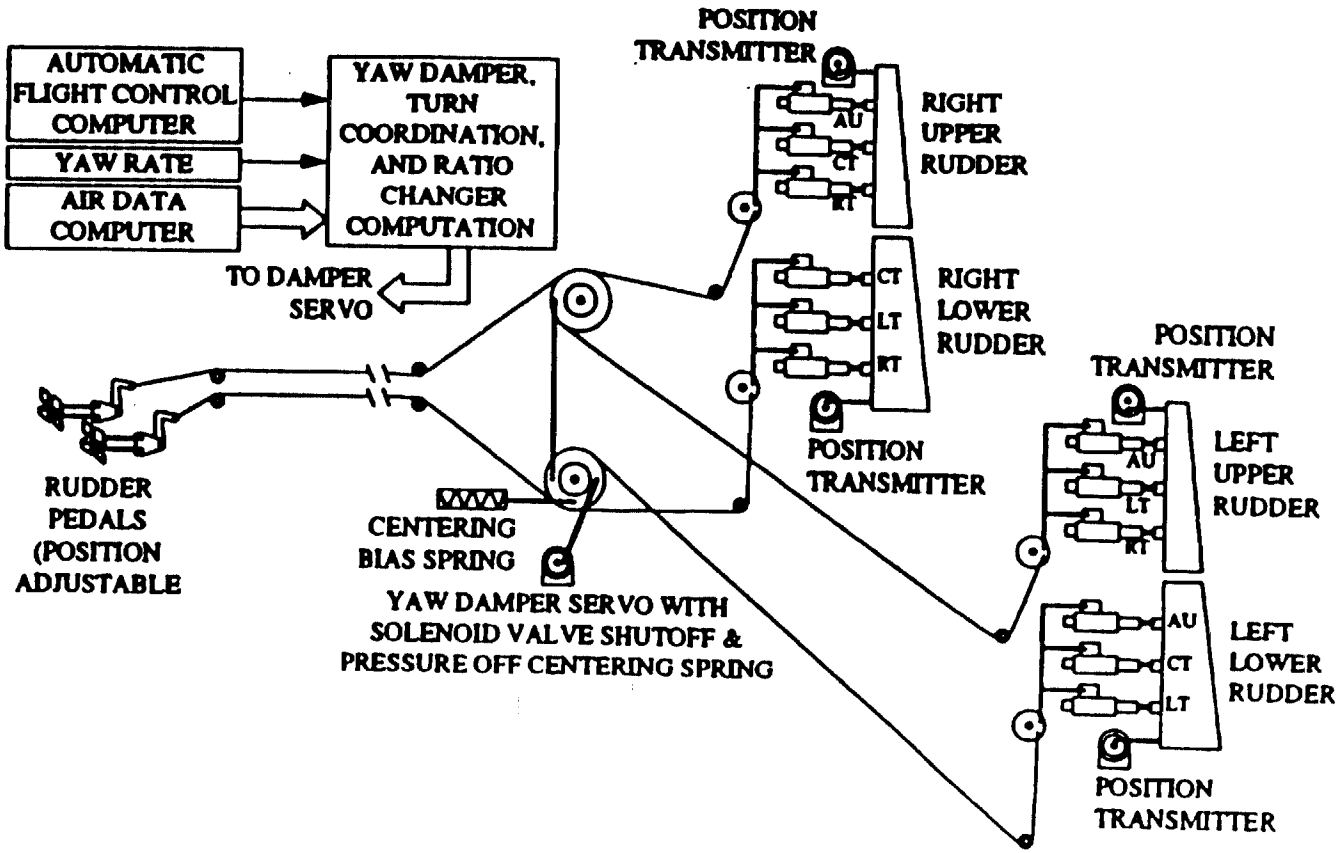

Fig. 8.5.3 Directional control layout

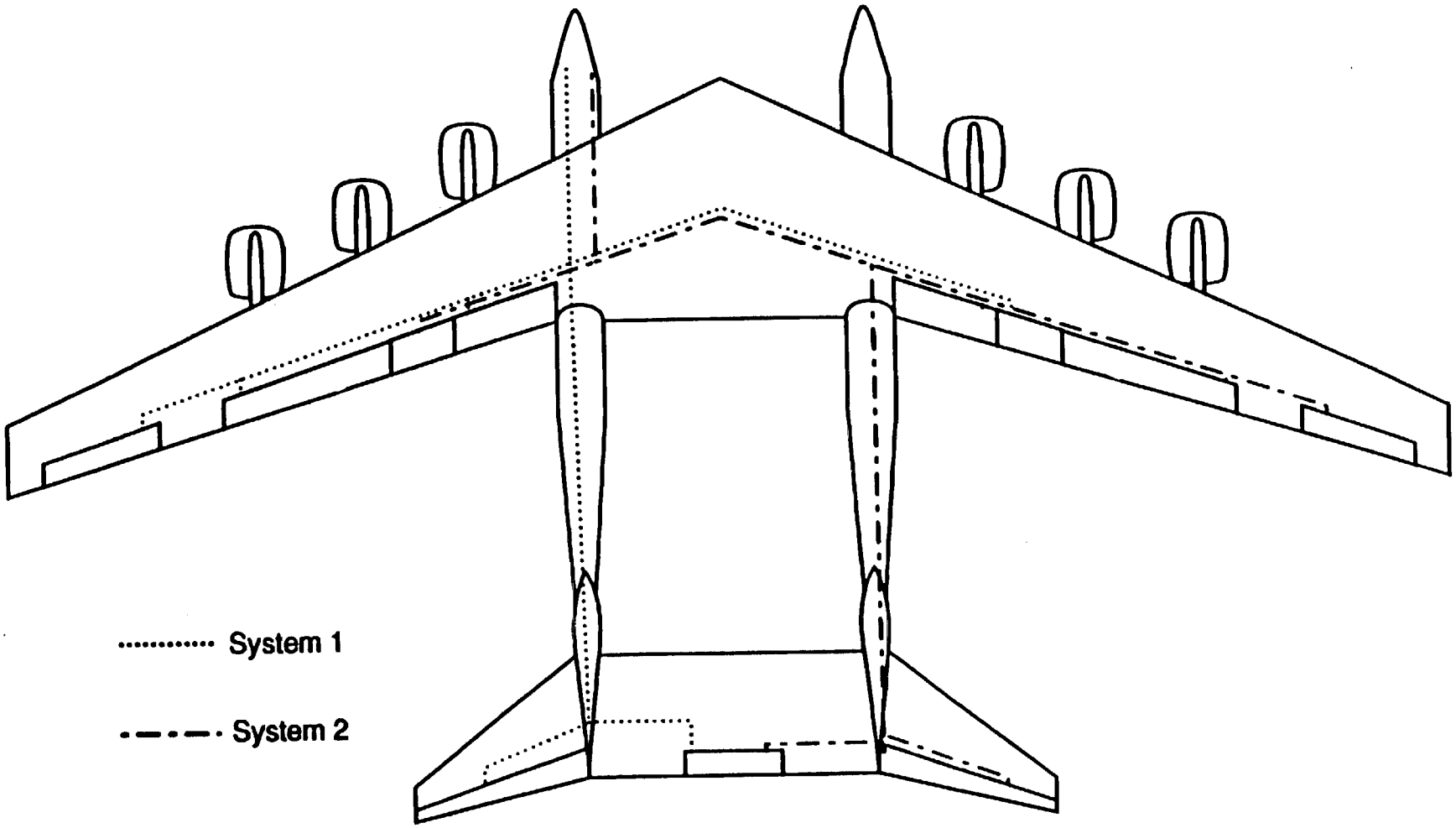

Fig. 8.5.4 Flight control cable layout

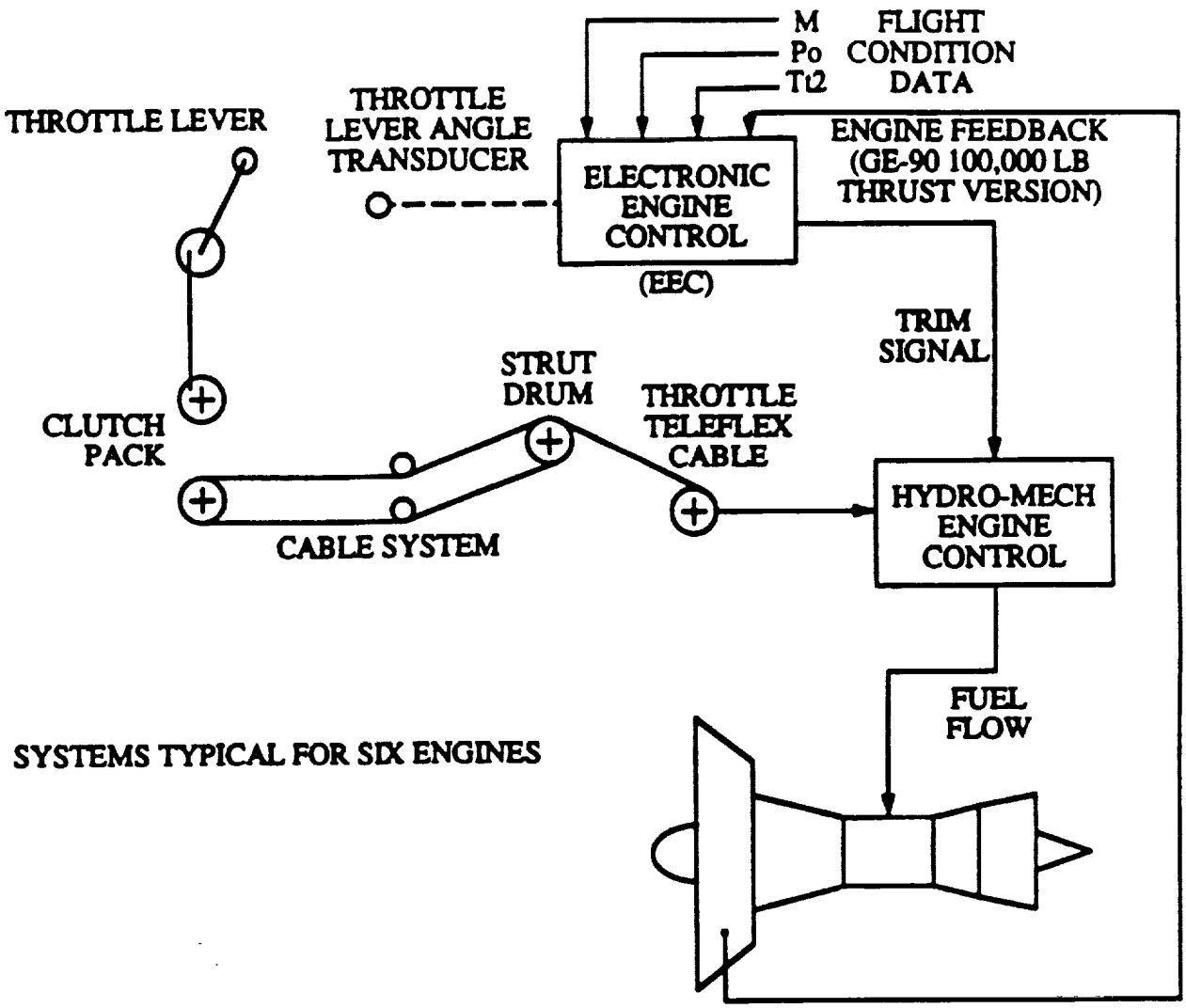

Fig. 8.5.5 Throttle control layout

Once the tanks were placed, the fuel lines and pumps had to be sized and placed. FAA regulations state that all fuel lines must be able to handle one and a half times the maximum fuel flow to the engines. The maximum fuel flow in our case occurs at take off with a thrust of 100,000 pounds per engine and a specific fuel consumption of 0.284 lbm/hr. So 28,400 lbm/hr or 9.4 ft^3/min, must be pumped. The pumps must therefore be able to pump 14.1 ft^3/min through 2 inch diameter fuel lines. Consult Figure 8.6.1 for tank and line placements.

Fuel lines were located between the first and third spars. In order to keep the center of gravity of the fuel at the center of gravity of the Eclipse at all time, normal one way flow baffles were not used, instead each tank is separated into several fuel cell inter connected by flow valves and pumps. A computer will keep the center of gravity of the fuel constant. Standard water drainage pumps and fuel venting lines are used much like those on the Boeing 747.

Surge tanks are located outboard of the main tanks to allow a volume for fuel to expand into. The auxiliary tanks are located inboard of the main tanks. Fueling is done through a single point located on the right wing. Cross feed lines run behind the first and third spars for fueling and to maintain airplane balance. The auxiliary power unit fuel is bled from the cross feed line behind the third spar.

8.7 Crew Issues

Since the current plans only call for use of the Eclipse once every other month, a training system is necessary to keep pilot proficiency. The most appropriate low cost method is a six degree of freedom ground based simulator. This simulator could be used on a regular basis to maintain pilot, copilot, and launch officer proficiency.

The simulator would give the pilot and copilot the flight experience which is vital to safe operations. No airplane of this size with a twin fuselage configuration exists. The pilot seat in the left fuselage will require retraining the pilot and copilot both for take off and landing as the motion cues will be quite different.

If deemed necessary, a flying simulator could easily be made at a future date. This simulator would employ the software designed for the ground based simulator to alter the flight characteristics of a business jet or small commercial jet to mimic the characteristics of the Eclipse. This used in conjunction with the ground based simulator would provide more than

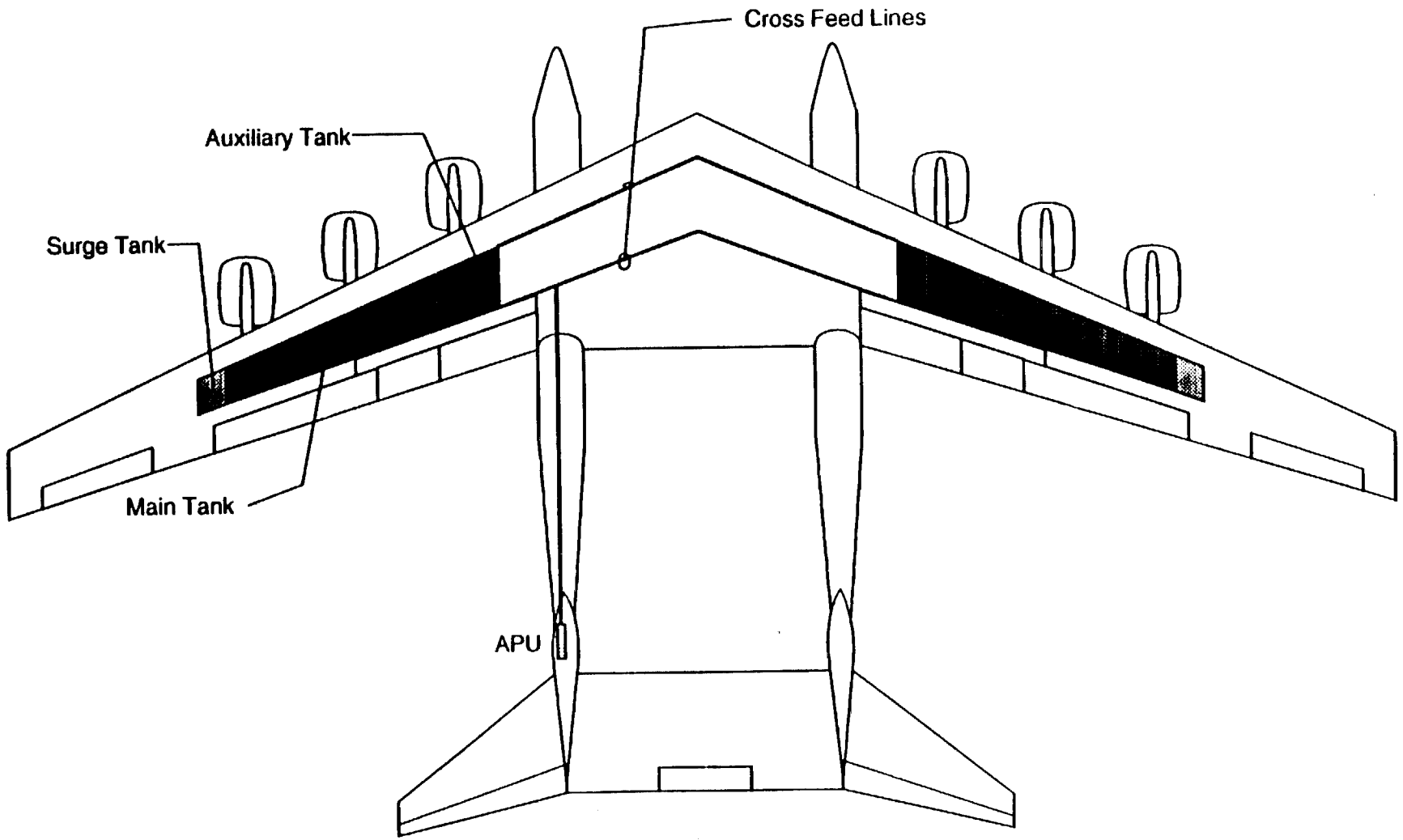

Fig. 8.6.1 Fuel system layout

sufficient training for the flight crew. The drawback to the flying simulator is the cost associated with maintenance of the simulator when not in use.

The cockpit is located in the left fuselage. The pilots sit on a raised platform in the cockpit for enhanced visibility over the nose. The launch panel operator sits on the right hand side of the fuselage, behind the raised platform. A galley and lavatory are provided in the cabin for crew comfort during the mission.

(This page left intentionally blank.)

9. COST ANALYSIS

There may be no greater challenge that this airplane must surmount than its budget. This section gives the background on the methods used to calculate the life cycle cost and per mission cost of the Eclipse. It is followed by the discussion on the financial viability of this project and the number of missions required to be flown in order to meet the initial cost goal of $10 million per mission for the airplane. Finally, a mission cost, including the Gryphon, is presented.

9.1. Cost Analysis Method: Overview

All cost analysis methods used for this section is based on statistical methods.[8] These methods are derived from empirical data collected from all types of existing airplanes. The take off weight of the Eclipse, at 1,227,000 pounds, is greater than the heaviest weight from the empirical data which could have effected the accuracy of applying this method to this particular cost analysis.

Since only two airplanes will be built, this program can be typified as a prototype production. Prototype production costs per airplane are higher than comparable manufacturing costs for a full production run. The Eclipse will cost significantly more than a comparably sized commercial or military airplane for this reason. However, there is no other airplane which can accomplish this mission. The question then becomes should the mission be modified to lower airplane cost or is this purchase price justified.

9.1.1. Airplane program

The overall stages of design, manufacturing, operation, and disposal make up the airplane program. The airplane program can be divided into six phases:

Phase 1 - Planning and Conceptual Design

The planning phase includes mission requirement research and deriving mission specification. The early conceptual design and cost analysis done by the Eclipse design team are in this phase. Although the cost of design by the design team is very inexpensive, the cost of further initial design required for the real production can be significant.

Phase 2 - Preliminary Design and System Integration

In this phase, serious design trade studies are conducted to find out what combination of technology and cost which might result in a viable airplane.

Phase 3 - Detail Design and Development

For most airplane program, during this phase the airplane and system integration design is finalized for certification flight testing and for production. However, this program requires minimal certification and will not be mass produced. Therefore, the cost for this phase will be significantly lower than the usual programs. The acquisition cost for the Eclipse is included in this cost as the procurement of test articles.

Phase 4 - Manufacturing and Acquisition

During this phase, the airplane is manufactured and delivered to the customer. No airplanes are delivered during this phase for this program and consequently, there is no cost associated with it.

Phase 5 - Operation and Support

The plane is acquired and operated. Support activities required for the operation are included in this stage.

Phase 6 - Disposal

The airplane is no longer operable. Disposal activities include destruction of the airplane and disposal of the remaining materials. In this case, there is no disposal cost as the airplanes will be donated to a museum.

Table 9.1.1 lists the specifications used for the cost analysis of the airplane.

Table 9.1.1 Airplane cost analysis specifications

Take off weight	1,260,000 lbf
Maximum sea level velocity	300 keas
No. of airplane to be produced	2 airplanes
No. of missions total	60 missions

The life cycle cost of is defined as the total cost for the six phases:

$$LCC = C_{RDTE} + C_{ACQ} + C_{OPS} + C_{DISP} \quad (9.1.1)$$

where:

LCC = life cycle cost [$]

C_{RDTE} = research, development, testing, and evaluation cost (Phase 1-3) [$]

C_{ACQ} = acquisition cost (Phase 4) [$]

C_{OPS} = operations cost (Phase 5) [$]

C_{DISP} = disposal cost (Phase 6) [$]

The acquisition cost is omitted from this analysis because due to the very low production number, all of the airplanes required for the mission are built during the research and development phase. Also the most of the flight testing cost was eliminated because the Eclipse is an experimental airplane and does not need extensive flight testing for certification.

9.1.2 Prototyping cost

The mission specification only requires one fully operational Eclipse and one additional Eclipse for spare parts and emergency purposes. Due to the low production number, the Eclipse airplane program can is a prototype program. A statistical relation, based only on a reduced empty weight, for estimating the cost of developing, manufacturing, and flight testing of a prototype program is used for this estimation:[8]

$$C_{PROT} = (1115.4)(10^3)(W_{ampr})^{0.35}(N_{prot})^{0.99}\frac{CEF_{thenyear}}{CEF_{1973}} \qquad (9.1.2)$$

where:

C_{PROT} = total cost for prototype program [$]

W_{ampr} = empty structural weight [lbf]

N_{prot} = number of prototypes to be built

$CEF_{then\ year}$ = cost escalation factor for 1993

CEF_{1973} = cost escalation factor for 1973

The cost estimation of the entire program derived from this method for the Eclipse using this method is $450 million. This figure is attractive, but appears low when compared to approximately $400 million to purchase two Boeing 747s, and was used only as a ball park estimations and as a guide for the later, more extensive, cost analysis.

9.1.3 Research, development, test, and evaluation cost

The research, development, test and evaluation (RDTE) cost is accumulated during phases 1 through 3. The RDTE cost is defined as following:

$$C_{RDTE} = C_{aed_r} + C_{dst_r} + C_{fta_r} + C_{fto_r} + C_{tsf_r} + C_{pro_r} + C_{fin_r} \qquad (9.1.3)$$

where:

C_{aed_r} = airframe engineering and design cost [$]

C_{dst_r} = development support and testing cost [$]

C_{fta_r} = flight test airplane cost [$]

C_{fto_r} = flight test operations cost [$]

C_{tsf_r} = test and simulation facilities cost [$]

C_{pro_r} = RDTE profit [$]
C_{fin_r} = RDTE finance cost [$]

Most important factors in calculating the airframe engineering and design cost are the empty structure weight and the maximum sea level velocity. It is assumed that the design incorporates only those technologies and materials which are readily available. It is also assumed that computer aided design is extensively used in the design process.

Due to the experimental and low production volume nature of the Eclipse airplane program, the cost of producing all of the required airplanes (one operational and one spare) is included in the flight test airplane cost.

The flight test operations cost will only include the cost of establishing the air worthiness of the Eclipse.

The test and simulation facilities cost is the cost of building a new dedicated test facilities. Although the program will require the use of existing test facilities whenever possible, due to the size of the Eclipse a special test facilities may be required.

The manufacturing company involved in this project will require a significant amount of profit. Usually the profit margin is set at 10% of the entire cost. However, due to the weak industry demands, the profit levels are currently very low for most companies. For the Eclipse airplane program the profit margin is set at 7%.

In most cases, due to the large amount of capital required, the manufacturer will borrow money to finance the RDTE phases. The finance cost is defined as the interest payment accumulated due to the borrowed capital. The current level is set a conservative 12%. It is of interest to note that it might be possible for this project to be considered for low interest governmental loans.

9.1.4 Operating cost

For the purpose of calculating the operating cost of the Eclipse airplane program, the military operating cost estimate methods are used. The military operating cost was chosen over the civilian operating cost because of the Eclipse airplane is an experimental airplane. The overall operation and missions will be similar to a military nature.

The program operating cost can be broken down as follows:

$$C_{OPS} = C_{POL} + C_{PERSDIR} + C_{PERSIND} + C_{CONSMAT} + C_{SPARES} + C_{DEPOT} + C_{MISC} \quad (9.1.4)$$

where:

C_{POL} = fuel, oil, and lubricant cost [$]

$C_{PERSDIR}$ = direct personnel cost [$]

$C_{PERSIND}$ = indirect personnel cost [$]

$C_{CONSMAT}$ = consumable material cost [$]

C_{SPARES} = spares cost [$]

C_{DEPOT} = cost associated with depots [$]

C_{MISC} = miscellaneous cost [$]

The cost of fuel, oil, and lubricant used depends on the type of airplane, mission of the airplane, annual utilization, and number of airplanes in active service. Compared to other costs in this program, this cost is almost nothing.

The direct personnel cost includes the salaries of the air crews and all maintenance crew. The personnel cost greatly depends on the personnel's skills and experience.

The indirect personnel would include those people in administration level and other support crews.

The consumable materials cost include degradable parts which must be restocked after each missions.

The spares cost is the cost of replacing all parts which are worn out and must be replace due to the operations.

The depot cost is the cost of overhaul, maintenance, and storage facilities.

The following miscellaneous cost elements contribute to the operating cost of the Eclipse:

1. Requirements for technical data to support maintenance functions
2. Requirements for training, training data and training equipment
3. Requirements for support equipment

9.1.5 Disposal cost

Although it is common standard practice to estimate the cost of the disposal when the airplane is no longer operable, due to the uniqueness of the Eclipse, it is reasonable to assume that the airplane can be donated to a museum. Thus, the cost of disposal for this airplane is neglected.

9.1.6 Life cycle cost

The actual life cycle cost of the Eclipse airplane, based on six missions each year for ten operational years, is found in Table 9.1.2.

Table 9.1.2 Eclipse life cycle cost (in millions of 1993 dollars)

Research, Development, Test and Evaluation Cost	$1.697 billion
Airframe Engineering and Design Cost	$327
Development Support and Testing Cost	$37.0
Airplane Manufacturing Cost	$999
Flight Test Operations Cost	$0.838
Test and simulation Cost	$16.6
RDTE Profit	$116
Cost of Finance	$199
Operation Cost	$18 million
Fuel, Oil, and Lubricants Cost	$3.45
Direct Personnel Cost	$5.05
Indirect Personnel Cost	$2.88
Consumable Materials Cost	$0.144
Cost of Spares	$2.34
Depot Cost	$3.60
Miscellaneous	$0.540
Total Life Cycle Cost	$1.715 billion
Cost per Mission	$28.6 million

9.2 Project Viability

The accuracy of the methods described earlier are questionable since the weight of the Eclipse is probably out of the accurate range for these methods. But as it currently stands the viability of the Eclipse airplane program is seriously threaten by the cost per mission. Based on the prototyping cost mentioned earlier in the chapter, the cost per mission of under $10 million was deemed possible. However, the more intensive method of cost estimation has resulted in the cost per mission of $28.6 million, almost three times over the recommended cost.

The biggest factor contributing to the high cost per mission is the conservative number of missions planned per year. The six missions per year for 10 years is not enough of missions to adequately defend this project. The relationship between the number of mission and the cost per mission is clearly presented in the Figure 9.2.1. By increasing the number of missions from 60

to 100, the cost per mission can be reduced from $28.7 million to $17.2 million. The target goal of $10 million per mission can be achieved by increasing the total to 175 missions.

The total number of missions can be increased in three ways. First, it can be increased by increasing the number of missions per year. However, market studies show that finding more than twelve customers per year (for six missions) will be very difficult to achieve. Another way to increase the total number of missions is to increase the operational life span. Most airplanes have operational life of more than 25 years. To use the Eclipse airplane for ten years when it is only flying six missions a year would be a great waste. The third way involves finding another mission for the Eclipse. While this would increase the number of missions, it would also increase the possibility of losing the airplane.

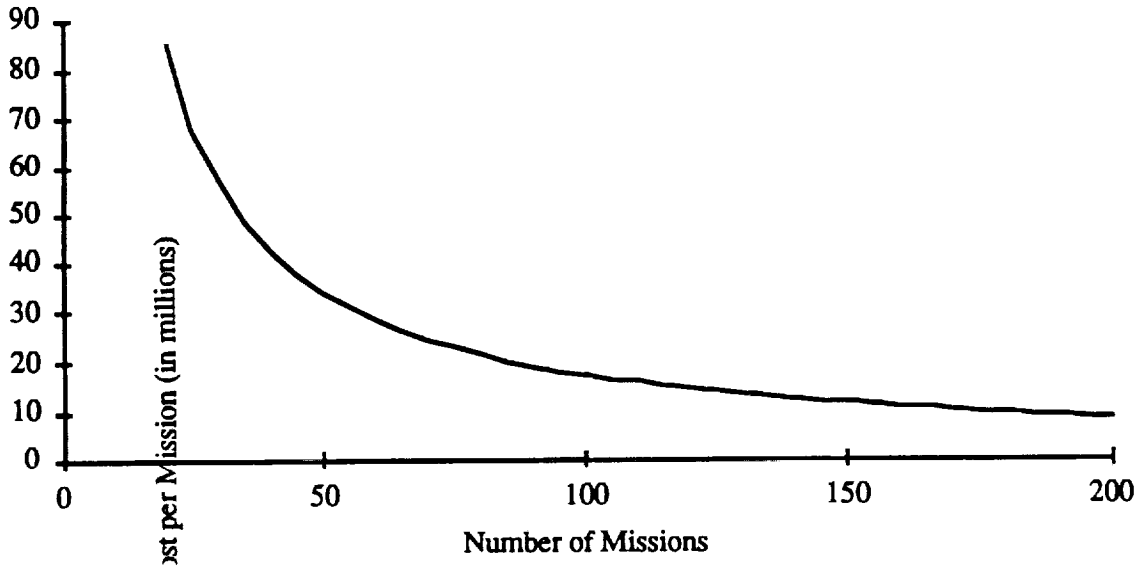

Fig. 9.2.1 Cost per mission versus number of missions

9.3 Total Mission Cost

Based on the single vehicle cost of the Gryphon, a total mission cost for a flight with a typical space booster can be calculated. The Gryphon is expected to cost $22.1 million per vehicle.[15] Adding this to the $28.6 million per mission for the airplane, a total cost of $50.7 million is anticipated for a vehicle launch. This is a very competitive cost for today's markets, even thought the original cost estimates were not met.

9.4 Future Recommendations

In order to secure the economic viability of the Eclipse airplane, a more detailed approach to the cost analysis must be found. More research is required to find an accurate method for estimating the manufacturing cost of the airplane of this magnitude. There may be ways to decrease the overall project cost to about $1.5 billion. This high cost could still represent a stumbling block to the program, however, as it is difficult to raise this much venture capital.

There are also many methods of reducing the overall cost which should be considered. One way to reduce the cost is possible leasing of the engines. Since the engines will be used only six times a year, it might be possible to lease the engines from General Electric rather than purchasing them. Another option would be to redesign with a high degree of commonality with an existing aircraft which would reduce part costs.

10. WIND TUNNEL TESTING

One of the original goals of the design project was to carry out wind tunnel testing on a model of the Eclipse to check the validity of the analytical methods. Fortunately, there was an opportunity to do testing in the beginning of June so a model was constructed and subsequently tested.

10.1 Model Fabrication

Due to the size of the Eclipse, the scale of the model had to be very small. A scale of 1:120 offered easy conversion and a wing size close to the maximum which could be manufactured on the mill. In order to accurately model the wing airfoil section, the wing was milled from a single piece of aluminum. The fuselages were made from wood which was cut to shape. The tails have an aluminum core with balsa wood added for the proper thickness and shape. They were then fiberglassed for durability. Flow on the wing was tripped with a strip of tape which was attached at the transition point predicted by the computational fluid dynamics work.

The first step in making the wing was to create a model of the wing in SDRC I-DEAS. This model was then used to generate computer numerical control (CNC) mill cutter paths. After post processing, the CNC mill cutter paths were checked for errors. Finally, the paths were run on a Bridgeport three axis numerical control mill. Finally, the wing was polished. Unfortunately, the wing was too thin at the trailing edge and was easily damaged. To avoid this, the rear 1/16" of the wing was removed. The manufacturing of the wing was supported by a National Science Foundation contract, #USE-91513228.

10.2 Test Results

Testing was conducted in the University of Michigan 5'x7' subsonic wind tunnel at speeds of 100 and 150 mph. The test data was then scaled to the 10,000 foot low speed loiter condition which corresponds to $Re = 39.4 \times 10^6$. Figures 10.2.1 and 10.2.2 are the lift curve and drag polar comparisons, respectively.

As can be seen from the lift curves, the slope is almost exactly as predicted. However, the zero lift angle of attack is not correct. This is most likely due to the lift effects of the tail and an improper mounting angle for the wing on the model. Also, there is a difference in the slope between the clean and with payload conditions. The assumption was made that flow would be

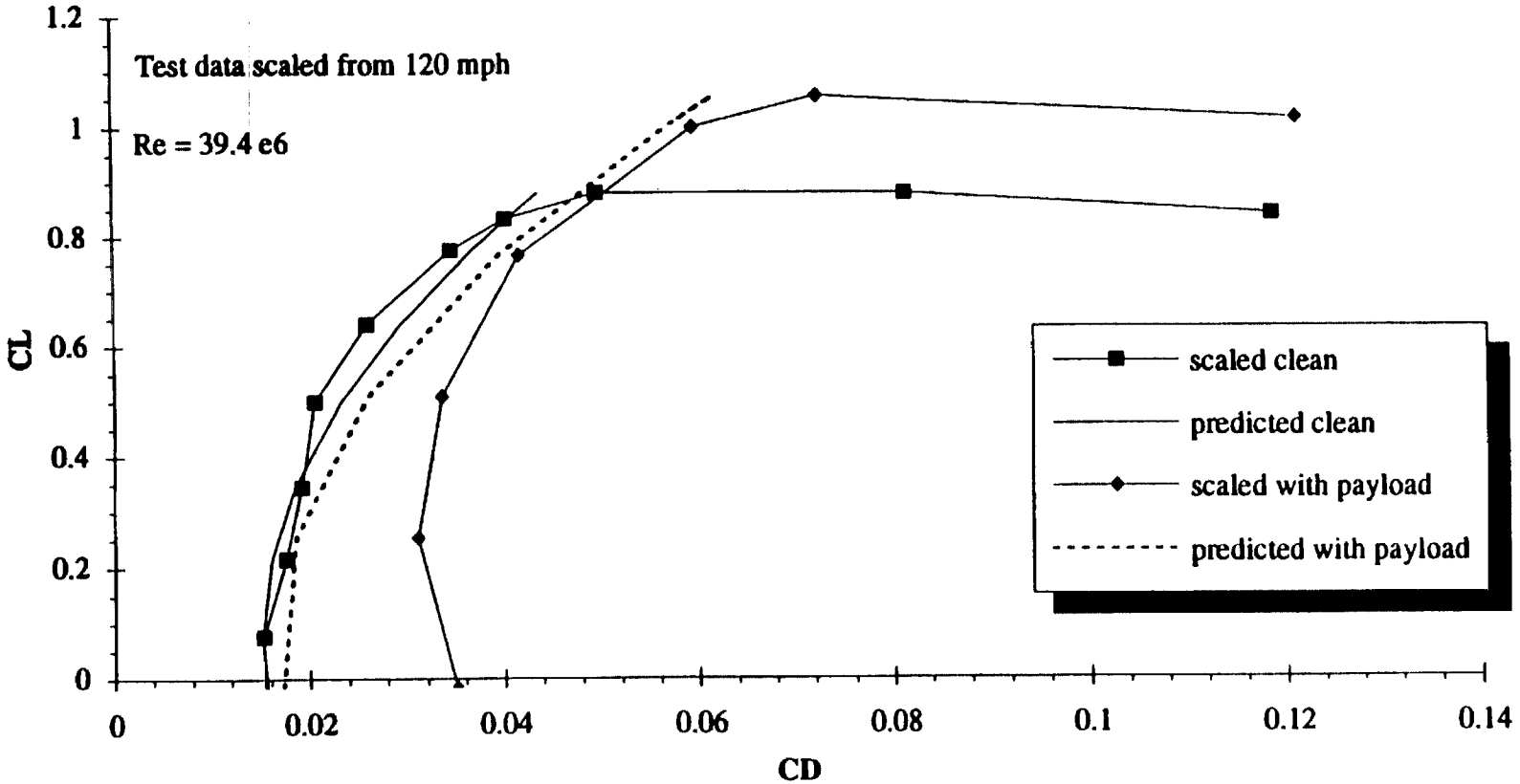

Figure 10.2.2 Wind tunnel drag polar comparison with predicted results

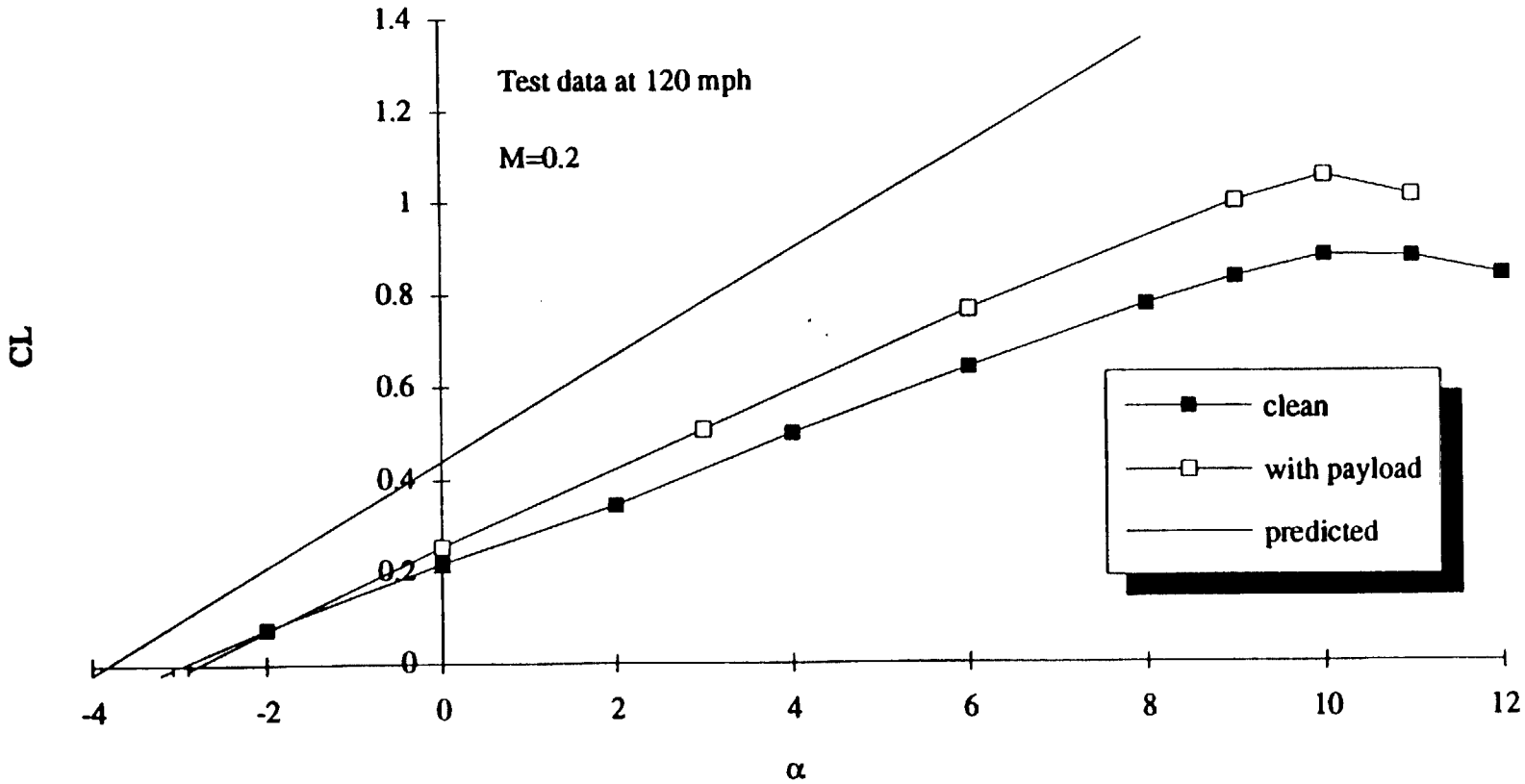

Figure 10.2.1 Wind tunnel lift curve comparison with predicted results

forced parallel to the wing and therefore not be altered by the payload. The change in slope is most likely due to the scale of the model, where the Reynold's number is not high enough to allow for the aforementioned assumption.

The clean drag polars show good agreement. The configuration with payload attached has a large discrepancy in C_{do}, however. This could be from a faulty prediction of the zero lift drag for the payload. Another explanation is that the scale of the model, with low Reynold's number, made for a large amount of choked flow between the fuselages. On the real model, the boundary layer would not be as large and therefore less choking would occur, lowering the drag.

11. CONCLUSIONS & RECOMMENDATIONS

The design presented for the Eclipse within this report meets or exceeds all of the mission specifications set out for the airplane. Namely:

- Payload capacity is 500,000 pounds and the payload can be dropped in flight
- Launch altitude is 43,500 feet, which is above the 40,000 foot specification
- The mission radius is 750 statute miles
- The airplane is capable of operating from existing runways
- Able to perform a 2.2g post launch maneuver
- Utilizes existing production methods and equipment

The Eclipse has some unusual design configurations to meet these specifications. Most noticeable are the twin fuselage design and the high aspect ratio wing. The twin fuselages allowed for better payload and landing gear integration while the high aspect ratio wing was necessary for maneuverability at high altitude. The Eclipse is powered by six GE-90 turbofan engines rated at 100,000 pound of thrust each. These are necessary for flight to altitude. There is a large number of wheels to distribute the loads on the runway. The other systems are modeled after similar systems on existing airplanes.

The design team has used some extra methods to get a better idea of some numbers which were questionable in Class II methods. An attempt to obtain better high angle of attack data using computational fluid dynamics was made. An analytical wing weight model was used to better model a significant portion of the airplane empty weight. Also, an in-depth performance analysis was made to better estimate airplane position and speed as well as fuel consumption. Wind tunnel testing was done to verify some of the assumptions which were made in the aerodynamics calculations.

It is technologically feasible to design an airplane capable of fulfilling the mission requirements. While the large up-front cost for the airplane may be prohibitive, if the airplane can be funded, financial feasibility for the program can be obtained in one of three ways: more Gryphon launches per year, a longer lifetime, or alternate missions for the Eclipse

The next logical step is to incorporate the knowledge gained in the wind tunnel testing into the calculations. Also, while most calculations were iterated to closure, there are some areas where more calculations could be done. Further discussions with the Gryphon design team could also help to optimize the design.

(This page left intentionally blank.)

12. REFERENCES

1 Roskam, J., *Airplane Design Part I: Preliminary Sizing of Airplanes*, Roskam Aviation and Engineering Corp., Ottawa, Kansas, 1989.

2 Roskam, J., *Airplane Design Part II: Preliminary Configuration Design and Integration of the Propulsion System*, Roskam Aviation and Engineering Corp., Ottawa, Kansas, 1989.

3 Roskam, J., *Airplane Design Part III: Layout Design of Cockpit, Fuselage, Wing and Empennage*, Roskam Aviation and Engineering Corp., Ottawa, Kansas, 1989.

4 Roskam, J., *Airplane Design Part IV: Layout Design of Landing Gear and Systems*, Roskam Aviation and Engineering Corp., Ottawa, Kansas, 1989.

5 Roskam, J., *Airplane Design Part V: Component Weight Estimation*, Roskam Aviation and Engineering Corp., Ottawa, Kansas, 1989.

6 Roskam, J., *Airplane Design Part VI: Preliminary Calculation of Aerodynamic, Thrust, and Power Characteristics*, Roskam Aviation and Engineering Corp., Ottawa, Kansas, 1989.

7 Roskam, J., *Airplane Design Part VII: Determination of Stability, Control and Performance Characteristics: FAR and Military Requirements*, Roskam Aviation and Engineering Corp., Ottawa, Kansas, 1989.

8 Roskam, J., *Airplane Design Part VIII: Airplane Cost Estimation: Design, Development, Manufacturing, and Operating*, Roskam Aviation and Engineering Corp., Ottawa, Kansas, 1989.

9 Berry, D.L., *Civil Aircraft Propulsion Integration: Current and Future*, Boeing Commercial Airplane Company, Seattle, Wash., Unpublished, Nov. 12, 1992.

10 Harris, C.D., "Aerodynamic Characteristics of a 14-Percent-Thick NASA Supercritical Airfoil Designed for a Normal-Force Coefficient of 0.7," NASA-Langley Research Center, Hampton, Virginia, NASA TM X-72712, July 1975.

11 Raymer. D.P., *Aircraft Design: A Conceptual Approach*, AIAA Educational Series, Washington, D.C., 1992.

12 Udin, S.V., and Anderson, W.J., "Wing Mass Formula for Twin Fuselage Aircraft," *Journal of Aircraft*, Vol. 29, Sept.-Oct. 1992, pp. 907-914.

13 Poth, S.M., Jr., et al., *Design of the Pegasus III Carrier Vehicle*, University of Michigan, Ann Arbor, Mich., Dec. 1992.

14 Choi, R., et al., Aerospace 481 Maize Team Report, University of Michigan, Ann Arbor, Mich., Dec. 1992.

15 Fisher, M.A., et al., *Project Gryphon: Air Launched Space Booster*, University of Michigan, Ann Arbor, Mich., June 1993.

16 Lewis, R.J., Sr., *Big Engine Data*, General Electric Aircraft Engines, Evendale, Ohio, Unpublished, Nov. 16, 1992.

17 Bengelink, R., Boeing Commercial Airplane Co., Seattle, Wash., Personal Conversation, Feb. 1993.

18 Vinh, N.X., Aerospace 440 Vehicle Systems Performance Unpublished Lecture Notes, University of Michigan, Ann Arbor, Mich., Jan.-May 1993.

19 De Zeeuw, D., Quadtree CFD Code, University of Michigan, Ann Arbor, Mich., Feb. 1993.

A. GRYPHON SUMMARY PAPER

PROJECT GRYPHON : AIR LAUNCHED SPACE BOOSTER

University of Michigan
Aerospace Department - Space System Design
Ann Arbor, Michigan

Professor Joe Eisley
James Akers, Teaching Assistant
Mike Fisher, Asst Project Manager
Krista Campbell, Adam Nagaj, Elizabeth Hilbert, Alan Ristow, Ron Shimshock

Abstract

The Gryphon Design Team has developed a next generation 500,000 lb air launched space booster. The Gryphon is launched from a 1.2 million lb aircraft, the Eclipse, at 44,000 ft. The primary purpose is the delivery of 7,900 lb to Geosynchronous Transfer Orbit (GTO) and 17,000 lb to Low Earth Orbit (LEO). With these payload capabilities, the Gryphon is able to beat out competitor launch vehicles cost per pound by 50% which allows investors a 15% return on their investment. The design has also allowed for the ability to supply Space Station Freedom, based on the Space Shuttles capabilities. Since the Gryphon was designed to compete with existing vehicles, cost has been minimized in all areas. Therefore, only 'off the shelf' technology has used in the design process.

Introduction

The goal of the Gryphon Design Team was to develop a 500,000 lb air launched space booster with the capability of delivering 7,900 to GTO and 17,000 lb to LEO. These payload goals were determined in order to beat the competition's cost by 50% to insure investor's of a 15% return.

The task of designing the Gryphon was daunting. No project of its size and nature had been previously undertaken. OSC has begun an initial study of a similar sized launch vehicle called Pegasus III, but they have yet to decide whether they will continue. An additional challenge stemmed from the 'real world' application of the Gryphon, since there is current commercial interest. This restriction has not allowed for the design of components and systems to be developed in the 'future', or without cost constraint. With the added dimension of a 14 week semester, the Gryphon has been designed as efficiently as possible, above and beyond all of the limitations imposed.

Reason for the Configuration

Robert Lovell of Orbital Sciences Corporation presented the idea of a large air launched space booster based on his department's belief in a market opportunity between the Space Station Freedom resupply needs and the commercial communications industry. The 500,000 lb weight suggestion was based on his intuitive knowledge of available engines and their capabilities. Other than his initial weight recommendation and stipulation of a 15% return, the entire project's development was left to the design team.

Unlike the Pegasus, which is carried underneath a L1011, the Gryphon's weight caused an entirely new aircraft to be developed in order to carry it into the upper atmosphere. The Eclipse Design Team, which designed the carrier airplane, specified a drop at approximately 40,000 ft at a speed of 500 mph. With this knowledge, the technical groups proceeded in their research and design. At the start, the Pegasus was used as a baseline and many aspects were designed as larger upgraded versions of those found on the Pegasus. However, it was quickly realized that extrapolating components from a 40,000 lb vehicle to a 500,000 lb vehicle was not always possible. Even though many aspects from the Pegasus could not be used, the Gryphon still resembles current launch vehicles. All the systems and components are currently available. Its final configuration results from a combination of cost, simplicity, and available technology. Figures 1 and 2 show a transparent view of the Gryphon and how the Eclipse and Gryphon look while attached.

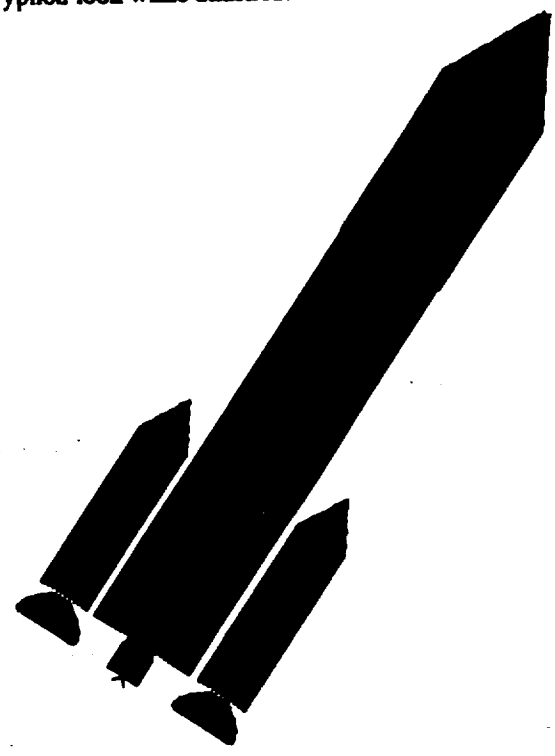

Fig 1 Transparent View of Gryphon

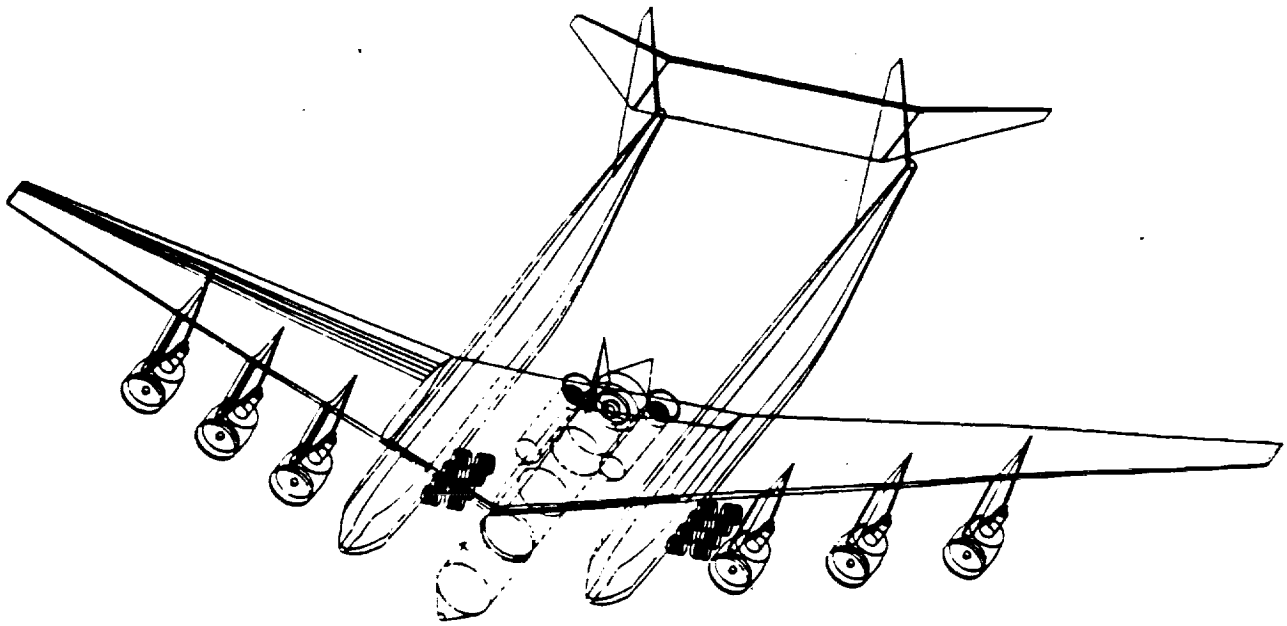

Fig 2 Gryphon and Eclipse attached

Cost Analysis

The most important aspect of this project is to give investors a 15% return on their investments. To achieve this, the cost (per pound of payload) of the Gryphon was determined in order to beat the launch prices (also per pound of payload) of chief competitors by at least 50%. This leaves the other 50% for financing, insurance, and profits while still having a competitive price.

Gryphon's main competitors in the satellite launch market are the Ariane 4, Atlas Centaur, and Titan 3. The price data for these and other launchers are listed below in Table 1. Note that Ariane prices are in 1990 dollars, Atlas and Titan prices are in 1991 dollars, and numeric figures are averages.

Table 1 Launch Prices of the Competition

Launch Vehicle	Payload Size (lb)	Launch Price	Price per Pound
Ariane 40	4,190	$ 65 million	$ 15,513
Ariane 42P	5,730	$ 67 million	$ 11,692
Ariane 44P	6,610	$ 70 million	$ 10,590
Ariane 42L	7,050	$ 90 million	$ 12,766
Ariane 44LP	8,160	$ 95 million	$ 11,642
Ariane 44L	9,260	$ 115 million	$ 12,419
Centaur	5,148	$ 60 million	$ 11,655
Titan 3	10,978	$ 110 million	$ 10,020

Using the market average price per pound of the competition derived from Table 1 and an inflation factor of 4.5% per year, a project goal cost per pound of $ 6,200 was determined. This cost per pound translates into a payload of 7,900 lb to GTO and a per mission cost of $49 million.

The final cost analysis is given below in Table 2. The costs given are high estimates and include a fifty million dollar development cost (which is what OSC used for their Pegasus program).

Table 2 Cost Analysis

Airplane Cost	$ 1,000 million
Project Costs	$ 106 million
Vehicle Cost	$ 28 million
Airplane Operating Costs	$ 2 million

The total mission cost was calculated by dividing the one-time costs (the airplane and project costs) by sixty launches and adding the per launch costs for the vehicle and plane operation. Sixty launches was chosen as a realistic estimate for the number of launches that would be performed over ten years. This estimate is based on the recent satellite market. Table 3 shows the final mission cost of the Gryphon. It should be noted that this cost estimate meets the project goal of $49 million per launch.

Table 3 Cost of Gryphon

Total Mission Cost (60 launches)	$ 48.3 million

Per Launch Cost

The per launch cost of the Gryphon is $27.9 million, while the per launch cost of the Eclipse is $2 million. A $1 billion fixed cost of the Eclipse must be evenly spread over each launch. For a projected duration of 60 launches, this calculates to a total average cost per launch of $46.6 million. The minimum price that can be charged per launch and still turn a profit in the last year is $65.2 million. This includes an additional 18% for insurance. Disregarding the amount per launch towards insurance premiums, the Gryphon grosses $55.2 million per launch. The net profit is the amount grossed per launch minus the total expenses per launch resulting in a net profit margin of $8.6 million per launch.

Vehicle Configuration

The Gryphon consists of three stages for the GTO configuration. For the LEO configuration, the third stage engine and propellant tanks are removed and replaced with pure payload. Both configurations use solid and storable liquid fuels. For the GTO version, a cryogenic third stage is employed.

All of the major components on the Gryphon are listed in Table 4 and the overall parameters in Table 5. A picture detailing all of the major systems within the Gryphon is shown in Figure 3.

Table 4 Major Components

Stage 1	Stage 2
2 Castor Solid Rocket Motors	2 LR91 Liquid Rocket Motors
LR91 Liquid Rocket Motor	Gryphon-Eclipse Rings 3 - 8
Gryphon-Eclipse Rings 1 & 2	Plane Attach Rings 2 & 3
Engine Mount	External Skin
Plane Attach Ring 1	Strut Support Ring
Vertical Tail	Engine Mount
Interstage Ring	Interstage Ring
Aft Nozzle Cover	
Fairing Attach Rings	

Stage 3
1 RL10A-4 Cryogenic Liquid Fuel Rocket Motor
Payload Interface
External Skin
Engine Attach
Power/Avionics Ring
Cabling
Hydrazine/Oxidizer & Tanks
Control Thrusters
Venting System
Thermal Control
Batteries
CPU
Radar Transponder
Telemetry Transmitters
GPS
Inertial Guidance (IMU)

Table 5 Overall Parameters

Parameter	GTO	LEO
Stage 1,2,3 and ANC	479,056 lb	476,368 lb
Components on Eclipse	10,435 lb	10,435 lb
Total Gryphon Weight	489,491 lb	486,803 lb
Total Length with ANC	124 ft 3 in	104 ft 5 in
Total Length without ANC	106 ft 3 in	86 ft 5 in
Width	32 ft 2 in	32 ft 2 in
Height	30 ft 0 in	30 ft 0 in

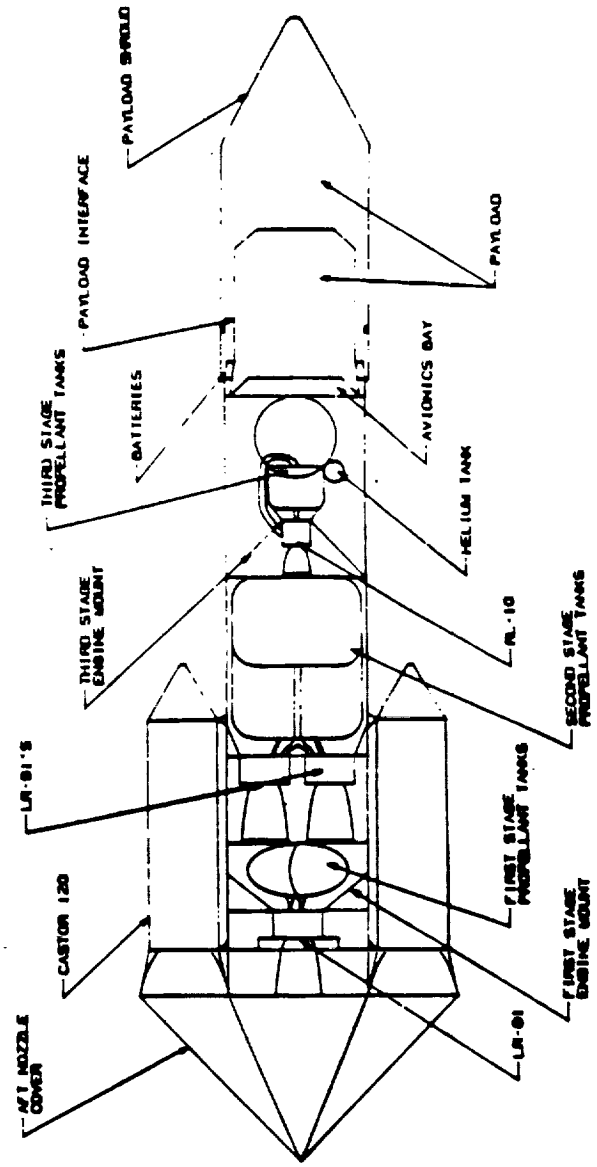

Fig 3 Internal Components

Mission Analysis

Trajectory

Analysis of the Gryphon's ascent trajectory was completed using nomographs and a series of equations. Initial vehicle parameters were read from the nomographs, and the results were substituted into the appropriate equations. A MATLAB routine was written to solve the system of equations that yielded the second stage trajectory.

Initially, the Gryphon is dropped from the belly of the Eclipse aircraft. The aerodynamic shape of the Gryphon causes it to pitch up approximately 20 degrees during the ensuing 10 second drop. At this point, the first stage engines ignite and the Gryphon begins its ascent into space.

The Gryphon pitches upward at a rate of 6.25 degrees per second until it reaches a pitch angle of 10 degrees from vertical. Pitch control is achieved by gimballing the engine nozzles. The Gryphon pitches back down before second stage ignition, to an angle of 70 degrees from vertical. Pitch

down is achieved via a gravity turn in order to minimize gravitational energy losses.

The first stage engines burnout at an altitude of 130,397 feet and a velocity of 7,297 feet per second. Second stage ignition follows, accelerating the Gryphon to a circular parking orbit. The engines burn out at an altitude of 574,240 feet and a velocity of 24,864 feet per second. At this point, the vehicle has entered low Earth orbit (LEO). The payload shroud is jettisoned along the way, at an altitude of 200,000 feet.

The method of analysis for the second stage assumes a non-atmospheric, low altitude circular orbit and a constant pitch rate of 0.075 degrees per second.

Once the parking orbit is reached, the second stage is ejected and the Gryphon orbits until it reaches the proper position for insertion into geotransfer orbit (GTO). Finally, the third stage engine ignites, and GTO insertion is completed.

Aft Nozzle Cover Design

The aft nozzle cover (ANC) was designed to reduce the drag of Gryphon while it is being carried by the launch plane. Since the ANC is dropped into the ocean following separation from the plane, the goals for this design were to make it as light and inexpensive as possible. Initial designs have the ANC being constructed out of reinforced molded fiber glass, this should reduce weight, while giving the ANC enough strength to support its own weight and any loads incurred during the plane flight, separation and drop.

Propulsion

When designing the Gryphon's propulsion system three goals were recognized. The first goal was to assure the safety of the vehicle. This space booster is attached to an aircraft carrying crew members. Dangers of the different propellants had to be explored to minimize potential hazards to these personnel and the airplane. The second goal was to have the minimal amount of complicated connections with the Eclipse. The third goal involved the overall vehicle weight of approximately 500,000 lb. This weight required a study into high performance engines that would give as much thrust as possible for minimal propellant.

System Selection

Many various staging configurations were investigated. However, each version tested resulted in severe limitations, as seen in Table 6.

Table 6 Rejected Configurations

Configuration	Drawback
All solid fuel	Not enough payload, Too heavy
No cryogenic fuels	Not enough payload, Too heavy
Cryogenic Stage 2	Safety concerns
Extra Stage	Too expensive

Consequently, the final design resulted in a three stage system composed of:

Table 7 Propulsion Configuration

Stage	System	Fuel
1	2 Castor 120's	Solid
1	1 LR91-AJ-11	Storable Liquid
2	2 LR91-AJ-11	Storable Liquid
3	1 RL10A-4	Cryogenic Liquid

The chosen configuration allows for the Gryphon to meet its payload and ultimately it cost goals. The combination of the three fuel types allows for a successful orbit, while minimizing possible hazard.

Staging

The first stage engines include a LR91-AJ-11 mounted in the middle of the main body and two Castor 120 solid rocket boosters attached symmetrically to the sides. The elliptical propellant tanks, containing nitrogen tetroxide for oxidizer and Aerozine-50 for fuel, are mounted just ahead of the LR91. Control of the booster is provided by a vertical tail and gimbaled nozzles on all three engines.

After the Stage One engines and structure have jettisoned and a coast phase is completed, two LR91-AJ-11's ignite for the second stage. The propellants are the same for the first stage LR91 but are contained in two large, nearly cylindrical tanks. Gimbaled nozzles again provide stability.

For a GTO mission, these engines are released and after another coast phase, a RL10A-4 engine ignites and burns cryogenic propellant. Liquid oxygen is supplied from a nearly cylindrical tank just ahead of the engine and liquid hydrogen is supplied from a spherical tank attached in front of the oxidizer tank. The RL10's vectorable nozzle provides control along with RCS thrusters. For a LEO configuration, this stage is not needed and orbit can be established after the second stage. Refer to Figure 4 to see the overall propulsion system configuration.

Payloads

The Gryphon was designed with the goal of meeting several important payload delivery criterion. These payload related criterion consisted of the following:

- The delivery of 7900 lb, including payload support structures, to GTO
- The delivery of 17,000 lb, including payload support structures, to LEO
- The maximization of usable payload envelope
- The capability for multiple-satellite deployments to both LEO and GTO
- The compatibility of delivering Space Station Freedom related payload packages

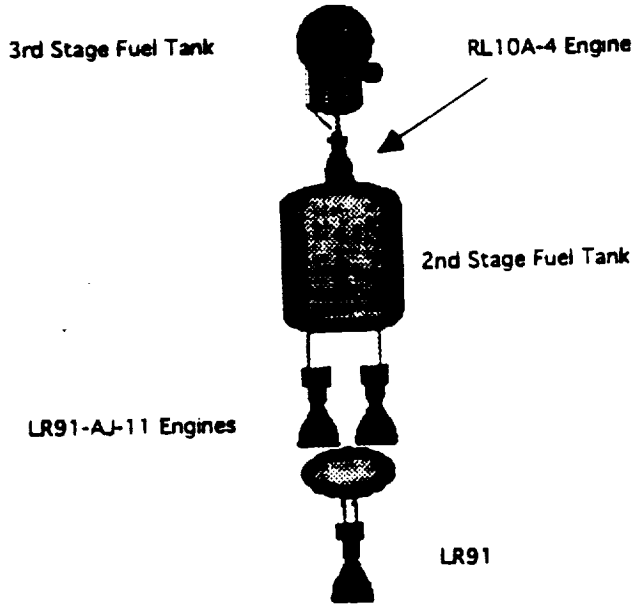

Fig 4 Overall Propulsion System

These goals acted as the driving force behind the design of the Gryphon. The delivery weights of 7900 and 17,000 lb for GTO and LEO missions were decided upon after careful consideration of the likely market demand and the cost analysis. The geosynchronous delivery limit will allow the booster to carry a large majority of the currently existing commercial communication satellites to their transfer orbits, utilizing either single or multiple payload configurations. The low earth capability will allow for the delivery of a large variety of scientific satellites, either in single or multiple configurations. This 17,000 lb limit and 15 ft diameter will also allow for the delivery of payload packages to the Space Station Freedom.

Payload Bay Dimensions

The volume of the Gryphon payload envelope was maximized in order to ease satellite design and payload configuration constraints. The maximization of the payload envelope provides several attractive features for potential booster customers. First, a large payload volume allows customers to relieve launch cost burden by participating in multiple customer/satellite deployments. Second, a large payload bay eases the design constraints which commercial and scientific satellite producers must adhere to. Third, a large payload volume, in the case of the Gryphon allows for compatibility with proposed Space Station Freedom related payload packages. These packages have a large diameter of 15 ft and lengths between 10 - 15 ft and therefore are able to be delivered by few launch systems.

Satellites are usually cylindrical in shape when in the launch configuration. They cover a large range in size, but average 7-10 ft in diameter and 8-12 ft in length. The volume of the payload bay, approximately 19,675 cubic feet, is large enough to accommodate both of these payloads in various configurations (single, double, and possible triple stacked). The final design of the Gryphon payload envelope is shown in Figure 5.

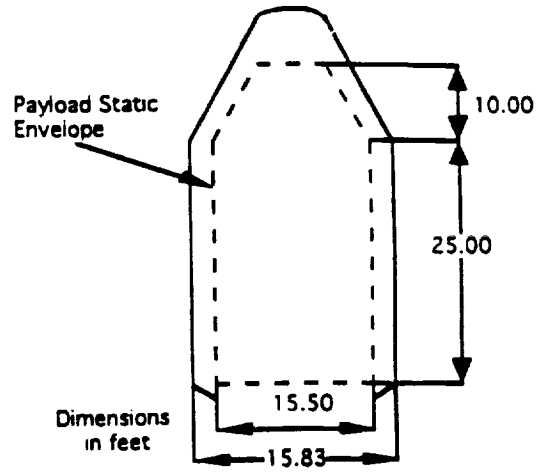

Fig 5 Payload Bay Dimensions

Space Station Freedom Options

The Space Station Freedom has been designed to be built and resupplied by the Space Shuttle. Although the shuttle may be the most efficient vehicle to boost the actual space station components into space, it is not the most efficient launch vehicle for some of the resupply missions. Therefore, the Gryphon has been designed to be capable of boosting some of the space station resupply payloads more cost effectively.

All resupply of the space station has been compacted into four main elements each designed to be held in the space shuttle payload bay. The major consideration in determining which elements the Gryphon would be able to boost was size and weight. Therefore, listed below (Table 8) are all of the elements with their respective sizes and weights (with cargo).

Table 8 Space Station Module Parameters

Module	Weight (lb)	Dimensions
PKM	34,750	Dia - 14.6 ft Length - 23 ft
MPLM	18,050	Dia - 14.6 ft Length - 12.5 ft
ULC	18,695	6.8 x 4.3 x 12.5 ft
PM	11,040	14.7 x 7.3 x 13.8 ft

Although all of the above modules are about the right size to fit into the Gryphon, the PLM is much too heavy to be considered. The PM is well below the maximum weight of 17,000 lb to LEO. The MPLM and ULC are just a little above the maximum weight. However, 41.6% of the MPLM's weight and 18.4% of the ULC's weight is in the carrier alone. If these packaging weights could be reduced by as little as 10%, the Gryphon would be able to handle these modules. Consequently, the Gryphon should be able to carry the MPLM, ULC, and PM.

Guidance, Navigation, and Control

Guidance, Navigation, and Control (GNC) is the most important responsibility of Mission Control. Mission Control must be able to accurately keep track of Gryphon's position, velocity, and acceleration in order to determine what attitude controls need to be implemented. The main areas of concern to assure the reliability of GNC are the location of Mission Control, telemetry, tracking, and command, inertial measurement, the global positioning receiver, and the on-board computer.

Mission Control. Since the Gryphon is similar to OSC's Pegasus and will be performing similar missions, there is no justification for building a new system. If the Gryphon uses the same existing ground support infrastructure the Pegasus utilizes, the missions will have already been matched to the system because of this mission similarity. Mission similarity will also have the advantage of reducing contractual negotiations required for the Gryphon.

Telemetry, Tracking and Command. The Gryphon project will employ all telemetry, tracking and command (TTC) services from the Eastern and Western Space and Missile Centers. All captive carry takeoffs from Kennedy Space Center will be supported by the eastern range, and all those from Vandenberg AFB will be supported by the western range.

Inertial Measurement Unit. Inertial reference is supplied by the strapdown inertial measurement unit (IMU), consisting of integration gyroscopes, linear accelerometers, and sensor electronics. A single gyro produces one component of the total angular inertial reference, which is known in body defined coordinates. Each accelerometer provides one component of the linear inertial constant, where each component corresponds to one body defined axis.

The Litton LR-81 system is the choice of this design. It is currently under contract for use and is thus readily available and cost effective, while providing the functions desired on the Gryphon system.

Global Positioning System Receiver. Using both cost effectiveness and reliability as primary criteria for selection, the Trimble Quadrex is the GPS Receiver chosen for use on Gryphon. Trimble also provided the six-channel GPS Receiver that was used on Pegasus, but the Quadrex is an improved version in that it includes a multiple antenna. The multiple antenna provides both better visibility and attitude determination.

Launch Panel Operator

It was decided that one additional crew member, onboard the Eclipse a Launch Panel Operator (LPO), would be needed to monitor the Gryphon's system's systems before and immediately after launch. Their responsibilities will include:

- Monitoring Gryphon and payload status
- Provide external power to Gryphon
- Switch between external and internal power (prior to launch)
- Update Gryphon IMU prior to release
- Download mission data to the flight computer and verify mission data
- Prepare and enable vehicle for drop
- Capture, record, and display data from the vehicle and payload

The LPO will be seated at a console that consisting of a ruggedized PC, display devices, a mass data storage device, and a precision IMU.

On-Board Computer

The on-board computer system interfaces with the sub-systems and determines the course of action that they should take. In short, it functions as the brains behind the Gryphon and plays a critical role in the success of the mission. Table 9 details the characteristics of the chosen computer for the Gryphon

Table 9 Characteristics of Gryphon Computer

Processor	32 bit, 68000 Motorola based
Architecture	Versa Module Europe Bus
Telemetry processor	16 bit
Weight	10 lb
Dimensions	4" x 8" x 8"
Temperature tolerance	-40 °C to +85 °C
Reliability	0.95 at end of 10-year period
Radiation protection	hardening to 1 Mrad
Vib. amplification	close to factor of 1

Communications System Overview

The Gryphon's communications system provided the link between the spacecraft and ground control after launch from the carrier aircraft. The communication system will transmit telemetry and tracking data to the ground control station and transmit termination commands, if necessary, from the ground to the Gryphon.

Tracking data will consist of position, velocity, attitude, and acceleration information received from the GPS and the IMU. If necessary, the termination command will be sent via an encoded (for security purposes) signal from the ground to be received and decoded by specific FTS (Flight Termination System) hardware on the Gryphon. All of the mission control components (i.e. the CPU, GPS, and Inertial Guidance Systems) are bolted to the top of the avionics bay (See Figure 3).

Structures

In general, each stage has the following structures:

- Engine mounts
- Propellant tank supports
- Interstage connections
- External skin with reinforcements

Additionally, the payload and avionics are supported by dedicated structures.

Investigation into the exact dimensions and structural capabilities of all of the structural components was done (where applicable) using laminate modeling, buckling analysis, ply failure analysis, stress analysis, finite element modeling and analysis and displacement analysis in SDRC I-DEAS.

Overall Structural Components

In the first stage, each Castor 120 has two sets of two attach struts which connect it to the main body of the Gryphon, which is a 1/64 in aluminum shell bolted to stringers and buckling rings. Each Castor 120 also has a conical fairing mounted on its top to reduce drag. The LR91 is held in place by an engine mount, and the LR91 and its propellant tanks are encased by a reinforced external skin. An interface ring links the skin with the interstage connector. The interstage connector sheaths the nozzles of the second stage engines.

The second stage consists of two LR91's affixed to the Gryphon by means of the second stage engine mount. The engine mount then transfers the thrust produced by the engines to the total vehicle The reinforced external skin covers the propellant tanks and support structure for this stage. An interface ring connects the skins of the second and third stage.

The third and final stage has an engine attach which unites the RL10 with the propellant tanks. A structure mount supports the engine and fuel tanks which are designed to carry the thrust load while a payload interface attach connects the third stage with the payload area.

The volume between the power/avionics ring and the payload interface attach comprises the avionics bay. Navigational modules are attached to the power/avionics ring via an adapter plate. In the dual-satellite configuration, the first payload is mounted directly to the power/avionics ring, and the second payload is mounted to the payload interface which surrounds the first satellite. A payload shroud encloses the entire payload/avionics area. As with the Castor 120 fairing, the payload shroud conically tapers to a point to reduce drag.

For a LEO launch, the third stage is removed and the second stage interface ring is attached directly to the payload interface attach. All other structures remain the same as for a GTO launch.

Payload Shroud and Solid Booster Fairings

Both the payload shroud and solid booster fairings are constructed of the same composite materials, but with different ply orientation and core thickness. The material used is a sandwich composite of 5056 aluminum honeycomb, with piles of 0.0055 inch carbon epoxy, both of which are from the Hexcel Corporation. The choice of this system is because of its strength, light weight, and extensive use in aerospace applications. Table 10 shows characteristics of the shroud and fairings.

Table 10 Shroud and Fairing Characteristics

	Overall Thickness	Aluminum	Carbon Epoxy	Number of Piles
Shroud	0.948 in	0.75 in	0.198 in	18
Fairings	0.485 in	0.375 in	0.11 in	10

Payload Interface

The Payload Interface (PI) supports and protects the payload during ascent. It is roughly 16 feet high and has a diameter which varies between 10 and 14 feet to adapt to various payloads. It can support two satellites with a maximum weight of 5000 lb each.

The PI consists of an aluminum skin that is 1/64" thick. The skin is reinforced with beam supports. Along the outside, eight I beams run the length of the PI. These are aluminum beams with a 1" I-beam cross section. Around the top of the PI, a ring is positioned to interface with an upper satellite. This ring was modeled as a 3" I beam section, made of aluminum. A second ring, 14' above the base of the PI, supports the structure against buckling and is a 1" I beam made of titanium. Finally, a third supporting ring is positioned 10' above the base of the structure. Again this ring mainly prohibits buckling, and is composed of titanium. The lower satellite is supported by a truss structure originating from the base of the PI, and running inside the skin. The entire structure weighs 636 lb.

Engine Mounts

Stage 1. The LR91 engine includes a 15" diameter attach ring used to join the engine to the structure. The base of the Stage 1 engine mount connects to this ring, and a tubular truss structure transmits the thrust load to the exterior hull via four attach points (see Figure 6).

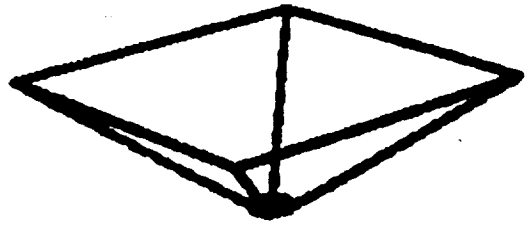

Fig 6 Stage 1 Engine Mount

The mount is constructed of A333 steel, due to its high yield strength (75 ksi), high stiffness, and availability in pipe form. Having a total weight of 349 lb, the mount is capable of transmitting 105,000 lb of thrust from an LR91 engine to the exterior hull. It has a height of 48" and fits inside the 180" hull diameter.

Stage 2. The Stage 2 Engine Mount holds two LR91 engines side by side and connects them to the external hull. The mount attaches to the engines at its base, similarly to the Stage 1 mount, and to the hull at six connection points on the top. The Stage 2 mount is shown in Figure 7.

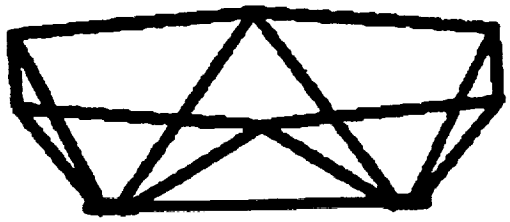

Fig 7 Stage 2 Engine Mount

The mount is constructed of A333 steel, due to its high yield strength (75 ksi), high stiffness, and availability in pipe form. With a total weight of 646 lb, the mount is capable of transmitting 210,000 lb of thrust to the exterior hull. It has a height of 40" and fits inside the 180" hull diameter.

Stage 3. The Stage 3 support structure has two primary functions. First, it supports stage 3 in the early stages of the mission and second, it connects the RL10 engine to the stage 3 spherical fuel tanks. Figure 8 shows the support structure and engine mount together.

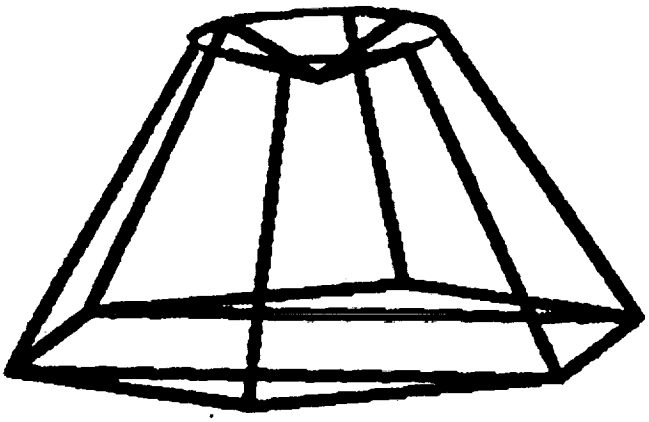

Fig 8 Stage 3 Engine Mount

During stage 1 and stage 2 burn, the structure acts as a support, carrying the 17,400 lb stage 3 under acceleration loads of up to 5 g's. After stages 1 and 2 burn out, the engine attach transmits 20,000 lb of thrust from the RL10 engine to load carrying fuel tanks. The support structure is a tubular aluminum truss with a total weight of 234 lb. Aluminum provides a high strength to weight ratio and an acceptable stiffness for this application. The Stage 3 structure has a height of 90" in order to accommodate the RL10 nozzle inside it, and its sides slope from a diameter of 180" where it connects with stage 2, to a 72" diameter at the fuel tank interface ring.

Attitude Control

To fulfill the requirements of attitude control and payload deployment, the Reaction Control System (RCS) will use Thrust Vectoring from the main rocket engines and an additional series of small hydrazine thrusters

Free Fall

Because of the danger of an explosion when the first stage main engines are ignited, the booster must be at least a half mile (2640 ft) from the airplane before ignition can occur. To ensure the half-mile separation distance, the Gryphon must drop through a vertical distance of 1188 ft for the LEO configuration and 1258 ft for the GTO configuration. The Mission Analysis Group determined that a vertical tail will provide the required yaw control.

During the free fall period, which lasts approximately 8.5 seconds, the booster pitches up 20 degrees to allow the main engines to propel the booster into the correct trajectory after ignition. A detailed aerodynamic analysis showed that this pitch-up maneuver can be satisfactorily accomplished by utilizing the aerodynamic forces that naturally result from the free fall. The maneuver calls for the separation of the ANC from the booster as soon as enough clearance exists between the booster and the plane. For both configurations, this occurs approximately 2.25 seconds after release at an absolute distance of 261 ft from the plane. The separation of the ANC shifts the booster's center of pressure forward nearly 10 ft, greatly increasing the aerodynamic pitch-up moments that result from the booster's downward velocity.

After 8.5 seconds the booster is pitched at the correct 20 degree inclination from horizontal. The vertical drop distances mentioned above are greater than those required for the minimum half-mile separation distance. The additional drop distance was required in order to complete the pitch-up maneuver.

The analysis showed that the engines were capable of regaining control of the booster's attitude and pitch rate, and that full recovery (0 angular velocity) occurred at 14.25 seconds. The final recovery angle for the LEO configuration (84 degrees from horizontal) is higher than that for the GTO configuration (62 degrees from horizontal). Because the center of mass for the LEO booster is closer to the base of the rocket, the moment arm of the aerodynamic forces is greater for this configuration. The resulting increase in the aerodynamic pitch-up moments on the booster cause the increase in the final recovery angle.

Preliminary analysis also showed that the hydrazine thrusters have sufficient thrust (100 lb) to provide control in the roll direction for the third stage.

Hydrazine Thrusters

The Hydrazine thrusters will serve four main functions. These include:

- Spin / Despin for payload deployment or maneuvering at Space Station Freedom
- Attitude corrections during all coast periods
- Roll control on stage 3
- Reorientation before entering GTO

The MR-104 hydrazine thrusters, manufactured by the Rocket Research Company, will be located immediately above the avionics section and attach to the payload interface ring. The tanks for the fuel and oxidizer will be located in the avionics bay. Two thrusters will be placed on each of the three axes: yaw, pitch and roll.

The tanks will be made from Stainless steel 347. The oxidizer and fuel weight will equal 450 lb. This will compensate for payload deployment, coast attitude control, roll control, and any unforeseen emergencies. The approximated time of use was based on a twenty-four hour mission.

Power Systems

The on-board power systems are composed of two major sub-systems: the principal system and the ignition system. The principal power sub-system supplies power to the on-board systems (such as the computer and communications equipment) while the ignition power sub-system supplies power to the engines for startup.

Principal Power Sub-System

The principal power sub-system will consist of lithium thionyl chloride batteries. This type of primary battery (non-rechargeable) is available off-the-shelf and is packaged in individual cells, each of which operates at a specific voltage and contains a fraction of the required power. It was determined, by examining the power requirements of all the Gryphon's on-board systems (See Table 11) that $Li/SOCl_2$ cells with an energy density of 642 W-h/kg and an open circuit voltage of 3.63 volts would optimize the power system performance while minimizing the cost and weight of the overall system. This sub-system will consist of four modules, each containing 8 cells and providing operational power to the Gryphon for 24 hours.

Table 11 Power Requirements of On-board Systems

Components	Power (W)
Flight Computer	250
GPS Receiver	3.5
Telemetry Transmitter (x2)	98
Radar Transponder	31
Communications	323
Thrusters	200
Inertial Receivers	200
Misc.	250
TOTAL	1356

Ignition Power Sub-System

Each of the rocket engines and the two solid rocket motors require 5 amps at 28 V DC. applied to it for up to 1 second to achieve ignition. This system consists of three modules of silver zinc primary cells. Each module will be completely independent and responsible for the ignition of all the rockets in each stage of the propulsion system. In order to meet the specifications of 5 amps at 28 V DC. for one second each module will need to contain 20 high rate silver zinc cells. Each of these cells contains 1.5 W-h of energy and operates at 1.4 volts. This means that each module will supply 30 W-h of energy at 28 V DC. which is more than is needed to activate each stage.

Thermal Control Systems

It is the goal of the thermal control system to keep all components within their specified temperature envelopes while minimizing cost and weight and maintaining reliability. The thermal control system for the Gryphon is concerned with two major areas. These areas are the external structure and the avionics bay. The external structure will use ablative coatings to provide thermal protection against aerodynamic heating during the ascent of the booster. The avionics bay will use a multi-component system which includes a helium purge, a heat sink radiator, enamel coatings, and multilayer insulation. This system will maintain the temperatures of all the electronic equipment located in the avionics bay.

Thermal Control of the External Structure

Because of hypersonic speeds during ascent, aerodynamic heating becomes an important factor in the design of the Gryphon. At speeds of Mach 8.0, temperatures of 4900°F can be felt by the booster. The composite material used for the external structure has a usable realm of up to 350°F, therefore, ablative coatings will be applied to surfaces where high heat rates occur to provide thermal protection. The ablative coatings that will be used for the Gryphon will consist of Firex and Thermal-Lag, because they are relatively inexpensive and they can be applied easily. The major surfaces exposed to high heat rates have been identified as:

- the nose cone of the payload shroud
- the nose cones of the solid rocket boosters
- the leading edge of the vertical tail surfaces

A maximum thickness of 2.5 inches of ablative coating will be applied to the stagnation surfaces of each of the mentioned surfaces. The coating will then taper as the heat rates decrease along the body of the Gryphon.

Thermal Control of the Avionics Bay

Spacecraft electronics typically have temperature limits from 0 to 80°F. The Lithium Thionyl Chloride batteries must operate at temperatures below 100°F. Consequently, a thermal control system must be provided in the avionics

bay. Thermal control of the avionics bay consists of a multi-fold system. The system includes: purging with helium, heat sink radiators, enamel coatings, and multilayer insulation.

Helium will be bled from the propulsion system and purged through the avionics bay. The purge will take place until the payload shroud is deployed. The helium purge provides forced convective cooling of the flight computer, the batteries, and certain transmitters. It will also be available for use after the payload shroud is deployed if the heat sink radiator fails. Helium was chosen since it was being used by the propulsion system for fuel tank pressurization. This option eliminated the need for two separate inert gas systems.

After the payload shroud is deployed, a heat sink radiator will provide cooling for the flight computer. The radiator has a surface area of 144 in^2 and is made of aluminum. Its outer surface will be coated with white enamel to improve radiative heat transfer effects.

Coatings will also be applied to critical components in the avionics bay. These coatings include white enamel and black paint, and they are used to increase or decrease radiative effectiveness. These coatings are simple devices that can be used to control the temperature passively and will add little weight or cost to the project.

Finally, multilayer insulation will be used to protect important electrical boxes and the electrical wiring against any radiative heat transfer. The insulation will consist of alternate layers of aluminized Mylar and a coarse netting. Multilayer insulation is the primary insulation used on most spacecraft and was chosen for this reason.

Gryphon Integration

To design the actual systems used in the putting the Gryphon together and attaching it to the Eclipse, several tasks needed to be completed. These include:

- Gryphon Assembly Building (GAB)
- Transportation and attachment of Completed Booster
- Physical attachment of Eclipse to Gryphon

Gryphon Assembly Building

The GAB is were the vehicle is assembled from its sub-components and the payload is integrated payloads. The GAB has been designed to have one completed Gryphon finished every two weeks.

Gryphon Assembly Building Layout. After considering several different building configurations, an assembly building with two parallel assembly lines was chosen. Two independent lines were chosen to allow greater flexibility in launch scheduling. If only one assembly line were used, launches could not be easily conducted in close succession. With two independent assembly lines, the assembly schedules could be staggered to provide one vehicle every two weeks, or two vehicles in close succession if launch windows require it. Having two independent assembly lines also allows for some protection from delays in any step in the assembly process.

The Gryphon Assembly Process. The various components are delivered to the GAB in the Stage Build-up Area. They are unloaded using an overhead crane. Each assembly line is equipped with an 80 ton overhead crane. The crane was sized at 80 tons to allow it to move the Castor 120 solid rocket boosters. These boosters weigh approximately 60 tons and are the heaviest component of the Gryphon.

Following completion in the Stage Build-up Area, the components are picked up with the 80 ton overhead crane and placed in position on the trailer in the Stage Integration area. This area of the GAB is equipped with a scaffolding system which can be pushed up close to the Gryphon being assembled to allow easier access to all areas of the Gryphon.

Following completion of Stage Integration and Integrated Vehicle Testing, the scaffolds are pushed back and the Gryphon is rolled on its trailer into the Payload Integration and Final Systems Check Area. In each line, this area is sealed off from the rest of the GAB and maintained at a class 10,000 clean room environment. This is necessary to protect the payloads from contamination prior installation of the fairing. The Payload Integration area of each line is also equipped with a 20 ton overhead crane to be used for hoisting payloads into position for integration with the Gryphon.

Following completion of the payload integration and all final systems checks, the completed Gryphon is rolled out of the GAB and to the waiting Eclipse for attachment.

Assembly Schedule. The assembly schedule of the Gryphon was based on the Pegasus's. Due to the much larger size and complexity of the Gryphon's liquid fueled stages, considerably longer times were assumed necessary for certain assembly steps. The following table compares the two assembly schedules.

Table 12 Pegasus/Gryphon Timeline Comparison

Step	Pegasus	Gryphon
Stage Build-up and Pre-Integration Testing	3 weeks	4 weeks
Stage Integration and Integrated Vehicle Testing	1 1/2 weeks	4 weeks
Payload Integration	1 week	2 weeks
Final Systems Tests	1 1/2 weeks	2 weeks
Total	7 weeks	12 weeks

Gryphon/Eclipse Interface

The main aspects necessary to attach the Gryphon to the Eclipse are the transportation trailer, the facility, and its location.

The Gryphon Transportation Trailer. The Gryphon Transportation Trailer (GTT) supports the 500,000 lb booster, transports the Gryphon to the Eclipse without

imparting undue shocks, and can make precise orientation adjustments for alignment..

The GTT was patterned after the trailer used by OSC to transport the Pegasus from its assembly building to the B-52 drop aircraft. The trailer used to transport the Pegasus is equipped with 24 standard seem-trailer wheels on 6 axles. By comparison then, the GTT would require 73 axles and 292 wheels. It was decided that the GTT should be based on a rail system to support the Gryphon's large weight.

In order to insure proper alignment of the Gryphon with the Eclipse during attachment, the GTT must be able to shift the Gryphon from side to side and also rotate several degrees. To allow for this, it was decided that the Gryphon will be supported in a cradle which rests on top of the trailer. Large screw jacks will be mounted horizontally at the front and rear and of the trailer. By operating the two screw jacks synchronously in either direction the cradle can be moved either left of right. Operating the screw jacks differentially allows the cradle can be rotated a few degrees to make the necessary adjustments.

The Gryphon will be brought out from the GAB on its trailer and rolled underneath the Eclipse from the rear. Once it is in position, it will be lifted by four hydraulic lifts (mounted in the ground). The screw jacks on the GTT will then be used to move the Gryphon either to the left or right or to rotate it to achieve proper alignment. If the fore and aft positioning is incorrect, the Eclipse can be pushed forward or backward slightly, or the Gryphon could be lowered, pushed forward or aft on the rails, and lifted up again. Once correct alignment has been achieved, the Gryphon will be raised the last few inches and the hydraulic interface mechanism closed, thus securing the Gryphon to the Eclipse. The GTT can then be lowered back onto its rails and removed.

Gryphon Facility Location

The location of the facility was based on the availability of rocket fuels on site, proximity to the equator for GEO launches, distance from large population centers, and the availability of a 10,000 ft runway.

Based upon these requirements it was decided that the Kennedy space center was the best place to locate the Gryphon Facility for GEO launches. However, a small percentage of the launches might be made to very high inclination (polar) orbits. For these orbits, Vandenberg Air Force Base was chosen as the launch site for the west coast. For these missions, a Gryphon would be ferried unfueled from Kennedy to Vandenberg by the Eclipse and then fueled and launched.

Aircraft/Booster Interface Mechanism

The best configuration was found to be two four point, attachment systems on the second stage, symmetric about the center of gravity. All of the pins lie within the second stage. With the exception of pins 1 and 2, a circular support structure had to be designed at the pin locations. The first two pins were purposefully placed at the interstage between stage 1 and stage 2 due to the structure required there. Pins 5 and 6 are placed at the attach ring required for the struts connecting the two Castor 120 engines. Some of the key aspects of this system are shown below (see Table 13).

Table 13 Characteristics of Gryphon/Eclipse Interface

Hook Cross Sectional Area	16 in^2
Maximum Pin Length	27 in
Total System Weight	11,104 lb
Total Pin Weight	1328 lb

Pin Layout. In order to fully analyze the different possibilities, a finite element model was constructed in I-DEAS . It was determined to run different configurations using finite element models in order to find the best pin layout on the Gryphon. The parameters determining the best pin configuration were:

- Distribution of forces on pins
- Stability of configuration
- Structural Dynamics

Having approximately the same force on each pin would mean only one type of hook and pin combination had to be designed. This would greatly reduce manufacturing costs. Due to the overall need to reduce costs and ability to meet the requirement, only one combination was chosen.

Required Hydraulic Force. The hydraulic force to operate the system was calculated using a worst-case-load. It was calculated by using the forces on the pin/hook combination, the friction coefficient between the pin and hook and the geometry and the lengths of the lever arm and connecting rods. The hydraulic pressure provided by the plane was given at 5000 psi. It was noted that pumps could be added for emergency pressure loss and additional hydraulic force if needed. Using the hydraulic pressure, the pistons were sized by calculating the worst-case load force required. After completing the detailed analysis in I-DEAS the pistons cross sectional area was found to be 10.54 in^2.

Materials. The material used for the structural members throughout the interface system is a heat treated, quenched and tempered, steel alloy ASTM-A242. This alloy was chosen due to the fact that it is the strongest construction material in yield shear strength.

G-Force Loads. The maximum G-Force was given from the Eclipse Design Team to be 2.5. This was then multiplied by the structural factor of safety and the dynamic loading coefficient to obtain the overall system factor of safety of 4.

Conclusion

Project Gryphon is the beginning investigation of a 500,000 lb air launched space booster. This Phase I study demonstrates the viability for a venture of this type.

Ultimately, the cost effectiveness of the Gryphon will determine its future. As demonstrated in this summary, the Gryphon has the capability of providing investor's a 15% return, which would provide a corporation a profitable endeavor. As with all projects, one can expect that changes will occur as the process develops. However, the initial results definitely merit continued study into large sized air launched space boosters. For a more detailed explanation of the process and analysis that went into the Gryphon, consult the Gryphon Air Launched Space Booster Report.

Acknowledgments

The author would like to acknowledge all those individuals involved in Project Gryphon. The 40 students of Aerospace 483 Space System Design at the University of Michigan deserve the credit for the work and commitment needed on a project of this nature. Although be restrained by a tight budget was quite difficult to work with, it helped the group feel as if its endeavors were realistic and worthwhile. And everyone should be commended for sticking together to meet the budget.

Special thanks also go to Professor Joe Eisley for all of his support and for providing all the resources needed to make for a technically sound project. Teaching Assistant James Akers must also be mentioned for all of his outstanding contributions. Without his guidance and support, we may have never gotten as far as was possible.

Robert Lovell of OSC presented the idea behind all of the work and must be thanked for his help. Also, Lisa Kuhout of NASA Lewis Research Center must be mentioned for providing support when needed.

B. AERODYNAMICS CALCULATIONS

B.1 CFD

For many design points of an aircraft, one important parameter is $C_{L_{max}}$. Due to the choice of a supercritical airfoil for the Eclipse, there is no available experimental high angle of attack data available. Therefore, computational fluid dynamics was employed in an attempt to acquire some of this needed data.

The first step in this process was to use a two dimensional Euler code to solve the inviscid case. Then, to try to predict separation, a second program was used to evaluate the boundary layer behavior using Thwaite's method. This program first searches for the stagnation point near the front of the airfoil. From this point, the airfoil is traversed as shown in Figure B.1.1. At each point along the surface, the flow velocity is known from the Euler code. This data is then used to create Figures such as B.1.2. This figure shows the flow velocity, U, tangential to the body surface as a function of s, the distance from the stagnation point. Thwaite's method calculates a parameter λ, such that

$$\lambda = 0.45\frac{U'}{U^6}\int_0^s U^5 ds \qquad \text{(B.1.1)}$$

when λ is less than or equal to -0.15, Thwaite's method predicts separation.

With this data, a third and final program was written to transform these effects into three dimensions. To do this, Prandtl's lifting line theory was modified to account for wing sweep. This resulted in Figure B.1.3 and B.1.4. Figure B.1.3 shows the spanwise effective angles of attack divided by the absolute angle of attack. From this, one could find the point along the wing that would stall first, and at what absolute angle of attack that stall would occur. Figure B.1.4 is the lift distribution during cruise.

Unfortunately, Thwaite's method estimates the effects of a laminar boundary layer. Results show that the airfoil used on the Eclipse depends upon turbulent flow. To be more specific, in the design condition of the airfoil (M=0.73, α=0°), separation was predicted at about 80% chord. This is obviously not a good model of the true performance of this airfoil.

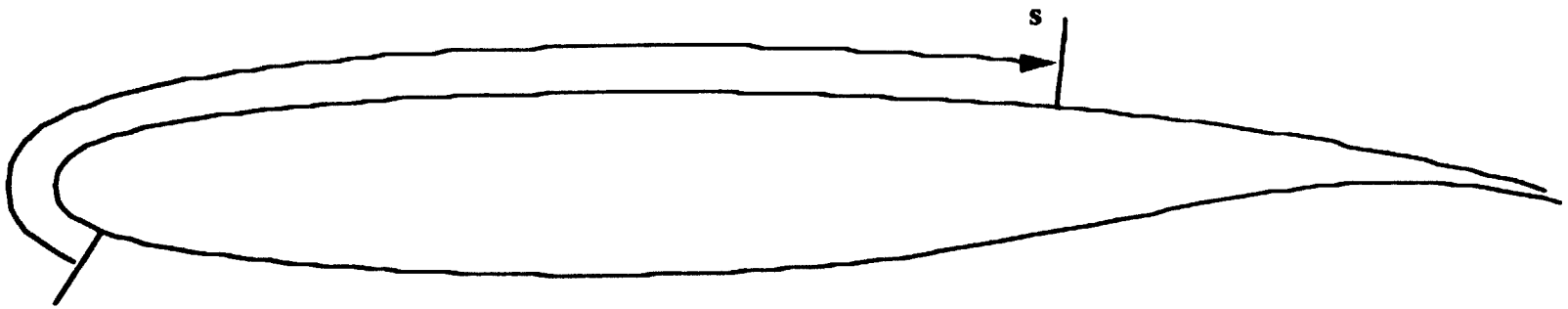

Figure B.1.1 Method of traversion of airfoil for boundary layer evaluation

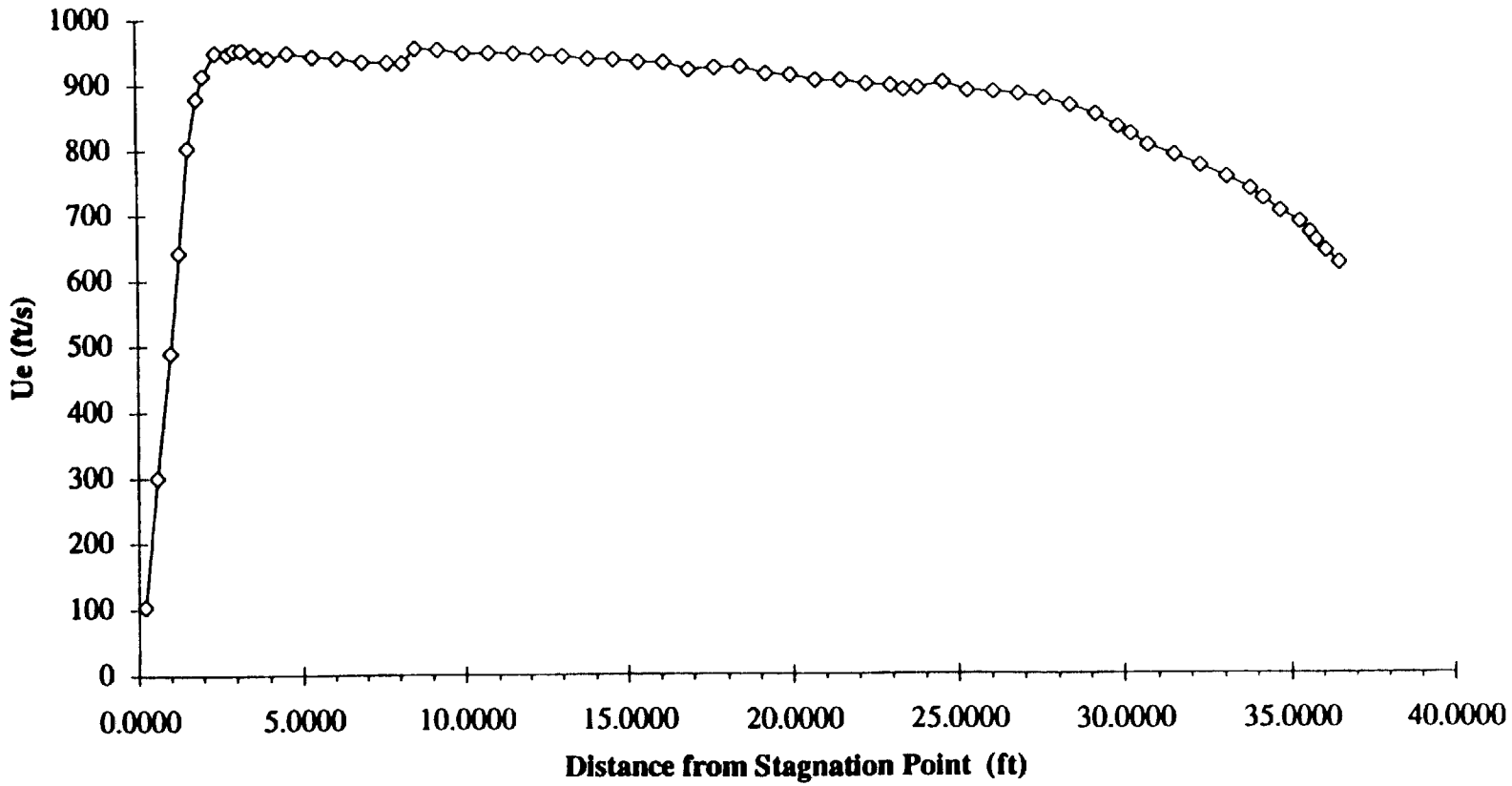

Figure B.1.2 Distance along airfoil from stagnation point versus flow velocity outside of boundary layer

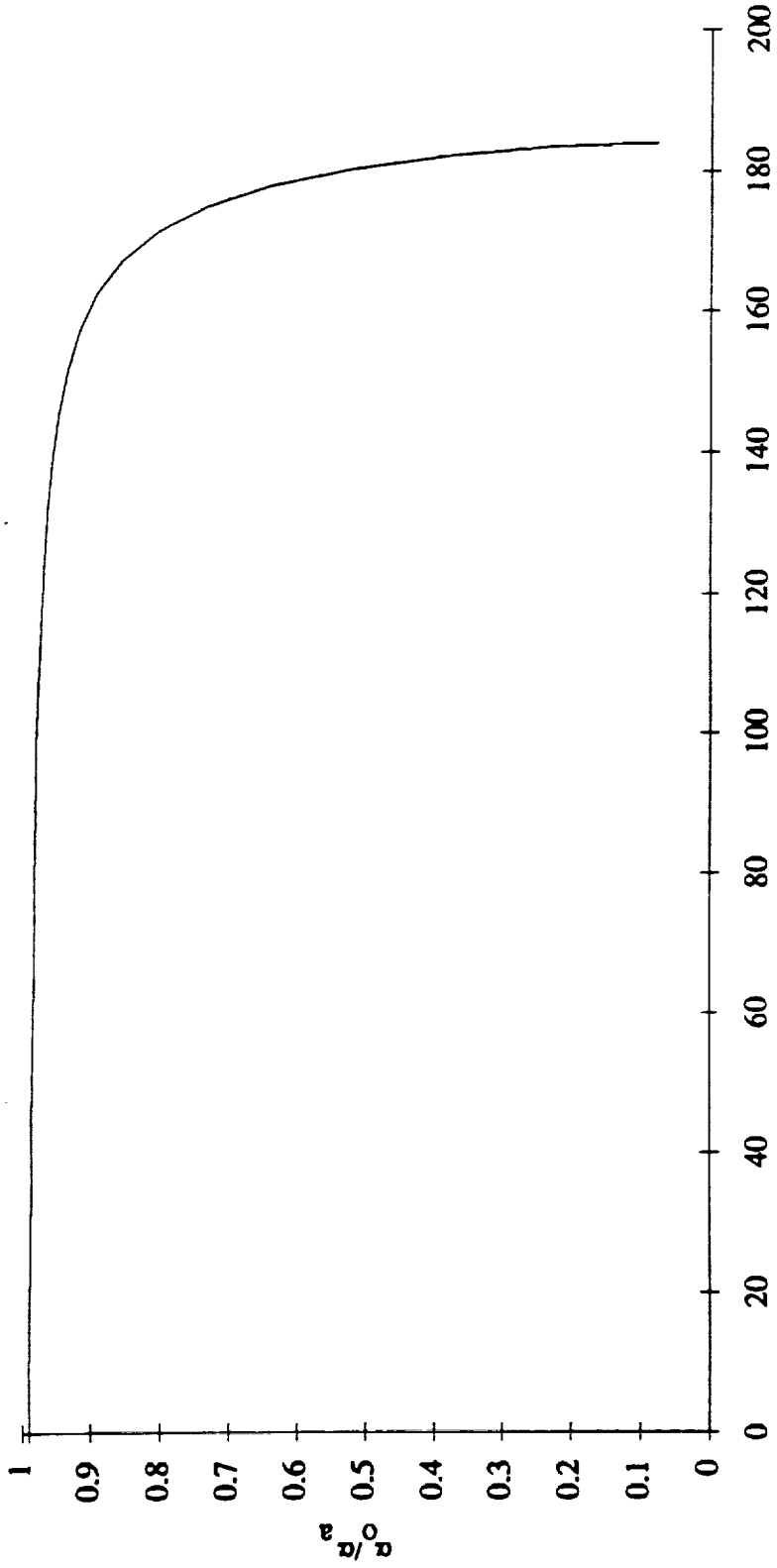

Figure B.1.3 Spanwise effective angles of attack / absolute angles of attack at cruise

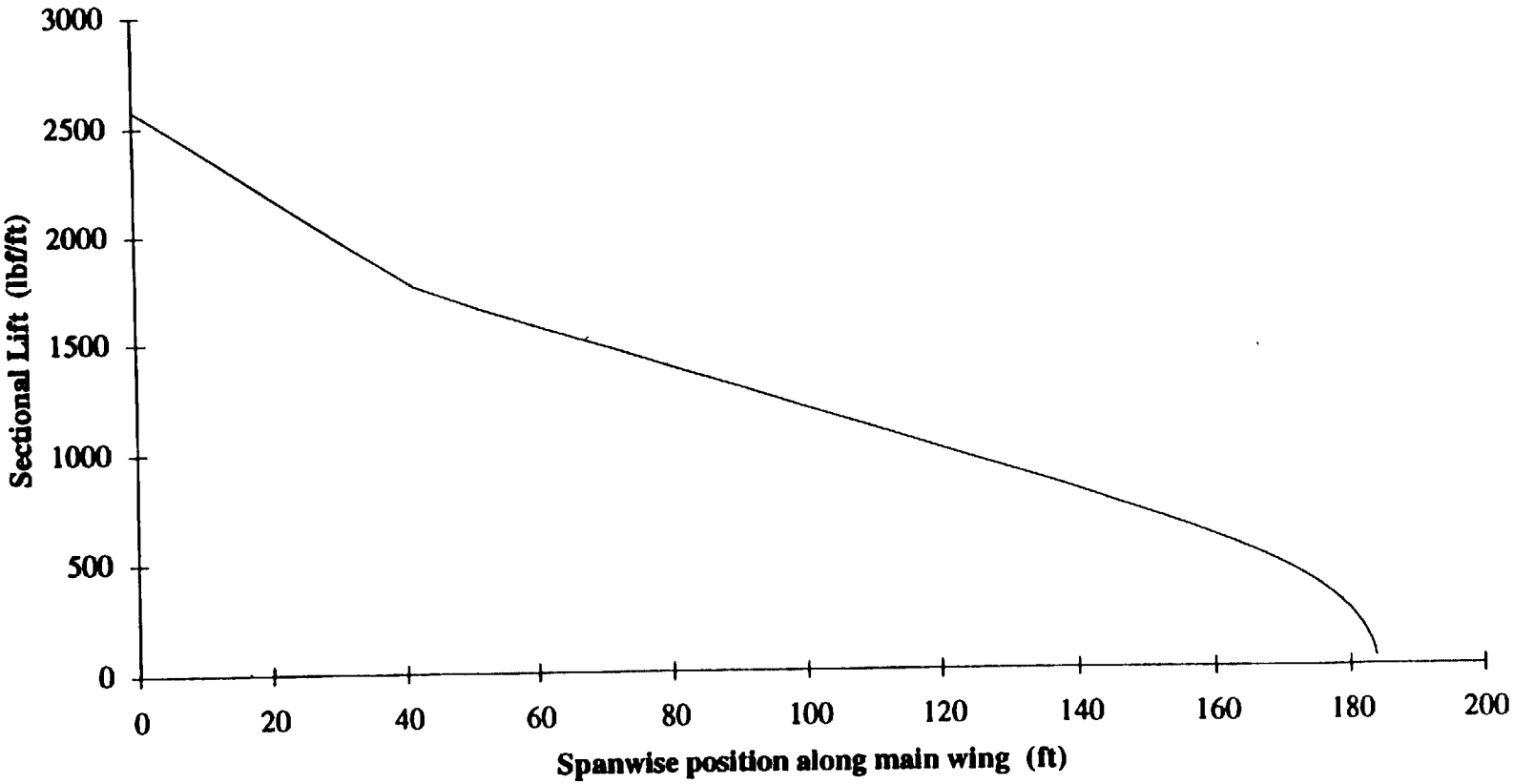

Figure B.1.4 Lift distribution at cruise

B.2 Lift

For each Mach Number:

$$C_{L\alpha_w} = \frac{2\pi \cdot A}{2 + \sqrt{A^2 \frac{\beta^2}{k_w^2}\left(1 + \tan^2 \Lambda_{c/2}\right) + 4}} \tag{B.2.1}$$

where:

$$\beta^2 = 1 - M^2 \tag{B.2.2}$$

$$k_W = \frac{C_{L\alpha}|_{M=0}}{2\pi} \tag{B.2.3}$$

Then, with the fuselages:

$$C_{L\alpha_{wf}} = C_{L\alpha_w}\left(1 + 0.025\frac{d_f}{b} - 0.25\left[\frac{d_f}{b}\right]^2\right)^2 \tag{B.2.4}$$

The horizontal tail lift curve slope is then:

$$C_{L\alpha_H} = \frac{2\pi \cdot A_H}{2 + \sqrt{{A_H}^2 \frac{\beta^2}{k_H^2}\left(1 + \tan^2 \Lambda_{c/2_H}\right) + 4}} \tag{B.2.5}$$

Now, to find the tail efficiency:

$$z_H = x_H \cdot \tan\left(\gamma + 1.62\frac{\alpha_W \cdot C_{L\alpha_w} + 0.2486}{\pi \cdot A}\right) \tag{B.2.6}$$

$$Z_W = -0.68\bar{c}\sqrt{C_{Do_w}\left(\frac{z_H}{c} + 0.15\right)} \tag{B.2.7}$$

$$\eta_H = 1 - \cos^2\left(\frac{\pi \cdot z_H}{2s_w}\right) \cdot \left(\frac{2.42\sqrt{C_{Do_w}}}{\frac{x_H}{c} + 0.3}\right) \tag{B.2.8}$$

with all parameters defined in reference 6.

Next, find the downwash, $\frac{d\varepsilon}{d\alpha}$:

$$\frac{d\varepsilon}{d\alpha} = 4.44\left(K_A \cdot K_\lambda \cdot K_H\sqrt{\cos\Lambda_{c/4}}\right)^{1.19}\left(\frac{C_{L\alpha_w}}{C_{l\alpha_w}|_{M=0}}\right) \tag{B.2.9}$$

where:

$$K_A = \frac{1}{A} - \frac{1}{1 + A^{1.7}} \tag{B.2.10}$$

$$K_\lambda = \frac{10 - 3\lambda}{7} \tag{B.2.11}$$

$$K_H = \frac{1 - \frac{h_H}{\sqrt{S \cdot A}}}{\left(\frac{2l_H}{\sqrt{S \cdot A}}\right)^{1/3}} \tag{B.2.12}$$

Now, the total airplane lift curve slope is:

$$C_{L\alpha_A} = C_{L\alpha_{wf}} + C_{L\alpha_H} \cdot \eta_H \frac{S_H}{S}\left(1 - \frac{d\varepsilon}{d\alpha}\right) \quad \text{(B.2.13)}$$

To then find C_{LoA}:

$$\alpha_{0L_w} \cong \alpha_{0l_{airfoil}} \quad \text{(B.2.14)}$$

$$C_{Lo_w} = -\alpha_{0L_w} \cdot C_{L\alpha_{wf}} \quad \text{(B.2.15)}$$

$$C_{Lo_{wf}} = \left(i_W - \alpha_{0L_w}\right) C_{L\alpha_{wf}} \quad \text{(B.2.16)}$$

$$C_{Lo_A} = C_{Lo_{wf}} + C_{L\alpha_H} \cdot \eta_H \frac{S_H}{S} i_H \quad \text{(B.2.17)}$$

And both C_{LoA} and $C_{L\alpha A}$ are calculated. This accounts for the linear portion of the lift curve, which is all that is estimated. Therefore, the final result is:

$$C_{L_A} = C_{Lo_A} + C_{L\alpha_A} \cdot \alpha_A \quad \text{(B.2.18)}$$

The results of these calculations are listed in Table B.2.1.

Table B.2.1 Lift curve and wing moment results

M	CLα w	Clo w	CLα wf	CLo wf	CLα h	dε/dα	CLα A	CLo A	CmoW	xacA	dCm/dCL
0.20	5.637	0.292	5.643	0.440	4.435	0.317	6.4353	0.4399	-0.1035	2.900	-0.1439
0.25	5.691	0.295	5.698	0.444	4.472	0.320	6.4924	0.4442	-0.1035	2.898	-0.1413
0.30	5.761	0.299	5.768	0.450	4.518	0.324	6.5643	0.4496	-0.1040	2.895	-0.1380
0.35	5.846	0.303	5.853	0.456	4.574	0.329	6.6529	0.4562	-0.1050	2.891	-0.1339
0.40	5.950	0.308	5.957	0.464	4.642	0.335	6.7605	0.4643	-0.1066	2.887	-0.1291
0.45	6.075	0.315	6.082	0.474	4.723	0.342	6.8899	0.4741	-0.1091	2.882	-0.1234
0.50	6.225	0.323	6.232	0.486	4.820	0.350	7.0448	0.4858	-0.1117	2.876	-0.1165
0.55	6.406	0.332	6.413	0.500	4.936	0.360	7.2303	0.4999	-0.1138	2.868	-0.1082
0.60	6.624	0.309	6.632	0.483	5.073	0.373	7.4562	0.4826	-0.1169	2.860	-0.0993
0.65	6.892	0.286	6.900	0.466	5.238	0.388	7.7306	0.4664	-0.1210	2.850	-0.0884
0.70	7.224	0.187	7.233	0.377	5.439	0.406	8.0747	0.3766	-0.1236	2.840	-0.0771
0.75	7.647	0.000	7.656	0.200	5.687	0.430	8.5159	0.2004	-0.1278	2.830	-0.0654
0.78	7.961	0.000	7.970	0.209	5.865	0.448	8.8270	0.2087	-0.1314	2.817	-0.0515
0.80	8.203	-0.425	8.213	-0.210	6.000	0.462	9.0929	-0.2101	-0.1329	2.816	-0.0507

B.3 Drag

$$C_{D_{clean}} = C_{Do_{clean}} + C_{Di_{clean}} \quad \text{(B.3.1)}$$

B.3.1 Zero-lift drag

Using the component breakdown method (virtually all of which is from reference 6)

$$C_{Do_{clean}} = C_{Do_W} + C_{Do_H} + 2C_{Do_V} + 6C_{Do_N} + 6C_{Do_P} + 2C_{Do_F} + C_{Do_{Misc\&Trim}} \quad \text{(B.3.2)}$$

Each component's zero lift drag was then estimated as follows:

Wing:

$$C_{Do_W} = R_{WF}{}^2 \cdot R_{LS} \cdot c_{f_W}\left(1 + \tfrac{t}{c}L' + 100\left[\tfrac{t}{c}\right]^4\right)\frac{S_{wet_W}}{S} \quad \text{(B.3.3)}$$

where R_{WF} is the wing/fuselage interference factor, R_{LS} is the lifting surface factor, and L' is the airfoil thickness location factor. All are as defined in reference 6.
note: R_{WF} is squared because the Eclipse has two fuselages.

Horizontal Tail:

$$C_{Do_H} = R_{LS} \cdot c_{f_H}\left(1 + \tfrac{t}{c}L' + 100\left[\tfrac{t}{c}\right]^4\right)\frac{S_{wet_H}}{S} \quad \text{(B.3.4)}$$

Vertical Tail:

$$C_{Do_V} = R_{LS} \cdot c_{f_V}\left(1 + \tfrac{t}{c}L' + 100\left[\tfrac{t}{c}\right]^4\right)\frac{S_{wet_V}}{S} \quad \text{(B.3.5)}$$

Nacelles:

Predictions of the nacelle drag as calculated from reference 6 gave unreasonably high results. This is due to the fact nacelles are treated as fuselages. Since the fan diameter of the GE-90 is so large, the fineness ratio is very poor. For this reason, a method found in reference 11 was used:

$$C_{Do_N} = R_{WF} \cdot c_{f_W} \cdot FF\,\tfrac{S_{wet_N}}{S} \quad \text{(B.3.6)}$$

where:

$$FF = 1 + 0.35\tfrac{D_{fan}}{l_N} \quad \text{(B.3.7)}$$

D_{fan} = fan diameter

l_N = length of the nacelle

Pylons:

$$C_{Do_P} = R_{WF} \cdot R_{LS} \cdot c_{f_P}\left(1 + \tfrac{t}{c}L' + 100\left[\tfrac{t}{c}\right]^4\right)\frac{S_{wet_P}}{S} \quad \text{(B.3.8)}$$

Fuselages:

$$C_{Do_F} = R_{WF} \cdot c_{f_F}\left(1 + \frac{60}{(l_F/d_F)^3} + 0.0025\frac{l_F}{d_F}\right)\frac{S_{wet_F}}{S} \quad \text{(B.3.9)}$$

where l_F is the fuselage length and d_F is the equivalent diameter as explained in reference 6.

Trim and Miscellaneous:

$$C_{Do_{Misc\&Trim}} = 0.10\left(C_{Do_W} + C_{Do_H} + 2C_{Do_V} + 6C_{Do_N} + 6C_{Do_P} + 2C_{Do_F}\right) \quad \text{(B.3.10)}$$

note: the fuselages and horizontal tail will later add to the zero-lift drag as explained in the lift-induced drag section.

Table B.3.1 lists the wetted areas used in these calculations and the zero-lift drag results are contained in Table B.3.2.

Table B.3.1 Wetted area breakdown

Wing	23000.0
Horizontal Tail	6560.0
Vertical Tail (each)	1435.0
Nacelles (each)	668.3
Pylons (each)	238.9
Fuselage (each)	6959.2

Table B.3.2 Zero-lift drag components during climb/cruise conditions (clean)

Altitude	Wing	H. Tail	V. Tail (each)	Nacelles (each)	Pylons (each)	Fuselages (each)	Trim and Miscellaneous	Total
0	0.00520	0.00300	0.00044	0.00014	0.00007	0.00100	0.00062	0.01297
5000	0.00537	0.00305	0.00044	0.00014	0.00007	0.00101	0.00063	0.01323
10000	0.00552	0.00294	0.00045	0.00014	0.00007	0.00103	0.00063	0.01331
15000	0.00566	0.00300	0.00046	0.00014	0.00007	0.00104	0.00065	0.01363
20000	0.00588	0.00254	0.00047	0.00014	0.00007	0.00104	0.00064	0.01339
25000	0.00604	0.00219	0.00049	0.00015	0.00007	0.00108	0.00063	0.01331
30000	0.00614	0.00221	0.00050	0.00015	0.00008	0.00110	0.00064	0.01352
35000	0.00632	0.00223	0.00051	0.00015	0.00008	0.00115	0.00066	0.01390
36000	0.00635	0.00225	0.00052	0.00014	0.00007	0.00116	0.00066	0.01392
37000	0.00639	0.00226	0.00052	0.00014	0.00007	0.00118	0.00067	0.01403
38000	0.00644	0.00228	0.00052	0.00015	0.00007	0.00120	0.00067	0.01415
39000	0.00648	0.00229	0.00053	0.00015	0.00008	0.00122	0.00068	0.01427
40000	0.00653	0.00231	0.00053	0.00015	0.00008	0.00124	0.00069	0.01440
41000	0.00657	0.00232	0.00054	0.00015	0.00008	0.00126	0.00069	0.01453
42000	0.00662	0.00234	0.00054	0.00015	0.00008	0.00128	0.00070	0.01467
45000	0.00676	0.00239	0.00055	0.00015	0.00008	0.00138	0.00072	0.01512
50000	0.00702	0.00248	0.00057	0.00016	0.00008	0.00161	0.00077	0.01608

B.3.2 Lift-induced drag

$$C_{Di_{clean}} = C_{Di_W} + C_{Di_H} + C_{Di_F} = \Delta C_{Do_{clean}} + C_{Di_{1clean}} \cdot C_{L_A} + C_{Di_{2clean}} \cdot C_{L_A}^{\ 2} \quad \text{(B.3.11)}$$

Each of these lift-induced drag components was then estimated as follows:

Wing:

$$C_{Di_w} = \frac{{C_{L_w}}^2}{\pi \cdot A \cdot e} \approx \frac{\left(1.05 \cdot C_{L_A}\right)^2}{\pi \cdot A \cdot e} \qquad \text{(no twist)} \qquad \text{(B.3.12)}$$

where:

$$e \approx 1.1 \frac{\frac{C_{L\alpha_w}}{A}}{R\frac{C_{L\alpha_w}}{A} + (1-R)\pi} \qquad \text{(B.3.13)}$$

R = leading edge suction parameter

Horizontal Tail:

$$C_{Di_H} = \frac{{C_{L_H}}^2}{\pi \cdot A \cdot e} \cdot \frac{S_H}{S} \qquad \text{(B.3.14)}$$

$$C_{L_H} \approx C_{L\alpha_H}\left[\alpha_A\left\{1 - \tfrac{d\varepsilon}{d\alpha}\right\} + i_H - \alpha_{0L_H}\right] = C_{L\alpha_H}\left[\alpha_A - \tfrac{d\varepsilon}{d\alpha}\alpha_{0L_H}\right] \qquad \text{(B.3.15)}$$

note: there is no incidence angle on the horizontal tail, and that it is a symmetric airfoil

additionally:

$$\alpha_A = \frac{C_{L_A} - C_{Lo_A}}{C_{L\alpha_A}} \qquad \text{(B.3.16)}$$

Therefore:

$$C_{L_H} \approx C_{L\alpha_H}\left(\frac{C_{L_A} - C_{Lo_A}}{C_{L\alpha_A}}\left[1 - \tfrac{d\varepsilon}{d\alpha}\right]\right) = C_{L_A}\left(\frac{C_{L\alpha_H}}{C_{L\alpha_A}}\right)\left(1 - \tfrac{d\varepsilon}{d\alpha}\right) - C_{Lo_A}\left(\frac{C_{L\alpha_H}}{C_{L\alpha_A}}\right)\left(1 - \tfrac{d\varepsilon}{d\alpha}\right) \qquad \text{(B.3.17)}$$

$${C_{L_H}}^2 \approx \left({C_{L_A}}^2 - 2C_{L_A} \cdot C_{Lo_A} + {C_{Lo_A}}^2\right)\left(\frac{C_{L\alpha_H}}{C_{L\alpha_A}}\right)^2 \left(1 - \tfrac{d\varepsilon}{d\alpha}\right)^2 \qquad \text{(B.3.18)}$$

$$C_{Di_H} = \frac{\left({C_{L_A}}^2 - 2C_{L_A} \cdot C_{Lo_A} + {C_{Lo_A}}^2\right)\left(\frac{C_{L\alpha_H}}{C_{L\alpha_A}}\right)^2 \left(1 - \tfrac{d\varepsilon}{d\alpha}\right)^2}{\pi \cdot A \cdot e} \cdot \frac{S_H}{S} \qquad \text{(B.3.19)}$$

Fuselages:

To avoid a term in $C_L{}^3$, reference 6 suggests that a "standard" angle of attack for the fuselage at each drag polar's conditions. This is done simply by balance of forces, and using the lift curve.

$$C_{Di_p} = \eta \cdot c_{d_c} \cdot \alpha^3 \frac{S_{proj}}{S} \tag{B.3.20}$$

$$\alpha = \frac{\frac{W}{\frac{1}{2}\rho v^2 S} - C_{Lo_A}}{C_{La_A}} \tag{B.3.21}$$

where η is the ratio of the drag of a finite cylinder with that of an infinite cylinder and c_{dc} is the experimental steady state cross-flow drag coefficient of a circular cylinder, as defined in reference 6.

B.3.3 Payload Drag

$$C_{D_{Gryph}} = C_{Do_{Gryph}} + C_{Di_{Gryph}} \tag{B.3.22}$$

$$C_{Do_{Gryph}} = K_{mid-tank} \cdot C_{Do_{mid-tank}} + 2K_{side-tank} \cdot C_{Do_{side-tank}} + C_{Do_V} \tag{B.3.23}$$

where:

$$K_{mid-tank} = K_{side-tank} = 1.3 \tag{B.3.24}$$

each component C_{Do} was then calculated in the same manner as with the aircraft.

$$C_{Di_{Gryph}} = C_{Di_{mid-tank}} + 2C_{Di_{side-tank}} \tag{B.3.25}$$

these were also calculated in the same manner as for the aircraft.

B.3.4 Drag Polar Integration

1) The first task is to reference the payload's drag to the aircraft's parameters. $C_{DoGryph}$ can be re-referenced by multiplication by S_{Gryph}/S. For $C_{diGryph}$, the task is more difficult. First, a lift curve for the Gryphon is found. From this, C_{LGryph} is a function of angle of attack.

2) now, a three-step method suggested by Mr. Ron Bengelink of the Boeing Aircraft Company is employed.[17]
   a) Over the portion of the wing which is directly affected by the presence of the Gryphon, 10% is added to the zero-lift drag. This area is shown in Figure B.3.1. This factor accounts for direct interference.
   b) 5% is now added to the entire system's zero-lift drag. This factor accounts for other interference.
   c) an angle of attack of zero is assumed over the Gryphon. The large chord of the Eclipse's wing will force the air around the Gryphon, giving an angle of attack of zero.

Tables B.3.3 to B.3.7 contain the final drag polars.

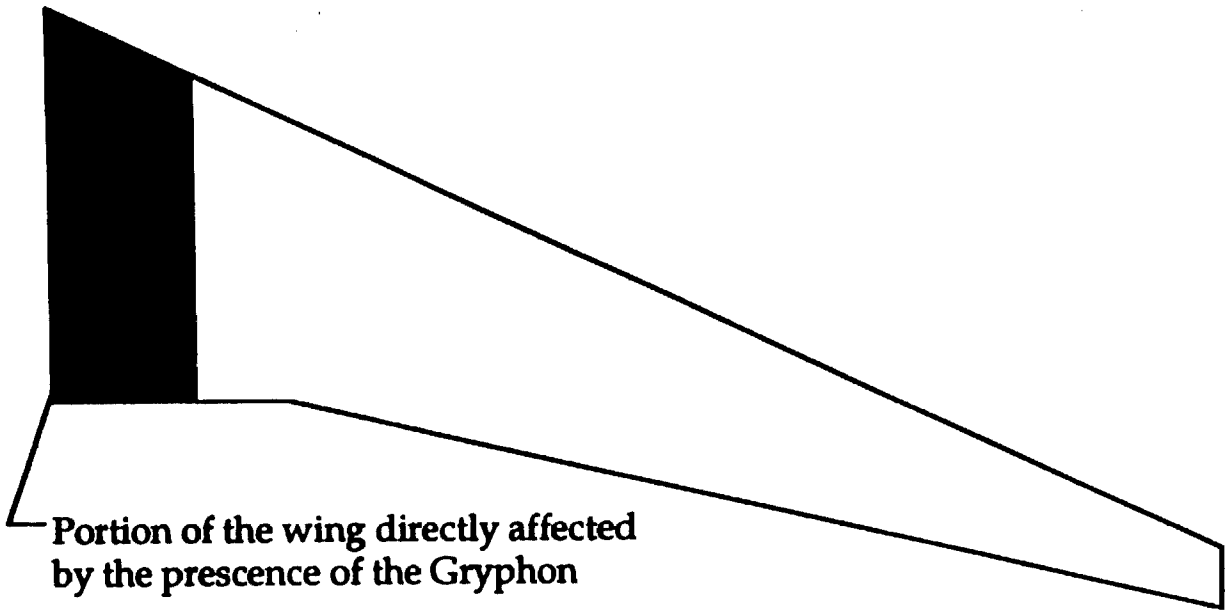

Figure B.3.1 Wing area directly affected by the prescence of the Gryphon

Table B.3.3 Drag polar results (clean)

Altitude (ft)	Speed (ft/s)	C_{do}	C_{di1}	C_{di2}	L/D_{max}
0	560	0.01291	-0.00493	0.04090	24.37
5000	600	0.01317	-0.00487	0.04044	24.21
10000	650	0.01326	-0.00452	0.03989	24.10
15000	650	0.01357	-0.00458	0.03988	23.83
20000	733	0.01336	-0.00309	0.03851	23.66
25000	750	0.01330	-0.00150	0.03785	23.05
30000	775	0.01351	-0.00141	0.03706	23.06
35000	760	0.01390	-0.00113	0.03637	22.81
36000	755	0.01392	-0.00112	0.03638	22.79
37000	755	0.01403	-0.00113	0.03638	22.70
38000	755	0.01414	-0.00113	0.03638	22.60
39000	755	0.01427	-0.00113	0.03638	22.50
40000	755	0.01439	-0.00113	0.03638	22.40
41000	755	0.01452	-0.00113	0.03638	22.29
42000	755	0.01466	-0.00113	0.03638	22.18
45000	755	0.01511	-0.00113	0.03638	21.84
50000	755	0.01607	-0.00113	0.03638	21.17

Table B.3.4 Drag polar results (with Gryphon)

Altitude (ft)	Speed (ft/s)	C_{do}	C_{di1}	C_{di2}	L/D_{max}
0	560	0.01509	-0.00518	0.04358	21.68
5000	600	0.01539	-0.00511	0.04309	21.55
10000	650	0.01550	-0.00474	0.04251	21.46
15000	650	0.01586	-0.00481	0.04249	21.22
20000	733	0.01565	-0.00325	0.04105	21.08
25000	750	0.01564	-0.00157	0.04035	20.55
30000	775	0.01589	-0.00148	0.03951	20.56
35000	760	0.01534	-0.00119	0.03879	20.34
36000	755	0.01538	-0.00118	0.03880	20.31
37000	755	0.01651	-0.00118	0.03879	20.23
38000	755	0.01665	-0.00118	0.03879	20.14
39000	755	0.01680	-0.00118	0.03879	20.05
40000	755	0.01695	-0.00118	0.03879	19.96
41000	755	0.01711	-0.00118	0.03879	19.86
42000	755	0.01728	-0.00118	0.03879	19.76
45000	755	0.01783	-0.00118	0.03879	19.44
50000	755	0.01902	-0.00118	0.03879	18.81

Table B.3.5 First loiter drag polars (with Gryphon at h = 44,000 ft)

M	V (ft/s)	C_{do}	C_{di1}	C_{di2}	L/D_{max}
0.45	484.76	0.01571	-0.00544	0.04409	21.18
0.50	538.62	0.01575	-0.00542	0.04367	21.25
0.55	592.48	0.01572	-0.00538	0.04318	21.39
0.60	646.35	0.01557	-0.00496	0.04262	21.48
0.65	700.21	0.01545	-0.00454	0.04196	21.55
0.70	754.07	0.01502	-0.00340	0.04119	21.57
0.75	807.93	0.01465	-0.00164	0.04028	21.30
0.78	840.25	0.01464	-0.00159	0.03996	21.45
0.80	861.80	0.01490	0.00150	0.03919	20.07

Table B.3.6 Second loiter drag polars (with Gryphon at h = 10,000 ft)

M	V (ft/s)	C_{do}	C_{di1}	C_{di2}	L/D_{max}
0.20	215.45	0.03927	-0.00548	0.04540	12.66
0.25	269.31	0.02167	-0.00548	0.04523	17.50
0.30	323.17	0.01788	-0.00548	0.04502	19.50
0.35	377.04	0.01682	-0.00547	0.04476	20.24
0.40	430.90	0.01637	-0.00546	0.04445	20.61
0.45	484.76	0.01615	-0.00544	0.04409	20.86

Table B.3.7 Second loiter drag polars (clean at h = 10,000 ft)

M	V (ft/s)	C_{do}	C_{di1}	C_{di2}	L/D_{max}
0.20	215.45	0.03126	-0.00522	0.04262	14.75
0.25	269.31	0.01797	-0.00522	0.04246	19.99
0.30	323.17	0.01512	-0.00521	0.04226	22.05
0.35	377.04	0.01433	-0.00521	0.04201	22.80
0.40	430.90	0.01399	-0.00520	0.04172	23.19
0.45	484.76	0.01382	-0.00518	0.04138	23.45

C. PERFORMANCE CALCULATIONS

C.1 Engine Start and Warm Up:

Assume 45 minutes at idle thrust (less than 10 % of take off thrust) with C_j around 1. Calculate fuel weight (W_{fuel} [lbf]) with:

$$W_{fuel} = T \cdot C_j \cdot \Delta t \qquad \text{(C.1.1)}$$

where:

T = idle thrust for the 6 engines [lbf]

C_j = specific fuel consumption [lbm/hr/lbf]

Δt = time [hr]

Take off weight (W_{to} [lbf]) is defined by:

$$W_{to} = W_{ramp} - W_{fuel} \qquad \text{(C.1.2)}$$

where:

W_{ramp} = ramp weight (before engine start) [lbf]

C.2 Take Off:

C.2.1 Fuel fraction:

Assume 2 minutes at maximum sea level thrust. Find the fuel flow from the General Electric engine data (see Appendix D).[16] Specific fuel consumption is found from:

$$C_j = \frac{F_f}{t} \qquad \text{(C.2.1)}$$

where:

F_f = fuel flow for one engine [lbm/hr]

t = uninstalled thrust for one engine [lbf]

Fuel weight is again found by:

$$W_{fuel} = T \cdot C_j \cdot \Delta t \qquad \text{(C.2.2)}$$

where:

T = total take off thrust [lbf]

C.2.2 Field length and time to lift off:

To obtain runway length (from zero velocity to lift off), calculate velocity to lift off (V_{lof}) from:

$$V_{stall} = \sqrt{\frac{2 \cdot W_{to}}{\rho \cdot S \cdot C_{l_{max}}}} \qquad \text{(C.2.3)}$$

where:

ρ = air density at airplane location [slug/ft^3]

S = wing reference area [ft^2]

$C_{l_{max}}$ = maximum C_l at take off (with flaps down)

Typically, $V_{lof} = 1.1V_{stall}$, however, for this case Vlof = Vmc = 231 ft/sec for adequate control power.

For a flat runway with no head wind, no thrust angle-of-attack (i.e. the engines are aligned with the airplane centerline), and maximum take off thrust available at sea level, the thrust varies from maximum take off thrust (T_o at zero velocity) to thrust at lift off (T_{lof} at the end of the runway). The thrust is influenced by the speed, according to the relationship:

$$T_{lof} = T_o\left(1 + c \cdot V_{lof}^2\right) \qquad \text{(C.2.4)}$$

where:

T_{lof} as found in engine data at Vlof

T_o as found in engine data at zero velocity

c = engine thrust correction factor

Solving for the engine thrust correction factor:

$$c = \frac{\frac{T_{lof}}{T_o} - 1}{V_{lof}^2} \qquad \text{(C.2.5)}$$

The acceleration force, F, varies from F_o (at zero velocity) to F_{lof} (at lift off velocity):

$$F_o = T_o - \mu \cdot W_{to} \qquad \text{(C.2.6)}$$

$$F_{lof} = F_o + V_{lof}^2\left[c \cdot T_o - \tfrac{1}{2}\rho \cdot S(C_d - \mu \cdot C_l)\right] \qquad \text{(C.2.7)}$$

where:

μ = friction coefficient (0.02 for concrete or asphalt runway)

Define the following engine performance parameters:

$$\eta = \frac{F_{lof}}{F_o} \qquad \text{(C.2.8)}$$

$$k1 = \frac{1}{1-\eta}\ln\left(\frac{1}{\eta}\right) \tag{C.2.9}$$

$$\text{when } \eta < 1 \Rightarrow k2 = \frac{1}{2\sqrt{1-\eta}}\ln\left(\frac{1+\sqrt{1-\eta}}{1-\sqrt{1-\eta}}\right) \tag{C.2.10a}$$

$$\text{when } \eta > 1 \Rightarrow k2 = \frac{1}{\sqrt{\eta-1}}\arctan\sqrt{\eta-1} \tag{C.2.10b}$$

Hence, the runway distance (x_g [ft]) is given by:

$$x_g = \frac{W_{to} \cdot V_{lof}{}^2 \cdot k1}{2g_o \cdot F_o} \tag{C.2.11}$$

where:

g_o = gravitational acceleration [ft/s^2]

The time to lift off (t_g [sec]) is given by:

$$t_g = \frac{W_{to} \cdot V_{lof} \cdot k2}{g_o \cdot F_o} \tag{C.2.12}$$

To calculate total field length, consider three distances:

x_1 = distance to accelerate from V_{lof} to V_2 [ft]

x_2 = flare arc distance [ft]

x_3 = obstacle clearance distance [ft]

Calculate:

$$V_2 = 1.2V_{stall} \tag{C.2.13}$$

where:

V_2 = flare arc velocity [ft/sec]

Use an average velocity ($\overline{V}$ average velocity [ft/sec]) to find x_1:

$$\overline{V} = \frac{V_{lof} + V_2}{2} \tag{C.2.14}$$

$$x_1 = \overline{V} \cdot \Delta t \tag{C.2.15}$$

where:

Δt = 2 sec (assumed)

Calculate flight condition to find x_2:

$$T_2 = T_o\left(1 + c \cdot V_2{}^2\right) \tag{C.2.16}$$

where:

T_2 = thrust at flare arc [lbf]

$$C_l = \frac{2W_{to}}{\rho \cdot S \cdot V_2^2} \qquad \text{(C.2.17)}$$

Obtain C_d from the drag polar.

$$\gamma_c = \frac{T_2}{W_{to}} - \frac{C_d}{C_l} \qquad \text{(C.2.18)}$$

where:

γ_c = flare arc [rad]

$$R = \frac{V_2^2}{g_o(n-1)} \qquad \text{(C.2.19)}$$

where:

R = flare arc radius [ft]

n = load factor [g] = 1.05 for a soft maneuver or 1.15 for a hard maneuver

$$x_2 = R \cdot \sin\gamma_c \qquad \text{(C.2.20)}$$

$$h_r = R - R \cdot \cos\gamma_c \qquad \text{(C.2.21)}$$

where:

h_r = height after flare arc [ft]

If $h_r > h_{obs}$, there is no need to add x_3. For this case, h_{obs} = 35 ft from the FAR 25 specifications. In this case:

$$h_r = 35 = 2R \cdot \sin^2\gamma_c \qquad \text{(C.2.22)}$$

Use this to obtain γ_c, and hence x_2.

Total field length for take off:

$$x_{tot} = x_1 + x_2 + x_3 \qquad \text{(C.2.23)}$$

C.3 Climb:

C.3.1 Exact solution:

From the equilibrium equations:

$$T_{req} = D + W_{airplane} \cdot \sin\gamma \tag{C.3.1}$$

where:

T_{req} = required thrust [lbf]

D = drag [lbf]

$W_{airplane}$ = current airplane weight [lbf]

γ = flight path angle (in reference to horizontal plane)

$$L = W_{airplane} \cdot \cos\gamma \tag{C.3.2}$$

where:

L = lift [lbf]

$$D = \frac{1}{2}\rho \cdot S \cdot V^2 \cdot C_d \tag{C.3.3}$$

where:

V = airplane velocity [ft/sec]

$$L = \frac{1}{2}\rho \cdot S \cdot V^2 \cdot C_l \tag{C.3.4}$$

For C_d and C_l assume a parabolic drag polar which varies with altitude:

$$C_d = C_{do} + K1 \cdot C_l + K2 \cdot C_l^2 \tag{C.3.5}$$

where:

Cdo, K1, K2 = constants which vary with speed and altitude

Find available thrust (Tavail [lbf]) from:

$$T_{avail} = t \cdot n - P \tag{C.3.6}$$

where:

P = Power extraction [lbf]

n = number of engines

Calculate rate of climb (ROC [ft/sec]):

$$ROC = \frac{(T_{avail} - T_{req}) \cdot V}{W_{airplane}} \qquad (C.3.7)$$

The maximum ROC is obtained at the condition where:

$$T_{avail} = \frac{3}{2}\rho \cdot S \cdot C_{do} \cdot V_{opt}^2 - \frac{2 \cdot K2 \cdot W_{airplane}^2}{\rho \cdot S \cdot V_{opt}^2} \qquad (C.3.8)$$

where:

V_{opt} = optimum speed for maximum ROC [ft/sec]

Solving for V_{opt}^2:

$$V_{opt}^2 = \frac{W}{3 \cdot \rho \cdot S \cdot C_{do}} \left(\frac{T_{avail}}{W} + \sqrt{\frac{T_{avail}^2}{W_{airplane}^2} + 12 \cdot K2 \cdot C_{do}} \right) \qquad (C.3.9)$$

V_{opt} is constrained and cannot exceed the critical Mach number (M_{crit}). Hence:

$$ROC_{max} = \frac{V_{opt}}{W_{airplane}} \left(\rho \cdot S \cdot C_{do} \cdot V_{opt}^2 - \frac{4 \cdot K2 \cdot W_{airplane}}{\rho \cdot S \cdot V_{opt}^2} \right) \qquad (C.3.10)$$

Note that the maximum ROC does not correspond to the condition of maximum climb angle (this corresponds to the condition of maximum lift to drag ratio). Calculate the climb angle for maximum ROC from:

$$\sin\gamma = \frac{ROC}{V_{opt}} \qquad (C.3.11)$$

$$\sin\gamma = \frac{C_l^2 \cdot T_{avail}}{W_{airplane} \cdot (C_l^2 + C_d^2)} - \sqrt{\left[\frac{C_l^2 \cdot T_{avail}}{W_{airplane} \cdot (C_l^2 + C_d^2)} \right]^2 - \frac{C_l^2 \cdot T_{avail}^2 - C_d^2 \cdot W_{airplane}^2}{W_{airplane} \cdot (C_l^2 + C_d^2)}} \qquad (C.3.12)$$

There are two unknowns, γ and C_l. To solve this use an interactive method:

1) Assume a C_l value
2) Find γ from equation (C.3.12)
3) Find V_{opt}
4) Find ROC

5) Check the assumed thrust with the one calculated at V_{opt}. Interact until values stabilize.

Another approach would be to plot power (P_a and P_r) versus velocity and graphically choose velocity at maximum excess power. This automatically gives ROC and climb gradient (that is, $\frac{ROC}{V}$).

C.3.2 Approximate solution:

When the climb angle is small ($\gamma < 15°$), the following assumptions are valid:

$$\cos\gamma = 1 \tag{C.3.13}$$

$$L = W_{airplane} \tag{C.3.14}$$

$$T_{req} = D = \frac{1}{2}\rho \cdot S \cdot V^2 \tag{C.3.15}$$

The maximum ROC occurs when $\frac{\partial ROC}{\partial C_l} = 0$. In this situation, obtain C_l from:

$$K2 \cdot C_l^2 + \frac{(T_{avail} + K1) \cdot C_l}{W_{airplane}} - 3 \cdot C_{do} = 0 \tag{C.3.16}$$

Obtain optimum velocity (V_{opt}):

$$V_{opt} = \sqrt{\frac{2W_{airplane}}{\rho \cdot C_l \cdot S}} \tag{C.3.17}$$

Note that V_{opt} cannot exceed M_{crit}. Calculate C_d from drag polar (equation C.3.5). Calculate drag:

$$D = W_{airplane} \frac{C_d}{C_l} \tag{C.3.18}$$

The flight path angle can be obtained through:

$$\sin\gamma = \frac{T_{avail} - D}{W_{airplane}} \tag{C.3.19}$$

Finally, get ROC from:

$$ROC = V \cdot \sin\gamma \tag{C.3.20}$$

The service ceiling is attained when ROC = 500 ft/sec. The propulsive ceiling is attained when ROC = 0 ft/sec and in this case:

$$\frac{1}{2}\rho \cdot V^{o2} = \frac{W_{airplane}}{S}\sqrt{\frac{K2}{C_{do}}} \qquad \text{(C.3.21)}$$

where:

V^o = velocity at L/D max (for minimum P_r) [ft/sec]

With rate of climb, calculate time to climb (E_{cl} [sec]):

$$E_{cl} = \frac{2500}{ROC} \qquad \text{(C.3.22)}$$

where:

2500 = altitude breakdown [ft]

Calculate horizontal velocity (V_h [ft/sec]):

$$V_h = V_{opt} \cdot \cos\gamma \qquad \text{(C.3.23)}$$

For each 2500 ft of climb, calculate the average horizontal velocity (V_h' [ft/sec]):

$$V_h' = \frac{V_{h_{final}} - V_{h_{initial}}}{2} \qquad \text{(C.3.24)}$$

where:

$V_{h_{final}}$ = velocity after climbing each 2500 ft

$V_{h_{initial}}$ = velocity before climbing each 2500 ft

Calculate the horizontal distance covered for each 2500 ft of climb:

$$Dist = E_{cl} \cdot V_h' \qquad \text{(C.3.25)}$$

Sum all these breakdowns and obtain total horizontal distance covered during climb. This distance is to be subtracted from the outbound cruise range. With each altitude breakdown from rate of climb, list the temperature, velocity of sound and obtain Mach number (M):

$$a = \sqrt{1.4 \cdot 1716 \cdot temp} \qquad \text{(C.3.26)}$$

where:

a = velocity of sound [ft/sec]

temp = air temperature (°R)

$$M = \frac{V_{opt}}{a} \qquad \text{(C.3.27)}$$

List thrust and fuel flow from General Electric data. Calculate C_j. Get W_{fuel} for each 2500 ft of climb:

$$W_{fuel} = E_{cl} \cdot C_j \cdot T \qquad \text{(C.3.28)}$$

where:

T = total uninstalled thrust [lbf]

C.3.3 Velocity constraints:

Sometimes it is not possible or desired to achieve V_{opt} for climb right after lift off because of FAR velocity constraints (250 knots below 10,000 ft of altitude). In this case, assume this velocity in the calculation. Above 10,000 ft, climb is performed at a constant indicated speed. Calculate actual speed (V_{act}):

$$V_{act} = \sqrt{\frac{\rho_o \cdot V_{ind}^2}{\rho}} \qquad \text{(C.3.29)}$$

where:

ρ_o = air density at sea level [slug/ft^3]

V_{ind} = indicated speed [ft/sec]

Perform the rest of the calculation as indicated above (item 3.2). When the critical mach number is reached, set the velocity based on this mach number.

C.4 Outbound Cruise:

The best L/D represents the best condition for C_j. Take the derivative of the drag polar, equal it to zero, and obtain the maximum value for L/D. This happens when:

$$C_l^\circ = \sqrt{\frac{C_{do}}{K2}} \qquad \text{(C.4.1)}$$

where:

$C_l^\circ = C_l$ at maximum L/D

$$C_d^\circ = 2C_{do} + K1 \cdot \sqrt{\frac{C_{do}}{K2}} \qquad \text{(C.4.2)}$$

where:

$C_d^\circ = C_d$ at maximum L/D

$$\left(\frac{C_d}{C_l}\right)_{min} = \sqrt{4C_{do} \cdot K2} + K1 \qquad (C.4.3)$$

C.4.1 Cruise at BCA and BCM :

The fuel consumption can be minimized by cruising at best cruise mach number (BCM), at the best cruise altitude (BCA). By definition for this case:

$$BCM = M_{crit} \qquad (C.4.4)$$

Calculate the weight ratio for each cruise distance breakdown:

$$\frac{W_{final}}{W_{initial}} = e^{\frac{\left(\frac{C_d}{C_l}\right)_{min} \cdot C_j \cdot \Delta s}{BCM \cdot a}} \qquad (C.4.5)$$

where:

W_{final} = weight after cruise segment [lbf]

$W_{initial}$ = weight before cruise segment [lbf]

Δs = distance covered in cruise segment [mi]

Note that, although BCM is constant (because the airplane reached the tropopause and the temperature is constant), BCA increases because of W_{fuel} consumed ($W_{airplane}$ is decreasing). From the equilibrium equation for steady cruise:

$$W = \frac{1}{2}\rho \cdot S \cdot C_l^{\circ} \cdot V^2 = \frac{1}{2}\rho \cdot BCM^2 \cdot a^2 \cdot S \cdot C_l^{\circ} \qquad (C.4.6)$$

where:

W = airplane weight [lbf]

Solve for:

$$\rho = \frac{2 \cdot W_{airplane}}{BCM^2 \cdot a^2 \cdot S \cdot C_l^{\circ}} \qquad (C.4.7)$$

Using the air density, find new cruise altitudes BCA for each cruise breakdown. Upgrade Cl_{max}, Cd_{min} and C_j for each new BCA. Calculate the airplane velocity and time required to cover each cruise distance breakdown:

$$V = BCM \cdot a \qquad (C.4.8)$$

$$V = \frac{Dist}{E_{cr}} \qquad (C.4.9)$$

where:

E_{cr} = time to cover each cruise distance breakdown

Now obtain W_{fuel} used for each breakdown:

$$W_{fuel} = E_{cr} \cdot C_j \cdot T \tag{C.4.10}$$

Sum all W_{fuel} for each breakdown to obtain total fuel used. If BCA is above the service ceiling, use the following method:

C.4.2 Service ceiling constraint:

If there is any ceiling constraint, fix the initial cruise altitude as a preset value (H_O). The specific fuel consumption will be higher than the one during cruise at BCM and BCA. Find ρ at H_O. Now, calculate new Mach number from the weight equation:

$$W_{airplane} = \frac{1}{2}\rho \cdot M^2 \cdot a^2 \cdot S \cdot C_l^{\circ} \tag{C.4.11}$$

$$M = \sqrt{\frac{2W_{airplane}}{\rho \cdot a^2 \cdot S \cdot C_l^{\circ}}} \tag{C.4.12}$$

Consider this Mach number constant during the cruise portion. The required thrust will be:

$$T = \frac{1}{2}\rho \cdot V^2 \cdot S \cdot C_d^{\circ} \tag{C.4.13}$$

With C_j from GE data, calculate W_{fuel} used for each cruise distance breakdown:

$$W_{fuel} = E_{cr} \cdot C_j \cdot T \tag{C.4.14}$$

C.5 Loiter Before Launch:

From the equilibrium equations:

$$L = W_{airplane} - T_{req} \cdot \sin\alpha \tag{C.5.1}$$

where:

α = angle of attack [rad]

$$D = T_{req} \cdot \cos\alpha \tag{C.5.2}$$

$$T_{req} = \frac{W_{airplane}}{\left(\frac{C_l}{C_d}\right) \cdot \cos\alpha + \sin\alpha} \tag{C.5.3}$$

For a given $W_{airplane}$, to obtain minimum thrust, we need the maximum value for the denominator in equation (C.5.3). Assuming a parabolic drag polar dependent of altitude, and from C_{l_α}:

$$C_l = C_{l_\alpha} \cdot \alpha + C_{lo} \tag{C.5.4}$$

$$C_d = C_{do} + K1 \cdot C_l + K2 \cdot C_l^2 \tag{C.5.5}$$

$$C_d = C_{do} + K1 \cdot C_{l_\alpha} \cdot \alpha + K1 \cdot C_{lo} + K2\left(C_{l_\alpha}^2 \cdot \alpha^2 + 2C_{l_\alpha} \cdot \alpha \cdot C_{lo} + C_{lo}^2\right) \tag{C.5.6}$$

Find the derivative of C_d in relation to α. The function is maximum when this derivative equals zero:

$$\frac{C_{l_\alpha} \cdot \cos\alpha}{B} - \frac{\left(C_{l_\alpha} \cdot \alpha + C_{lo}\right) \cdot \cos\alpha \cdot \left(K1 \cdot C_{l_\alpha} + 2 \cdot K2\left[C_{l_\alpha} \cdot \alpha + C_{lo}\right] \cdot C_{l_\alpha}\right)}{B^2}$$

$$- \frac{\left(C_{l_\alpha} \cdot \alpha + C_{lo}\right) \cdot \sin\alpha}{B} + \cos\alpha = 0 \tag{C.5.7}$$

where:

$$B = C_{do} + K1 \cdot \left(C_{l_\alpha} \cdot \alpha + C_{lo}\right) + K2 \cdot \left(C_{l_\alpha} \cdot \alpha + C_{lo}\right)^2 \tag{C.5.8}$$

Alternate method:
Note that for each Mach number, we have different values for C_{l_α}, C_{do}, C_{lo}, thus different lift to drag ratios and angles of attack. This leads to different thrusts. By comparing all these thrusts, choose the minimum amongst them. Match the corresponding Mach number to the minimum velocity required to sustain loiter and you consequently find the angle of attack:

$$V = \sqrt{\frac{2T_{min} \cdot \cos\alpha}{\rho \cdot S \cdot C_d}} \tag{C.5.9}$$

The initial loiter altitude is the same as the final cruise altitude. Consider this Mach constant during loiter. The altitude increase due to weight reduction. Consider C_l and C_d independent of altitude, though. Get C_j from GE data and calculate W_{fuel} used for each loiter time breakdown:

$$W_{fuel} = E_{loi} \cdot C_j \cdot T \tag{C.5.10}$$

where:

E_{loi} = loiter time breakdown

As $W_{airplane}$ decreases, find new altitudes with:

$$\rho = \frac{2T}{S \cdot C_d \cdot V^2} \qquad \text{(C.5.11)}$$

C.6 Inbound Cruise (Aborted Mission):

Same procedure as cruise out, only this time the initial altitude is that one reached after loiter.

C.7 Descent to 10,000 ft:

Consider flattest glide with maximum range. By doing this, assume idle thrust. Assume small flight path angle. Obtain velocity as a function of weight and altitude:

$$W = \frac{1}{2}\rho \cdot S \cdot V^2 \sqrt{\frac{C_{do}}{K2}} \qquad \text{(C.7.1)}$$

$$V = \sqrt{\frac{2W_{airplane}}{\sqrt{\frac{C_{do}}{K2}} \cdot \rho \cdot S}} \qquad \text{(C.7.2)}$$

Note that since ρ increases, V decreases. Also, the weight decreases and C_{do} and K2 vary with altitude. The vertical velocity (V_z [ft/sec]) is obtained from:

$$V_z = V \cdot \sin\gamma \qquad \text{(C.7.3)}$$

The horizontal velocity (V_h [ft/sec]) is:

$$V_h = V \cdot \cos\gamma \qquad \text{(C.7.4)}$$

Calculate the average velocity ($\overline{V}_h$ [ft/sec]) when computing distance covered. Time elapsed (Δt [sec]) can be obtained from:

$$\Delta t = \frac{Z_i - Z_f}{V_z} \qquad \text{(C.7.5)}$$

where:

Z_i = initial altitude for each breakdown [ft]

Z_f = final altitude for each breakdown [ft]

The horizontal distance (Dist [ft]) covered for each breakdown is:

$$Dist = \Delta t \cdot \overline{V}_h \qquad \text{(C.7.6)}$$

The minimum angle for this descent will be:

$$\tan(-\gamma) = \left(\frac{C_d}{C_l}\right)_{min} = 2\sqrt{K2 \cdot C_{do}} \qquad (C.7.7)$$

where:

γ = flight path angle [rad]

Note: C_j is not zero, i.e. the engines are not turned off. Use conventional values for mission fuel fraction and use weight breakdown. The distance covered during descent is credited to the cruise range.

C.8 Loiter at Constant Altitude:

Same as previous loiter, only this time ρ is constant:

$$V = \sqrt{\frac{2T_{avail} \cdot \cos\alpha}{\rho \cdot S \cdot C_d}} \qquad (C.8.1)$$

Consider velocity constant. C_d will decrease, and so will the angle of attack.

C.9 En Route Descent:

Use minimum rate of descent (V_z), to reduce the approaching velocity. Assume idle thrust.

$$V_{z_{min}} = 4 \cdot \sqrt{\frac{2 \cdot K2 \cdot C_{do} \cdot W_{airplane}}{\rho \cdot S}} \frac{K2}{\sqrt[4]{27 C_{do}}} \qquad (C.9.1)$$

Calculate V_z for each altitude breakdown. Consider drag polar dependent of altitude. The flight path angle is obtained from:

$$\tan(-\gamma) = 4 \cdot \sqrt{\frac{K2 \cdot C_{do}}{3}} = 2 \cdot \frac{\left(\frac{C_d}{C_l}\right)_{min}}{\sqrt{3}} \qquad (C.9.2)$$

The airplane speed is given by:

$$V_z = -V \cdot \sin\gamma \qquad (C.9.3)$$

The total time of descent is:

$$t = \sqrt[4]{\frac{27 C_{do}}{K2}} \sqrt{\frac{S}{2W_{airplane}}} \frac{\sqrt{\rho_{final}} - \sqrt{\rho_{initial}}}{2 \cdot \beta \cdot \sqrt{K2 \cdot C_{do}}} \qquad (C.9.4)$$

or, using the exponential atmosphere:

$$t = \sqrt[4]{\frac{27C_{do}}{K2}}\sqrt{\frac{S}{2W_{airplane}}}\frac{\sqrt{\rho_{initial}}\cdot\left(e^{\frac{\beta\cdot\Delta Z}{2}}-1\right)}{2\cdot\beta\cdot\sqrt{K2\cdot C_{do}}} \qquad (C.9.5)$$

where:

$1/\beta = 23{,}500$ ft

C.10 Landing and Taxi In:

C.10.1 Fuel fraction:

Assume 5 minutes at 50% thrust for touch-down and 30 minutes at idle thrust (less than 10% of total thrust) for taxi-in.

C.10.2 Runway length and landing time:

After touch-down, allow 3 seconds before brakes are applied.

The touch-down velocity (V_{td}) is:

$$V_{td} = 1.1V_{stall} \qquad (C.10.1)$$

The distance before braking (x_o) is:

$$x_o = 3V_{td} \qquad (C.10.2)$$

where:

x_o [ft]

The decelerating force (F) is computed from:

$$F = -\left[T + \frac{1}{2}\rho\cdot S\cdot V^2\cdot(C_d - \mu\cdot C_l) + (\mu+\theta)\cdot W_{airplane}\right] \qquad (C.10.3)$$

where:

θ = runway slope [rad]

μ = brake friction coefficient

For the most unfavorable scenario, assume a flat runway, no reverse thrust, and no head wind. Just disc brakes are operational. Under these circumstances, the decelerating force varies from F_{td} (at touchdown) to F_o (at full stop):

$$F_o = \mu\cdot W_{airplane} \qquad (C.10.4)$$

$$F_{td} = F_o + \frac{1}{2}\rho\cdot S\cdot(C_d - \mu\cdot C_l)\cdot V_{td}^2 \qquad (C.10.5)$$

Again, calculate:

$$\eta = \frac{F_{td}}{F_o} \qquad \text{(C.10.6)}$$

Calculate k1 and k2 as described previously (during take off). The distance with brakes applied (x_{g_b}) will be:

$$x_{g_b} = \frac{W_{airplane} \cdot V_{td}^2 \cdot k1}{2 \cdot g_o \cdot F_o} \qquad \text{(C.10.7)}$$

Time with brakes applied (t_g) is:

$$t_g = \frac{W_{airplane} \cdot V_{td} \cdot k2}{g_o \cdot F_o} \qquad \text{(C.10.8)}$$

Total landing distance from touch-down to full stop (x_g):

$$x_g = x_o + x_{g_b} \qquad \text{(C.10.9)}$$

C.11 Turning Performance:

C.11.1 Turning fuel fraction:

At any given moment of the mission, calculate the fuel fraction for a steady turn at constant altitude as follows:

$$L = n \cdot W_{airplane} \qquad \text{(C.11.1)}$$

where:

n = load factor

$$L = \frac{W_{airplane}}{\cos\phi} \qquad \text{(C.11.2)}$$

where:

ϕ = bank angle [rad]

The duration of the turn (Δt) is given by:

$$\Delta t = \frac{2\pi \cdot R_c \cdot N}{V} = \frac{2\pi \cdot R_c \cdot N \cdot V}{g_o \cdot \sqrt{n^2 - 1}} \qquad \text{(C.11.3)}$$

where:

R_c = turn radius (ft)

N = number of turns

Δt = seconds (if V is given in ft/sec)

$$R_c = \frac{V^2}{g_o \cdot \tan\phi} = \frac{V^2}{g_o\sqrt{n^2 - 1}} \qquad \text{(C.11.4)}$$

Obtain the fuel fraction from:

$$\frac{W_{final}}{W_{initial}} = e^{\frac{C_j \cdot \sqrt{\sigma} \cdot n \cdot C_d \cdot \Delta t}{C_l}} \qquad \text{(C.11.5)}$$

where:

σ = static temperature ratio

C.11.2 Post-launch maneuver:

With a turning maneuver, the airplane must recede as quick as possible from the booster. The purpose of this analysis is to predict the optimum attainable turn condition. Important observation: Turn is to be performed at critical Mach number. Since this is a high altitude maneuver, thrust available may impose some restrictions:

- If $T_{req} < T_{avail}$, the airplane can perform a turn and climb maneuver, or a turn at maximum rate at minimum radius.
- If $T_{req} > T_{avail}$, the thrust must be set as $T_{avail} = T_{req}$, and all available thrust is used for flat turning.

After payload release, the drag polar parameters change: use C_{do}, K1 and K2 for the 'clean' configuration.

The new airplane weight (W) is given by:

$$W = W_{airplane} - W_{payload} \qquad \text{(C.11.6)}$$

where:

$W_{payload}$ = space booster weight

From the equilibrium equations during turn:

$$W = L \cdot \cos\phi \qquad \text{(C.11.7)}$$

$$\cos\phi = \frac{1}{n} \qquad \text{(C.11.8)}$$

$$L = n \cdot W \qquad \text{(C.11.9)}$$

$$m = \frac{W}{g_o} \qquad \text{(C.11.10)}$$

$$\frac{m \cdot V^2}{R_c} = L \cdot \sin\phi \qquad \text{(C.11.11)}$$

where:

R_C = turning radius [ft]

$$\frac{T}{W} = \frac{n}{E} \qquad \text{(C.11.12)}$$

where:

E = lift to drag ratio (C_l/C_d)

Note that the thrust required for turning is greater than thrust required for loiter or cruise.

C.11.2.1 No constraints:

Use: n_s = limit load factor.

-For minimum radius at maximum rate:

For the minimum turning radius ($R_{c_{min}}$) along with maximum turning rate (φ'_{max}), use $C_{l_{max}}$ at turning stall speed:

$$V_{t_{stall}} = \sqrt{\frac{2n_s \cdot W}{\rho \cdot S \cdot C_{l_{max}}}} \qquad \text{(C.11.13)}$$

where:

$V_{t_{stall}}$ = stall speed for turning

n_s = limit load factor = ultimate load factor / 1.5

$$R_{c_{min}} = \frac{2 \cdot n_s \cdot W}{g_o \cdot \rho \cdot S \cdot C_{l_{max}} \sqrt{n_s^2 - 1}} \qquad \text{(C.11.14)}$$

$$\varphi'_{max} = g_o \sqrt{\frac{\rho \cdot S \cdot C_{l_{max}} \cdot \frac{n_s - 1}{n_s}}{2 \cdot W}} \qquad \text{(C.11.15)}$$

where:

φ' [rad/sec]

This maneuver requires turning at V_{stall}, which is not recommended (not even desired).

-For turning with climbing:

From the equilibrium equations for turn with climb:

$$T_{req} = \frac{1}{2}\rho \cdot S \cdot V^2 \cdot C_d + W \cdot \sin\gamma \qquad \text{(C.11.16)}$$

$$L = n \cdot W \qquad \text{(C.11.17)}$$

$$n = \frac{\cos\gamma}{\cos\phi} \tag{C.11.18}$$

Obtain C_l from:

$$n \cdot W = \frac{1}{2}\rho \cdot S \cdot V^2 \cdot C_l \tag{C.11.19}$$

From the drag polar, obtain C_d. The rate of climb is given by:

$$ROC = \frac{\left(T_{avail} - T_{req}\right) \cdot V}{W} \tag{C.11.20}$$

Obtain the flight path angle from:

$$ROC = V \cdot \sin\gamma \tag{C.11.21}$$

Obtain bank angle from:

$$\cos\phi = \frac{\cos\gamma}{n_s} \tag{C.11.22}$$

Calculate the turning radius:

$$R_c = \frac{V^2 \cdot \cos\gamma}{g_o \cdot \tan\phi} = \frac{V^2 \cdot \cos^2\gamma}{g_o \cdot \sqrt{n_s{}^2 - \cos^2\gamma}} \tag{C.11.23}$$

Obtain turning rate:

$$\varphi' = \frac{g_o \cdot \tan\phi}{V \cdot \cos\gamma} \tag{C.11.24}$$

C.11.2.2 Thrust and/or lift constraints:

If the available thrust is not sufficient, the best turn can only be performed at: $T_{avail} = T_{req}$. Also, the flight attitude cannot exceed E_{max}. Verify if turn is possible at E_{max} and T_{avail}, at limit load factor. If not, turn can only be performed at a lower load factor (n'), since the velocity is set at M_{crit}.

-For maximum practicable load factor:

By maximizing C_l/C_d, calculate maximum practicable load factor (n'):

$$n' = \frac{T_{avail} \cdot E_{max}}{W_{airplane}} \tag{C.11.25}$$

C_l can be obtained from the relationship:

$$n' \cdot W = \frac{1}{2}\rho \cdot S \cdot V^2 \cdot C_l \qquad \text{(C.11.26)}$$

C_d is obtained from:

$$T_{avail} = D = \frac{1}{2}\rho \cdot S \cdot V^2 \cdot C_d \qquad \text{(C.11.27)}$$

The turning radius (R_C) is given by:

$$R_C = \frac{V^2}{g_o \cdot \tan\phi} = \frac{V^2}{g_o\sqrt{n'^2 - 1}} \qquad \text{(C.11.28)}$$

The turning rate (φ') is given by:

$$\varphi' = \frac{g_o \cdot \tan\phi}{V} = \frac{g_o\sqrt{n'^2 - 1}}{V} = g_o\sqrt{\frac{\rho \cdot S \cdot C_l\left(\frac{n'-1}{n'}\right)}{2 \cdot W}} \qquad \text{(C.11.29)}$$

-For maximum turning rate:

Performed at:

$$C_d = \frac{T}{W}\sqrt{\frac{C_{do}}{K2}} \qquad \text{(C.11.30)}$$

Obtain C_l from drag polar. The load factor is:

$$n = \frac{C_l}{C_d}\frac{T_{avail}}{W_{airplane}} \qquad \text{(C.11.31)}$$

$$\varphi'_{max} = \frac{g_o}{W}\sqrt{\rho \cdot S \cdot C_l{}^\circ \cdot \frac{T \cdot E_{max}}{W - 1}} \qquad \text{(C.11.32)}$$

$$C_l{}^\circ = \sqrt{\frac{C_{do}}{K2}} \qquad \text{(C.11.33)}$$

$$E_{max} = \frac{1}{2\sqrt{K2 \cdot C_{do}}} \qquad \text{(C.11.34)}$$

-For minimum turning radius:

Performed at:

$$C_d = \frac{T^2}{2 \cdot W^2 \cdot K2} \qquad \text{(C.11.35)}$$

$$R_{c_{min}} = \frac{2 \cdot W}{\rho \cdot S \cdot g_o \cdot C_l^{\circ} \sqrt{\frac{E_{max}^2 \cdot T^2}{W^2 - 1}}} \qquad \text{(C.11.36)}$$

C.12 Other Mission Performance:

C.12.1 Minimum fuel mission

The minimum fuel mission performance is calculated as above, except the cruise segments are omitted.

C.12.2 Ferry mission

The ferry mission has a fixed cruise altitude of 35,000 ft and a fuel capacity of 350,000 pounds. Cruise performance is calculated so that all fuel is used, which determines the range.

(This page left intentionally blank.)

D. GENERAL ELECTRIC ENGINE DATA

SUBJECT: BIG ENGINE DATA

November 16, 1992

TO: David Levy

Hello Dave, please find data plots to check for usefulness. This is a 100K class advanced ultra high bypass (AUHB) engine. With, maybe, a center rotating L.P. system, driving a .3 radius ratio fan with a fan flow area of 76.6 square feet.

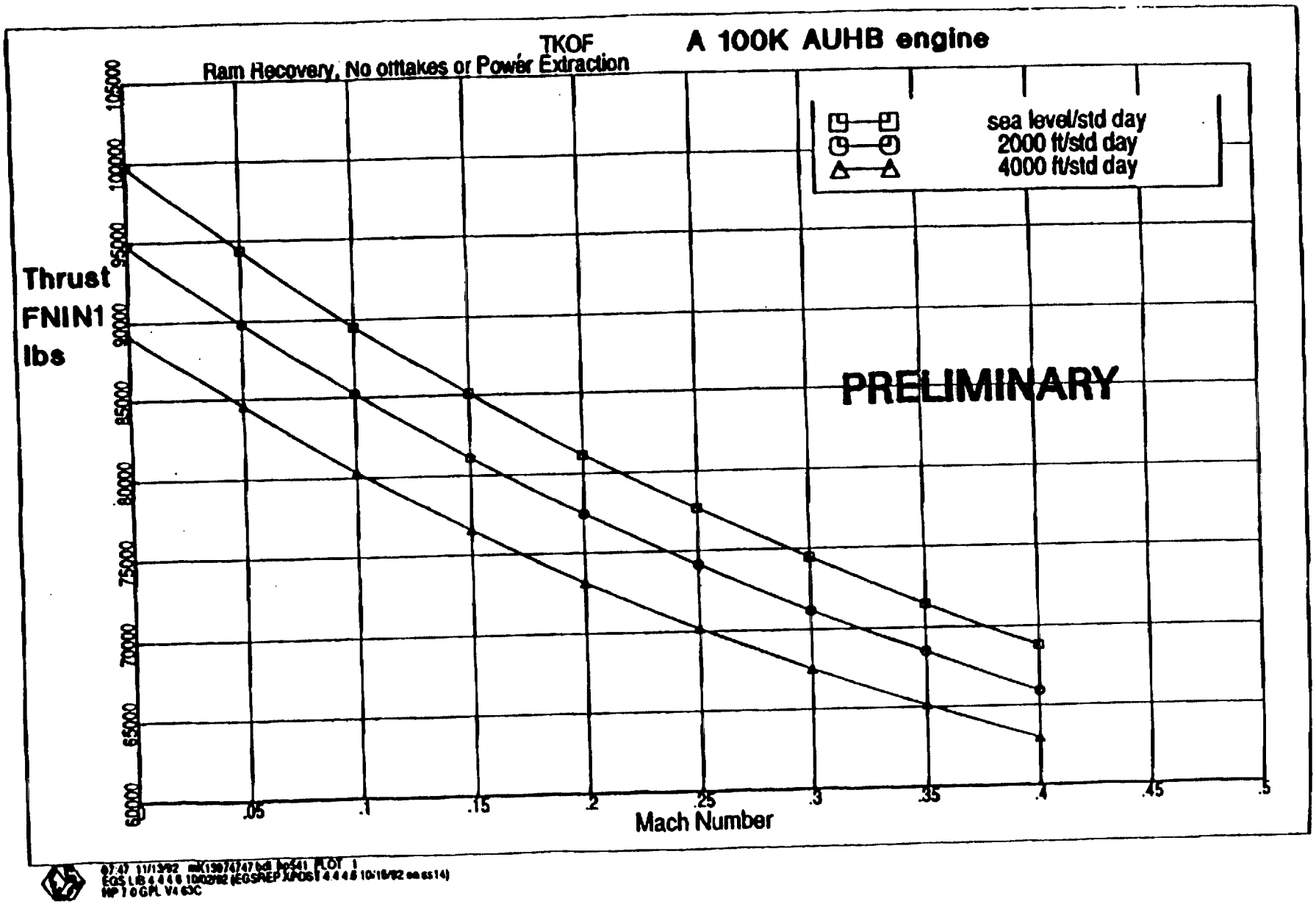
TKOF
A 100K AUHB engine
Ram Recovery, No offtakes or Power Extraction
sea level/std day
2000 ft/std day
4000 ft/std day
PRELIMINARY
Thrust
FNIN1
lbs
105000
100000
95000
90000
85000
80000
75000
70000
65000
60000
.05
.1
.15
.2
.25
.3
.35
.4
.45
.5
Mach Number

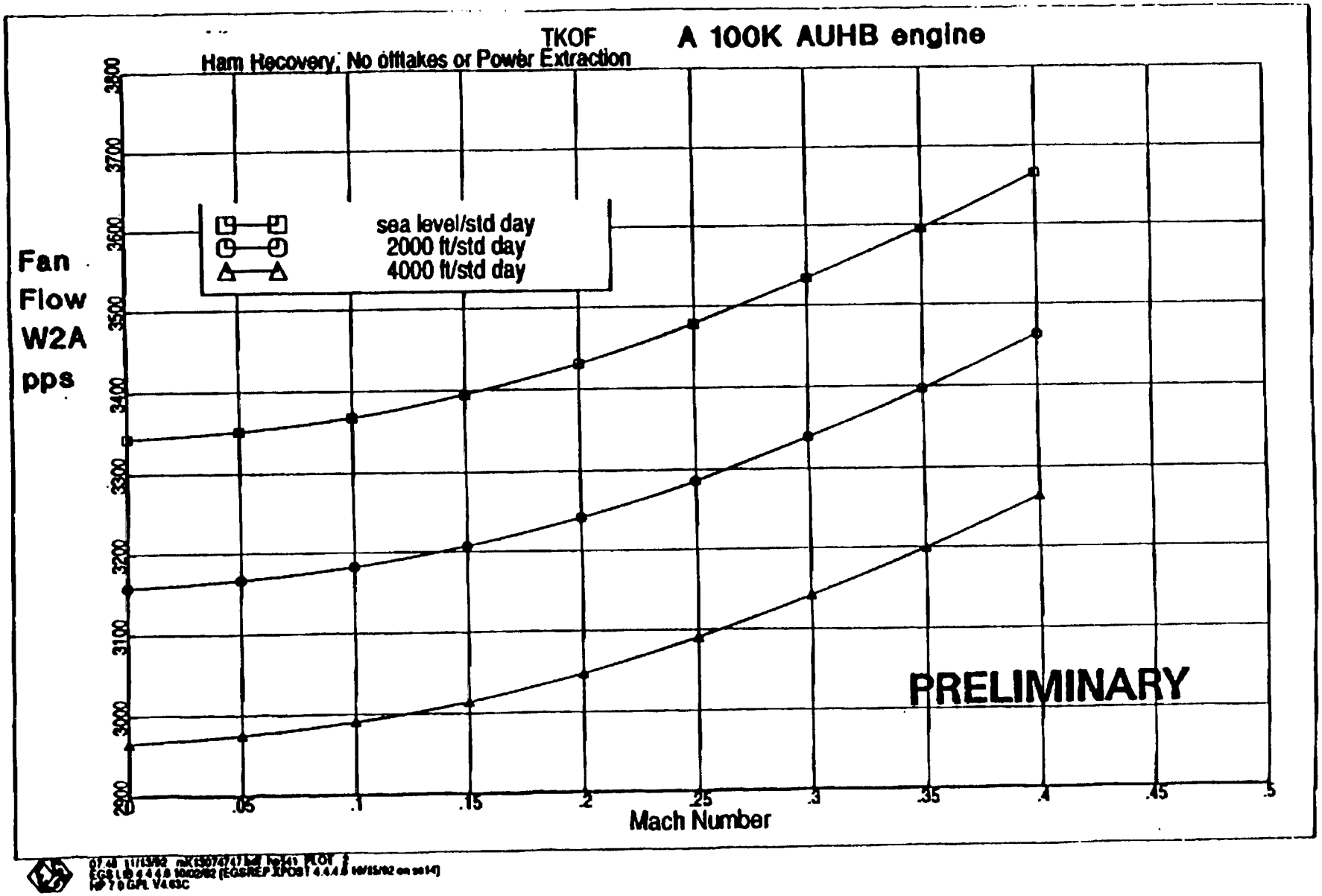
TKOF
A 100K AUHB engine
Ham Recovery, No offtakes or Power Extraction
sea level/std day
2000 ft/std day
4000 ft/std day
Fan
Flow
W2A
pps
3800
3700
3600
3500
3400
3300
3200
3100
3000
2900
.05
.1
.15
.2
.25
.3
.35
.4
.45
.5
Mach Number
PRELIMINARY

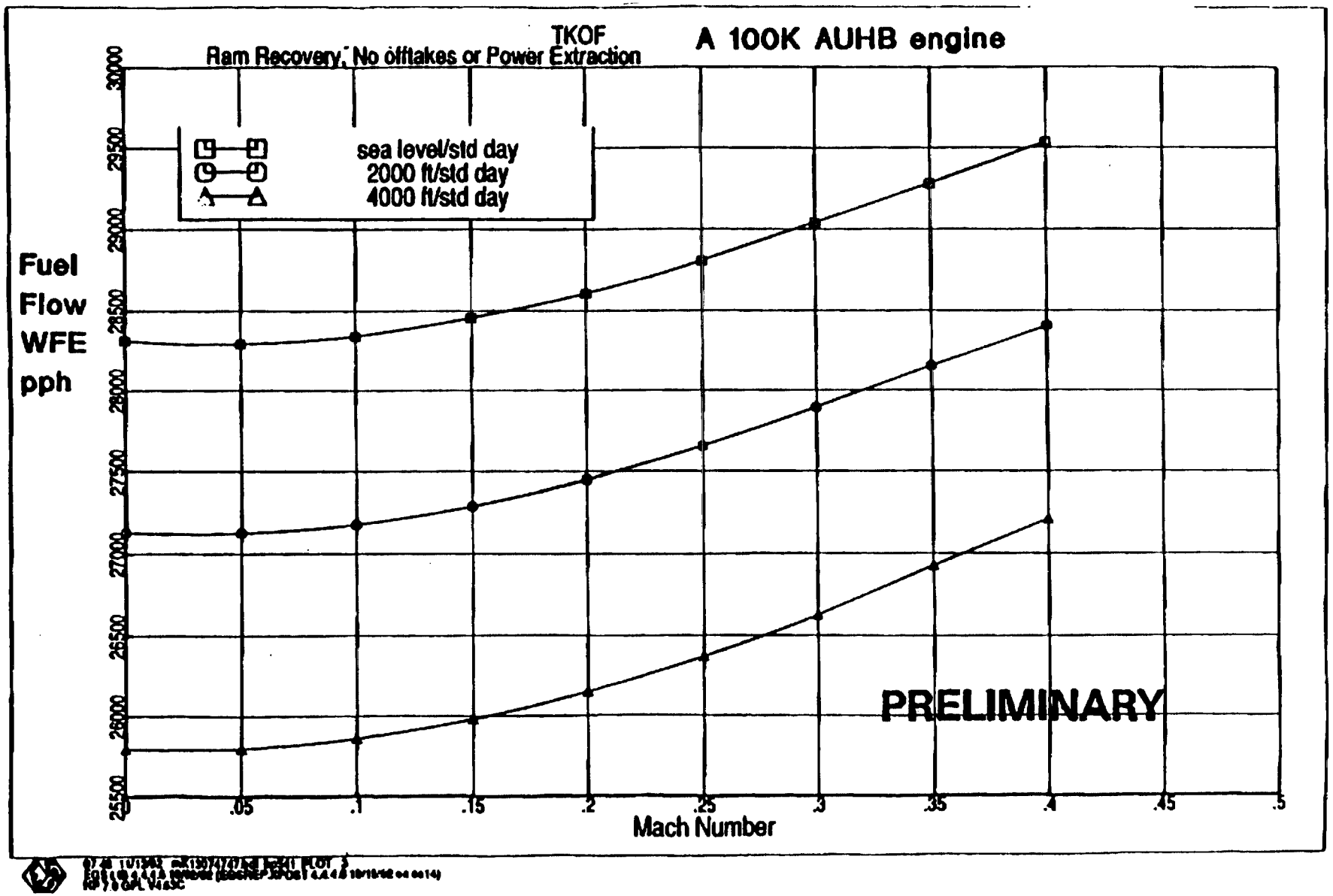
TKOF
A 100K AUHB engine
Ram Recovery, No offtakes or Power Extraction
sea level/std day
2000 ft/std day
4000 ft/std day
Fuel
Flow
WFE
pph
30000
29500
29000
28500
28000
27500
27000
26500
26000
25500
.05
.1
.15
.2
.25
.3
.35
.4
.45
.5
Mach Number
PRELIMINARY

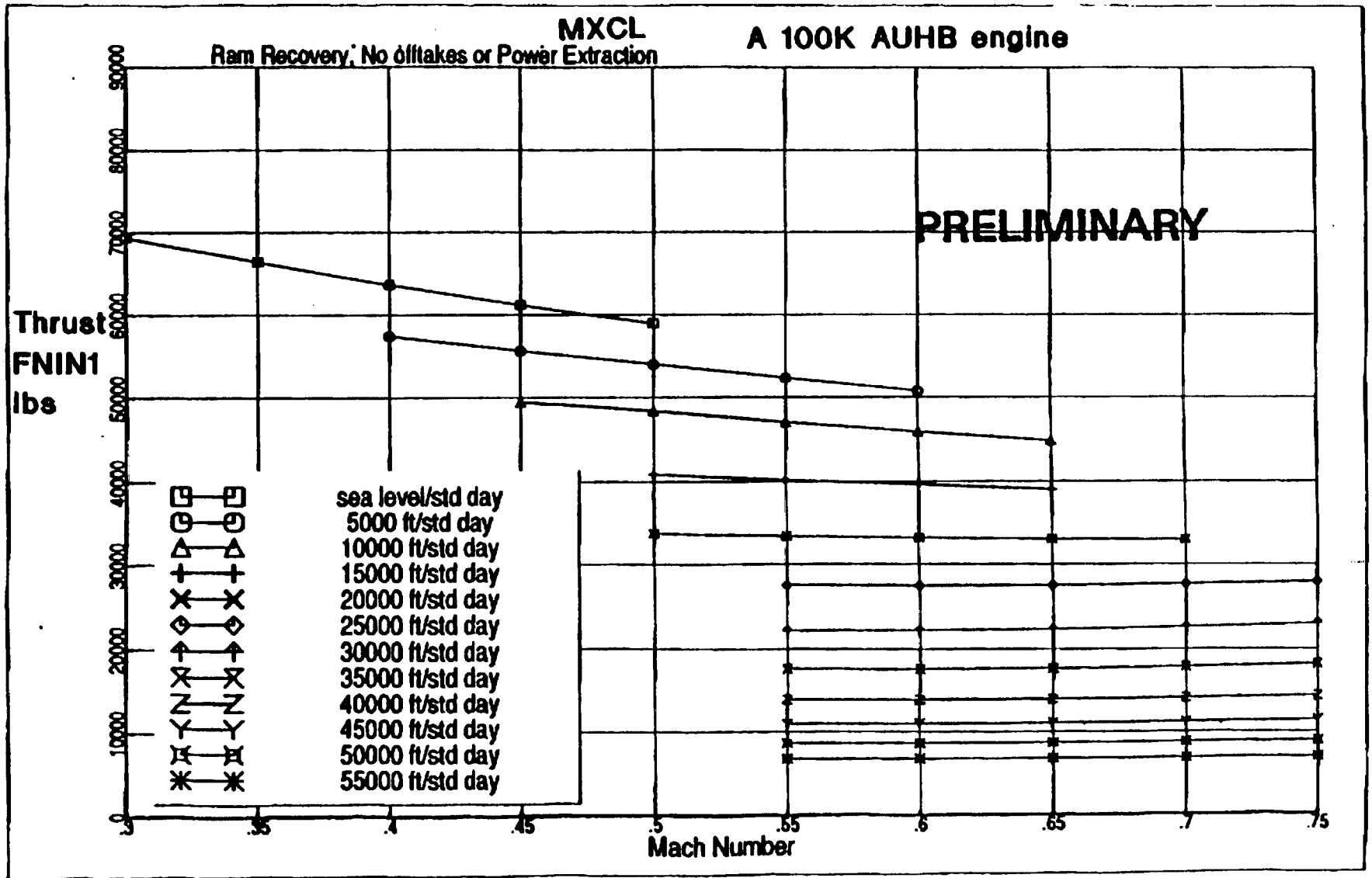
MXCL
A 100K AUHB engine
Ram Recovery, No offtakes or Power Extraction
PRELIMINARY
Thrust
FNIN1
lbs
sea level/std day
5000 ft/std day
10000 ft/std day
15000 ft/std day
20000 ft/std day
25000 ft/std day
30000 ft/std day
35000 ft/std day
40000 ft/std day
45000 ft/std day
50000 ft/std day
55000 ft/std day
Mach Number

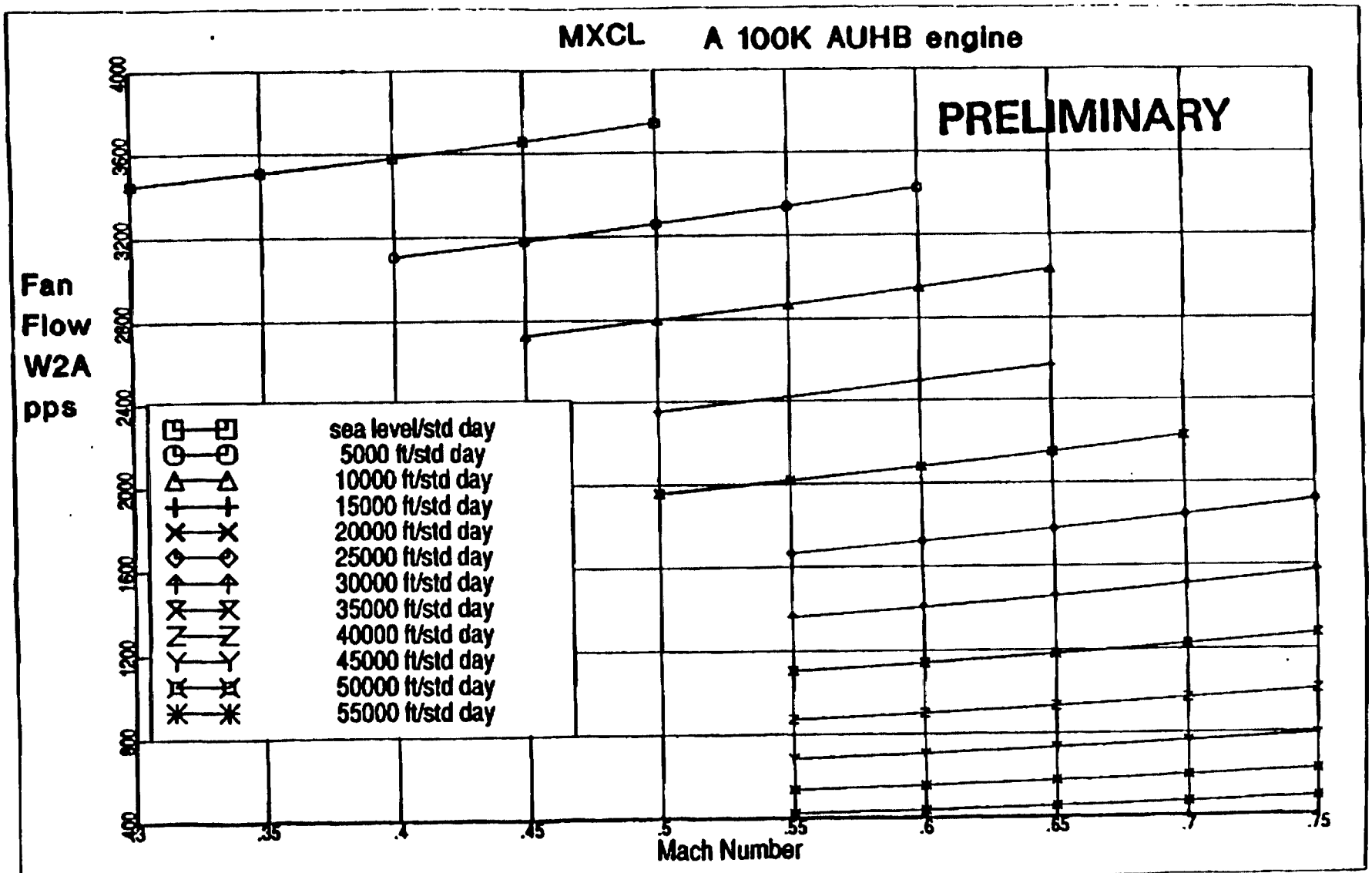
MXCL A 100K AUHB engine
PRELIMINARY
Fan Flow W2A pps
4000
3600
3200
2800
2400
2000
1600
1200
800
400
.3
.35
.4
.45
.5
.55
.6
.65
.7
.75
Mach Number
sea level/std day
5000 ft/std day
10000 ft/std day
15000 ft/std day
20000 ft/std day
25000 ft/std day
30000 ft/std day
35000 ft/std day
40000 ft/std day
45000 ft/std day
50000 ft/std day
55000 ft/std day

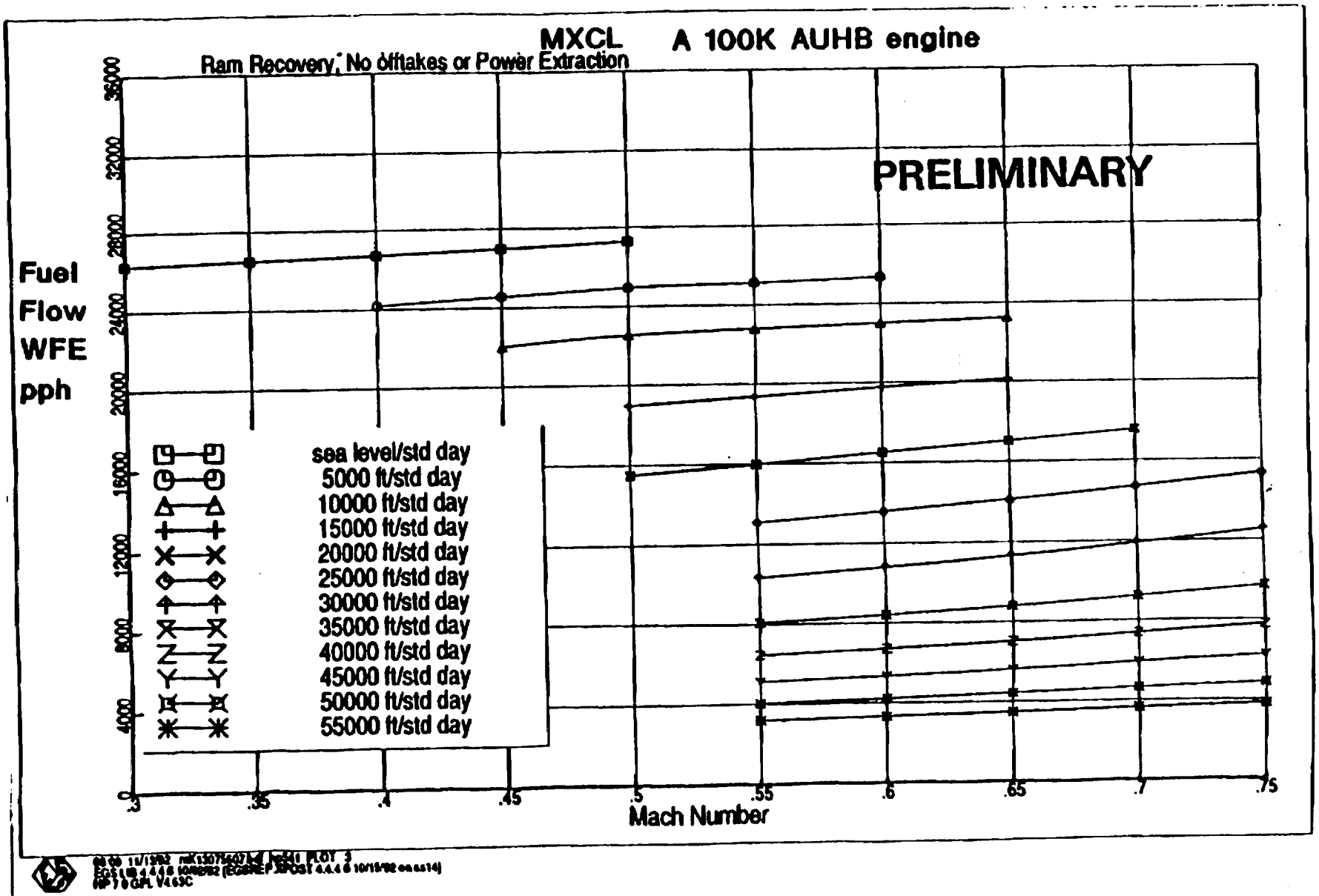
MXCL A 100K AUHB engine
Ram Recovery, No offtakes or Power Extraction
PRELIMINARY
Fuel Flow WFE pph
sea level/std day
5000 ft/std day
10000 ft/std day
15000 ft/std day
20000 ft/std day
25000 ft/std day
30000 ft/std day
35000 ft/std day
40000 ft/std day
45000 ft/std day
50000 ft/std day
55000 ft/std day
Mach Number

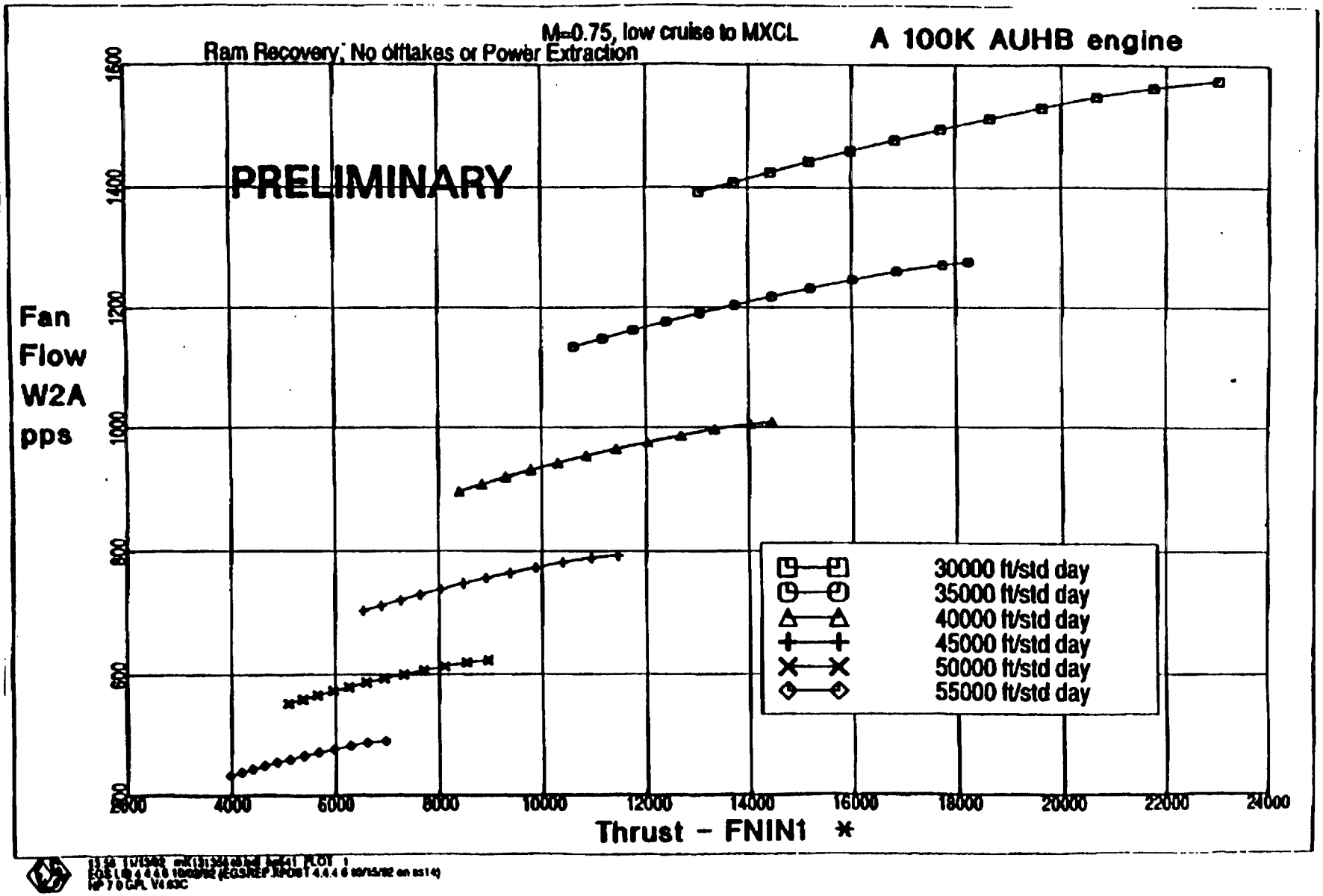
M=0.75, low cruise to MXCL
A 100K AUHB engine
Ram Recovery, No offtakes or Power Extraction
PRELIMINARY
Fan
Flow
W2A
pps
1600
1400
1200
1000
800
600
400
2000
4000
6000
8000
10000
12000
14000
16000
18000
20000
22000
24000
Thrust - FNIN1 *
30000 ft/std day
35000 ft/std day
40000 ft/std day
45000 ft/std day
50000 ft/std day
55000 ft/std day

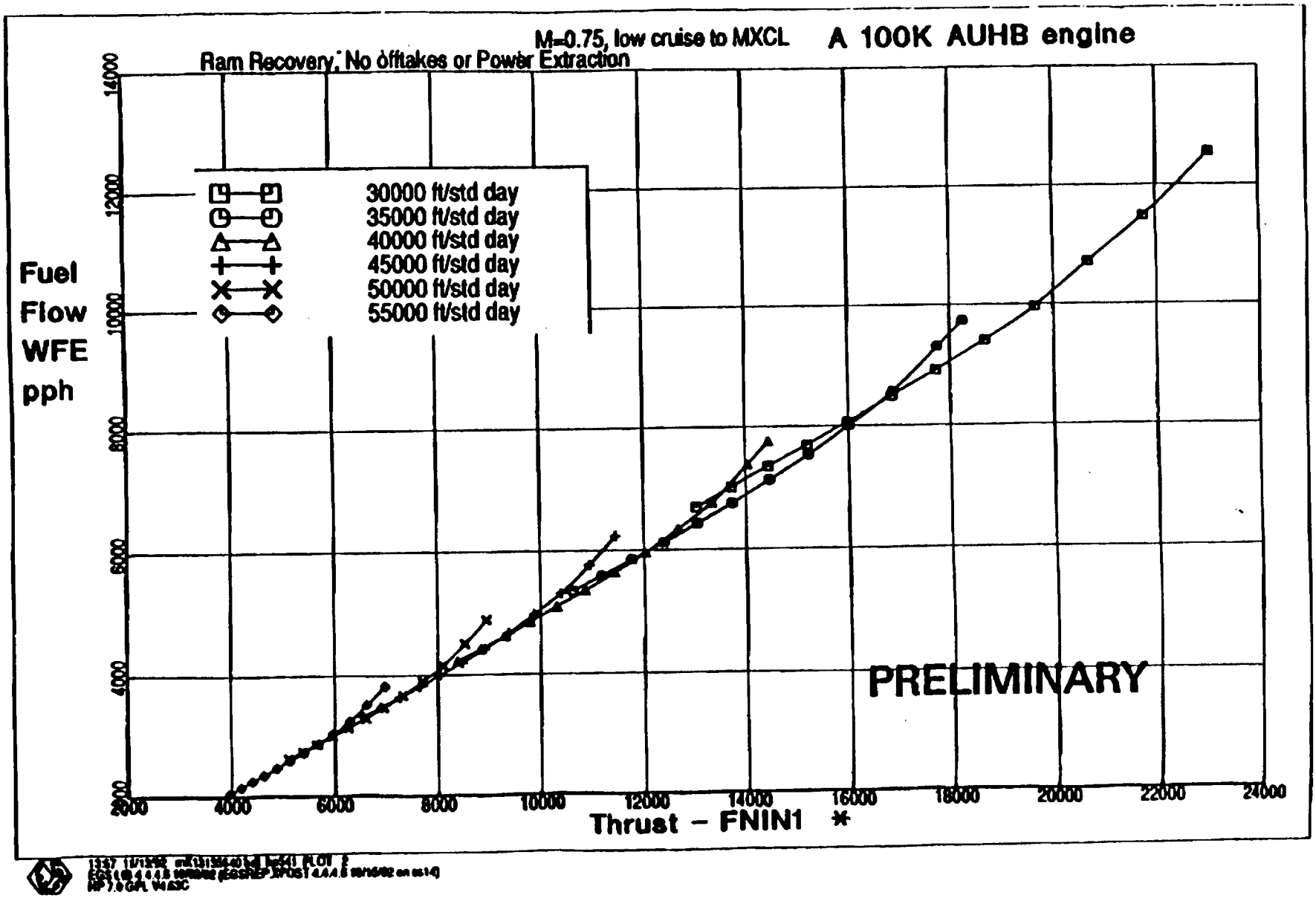
M=0.75, low cruise to MXCL
A 100K AUHB engine
Ram Recovery, No offtakes or Power Extraction
30000 ft/std day
35000 ft/std day
40000 ft/std day
45000 ft/std day
50000 ft/std day
55000 ft/std day
Fuel Flow WFE pph
14000
12000
10000
8000
6000
4000
2000
2000
4000
6000
8000
10000
12000
14000
16000
18000
20000
22000
24000
Thrust – FNIN1 *
PRELIMINARY

(This page left intentionally blank.)

E. WING WEIGHT CALCULATIONS

The wing weight calculations are based entirely on the *Wing Mass Formula for Twin Fuselage Aircraft* by Sergei Udin and Prof. Anderson.[12] The changes made reflect a different wing geometry and a different location for the change in wing taper ratio. This appendix details the formulas which differ and lists the results.

E.1 Formulas

The inboard taper ratio, λ_i, is less than one. This changes several of the equations. For the reduced aerodynamic quantities:

$$q_a(1) = \lambda_o \cdot q_a(z_f) \tag{E.1.1}$$

$$q_a(z_f) = \lambda_i \cdot q_a(0) \tag{E.1.2}$$

$$\frac{q_a(0)+q_a(z_f)}{2} z_f + \frac{q_a(z_f)+q_a(1)}{2}(1-z_f) = 1 \tag{E.1.3}$$

Assuming a linear distribution of reduced aerodynamic quantities, equations E.1.1, E.1.2, and E.1.3 can be solved to give:

$$q_a(0) = \frac{2}{z_f(1-\lambda_o\lambda_i)+\lambda_i(1+\lambda_o)} \tag{E.1.4}$$

$$q_a(z_f) = \frac{2\lambda_i}{z_f(1-\lambda_o\lambda_i)+\lambda_i(1+\lambda_o)} \tag{E.1.5}$$

$$q_a(1) = \frac{2\lambda_o\lambda_i}{z_f(1-\lambda_o\lambda_i)+\lambda_i(1+\lambda_o)} \tag{E.1.6}$$

Using a linear fit of these points, the reduced shear force and reduced bending moment are then:

$$Q_{a_o} = \frac{\lambda_i\left(1+\lambda_o+2\lambda_o z_f[z-1]-2z+z^2[1-\lambda_o]\right)}{(1-z_f)\left(z_f[\lambda_o\lambda_i-1]-\lambda_i[1+\lambda_o]\right)} \tag{E.1.7}$$

$$Q_{a_i} = \frac{z_f{}^2(\lambda_o\lambda_i-1)+z_f(2z-\lambda_i-\lambda_o\lambda_i)+z^2(\lambda_i-1)}{z_f\left(z_f[\lambda_o\lambda_i-1]-\lambda_i[1+\lambda_o]\right)} \tag{E.1.8}$$

$$M_{a_o} = -\frac{\lambda_i\left(1+\lambda_o+2\lambda_o z_f[z-1]-2z+z^2[1-\lambda_o]\right)(z-1)}{(z_f-1)\left(z_f[\lambda_o\lambda_i-1]-\lambda_i[1+\lambda_o]\right)} \tag{E.1.9}$$

$$M_{a_i} = -\frac{z_f^3(1+\lambda_i) + z_f\lambda_i\left(\lambda_o[z_f-1][z-1] - \left[z^2+z-1\right]\right) - z_f^2(3z+\lambda_i) + 3z^2 z_f + z^3(\lambda_i-1)}{z_f\left(z_f[\lambda_o\lambda_i - 1] - \lambda_i[1+\lambda_o]\right)} \quad \text{(E.1.10)}$$

From a linear approximation of wing mass spanwise distribution:

$$\frac{m_{s_o}}{m_{s_i}} = \frac{(1-z_f)(2+1.2\lambda_i)(\lambda_o+1)}{z_f(\lambda_i+1)(2+1.2\lambda o)} \quad \text{(E.1.11)}$$

$$q_{s_i}(z_f) = q_{so}(z_f) = \frac{(2+1.2\lambda_o)(2+1.2\lambda_i)}{0.8z_f(\lambda_o+\lambda_i)+(\lambda_o+1)(2+1.2\lambda_i)} \quad \text{(E.1.12)}$$

$$q_{s_i}(0) = \frac{0.8\lambda_i(2+1.2\lambda_o)}{0.8z_f(\lambda_i+\lambda_o)+(\lambda_o+1)(2+1.2\lambda_i)} \quad \text{(E.1.13)}$$

$$q_{s_o}(1) = \frac{0.8\lambda_o(2+1.2\lambda_i)}{0.8z_f(\lambda_i+\lambda_o)+(\lambda_o+1)(2+1.2\lambda_i)} \quad \text{(E.1.14)}$$

Using a linear fit of these points, the reduced shear force and reduced bending moment are then:

$$Q_{s_o} = -\frac{0.2\left([25+15\lambda_i][1+\lambda_o] + z_f\lambda_o[12\lambda_i+20][z-1] - 30z[\lambda_i+\lambda_o] + \lambda_i\lambda_o\left[3z^2-18z\right] - 50z + z^2[25+5\lambda_o+15\lambda_i]\right)}{(z_f-1)\left(2z_f[\lambda_i+\lambda_o]+[5+3\lambda_i][1+\lambda_o]\right)} \quad \text{(E.1.15)}$$

$$Q_{s_i} = -\frac{0.2\left(-z_f[25+15\lambda_i][1+\lambda_o] - 10z_f^2[\lambda_i-\lambda_o] + \lambda_i\lambda_o\left[3z^2+12zz_f\right] + z^2[25+5\lambda_i+15\lambda o] + 20zz_f\lambda_i\right)}{z_f\left(2z_f[\lambda_i+\lambda_o]+[5+3\lambda_i][1+\lambda_o]\right)} \quad \text{(E.1.16)}$$

$$M_{s_o} = \frac{0.2\left(-[25+15\lambda_i][1+\lambda_o] + 3z^3\lambda_i\lambda_o + [20\lambda_o z_f + 12\lambda_i\lambda_o z_f]\left[1+z^2\right] + z\lambda_i\lambda_o[33-21z-24z_f] + z\lambda_o[55-35z-40z_f] + z[45\lambda_i+75][1-z] + z^3[25+15\lambda_i+5\lambda o]\right)}{(z_f-1)\left(2z_f[\lambda_i+\lambda_o]+[5+3\lambda_i][1+\lambda_o]\right)} \quad \text{(E.1.17)}$$

$$M_{s_i} = \frac{0.2\left(z_f[25-25z+15\lambda_i][1+\lambda_o] + 15z^2z_f[\lambda_i-\lambda_o] + \left[15z_f^3\lambda_o\right][1+\lambda_i] + [10z-25]z_f^2\lambda_o - [15+30z_f]zz_f\lambda_i - 15z_f^2\lambda_i\right)}{z_f\left(2z_f[\lambda_i+\lambda_o]+[5+3\lambda_i][1+\lambda_o]\right)}$$

$$+\frac{0.2\left(-25z_f^2 - 25z_fz^2 + 25z + z^3[25+5\lambda_i+15\lambda_o] + \lambda_i\lambda_o\left[3z^3 - 15z_f^2 + 9z^2z_f - 12zz_f^2 - 15zz_f\right]\right)}{z_f\left(2z_f[\lambda_i+\lambda_o]+[5+3\lambda_i][1+\lambda_o]\right)} \quad \text{(E.1.18)}$$

In addition, the thickness distribution:

$$H_i = \frac{z_f - z}{z_f}\left(1 - \frac{T_f}{T_r}\right) + \frac{T_f}{T_r} \quad \text{(E.1.19)}$$

$$H_i = \frac{1-z}{1-z_f}\left(\frac{T_f}{T_r} - \frac{T_e}{T_r}\right) + \frac{T_e}{T_r} \qquad \text{(E.1.20)}$$

E.2 Solution

The equations were solved using Maple. A short FORTRAN program was then used to calculate the final wing group weight percentage. Two cases were solved. First, the actual configuration. Second, a configuration with the mass of both fuselages and the payload concentrated at the centerline. This second case allowed for comparison with existing aircraft. This second value was scaled to modern commercial aircraft and the percent change was taken from the first value as well. This resulted in a wing group weight of 12%. Also, there was a 0.4% savings due to the load distribution given by the fuselages and the payload. Figures E.2.1 and E.2.2 show the reduced shear force and bending moments. They clearly show the savings associated with the distributed loads. The "peaks" on the shear force plot are associated with, from the left, the payload mount, the fuselage, the three engines.

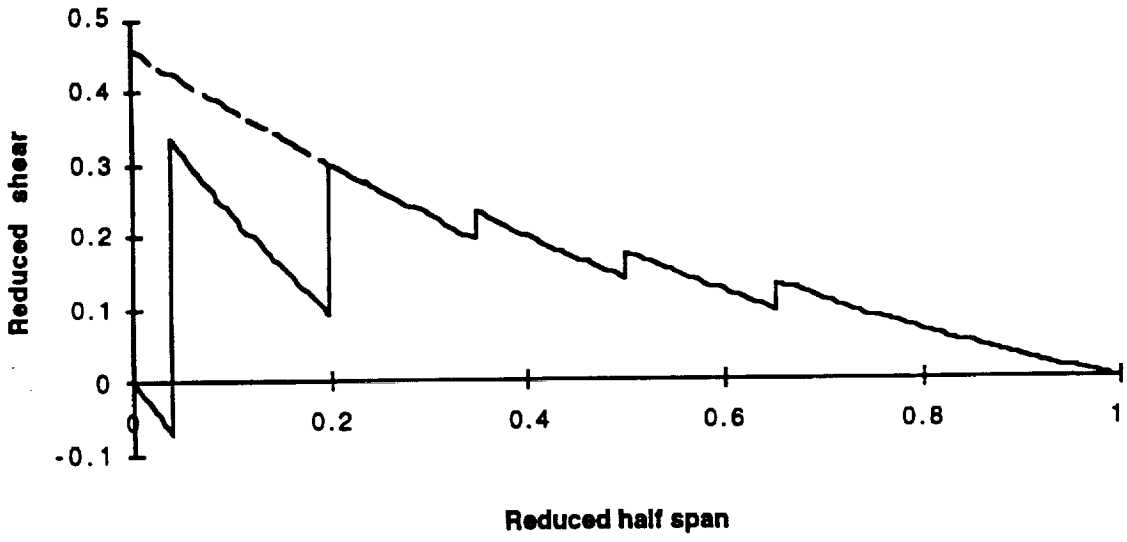

E.2.1 Wing reduced shear force

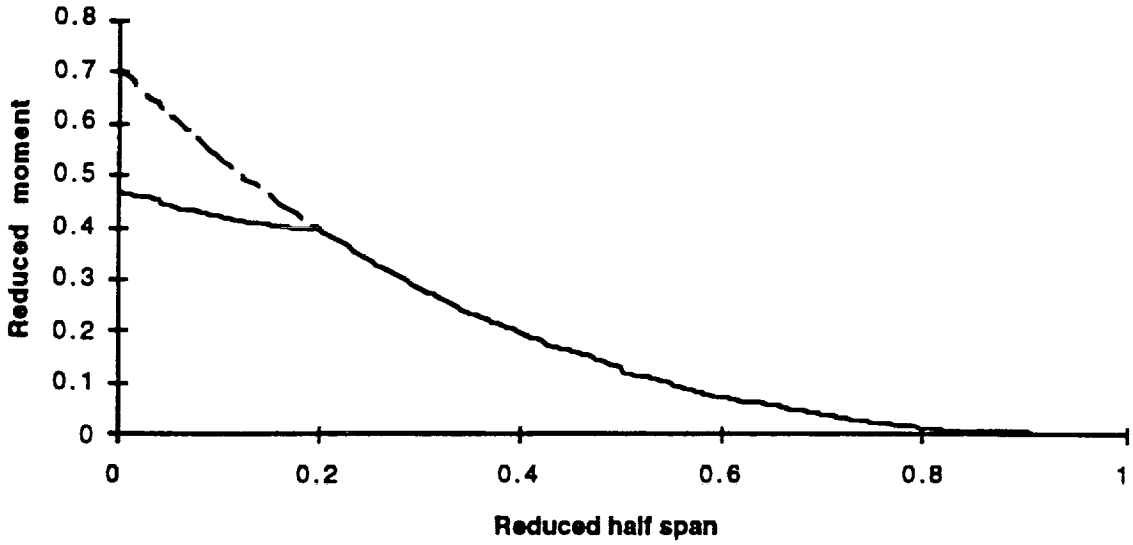

Fig. E.2.2 Wing reduced bending moment

F. LANDING GEAR CALCULATIONS

Static Landing Gear Loads:

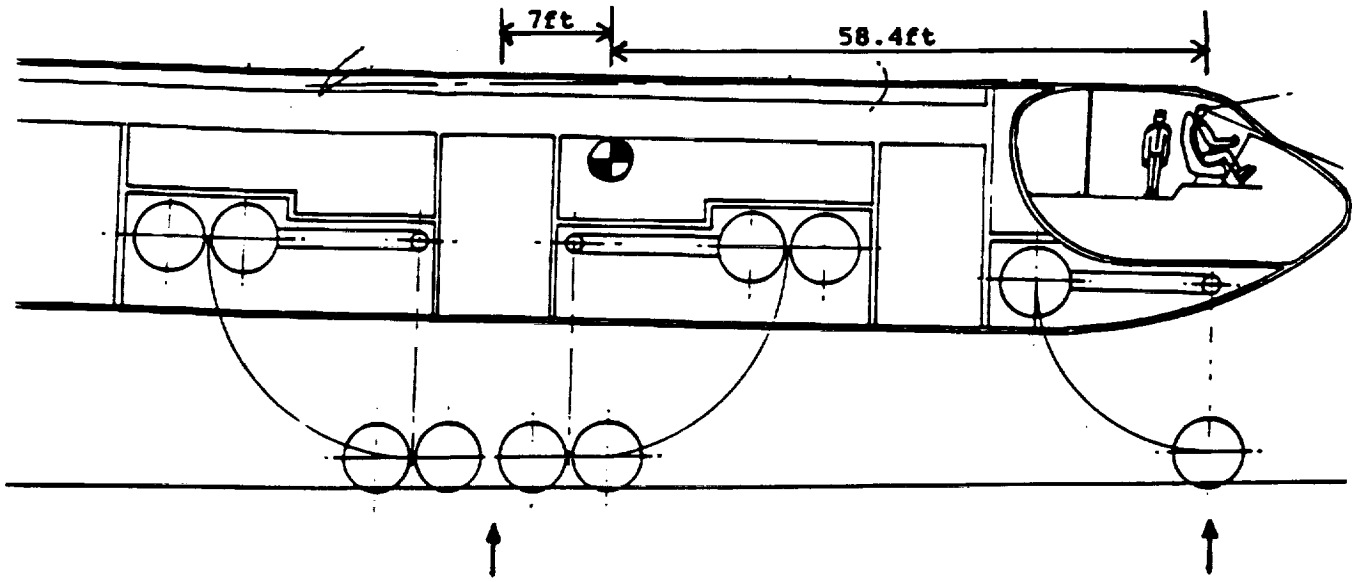

1,130,100 lbs	135,500 lbs
÷ 32 tires	÷ 6 tires
35,300 lbs/tire	22,600 lbs/tire
x 1.07 (FAR)	x 1.07 (FAR)
37,800 lbs/tire	24,200 lbs/tire
x 1.25 (future growth)	x 1.25
47,200 lbs/tire	30,200 lbs/tire

Nosegear Dynamic Loads:

$P_{n\,dyn} = W_{to}[l_m + a_x/g\ (h_{cg})]/n_t(l_m + l_n)$

$= 1{,}265{,}600[58.4 + .45\ (20)]/38(58.4 + 7.0)$

= 34,300 lbs = maximum dynamic load

Design Static Load = Maximum Dynamic Load / 1.50 = 22,900 lbs

x 1.07 (FAR)

24,500 lbs

x 1.25 (future growth)

30,600 lbs/tire

(This page left intentionally blank.)